6-1-2012

Ionic polymer metal composites as tactile sensors

Chris Mieney

Ionic Polymer Metal Composites
As
Tactile Sensors

By
Chris Mieney

Submitted in partial fulfillment of the requirement for the

Master of Science
In
Materials Science & Engineering

Dr. Kathleen Lamkin-Kennard Department of Mechanical Engineering	_____ (Thesis Advisor)
Dr. Benjamin Varela Department of Mechanical Engineering	_____ (Committee Member)
Dr. Brian Landi Department of Chemical & Biomedical Engineering	_____ (Committee Member)
Dr. Wayne Walter Department of Mechanical Engineering	_____ (Committee Member)

College Of Science

Rochester Institute Of Technology

June 2012

Permission to Duplicate

Permission Granted

Title:

Ionic Polymer Metal Composites As Tactile Sensors

I, Christopher M. Mieney, hereby grant permission to the Wallace Library of the Rochester Institute of Technology to reproduce my thesis in whole or in part. Any reproduction will not be for commercial use or profit.

Date: _____ Signature: _____

ABSTRACT

The field of electroactive polymers (EAPs) is rapidly growing. These materials are being scouted for use as linear actuators, specifically in the areas of artificial muscle design, and also for use as biomimetic sensors. IPMCs, or ionic polymer metal composites, are a form of EAP that are being proposed for application in both of these fields. IPMCs are composed of a solvated ionic EAP sandwiched between two metal electrodes. In the literature, there are a wealth of conceptual designs and data related to the use of IPMCs as actuators. However, sufficient data and characterization related to their use as sensors is grossly deficient. This research aims to rectify the gap between the theoretical concept of using these materials for sensing and actual proof of concept by quantifying voltage responses due to small force inputs in various electrolytes (LiCl, $NiCl_2$, $NiSO_4$, and De-Ionized water). Two different load profiles were implemented to evaluate the voltage response to a continuous input, to assess the feasibility of using IPMCs as a precision sensor, and to a cyclical input, to assess the feasibility of using IPMCs as a simpler binary sensor. Normal and reversed polarity voltage profiles were also collected to quantify the reversibility of the material response. Results from the study showed that the IPMCs showed a reversible response in all liquids tested. The results also showed that the response of the materials in LiCl was the least sensitive, but showed good repeatability, while the response in $NiCl_2$ exhibited the greatest sensitivity, but the worst repeatability. The response in $NiSO_4$ was slightly more sensitive than in LiCl and only slightly less repeatable, but the materials in $NiSO_4$ demonstrated an almost completely reversible response. Interestingly, the response in DI water was only slightly less sensitive than in $NiCl_2$ and results obtained using DI water demonstrated the feasibility of developing an IPMC sensor using DI water as the electrolyte. Overall, the data shows that regardless of the electrolyte of choice, IPMCs demonstrate a repeatable response to a force input and show promise for either precision or "binary" tactile sensors.

Abbreviations

1M – Molarity of 1

Al_2O_3 – Alumina

°C – Degrees Centigrade

cm - Centimeter

cm^2 – Square Centimeter

DI – De-Ionized

DOE – Design Of Experiments

E – Young's Modulus

EAP – Electro-Active-Polymer

g - Gram

HCl – Hydrochloric Acid

HDPE – High Density Poly-Ethylene

IPMC – Ionic Polymer Metal Composite

JPL – Jet Propulsion Laboratory

kPa – Kilo Pascal

L - Liter

Li - Lithium

LiCl – Lithium Chloride

mg - Milligram

min - Minute

mL - Milliliter

mm - Millimeter

N - (#_N) - Newton

N - (#N) – Normality

Na - Sodium

$NaBH_4$ – Sodium Borohydride

NH_4OH – Ammonium Hydroxide

$NiCl_2$ – Nickel Chloride

$NiSO_4$ – Nickel Sulfate

Pa - Pascal

PANI – Poly-Aniline

PDMS – Poly-Di-Methyl Siloxane

PPy – Polypyrrole

Pt - Platinum

SEM – Scan Electron Microscopy

TGA – Thermo-Gravimetric Analysis

µm - Micrometer

wt% - Weight Percent

Acknowledgements

I'd like to start by thanking my beautiful wife to be, Rachel, for her never ending support and patience and sticking with me through this. Next I'd like to thank my parents, Skip and Darlene, for their continued support and guidance. I'd also like to thank John and Bonnie Wadach for their encouragement. A special thanks to my boss and mentor Carolyn Fleming for all of her input and advice.

Without getting too deep, I'd like to thank God for the wisdom, foresight, and overall strength granted to me, so I could once again persevere. Many people from many different schools of thought say that God and science do not mix. As I progress further into science, it is becoming more and more apparent, that you cannot have one without the other.

It's been quite the journey and I've learned much along the way. I've always been a very practical thinker and decided to pursue science to strengthen my weaker theoretical side. The skills I have learned, I will have forever and look forward to honing them even more in the future. I'd like to thank my advisor and committee for their input and wish them all the best in their future research.

Table Of Contents

Introduction

Ionic polymer metal composites (IPMCs) are a type of electroactive polymer (EAP). EAPs are polymers that react to an electric stimulus and in doing so can undergo a change in shape, area, and at times volume. EAPs are usually grouped into two categories, electronic and ionic, which is dependent on their activation mechanisms.

Electronic EAPs (i.e. dielectrics, electrostrictive, electrostatic, piezoelectric, and ferroelectric) can hold an induced displacement under a DC voltage and can operate in air with no major constraints, such as the need to remain solvated (wet). Electronic EAPs have exhibited linear strain rates, up to 380%, but require a large actuation voltage; in the mega-volt range. The high actuation voltage required of electronic EAPs is their major drawback and reason for not being more readily implemented into bio-mimetic designs to date.

Ionic EAPs (i.e. gels, polymer-metal composites, conductive polymers, and carbon nanotubes) generate movement as a result of the diffusion of ions and can be actuated under an induced voltage in the millivolt range. Ionic EAPs require an electrolyte, must remain solvated, and with the exception of conductive polymers, have difficulty holding a displacement under a DC voltage. All of the forms of EAPs listed here are also classified as transducers and therefore not only have application in the actuator industry, but also in the area of sensors.

IPMCs, in particular, are an attractive technology for the sensor industry, specifically low force (tactile) sensing. The most attractive attribute of IPMCs for tactile sensing is the relatively low stiffness of the materials, which results in a tip deflection under relatively low induced forces. IPMCs are manufactured from a class of polymers called polyelectrolytes. Polyelectrolytes transmit positive or negative charges that are covalently bound. Nafion® and Flemion® are two polyelectrolytes manufactured by the Dupont™ and Asahi Glass Co.,

respectively. Nafion or Flemion are commonly the polymers of choice in the fabrication of IPMCs as a result of their availability [1].

Main Objective

The proposed research is a requisite first step leading to the development of a composite tactile sensor. A composite tactile sensor would be able to do sensitive tactile sensing as well as larger force sensing. Advantages of a composite tactile sensor would include a greater versatility of the sensor with minimal packaging since there would essentially be two sensors contained in one package. For example IPMCs could be integrated in series with a piezoelectric sensor into one combined sensor package. The IPMC could be used for sensing lower forces, while the piezoelectric would not output detected force data until a pre-determined force requirement was met. However, in order for this type of composite sensor to be realized, the tactile sensing ability of IPMCs must first be quantified. Thus, the main focus of this thesis was to characterize IPMCs and their operation as a potential tactile sensor, by quantifying the voltage output due to force and displacement inputs, for the eventual integration into a "composite sensor."

Background

Nafion® N117 is most often the polymer of choice for manufacturing IPMCs and is usually bonded on either side with a highly noble and conductive material, i.e. gold or platinum, for maximum operational efficiency. A representative IPMC can be seen in Figure 1. Efficiency is most often hindered by poor electrode conductivity and therefore one of the most important criteria for defining a good IPMC is the quality of the electrodes. The lower the resistance of an electrode, the less power required for actuation. The reverse would be true for sensing where a lower resistance would yield a more precise electrical output; e.g. voltage or capacitance

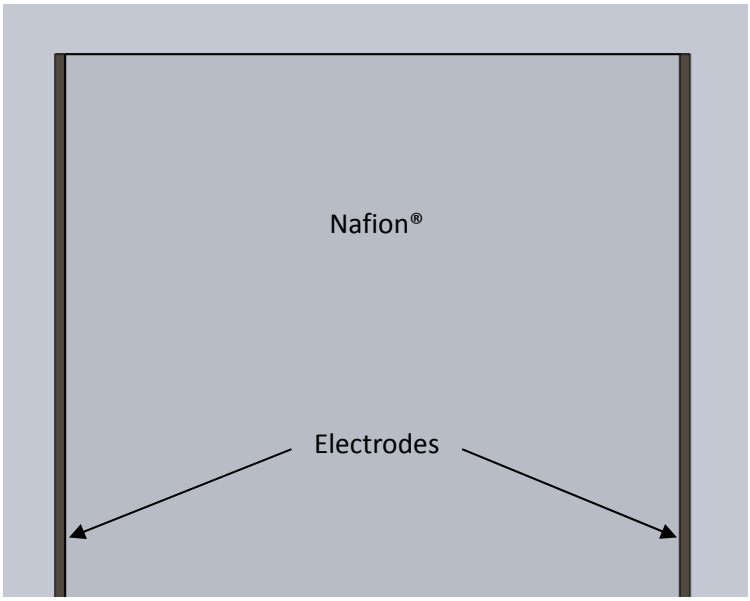

Figure 1. Representative IPMC with Nafion® N117 plated with 3µm electrodes

Ion implantation and electroless plating are among the methods used for the application of electrodes onto a polyelectrolyte. Ion implantation is a process where the ions of a material are accelerated through an electric field into the surface of a substrate as shown in Figure 2. The accelerator electrostatically accelerates the ions from an ion source onto the substrate. Acceleration energies typically range between 10 and 500 keV, where the greater the energy, the greater the penetration of the ions into the substrate.

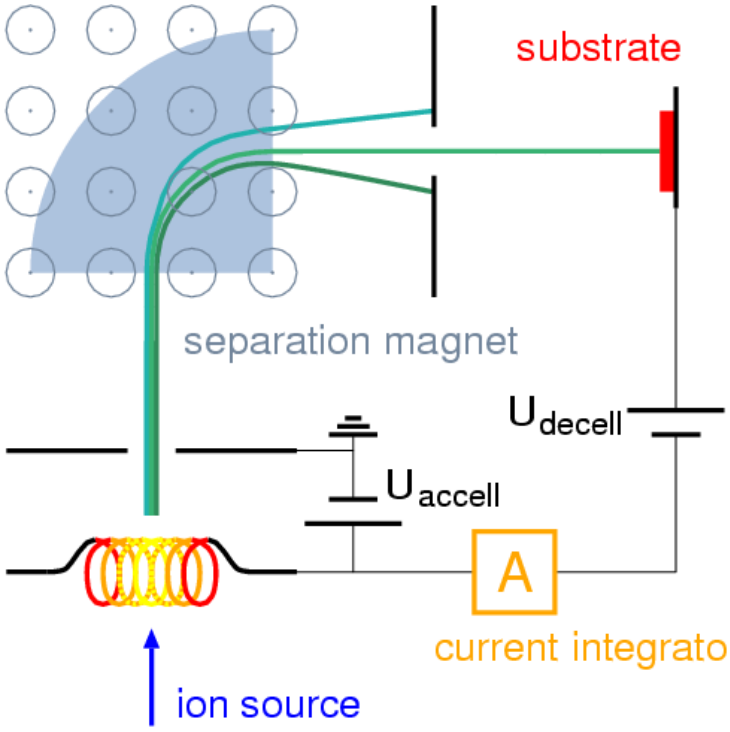

Figure 2. Representative Ion Implantation setup [5].

In the case of IPMCs, gold or platinum is generally the material being accelerated and the substrate is usually Nafion®.

Electroless plating is perhaps the most economical means of depositing electrodes onto the polymer substrate. Deposition is achieved through a pH and temperature controlled solution process. Electroless plating starts with a metal salt, generally a platinum complex for IPMCs, a reducing agent, sodium borohydride or similar compound, and pH balancer, sodium hydroxide or ammonium hydroxide. Sodium borohydride is generally the reductant of choice, resulting from its ability to deposit principally elemental metal, as seen in electroless nickel baths [4]. In theory, almost any metal can be deposited on a surface from a metal salt solution, with the necessary surface preparation and desired adhesion being the only aspects of concern. As a result of the high cost of platinum, another suitable metal such as Nickel or Cobalt may yield acceptable results as an electrode, while keeping cost minimal, since Cobalt and Nickel are much

less expensive than Platinum. To date, however, there is limited evaluation of these other metals as viable electrode materials and could be an interesting area for future research.

Several methods exist for evaluating the quality of an electrode, one of which is sheet resistance. An electrode with lower resistance is said to be of a higher quality. A large electrode resistance can be due to many factors that include, but are not limited to, insufficient electrode thickness, micro cracks, and inhomogeneous deposition [3]. Detrimental cracks in the electrode can result from plating that is either too brittle and/or overstraining of the IPMC. Inhomogeneous deposition and insufficient thickness are largely dependent on the type of processes used for electrode deposition. Thus, electroless plating is the most ideal from an all around perspective. It has a lower cost than other methods, such as ion implantation, and yields a very uniformly thick, homogeneous layer.

Several discrepancies exist in the literature with respect to cracks in the plating and overall performance of IPMCs., M. Shahinpoor and K. J. Kim [2] report on different plating schemes for the construction of IPMCs. For the "surface electroding process" the plating appears to have micro and macro cracks as shown in Figure 3.

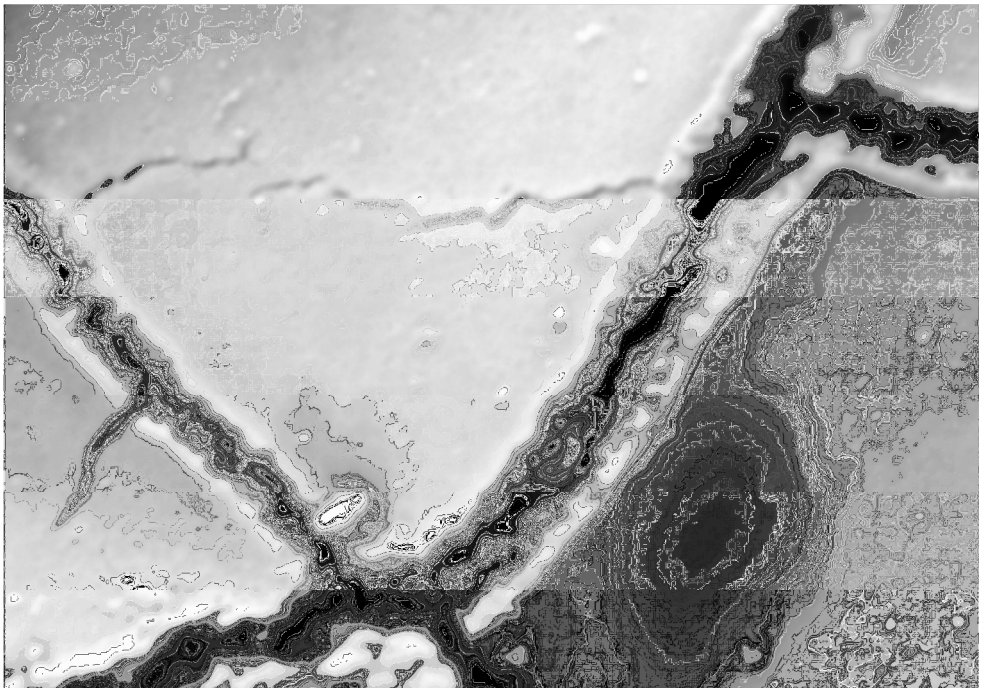

Figure 3. SEM surface view of platinized IPMC [2].

The authors further describe how the platinum electrode is porous and that the leakage of water through the electrode reduces the efficiency of the IPMC during electrochemical conversion. The authors suggest that as the IPMC is operated, either as an actuator where a bias is applied and the differential swelling causes motion, or as a sensor where the membrane is mechanically deformed resulting in charge buildup on the electrodes, water will leak through the electrode causing the energy conversion to be less efficient.

Punning et. al. [17] characterized the surface resistance of IPMCs as it applies to actuators and sensors. The authors refer to cracks in the plating as "fractionation." The authors confirm the findings of Shahinpoor and Kim, that the IPMC has a cracked surface appearance, seen in Figure 3 and describe the surface as being comprised of discrete particles. The operation of the IPMC is then attributed to the conduction of metal islands on the surface. This terminology of "metal islands" is interesting, as it is usually found in the literature when referring to conductive particle impregnation of polydimethysiloxane (PDMS), a dielectric EAP. These

discrete conductive particles on the surface of the IPMC are illustrated in Figures 5 and 6. Punning et. al. [17] also describes how the surface resistance of an untested IPMC was very low, but the "operational performance of the sample was reported to be very weak" due to the large stiffness of the strip; which is assumed to mean that it did not show a large displacement under the applied voltage. The authors evaluated samples that had been previously tested multiple times and found their performance to be well above the untested sample. Thus, the authors concluded that the untested sample was mechanically stiffer than the used samples [17,2]. From an actuation standpoint, a sample with a higher stiffness would require more voltage to obtain the same deformation as a sample with a lower stiffness. For sensing applications, this would roughly translate to more force necessary to obtain a similar voltage output for a sample that was more flexible. Overall, the literature suggests that there exists a degree of "pre-straining" necessary for IPMCs to function ideally, along with a happy medium between cracked or "fractioned" plating and performance.

IPMCs fall under the ionic class of EAPs, which need to remain "solvated." De-Ionized (DI) water is the more common of the solvents used to solvate IPMCs since it is readily available with limited safe use instructions. In addition to DI water, other solvents have also been used with IPMCs, such as ethylene glycol, glycerol and crown ethers [1]. It is important not to confuse the solvent with the electrolyte. The solvent is merely the carrier medium for the ions to be exchanged that can be readily absorbed by the polymer, in our case Nafion®. The use of other solvents results in a change in how the IPMC will react to an external stimulus, such as voltage for actuation or an induced force for sensing. Changing the solvent environment in which an IPMC is operated could shift the capacitive operating range of the sensor. The capacitive operating range can be modeled using:

$$C = \varepsilon\varepsilon_0 \frac{A}{d} \qquad (1)$$

where ε_0 is the permittivity of free space, ε is the dielectric constant, A is the area where opposing electrodes overlap "active area" and d is the distance between parallel plates [15]. Since the capacitive response of the material and the material's dielectric constant are directly proportional, a specific capacitance range could theoretically be targeted simply by using a solvent with a dielectric constant that would yield the desired capacitance range for a given application. This targeting of a specific capacitive range helps illustrate the broad spectrum of possible applications for these materials as tactile sensors.

Punning et. al. [16] reports on a self sensing actuator using IPMCs , since IPMCs are transducers by nature. Throughout actuation, measurements of voltage and changes in surface resistance were documented. This study further validates the applicability of IPMCs as sensors and Punning [17] provides significant detail on the characterization of IPMCs as sensors through surface resistance measurements.

The sensing nature of IPMCs is attributed to charged particle migration within the polyelectrolyte stemming from electrochemomechanical effects. During fabrication of IPMCs, the proton group is usually replaced with a metal cation, generally Li^+ or Na^+. This is of great importance since it drives the sensing nature of the material. Mechanical deformation of the material through bending forces these mobile, hydrated cations to one side of the material. The surplus of positive ions on one side of the membrane causes a voltage gradient at the IPMC electrodes as shown in Figure 4 [17].

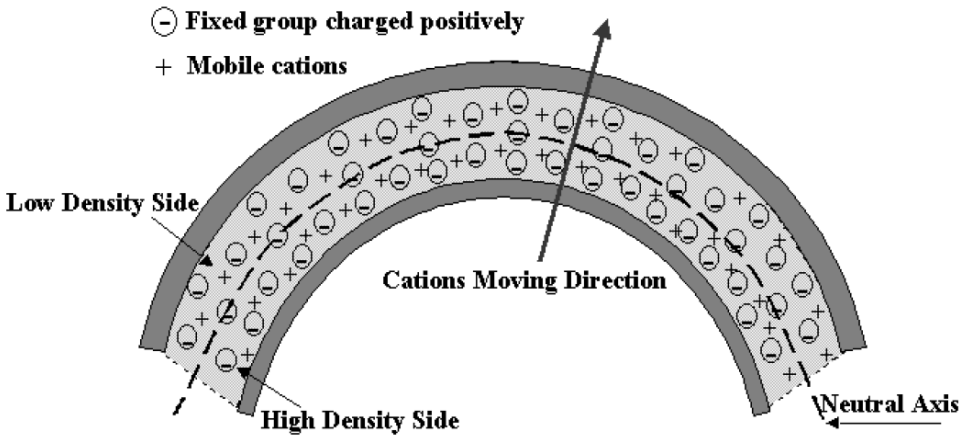

Figure 4. Charge distribution due to mechanical deformation [18]

Figure 5 illustrates how the surface resistance on the compressing side of the IPMC changes very little when bent.

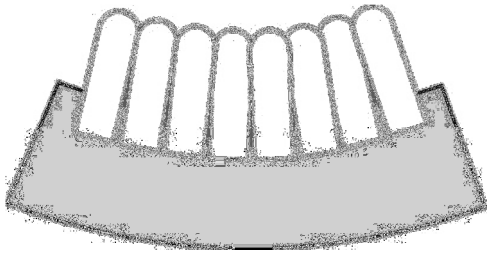

Figure 5. Conductive particles on the compressed surface [17]

On the stretching surface, however, the surface resistance changes drastically as seen in Figure 6. This is the change in surface resistance most likely resulting from the inability of the conductive particles on the compressing side to get any closer together. Conversely on the expanding side, it is with ease that the particles are able to distance themselves, therefore increasing surface resistance.

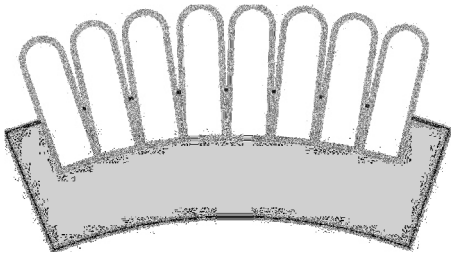

Figure 6. Conductive particles on the stretched surface [17]

Similar findings were found during the compression and stretching of an IPMC. Upon compression across the thickness, surface resistance changed very little, whereas upon stretching of the membrane, surface resistance increased drastically [17].

From the work presented by Punning et. al. [17] and how surface resistance changes with bending as opposed to compressing the membrane, voltage output is thought to be greater when charge migration is induced from bending rather than compressing the material as seen in Figure 4. Bending of the material causes the cations to migrate. If the membrane were to simply be compressed across the thickness, it is thought that drastic cation migration would not be instigated and therefore negligible voltage output would be observed. Lower voltage outputs under compression would suggest that the more points of bending achieved, the greater the possible voltage output; since a bend causes ions of the same charge to migrate from regions with a high density of ions to a low one, resulting in a voltage change. Thus, it would stand to reason that an IPMC tested in a 3 point bend scenario should yield easily measureable results.

Literature Gap

In the literature there are multiple entries referring to the applicability of EAPs as biomimetic sensors and actuators [6,8]. However, most of the information in the literature focuses on experimental characterization or design criteria associated with actuation applications. For example, Bar-Cohen et. al. [6], mentions using IPMCs as an ultrasonic sensor based on the capability of the materials to detect sound waves in the spectral range. A full page was devoted to the conceptual design of this setup in addition to identification of some input parameters. Experimental data presented in the paper, however, revealed that there was no measurable response in the spectral range and the remainder of the paper subsequently focused on IPMCs as actuators. Shahinpoor et. al. [9] discuss recent findings on the biomimetic sensing

and actuator abilities of IPMCs. A discussion about using IPMCs as sensors and some data on the voltage response to tip displacement of an IPMC follows over the course of three pages. The remaining 12 pages then go on to discuss (in much more detail) the application of IPMCs as actuators along with detailed actuation data.

The ratio of sensing to actuation data is quite common in the literature and illustrates the great need to bridge the gap in characterization of IPMCs as sensors. Kim [8] clearly describes the transducer nature of IPMCs, where a measurable charge builds up on the electrodes as a result of an imposed bending stress. Kim [8] presents the following governing equations for "*linear irreversible thermodynamic*" correlation relating charge transport and solvent transport that are applicable to actuation or sensing:

$$J = \sigma E - L_{12}\nabla p \qquad (4)$$

$$Q = L_{21}E - K\nabla p \qquad (5)$$

where J is the current density normal to the membrane, Q is the flux, E is the electric field, ∇p is the pressure gradient, σ is the electrical conductance, L_{xx} is the cross-coefficient, and K is the permeability. Despite a brief discussion of the potential use of IPMCs as transducers, the paper focuses primarily on the actuation potential of IPMCs, in particular, force-displacement characteristics and applications to Robotic Flapping Wings [8]. Bennett and Leo [7], give sufficient background on the function of IPMCs as mechanical sensors, but fall short with the physical characterization logistics of IPMCs being used as a sensor. There is adequate information on the test setup used, however, the results for the sensor, are again dwarfed by the actuation data. Overall in the literature, the amount of data that focuses on IPMCs as sensors, specifically true tactile sensors, is limited. Thus, there is a significant need to characterize these

materials as tactile sensors and quantify the voltage output ranges of this mode of operation. This thesis work seeks to address this need.

Most sensing data available for EAPs characterizes operation on the kPa or MPa scale and would not be applicable for tactile sensing. For example, a polyurethane thin film was proposed by Suzuki et. al. [12], as a material for a polymer tactile sensor. The measured capacitance output in the pF range, however, the force input was still in the 0.1 to 2 kPa range. For a practical tactile sensing application, the desired force input should aim to be in the range of a Pascal instead of hundreds to thousands of Pascals. Wang et. al. [13] created an all polymer pressure sensor from polyanaline (PANI), polypyrrole (PPy), and poly(3,4-ethylenedioxythiophene) doped with poly(styrenesulfonate). The sensor created by Wang et. al. [13] generated a resistance change in the kΩ range with a pressure input that started at around 20 kPa. Wang et al. further suggested that with manipulation of the chemical composition and other relevant parameters, this sensor could be much more marketable [13].

IPMCs as tactile sensors would need no such change in chemistry. IPMCs produce a measurable electrical output with limited force input and need only to be properly characterized. Conductive particle impregnated elastomers have been investigated for their pressure sensing ability, but only report a voltage change on the 100 kPa to 3 MPa scale [10,11]. For realistic tactile sensing, a fingertip type response is required with a measureable response to external stimuli in the Pascal range, as opposed to the kilo or mega Pascal range. Based on the low mechanical stiffness of IPMCs and their transducer nature, it is anticipated that IPMCs will have a response in the Pascal range and thus, may indeed be the necessary material for tactile sensing.

The long term objective of this research is to design and build a "composite" tactile sensor where an IPMC could be deposited in some way on top of a piezo-transducer. A

constantly increasing force would then be applied and the voltage from the IPMC and piezo transducer would be collected separately. At some force threshold, the IPMC would stop sensing and the piezo would begin since IPMC's are thought to be more accurate than piezos in the lower force range due to their lower stiffness.

Statement of Work

The goal of the thesis was to characterize the sensing response of IPMCs by quantifying voltage changes due to small induced mechanical deformation in the presence of different electrolytes. Through utilization of a test rig, shown in Figure 7, specifically designed for the characterization of IPMCs as sensors, force verses voltage and displacement verses voltage data was obtained in the presence of different electrolytes.

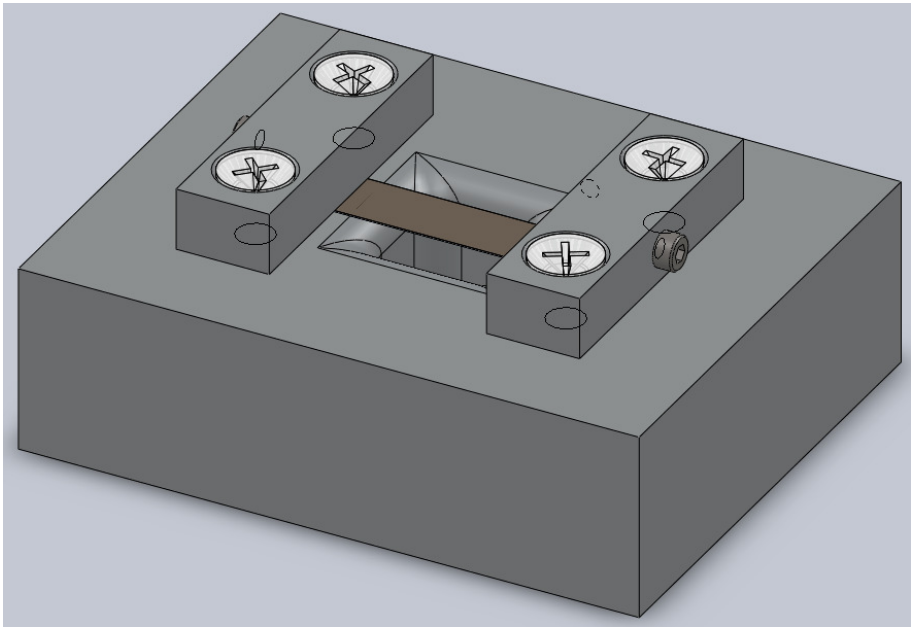

Figure 7. IPMC Sensor Test Rig

The test rig was designed to be immersed and fit onto a tensile testing machine to characterize the voltage response of IPMCs in an aqueous environment as a force is applied. Along with the ability to obtain accurate strength data, tensile testing machines are also able to output a very specific amount of force or strain, therefore allowing characterization of the electrical response

of an IPMC under an applied stress or strain (or mechanical deformation). The tensile testing machine utilized for this testing was an Instron® model 4206 controlled by a Merlin version 5 software package.

A force verses voltage analysis was performed for both normal polarity and reversed polarity on four different IPMCs. The four different liquids evaluated were: DI Water, 1M LiCl, 1M $NiCl_2$, and 1M $NiSO_4$. The 1M LiCl was used as a control solution since it is generally the electrolyte of choice in many literature sources. DI water was evaluated to determine its feasibility for this type of operation, stemming from its relatively low cost and limited safe use instructions. From a production standpoint this is of moderate importance. $NiSO_4$ was chosen to evaluate the use of a non chloride from of metal salt. The sulfate form was chosen to determine if the chloride form is truly necessary. A sulfate was selected in hopes of getting away from the need for noble metals as electrodes resulting from the aggressive nature of the chloride ion. $NiCl_2$ was tested for a comparison of chloride to sulfate forms of a metal salt, in order to keep the cation constant from the chloride to sulfate metal salt.

To test the voltage response of IPMCs, two force vs. time profiles were developed. The first incorporated a constantly increasing force over time at a rate of 30 mm/min, to characterize the IPMCs response to force (linear, logarithmic…) and to evaluate whether it is able to operate as a true tactile sensor. The next profile created was a cyclic profile, where a constant force was applied and removed for 3 cycles at a rate of 30 mm/min up to a load of 2.5 N with 2 second holds at 0 N and 2.5 N The second profile was used to evaluate IPMCs viability as binary tactile ("simple" touch [21]) sensors. The binary profile would be less desirable than the first profile, but would still be beneficial working under the theory that IPMCs have a very low stiffness (E, Young's Modulus) and require very low force to deform (ergo "precision tactile"). The binary

result could serve as a simple yes or no check for low force contact sensing. In both cases, the Instron® was setup to output force vs. time and a digital multimeter was used to read the voltage response of the IPMCs, by outputting voltage vs. time to a Microsoft Excel™ file. The voltage output along with the applied force and displacement verses time were plotted on 3-axis graphs with time on the horizontal axis.

IPMC Production

IPMCs were fabricated for this study using the recipe published by JPL [25]. Nafion® N117 was purchased from Ion Power, Inc (http://www.nafionstore.com/NAFION_Membrane_N117_p/n117.htm) and was processed according the JPL recipe, detailed in Appendix L. A 5 cm by 6 cm Nafion® N117 section was roughed with 600 grit wet sandpaper under dry conditions. The roughened membrane was then immersed in an ultrasonic cleaner, containing DI water, for 5 minutes. Following the washing the membrane was boiled in a 2N solution of hydrochloric acid (HCl) for 30 minutes and then boiled in DI water for 30 minutes. After preparing the 5% NH_4OH, 1 mL of the solution is added to the platinum ammine complex. The platinum ammine complex contains 2 mg of Tetraammineplatinum(II) chloride hydrate per mL of DI water and 3 mg of Tetraammineplatinum(II) chloride hydrate per cm^2 of membrane area. Following this step, the roughened and washed membrane was immersed in the solution of platinum ammine complex and 5% NH_4OH for 16.5 hours, referred to as the adsorption step in the recipe.

For primary plating, a 5 wt% aqueous solution of sodium borohydride ($NaBH_4$) was prepared by adding 2.5 g of $NaBH_4$ to 50 mL of DI water. The membrane was first rinsed in DI water and 180 mL of stirring DI water was brought up to 40°C. The membrane was put into the stirring water and 7 additions of 2 mL of the 5 wt% $NaBH_4$ were added every 30 minutes. Over

the course of these additions, the bath was gradually brought up to 60°C. After the 1st addition of the $NaBH_4$, the bath pre-maturely reached 50°C. The hot plate was turned down in order to bring the bath back to ~40°C and the gradual increase of temperature was resumed. Since the bath was eventually raised to 60°C, there was no cause for concern over the premature rise. After the 7th addition of the $NaBH_4$, 20 mL of the solution was added to the 60°C bath and allowed to stir for an additional 1.5 hours. Following this, the membrane was rinsed in DI water and then immersed in 0.1N HCl for 1 hour. After that, the membrane was stored in DI water overnight awaiting secondary plating.

For secondary plating 120 mg of Tetraammineplatinum(II) chloride hydrate was added to 240 mL of DI water. 5 mL of the 5% NH_4OH was then added to that solution and brought up to 40°C. 6 mL of the 5% hydroxylamine hydrochloride and 3 mL of the 20% hydrazine solution was then added 8 times every 30 minutes for a total time of 4 hours. Over the course of the additions, the bath temperature was gradually raised up to 60°C**.** The endpoint of the bath was then checked by sampling a small amount, allowing it to cool, slowly adding sodium borohydride in powder form and bringing the solution back up to temperature. If any platinum had remained, it would have formed dark particulate in the solution and if enough were present, could have turned the solution opaque. There was no change in appearance to the bath signifying that no platinum remained in the solution. The membrane was then rinsed in DI water and boiled in the 0.1N HCl followed by storage in DI water until use.

Note on Water

ASTM D1193 specifies Class I DI water to have an electrical resistivity value of 18 MΩ-cm (minimum) at 25°C. The DI water mentioned here had an electrical resistivity value of 17.2

MΩ-cm according to the readout of the Barnstead Nanopure machine from where the DI water was obtained.

Material Characterization

Following material production, a detailed characterization of the produced IPMCs was performed. Based on the amount of platinum added during the production process, and the measured density of platinum, a maximum theoretical plating thickness was determined. This was calculated by determining the amount of platinum (Pt) in moles that is available from the tetraammineplatinum(II) chloride hydrate complex. Taking the amount of complex in grams that is added to the reaction and dividing from that the molecular mass of the complex, gives the amount in moles of Pt available to be deposited during the chemical plating operation. A multiplication of the moles of Pt available and the molecular weight of Pt, gives the amount in grams of Pt that could theoretically be deposited onto the membrane. Multiplying the measured density of Pt and the surface area of the membrane yields g/cm of Pt. Dividing this number from the amount of Pt in grams that is available gives the maximum thickness in cm that is theoretically possible from the amount of Pt complex added. These calculations are illustrated in Figure 8.

$Pt(NH_3)_4Cl_2 \cdot H_2O$

Pt	195.084	1	195.084
N	14.0067	4	56.0268
H	1.00794	14	14.11116
Cl	35.453	2	70.906
O	15.9994	1	15.9994
			352.1274 g/mol

Pt Density 21.46 g/cm^3 measured at 25°C (ASM)
Nafion thickness 0.007 in = 0.01778 cm

Surface Area = (2LH)+(2LW)+(2HW)
60.39116 cm²

added 180.6 mg Pt complex for primary plating and 120 mg Pt complex for secondary
that's 0.3006 g Pt complex for entire process

$\frac{0.3006 \text{ g}}{352.12736 \text{ g/mol}}$ = 0.000854 mol Pt complex available to membrane

0.0008536 mol x 195.084 g/mol = 0.166537 g Pt available to Nafion

21.46 g/cm³ x 60.39116 cm² = 1295.9943 g/cm (Density x Surface Area)

$\frac{0.166537 \text{ g Pt}}{1295.9943 \text{ g/cm}}$ = 0.000129 cm theoretical plating thickness

~1.29µm plating thickness (theoretical)

Figure 8. Theoretical Electrode Thickness Calculations

The calculations show that the maximum thickness achievable from the amount of the platinum added is approximately 1.29 µm. This is not realistic, however, since it assumes that all of the platinum was adsorbed during the adsorption step and that all of the platinum consumed during plating was indeed deposited onto the Nafion® substrate. Alongside the theoretical calculations a number of other characterization methods were performed. These included: Thermogravimetric Analysis (TGA), metallographic cross sectional analysis, and Scan Electron Microscopy (SEM) which incorporated pictures, elemental maps and a line scan across the fracture face.

The TGA sample was prepared by sandwiching a small IPMC between two index cards and then removing a 7 mm circular section with a hole punch. This 7 mm sample was then run through a standard TGA profile displayed in Figure 9; first in nitrogen, to hinder oxide formation, and then in air, to compare to the value found for nitrogen. The TGA went up to 800°C, which is far above the melting point of the Nafion® polymer and still much below the

melting point of Pt. This guarantees that the mass remaining at the end of the run is solely Pt, aka the electrode.

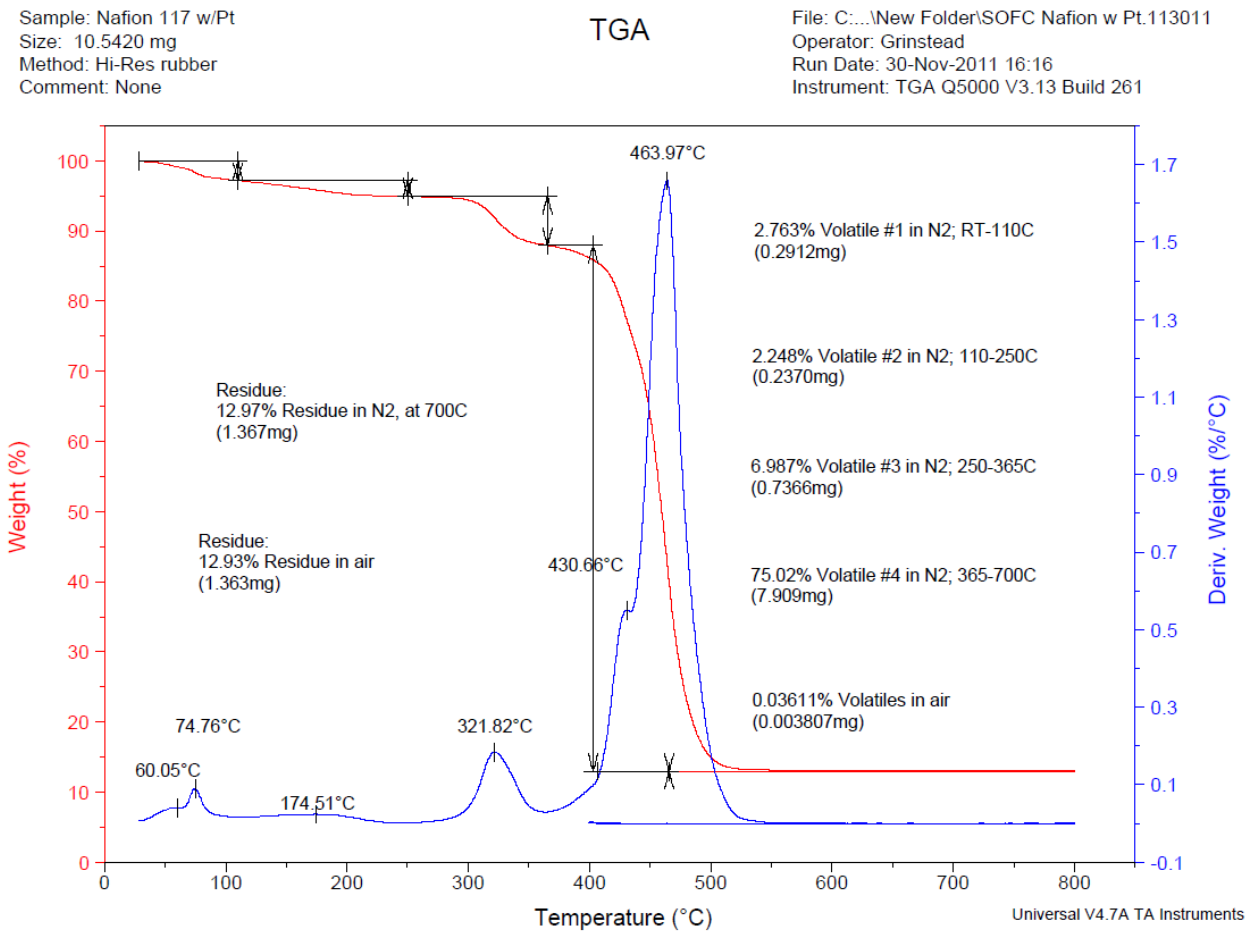

Figure 9. TGA Thermogram of IPMC

Since the remaining mass for air was less than that of nitrogen, the air value was used for calculating the average actual plating thickness; in order to represent the minimum amount of plating present. More calculations were then carried out using the TGA data where, instead of using the amount of Pt that was added to the membrane via the Pt complex, the physical amount present that was determined via the TGA was used and the calculations were carried out in the same manner and are pictured in Figure 10.

Pt Density	21.46	g/cm^3	measured at 25°C (ASM)
IPMC Sample Diameter	0.7	cm	

Area = $\pi d^2/4$

= 0.3848451 cm^2

SA= 0.7696902

0.001363 g Pt available to Nafion® (from TGA)

21.46 g/cm^3 x .3848 cm^2 = 16.5176 g/cm (Density x Surface Area)

$\frac{0.001363 \text{ g Pt}}{16.5176 \text{ g/cm}}$ = 8.25183E-05 cm plating thickness

~825 nm (average actual)

Figure 10. Average Actual Electrode Thickness Calculations

An average actual thickness of approximately 825 nm was determined based on the final mass found at the end of the TGA.

A small section of IPMC was mounted in lucite and then polished from 60 grit wet down to 1 micron diamond on nylon. From the metallographic analysis it can be seen (Figure 11) that variations exist in the plating thickness, hence the term “average actual thickness”.

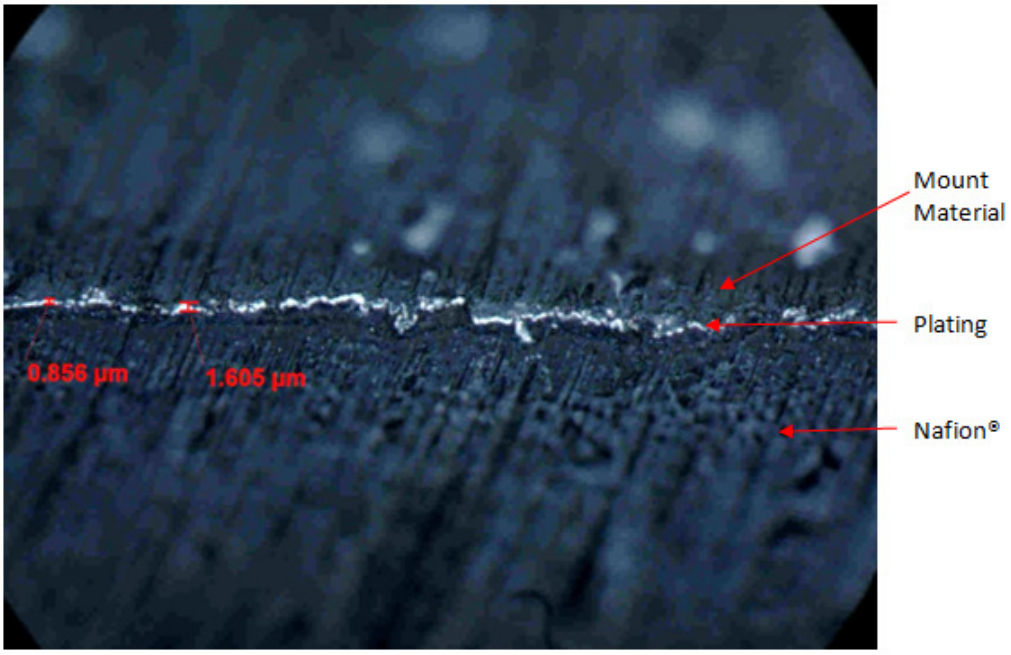

Figure 11. Metallographic Cross Section of the IPMC

The SEM analysis was performed on an Amray SEM with a Semtech Violin digital detector at 15 kV. The sample was obtained by stretching a small piece of IPMC until fracture. The according fracture face was then oriented in the SEM so that the image was as close to perpendicular as possible.

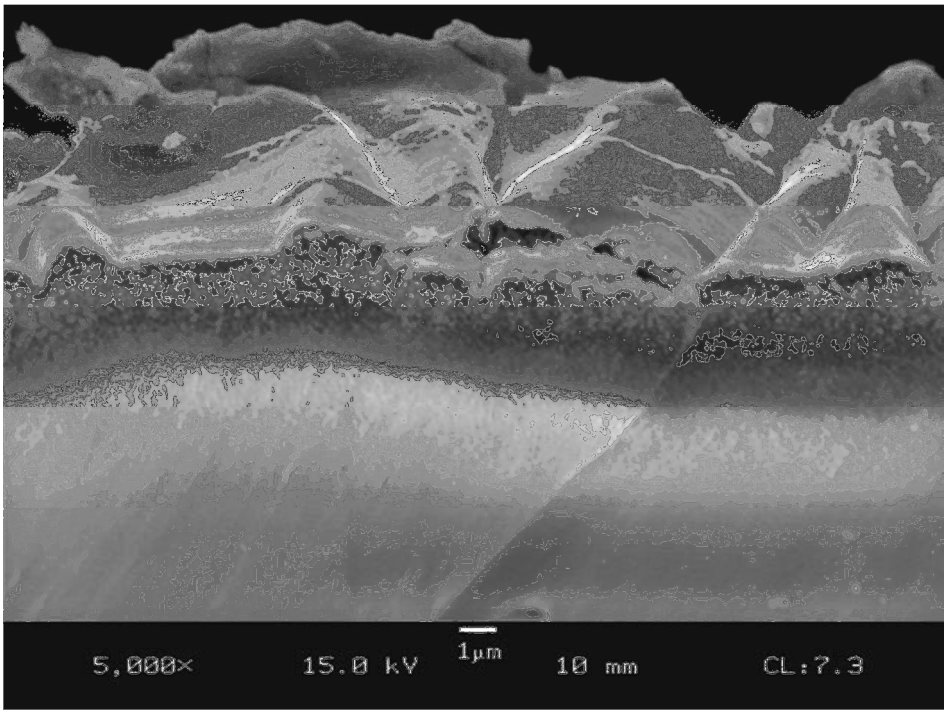

Figure 12. SEM of IPMC Fracture Face

The image seen in Figure 12, taken at 5000x, shows the plating, the inter-dispersed zone, and the Nafion® itself. Since Nafion® is a ductile material, the image is not completely perpendicular, however, a somewhat perspective view of the top of the sample is seen. This is difficult to avoid, since ductile materials fail in a cup and cone geometry. The ductile failure could also play a role in the "rippled" look of the plating which also would suggest a well adhered electrode.

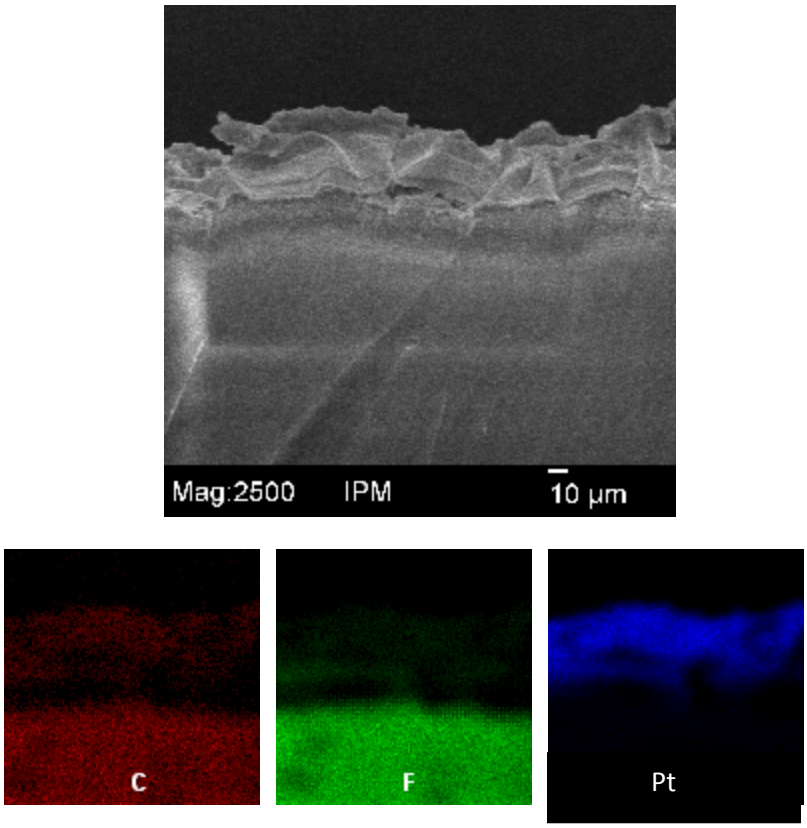

Figure 13. IPMC Elemental Map

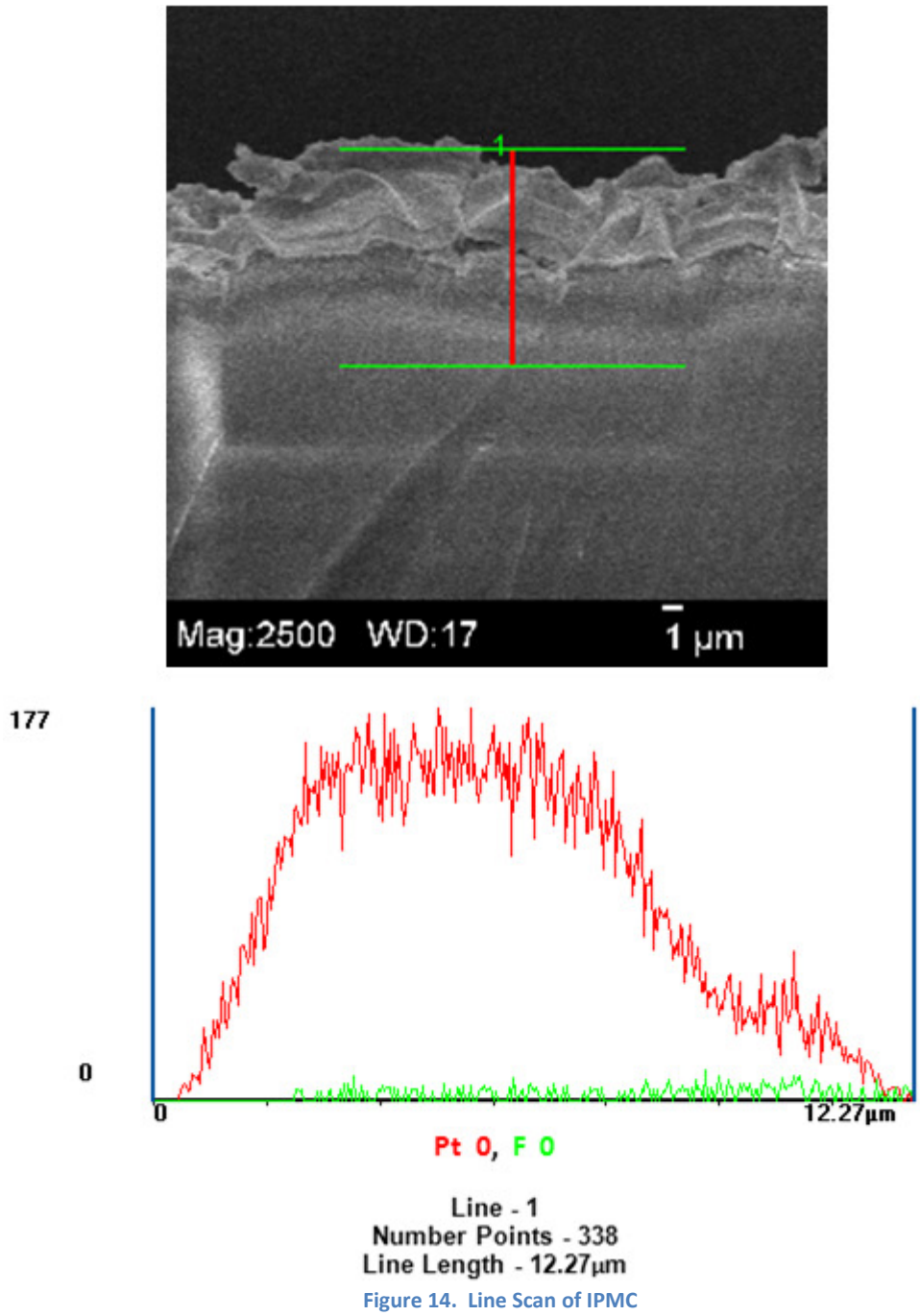

Figure 14. Line Scan of IPMC

An elemental map (Figure 13) and line scan (Figure 14) were then performed on the material to see how the Pt was dispersed into the Nafion®. Line scans are generally performed by identifying elements of interest and drawing a line to search along for these elements. Generally, samples are mounted then cross sectioned and polished flat, allowing the face to be looked at almost completely perpendicular. In this case, to avoid the drag in of contaminants that could

occur during polishing and to obtain a high resolution image at high magnification, the sample was simply stretched until fracture to obtain a fracture face for viewing. A fracture face was used since it gives the optimal scenario for high resolution high magnification imaging. It is important to note that the line length is not the plating thickness. As previously mentioned, the sample is at a slight angle, so the line scan encompasses a small amount of the top of the plating. The purpose of performing the line scan was solely to obtain a graphical representation of the inter-diffusion layer of Pt particles into the Nafion® substrate, not to determine plating thickness. The Pt inter-diffusion layer can be seen in Figure 14 where the concentration of Pt begins to gradually decrease.

Experimental Methods

Four different IPMC samples (1 cm x 6 cm) were tested in a 3 point bend mode. For each sample, a different electrolyte was prepared: 1M lithium chloride (LiCl), 1M nickel chloride ($NiCl_2$), 1M nickel sulfate ($NiSO_4$), and class II (17.2 Ω-cm) deionized water (DI water). Each IPMC sample was paired with one electrolyte and only tested in the presence of that liquid. Each sample was then removed from storage in a DI water solution and set up in the test rig.

Each IPMC sample was laid flat centered across the rig and perpendicular to the top electrodes. Thin plastic was placed on either side of the IPMC at the extremities of the top electrodes, where there was no contact with the IPMC. The plastic was used to ensure that the top electrodes could not make contact with the base of the rig, resulting in a short circuit. After the IPMC was held flat, one of the top electrodes was affixed with the nylon screws and tightened only to the point where the IPMC would not slip when the load was applied. A pair of

tweezers were used to pull the IPMC taut while the other electrode was tightened against the sample.

The test rig with sample affixed, was then immersed into one of the liquids in a 3L beaker sitting below the probe on the Instron® (Model #4206). The probe used to apply the force input to the material was a 1.5 cm wide piece of high density polyethylene (HDPE). The end was rounded with a radius of 3 mm to avoid sharp corners coming in contact with the sample. The probe was attached to a 10 Newton (N) load cell with an accuracy ± 0.025% the total range. Prior to testing, the probe was lowered into the beaker and the gage length was set to zero just as the probe made contact with the top of the sample, as seen in Figure 15.

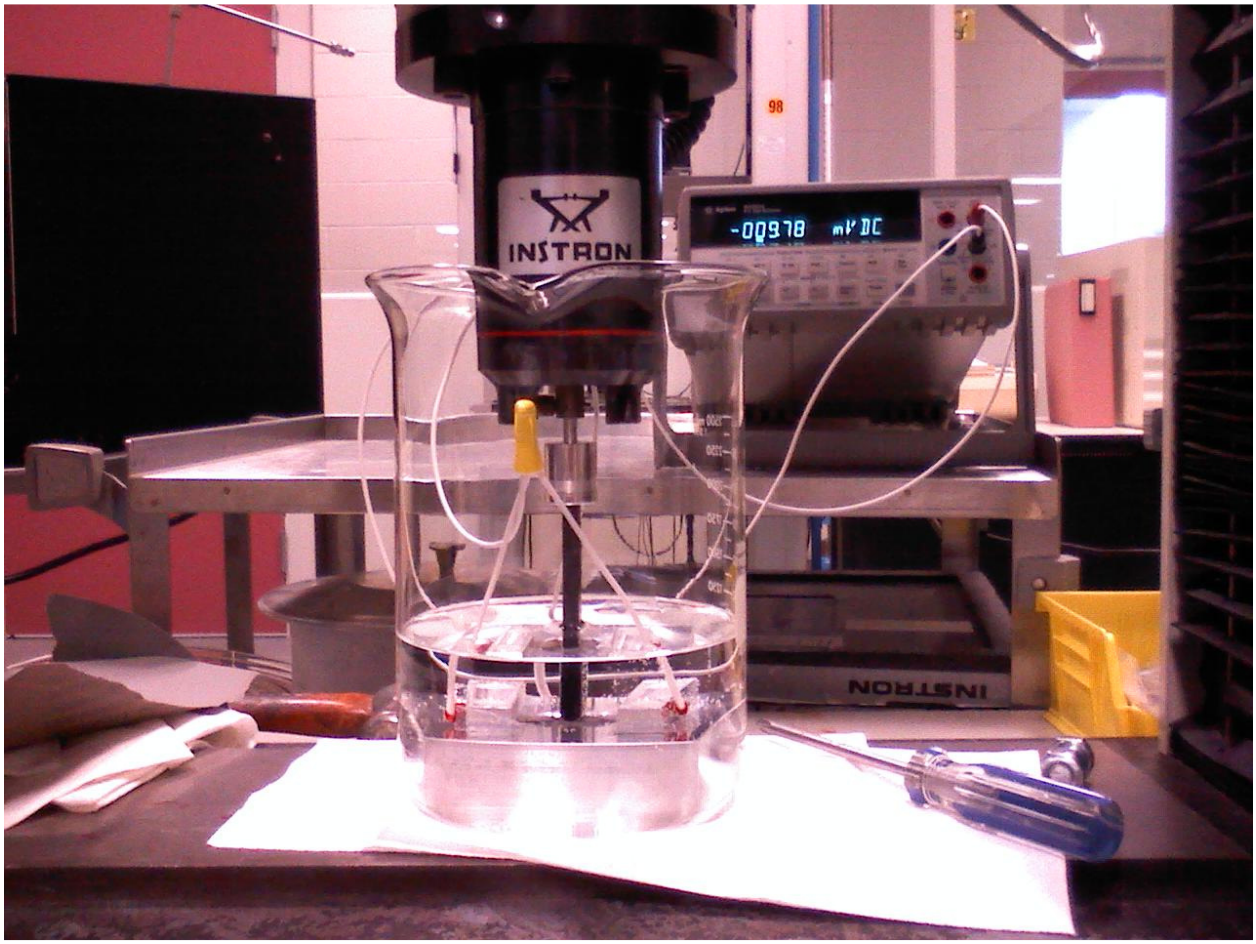

Figure 15. IPMC tactile sensor test setup

The leads from the rig were connected to an Agilent (model 34401A, accuracy of ± (0.00300% of reading + 0.00300% of range) for the 100.0000 mV range) multimeter with the RS-232 output connected to a laptop computer to collect the voltage output of the IPMC throughout testing. The load cell was re-balanced (zeroed out) before each run. Both computers were then started at the same time. Voltage and time were collected every 200 milliseconds on the laptop, pictured on right of Figure 2, while the Instron® computer (running Merlin version 5 Instron® control software), pictured left in Figure 16, instructed the Instron® to apply the desired load profile every 200 milliseconds while it collected (to a raw ASCII text file) the measured force, displacement, and time data.

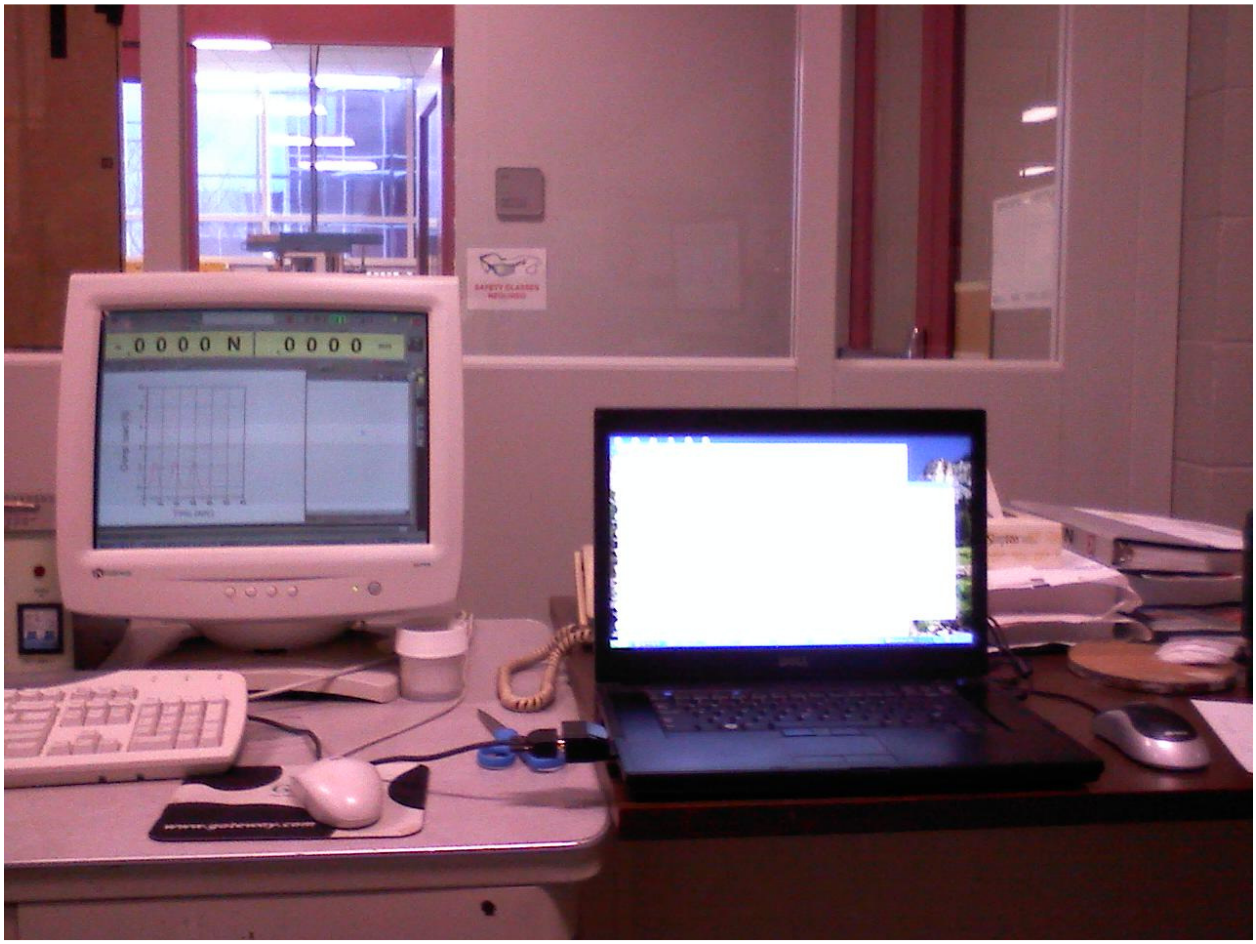

Figure 16. Instron® and voltage collection computers

Voltage for each sample was recorded while two different force profiles were sequentially applied to the sample, a constantly increasing load and a cyclic load. The applied force was increased at a rate of 30 mm/min up to a load of 2.5 N. The cyclic load profile used the same rate of increase up to the same 2.5 N load with a 2 second hold at 2.5 N. The force was removed at a rate of 30 mm/min and held at 0 N for 2 seconds and then repeated for a total of 3 cycles. At the end of each load profile, the machine returned to its starting position. The leads going to the multimeter were then reversed with the positive lead going to the negative terminal and negative lead to the positive terminal and both load profiles were then repeated. The reversal in polarity was done to compare the data with the findings of Shahinpoor et. al. [9], in which IPMC's to be evaluated as sensors were tested face up and face down in order to demonstrate how one side could be more sensitive than the other.

After testing was done in each liquid, the beaker and probe were cleaned with an Alconox® powdered detergent, rinsed 6 times with tap water and allowed to dry. The test rig was also cleaned, but only rinsed to the point where there was no more soap on the surface. The faces of the top electrodes and base of the rig, which are the faces that contact the two top and bottom faces of the IPMC, were then re-polished to ensure proper surface finish and electrical contact to the sample. The polishing was done with 800 and 1200 grit silicon carbide wet paper and a finish polish on Metcloth with .3 μm α-Al_2O_3. The rig was then solvent cleaned with acetone and re-washed according the procedure used on the beaker and probe.

The LiCl was the first liquid to be evaluated and the constantly increasing force profile was run first. Initially, the voltage response of the material was not as expected, meaning that there was no discernible voltage change when the load was applied. Since Punning et. al. [17] theorized and later concluded that the sensing output of an IPMC has a correlation to bending

radius, this stood to reason that the radius of the probe may be too small. A piece of 1/2 inch Teflon tubing was cut so that its length was just slightly greater than the width of the probe. A razor blade was used to slice it open along its length and the tube was then opened along this cut and the probe was inserted into the opening increasing the probes radius to 8 mm as opposed to 3 mm. The constant increasing force profile was then re-run and the ensuing voltage response of the IPMC was as expected. This change in response due to increase in bending radius further validates Punning's findings. It should be noted, however, that the inability to detect a change in voltage of the material before the radius of the probe was increased, does not mean that there was no response. The response merely showed that the equipment employed for detecting the response may have not been sensitive enough or that some sort of amplification may be necessary to detect voltage outputs with a smaller bending radius. Tests were then performed in $NiCl_2$, $NiSO_4$, and DI Water.

Results

The purpose of the research was to evaluate the feasibility of using IPMCs as tactile sensors. Feasibility was assessed by evaluating the voltage response resulting from an applied load for four different samples in four different electrolytes: 1M LiCl, 1M $NiCl_2$, 1M $NiSO_4$, and DI Water. The 1M LiCl was evaluated since it is the most common electrolyte used in the literature for actuation of IPMCs and 1M $NiCl_2$ was evaluated as an alternative to the LiCl. The 1M $NiSO_4$ was chosen to investigate the feasibility of a sulfate form of metal salt in hopes that it might be less corrosive to the electrodes of the IPMC due to the aggressive nature of the Cl^- ion. Use of a non-chloride metal salt would possibly enable non-noble metal electrodes to be used on IPMCs, in turn bringing down their cost. The DI Water was investigated to determine its feasibility for its cost effectiveness and has limited safe use instructions.

Each sample was tested four times per polarity and exposed to two different load profiles, which will be referred to as constant and cyclic, using an Instron® (Model #4206). For the constant load profile the probe displaced the center of the clamped IPMC vertically downward at a rate of 30 mm/min up to a maximum load 2.5 N. Ideally, this would have been applied at a rate of force per unit time e.g. 0.xx N/min, but was not within the capabilities of this particular Instron®. For the cyclic load profile, the probe displaced the center of the IPMC at a rate of 30 mm/min up to a load of 2.5 N and held there for 2 seconds. The load was then removed at a rate of 30 mm/min and held at 0 N for 2 seconds. This cyclic load profile was repeated 3 times for a total of 3 cycles. The purpose of applying a constantly increasing load was to quantify the trend of increasing voltage output with increased force to evaluate IPMCs as true "tactile" sensors. The cyclic load was evaluated as a contingency, to determine IPMCs feasibility as more of a binary touch sensor, as opposed to a true tactile sensor; by evaluating their ability to sense surface contact for small loads.

The multimeter used to record the voltage output of the material had an accuracy of ± .006 mV roughly translating to 6% error associated with the voltage measuring system and applies to all measurements taken. Other sources of experimental error could include slippage of the IPMC in the rig during operation or overstraining of the IPMC if a load beyond the elastic region were applied. Another source of error that is difficult to mitigate is the starting position of the probe. If the probe is not in contact with the IPMC prior to loading of if the IPMC starts with a degree of "pre-load" then the voltage outputs could become slightly skewed.

Figure 17 shows the typical constantly increasing load profile applied by the Instron® and Figure 18 shows the typical displacement of the center of the membrane from its flat equilibrium state.

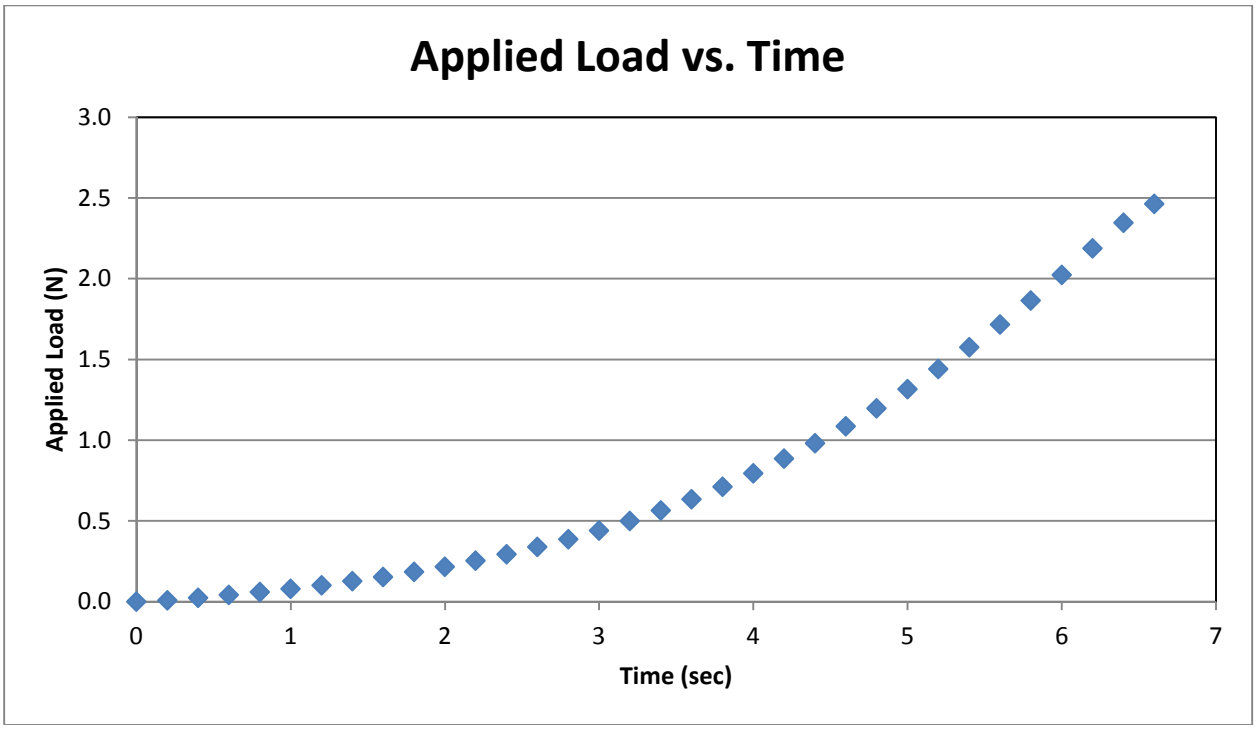

Figure 17. Typical applied load for constant applied load profile

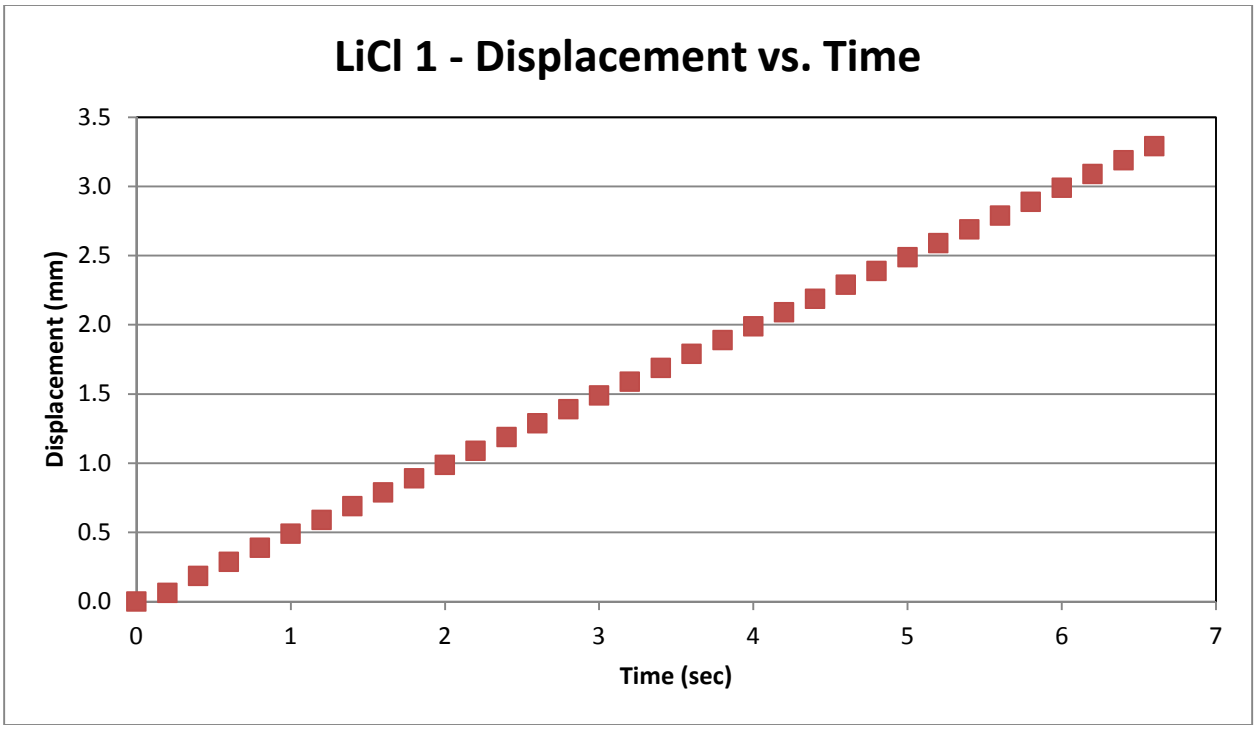

Figure 18. Typical displacement for constant load profile

For every sample and load profile, the material was evaluated with normal and reversed polarity.

For normal polarity, the base of the test rig, where the bottom face of the IPMC was in contact,

was attached to the negative terminal of the multimeter and the top electrodes of the test rig, in which the top face of the IPMC was in contact with, was attached to the positive terminal of the multimeter, pictured in Figure 19.

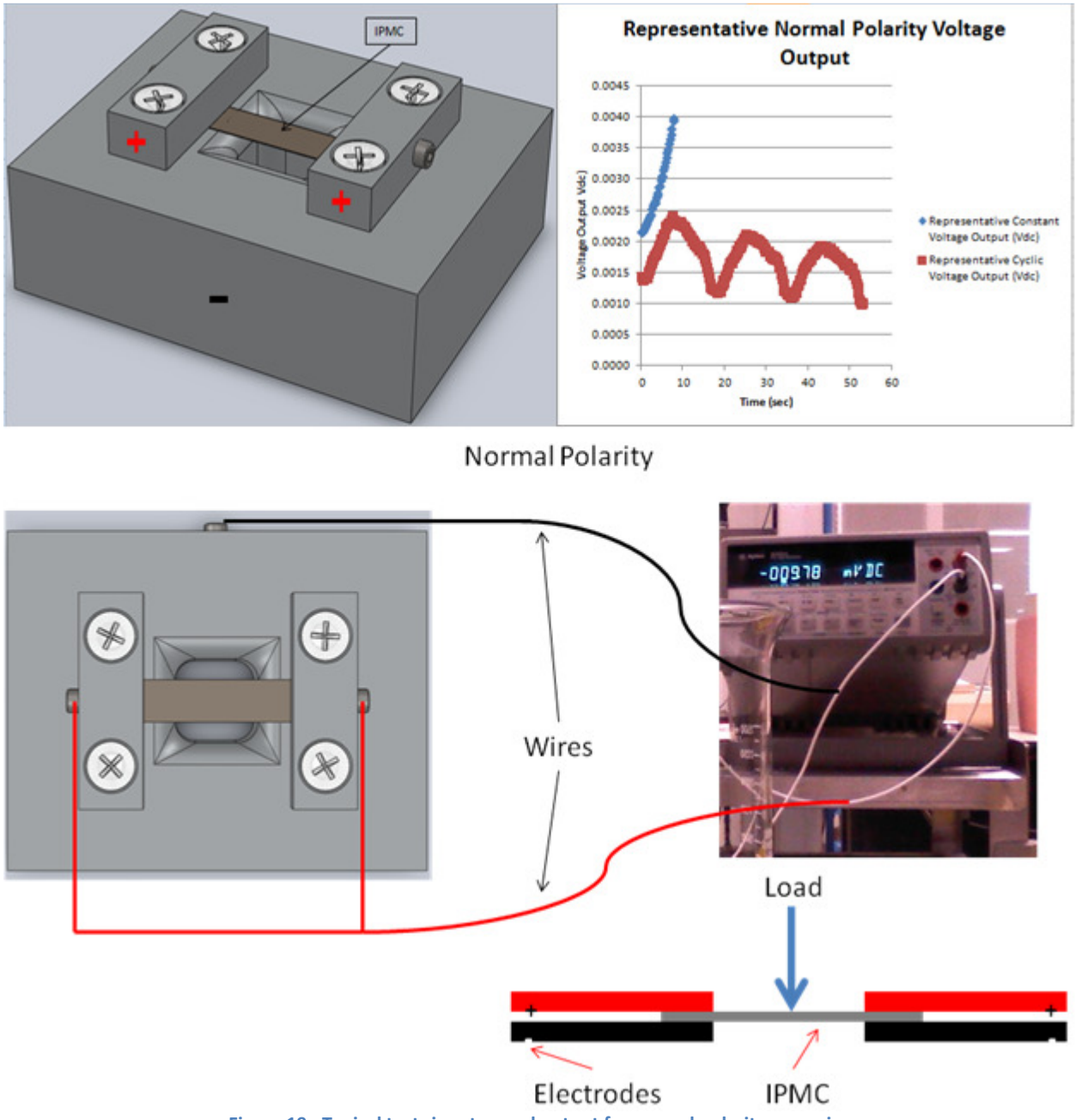

Figure 19. Typical test rig setup and output for normal polarity scenario

Reversed polarity means that the leads were then reversed with the base of the test rig plugged into the positive terminal and the top electrodes plugged into the negative terminal.

LiCl Constant Results

Figures 20-23 show a summary of the 1M LiCl constant data for both the "normal" and reversed polarity test cases (4 test runs per polarity). Figure 20 shows the applied load and raw voltage output vs. time for normal and reversed polarity where Figure 21 shows the displacement and raw voltage output vs. time for normal and reversed polarities. Figures 22 & 23 show the same applied load and displacements with voltage change vs. time. The 1M LiCl sample resulted in a maximum voltage change of +.189 mV and -.247 mV for reversed and normal polarity, respectively, seen in Figures 22 & 23.

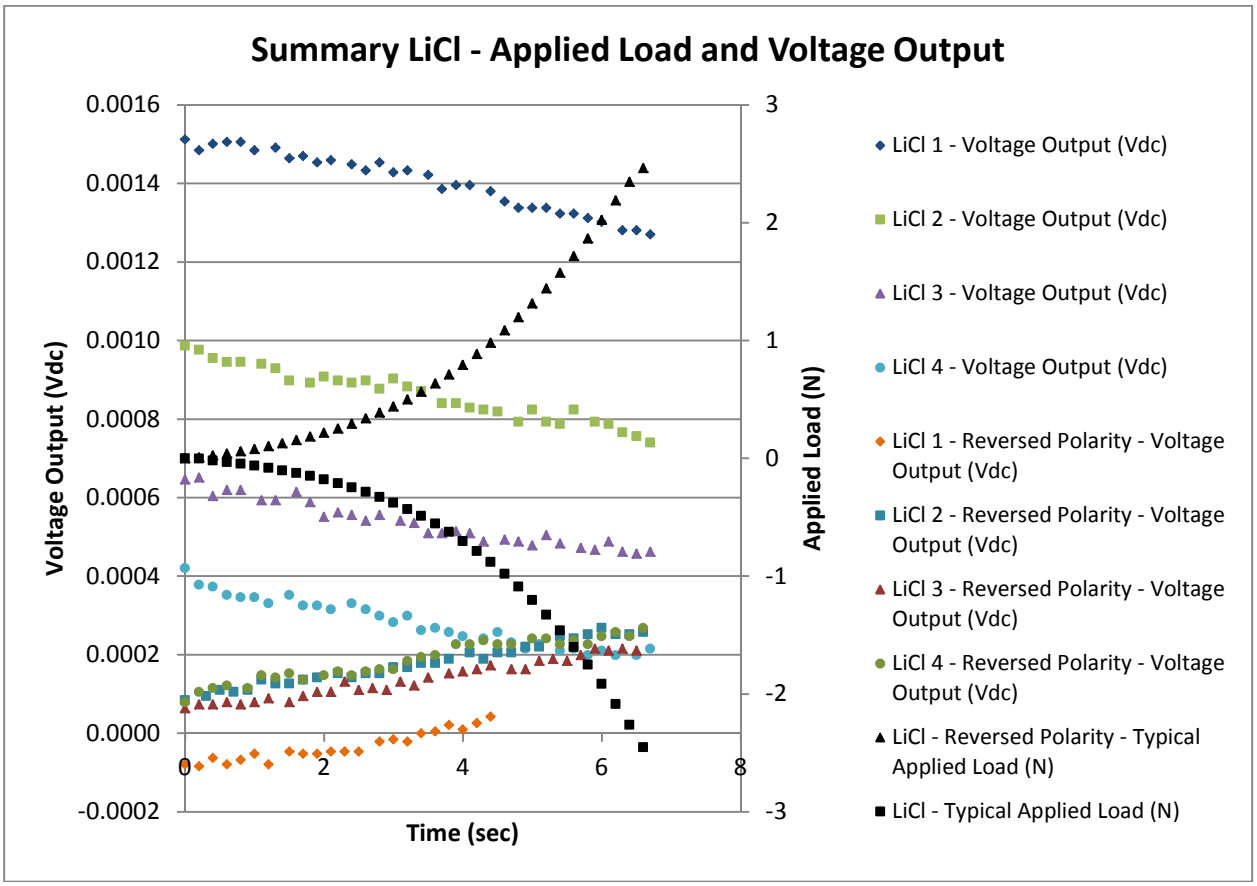

Figure 20. Summary of normal and reversed polarity LiCl electrolyte constant load scenario, load and voltage output, all plots verse time, note decreased variation as test number increased

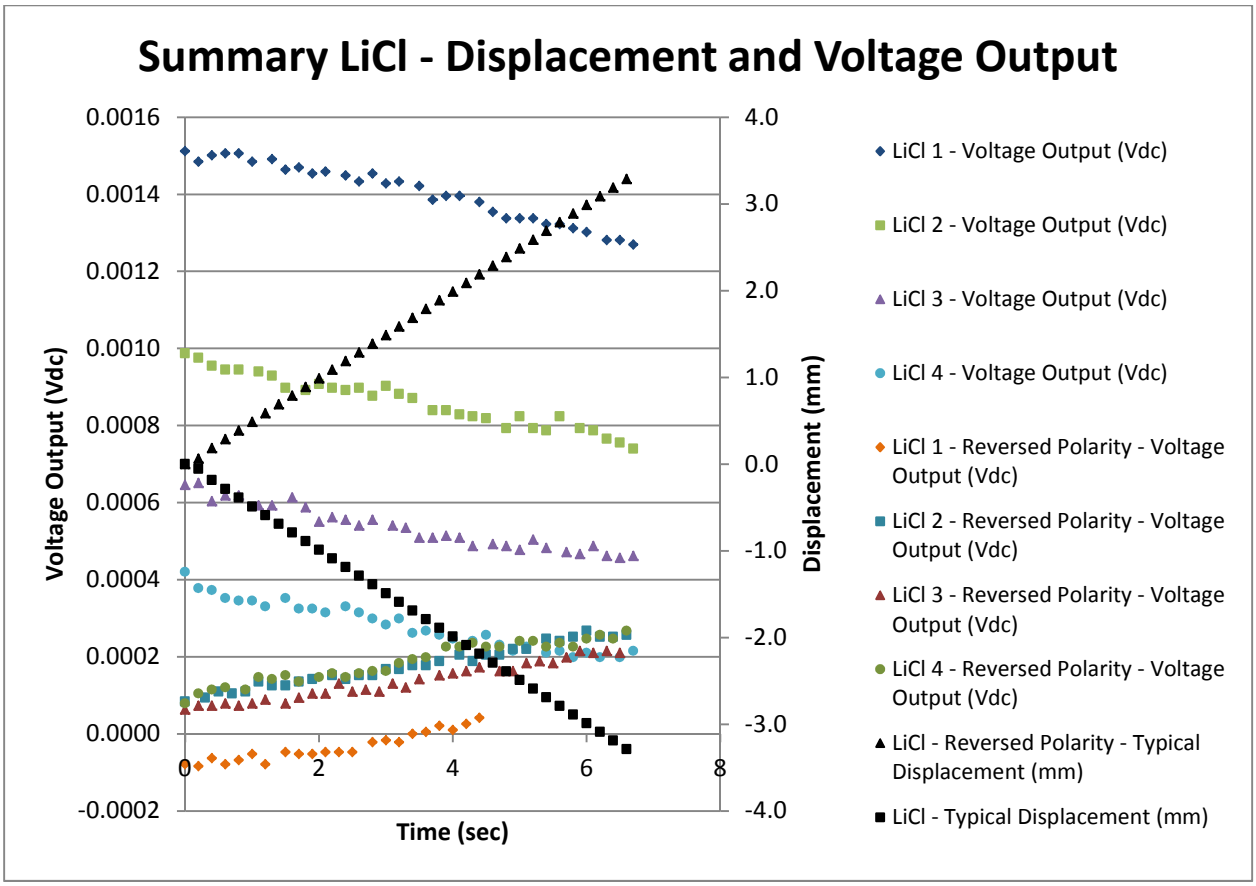

Figure 21. Summary of normal and reversed polarity LiCl electrolyte constant load scenario, displacement and voltage output

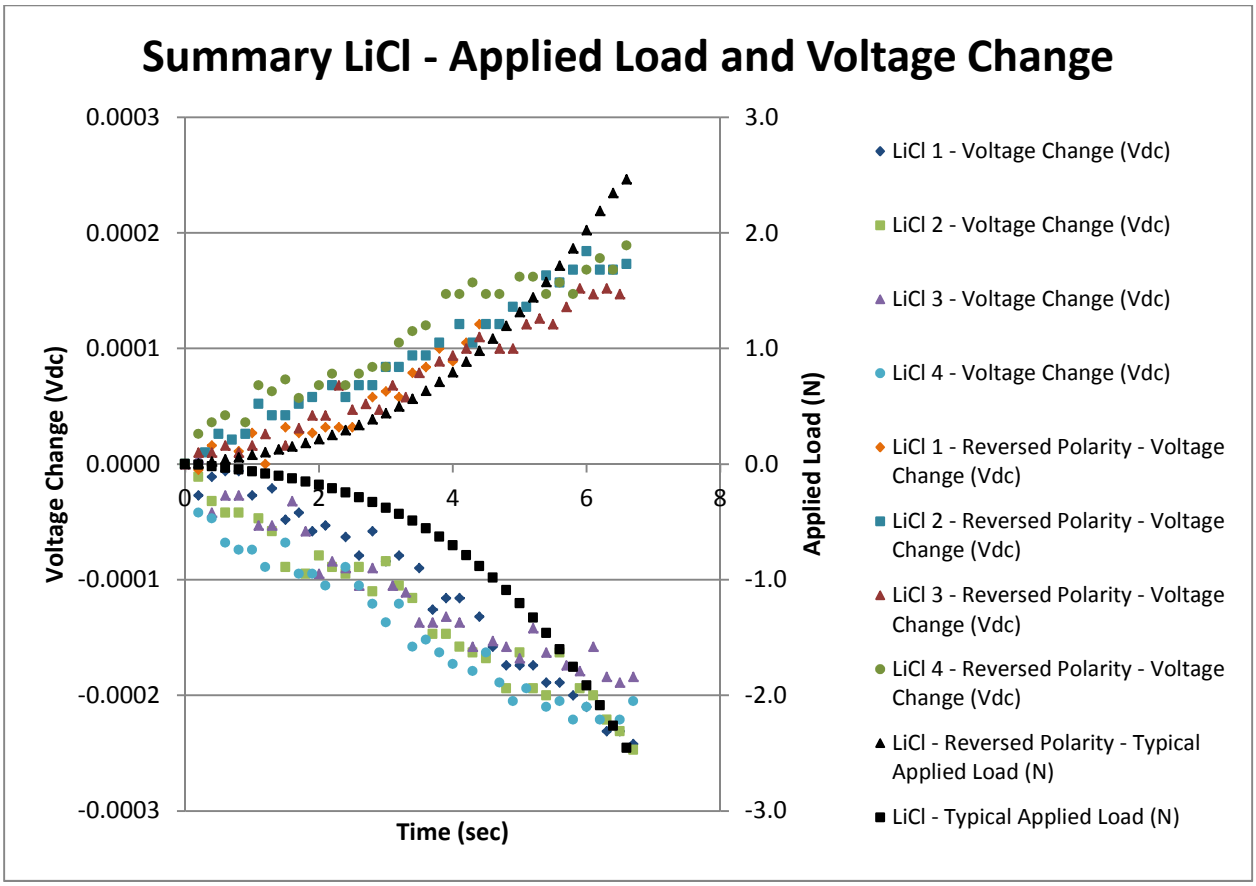

Figure 22. Summary of normal and reversed polarity LiCl electrolyte constant load scenario, load and voltage change, note negative voltage change for normal polarity

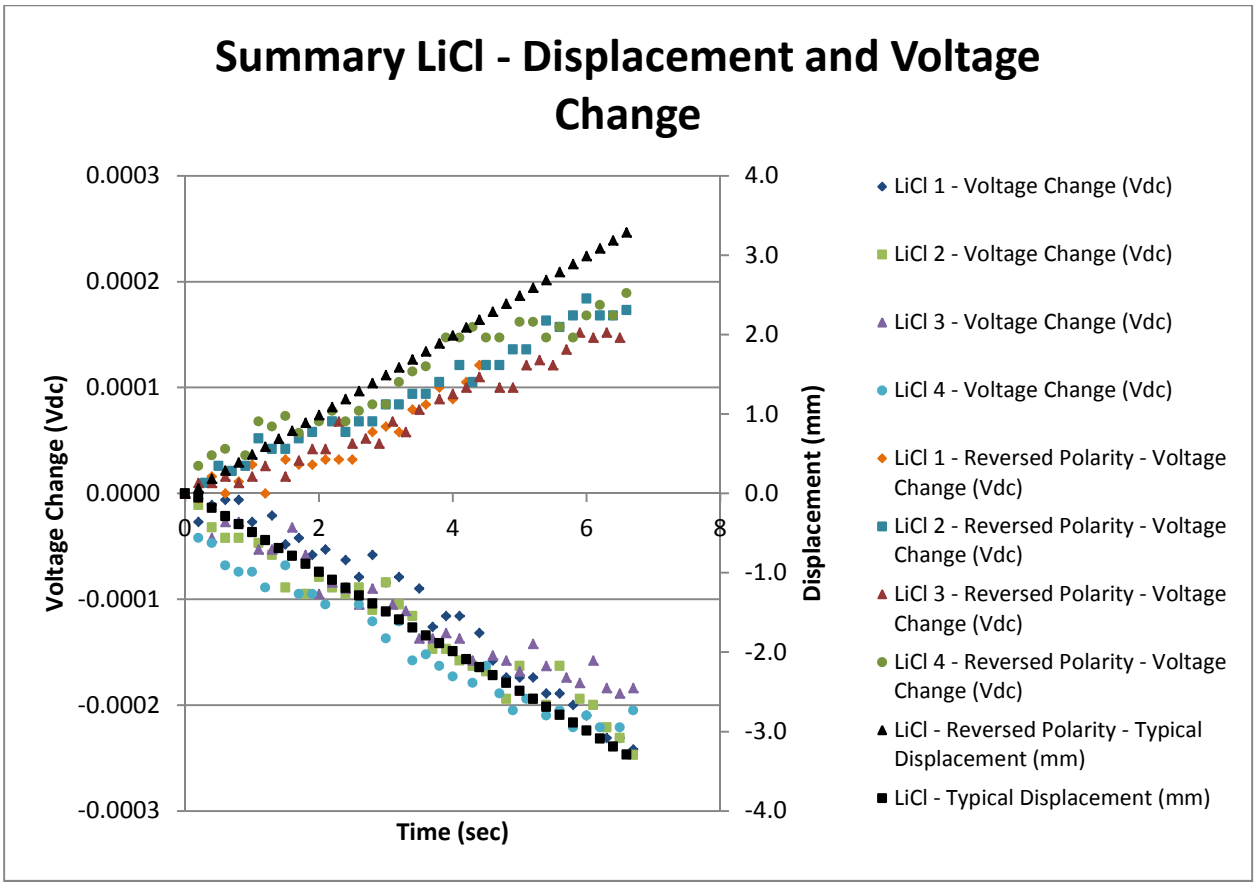

Figure 23. Summary of normal and reversed polarity LiCl electrolyte constant load scenario, displacement and voltage change

Even though the voltage changes are fairly small compared to the other liquids tested, the data is tightly grouped for test runs 1-4 and 5-8, displaying the repeatability of the study. The voltage change was determined by subtracting the starting voltage from every subsequent voltage, since the voltage did not start at zero. A closer look at the individual data sets for each run can be seen in Figures 68-99 in Appendix B, where LiCl 1 – 4 refers to the test run number for LiCl for both polarities. It is evident from Figures 68-99 Appendix B, that the raw voltage output for the individual runs decreases as the run number increases which is clearly seen in the summary of the raw voltage output in Figures 20 & 21. Interestingly, even though the raw voltage output seems to drift, the voltage change due to mechanical deformation does not which is summarized in Figures 22 & 23. The drifting raw voltage output is not surprising due to the hysteretic nature

of IPMCs. For some unknown reason, the Instron® only applied a maximum load of ~.9 N for the first test run of LiCl for the reversed polarity test case (LiCl 1 - Reversed Polarity) pictured in Figures 84-87 Appendix B.

$NiCl_2$ Constant Results

Figures 24-27 show a summary of the 1M $NiCl_2$ constant data for both the "normal" and reversed polarity test cases (4 test runs per polarity). Figure 24 shows the applied load and raw voltage output vs. time for normal and reversed polarity where Figure 25 shows the displacement and raw voltage output vs. time for normal and reversed polarities. Figures 26 & 27 show the same applied load and displacements with voltage change vs. time. Though the distribution is not as tightly grouped, the voltage output is higher than that of the LiCl with a maximum voltage change of 2.341 mV and -2.693 mV for normal and reversed polarity respectively. Figures 100-131 Appendix C, contain the individual data sets for $NiCl_2$.

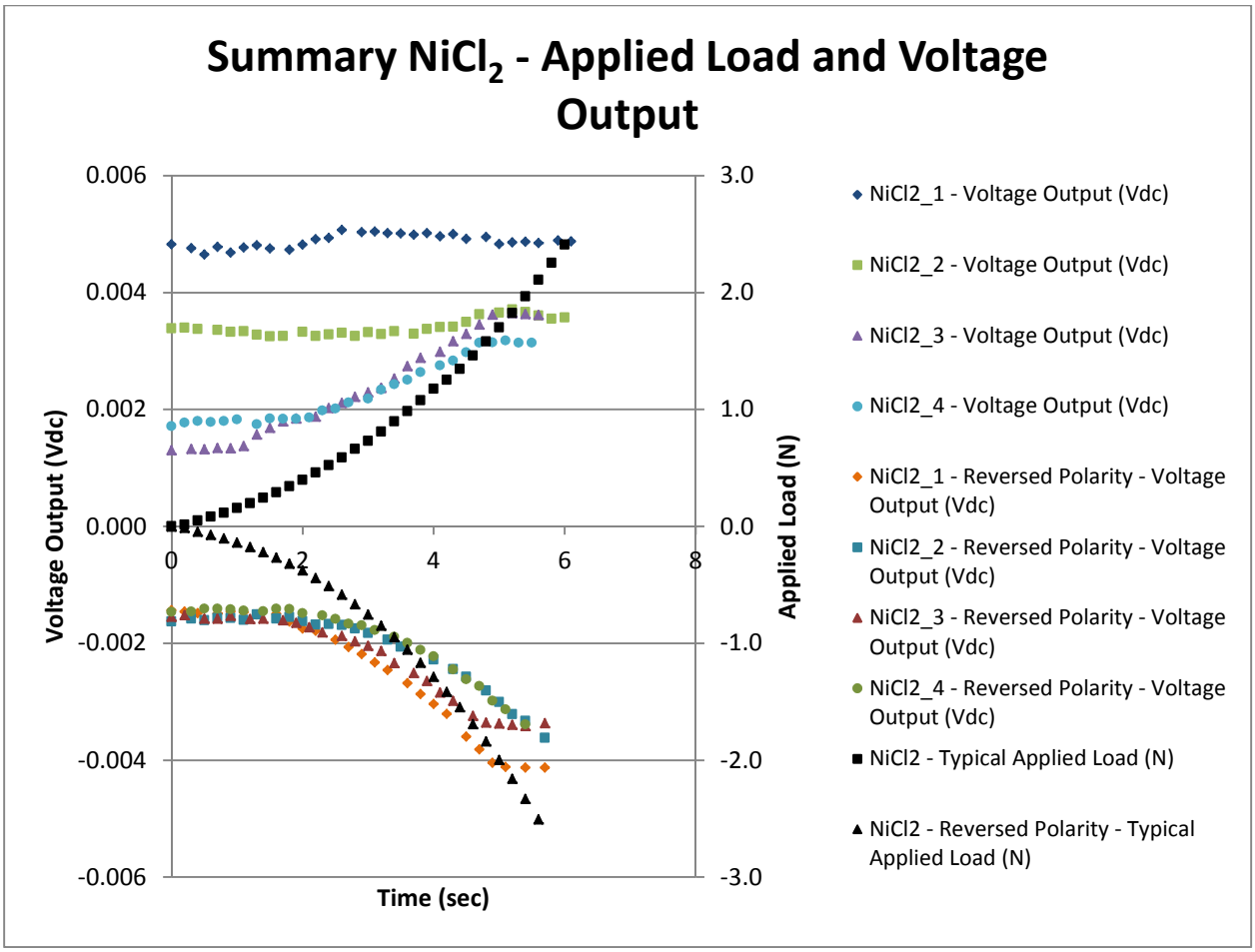

Figure 24. Summary of normal and reversed polarity $NiCl_2$ electrolyte constant load scenario, load and voltage output, note decreased variation in voltage output as test number increased

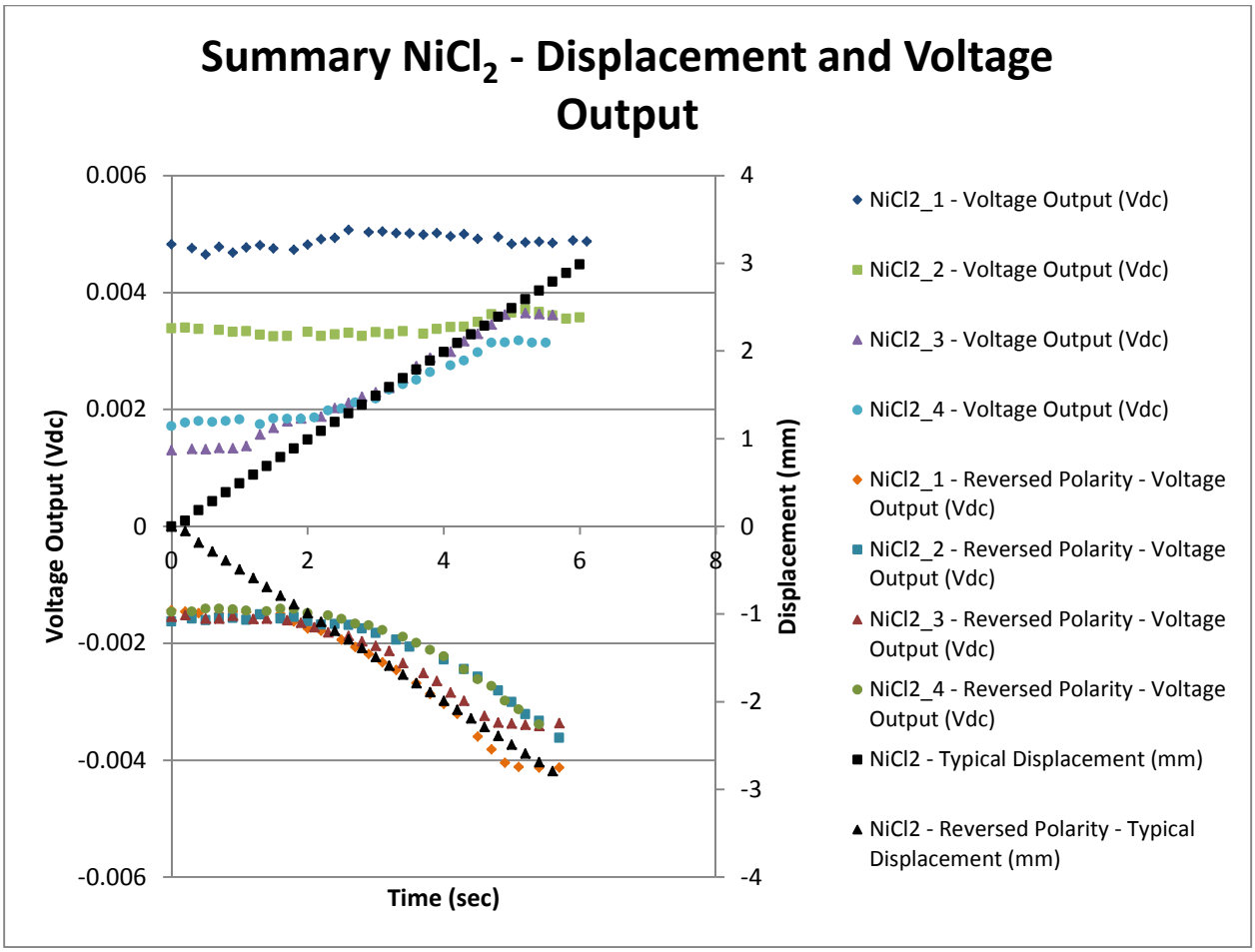

Figure 25. Summary of normal and reversed polarity $NiCl_2$ electrolyte constant load scenario, displacement and voltage output

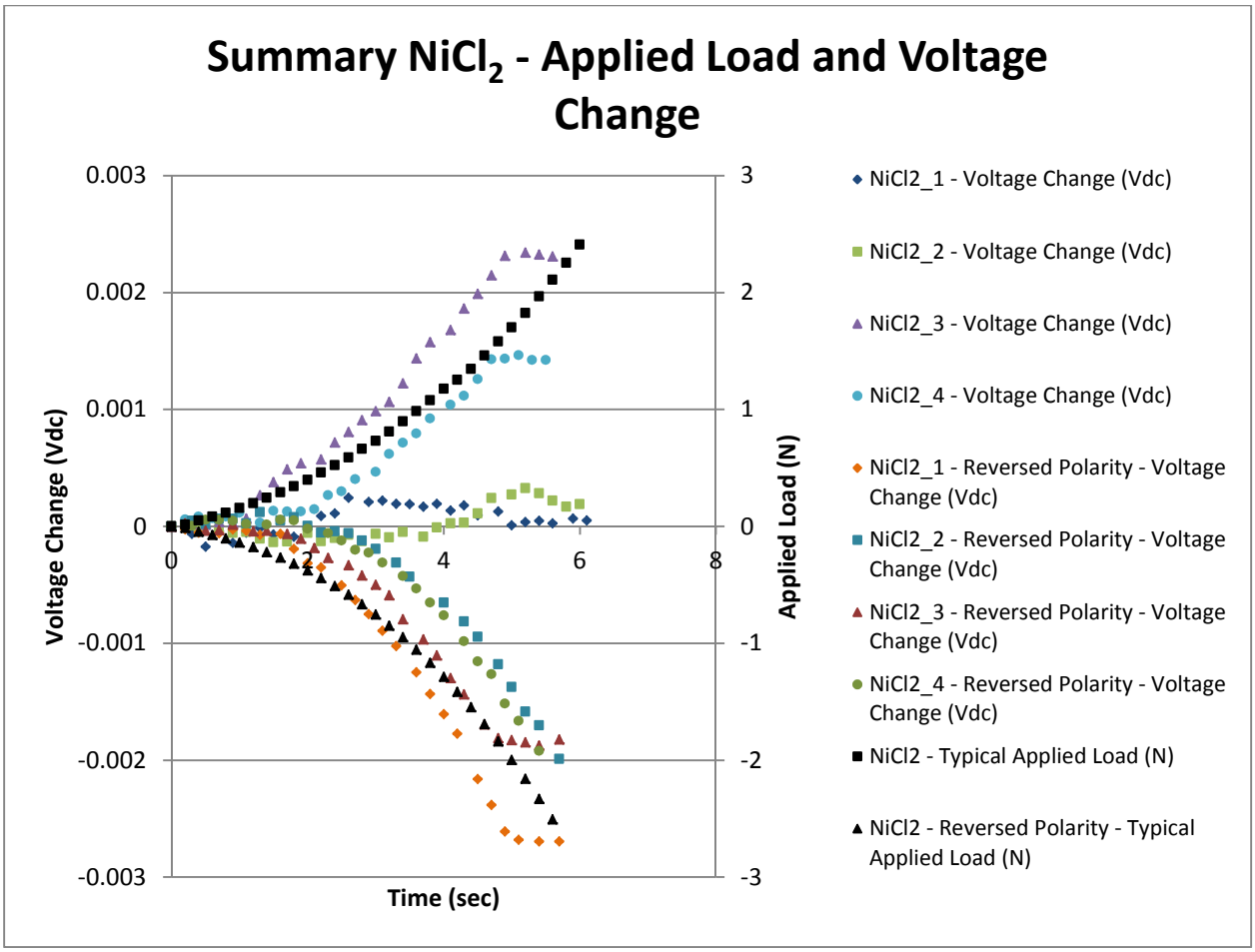

Figure 26. Summary of normal and reversed polarity $NiCl_2$ electrolyte constant load scenario, load and voltage change

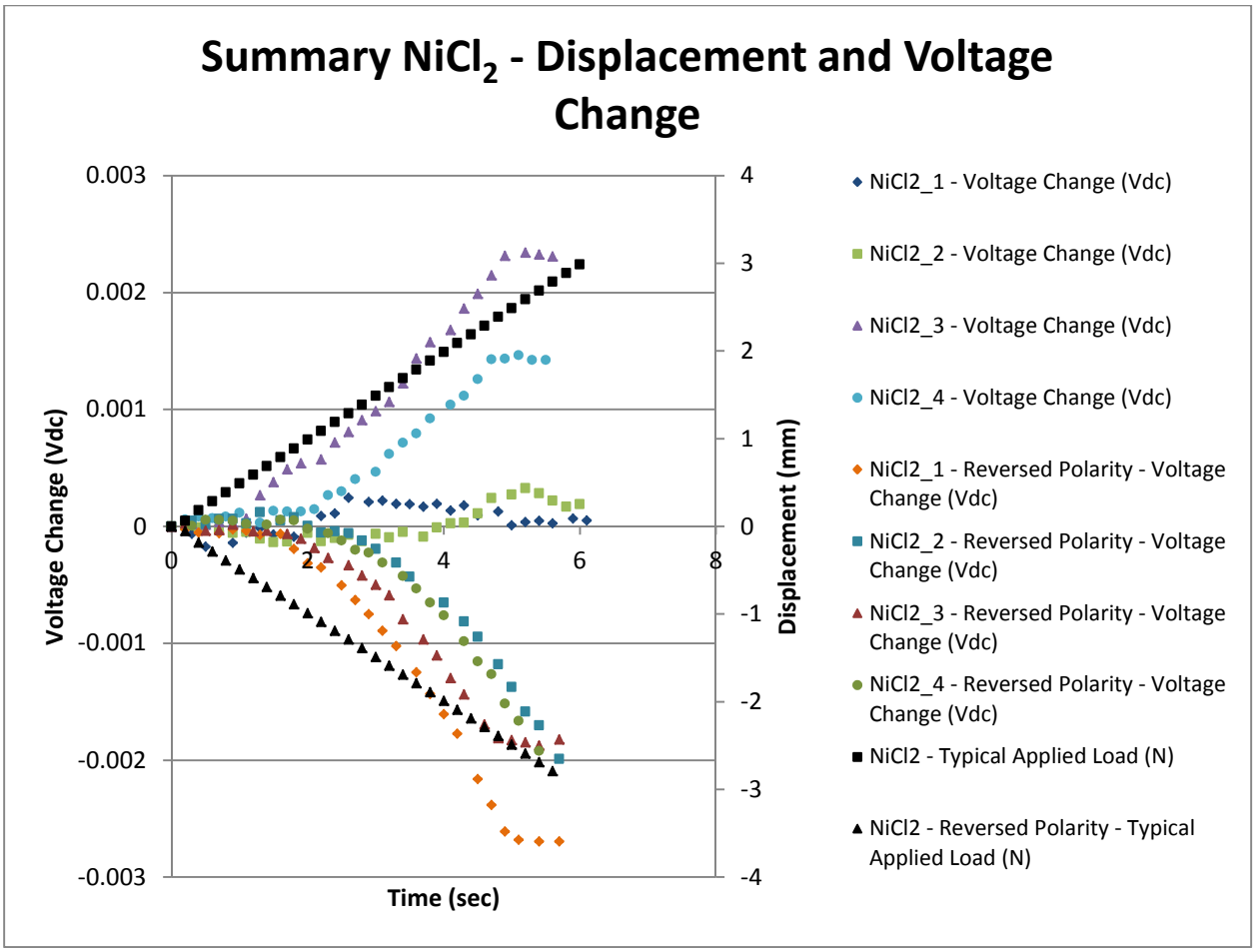

Figure 27. Summary of normal and reversed polarity $NiCl_2$ electrolyte constant load scenario, displacement and voltage change

Figures 108-131 in Appendix C show a slightly delayed response in the voltage output evident by the zero slope regions with a linear region in between. This is likely attributed to the ionic nature of the material since the voltage output is due to the diffusion of ions and diffusion is a time dependant phenomenon which would result in a delay of the voltage output.

$NiSO_4$ Constant Results

The $NiSO_4$ yielded results between the LiCl and the $NiCl_2$, with a slightly higher voltage output than the LiCl, but a tighter grouping of the voltage output than the $NiCl_2$. Figures 28-31 show the summary of the results for the 8 runs with $NiSO_4$.

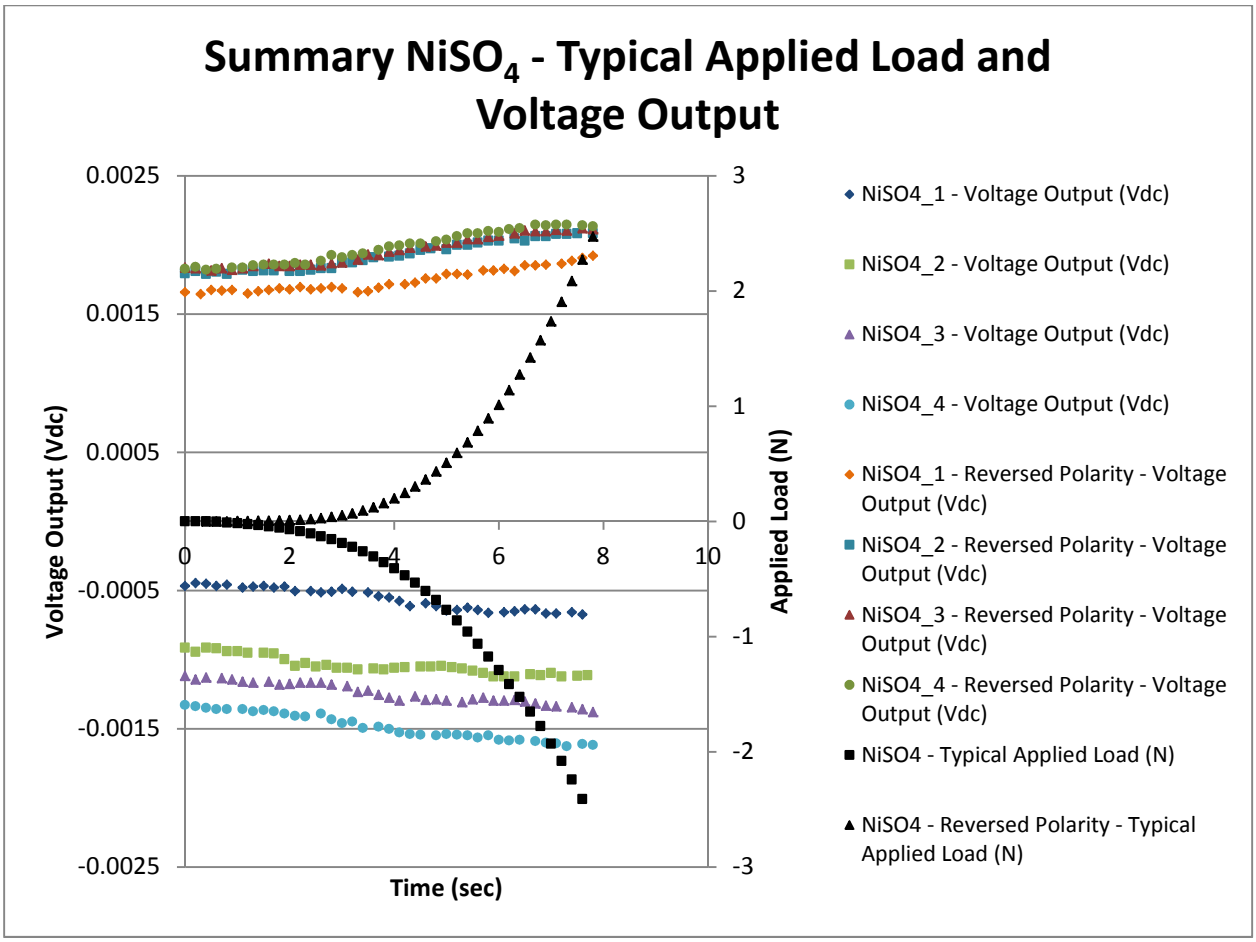

Figure 28. Summary of normal and reversed polarity $NiSO_4$ electrolyte constant load scenario, load and voltage output, note decrease in voltage data variation as test number increased

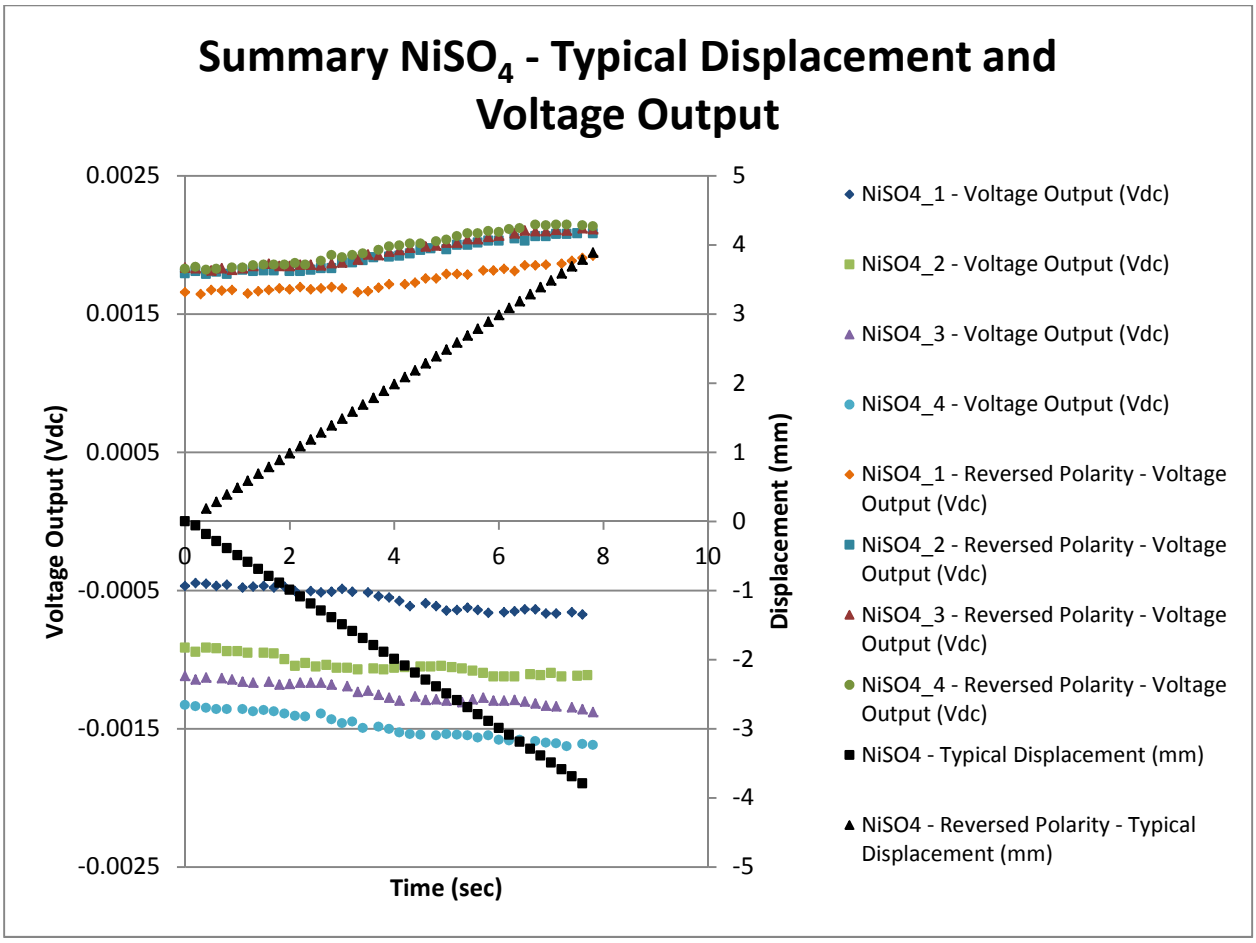

Figure 29. Summary of normal and reversed polarity $NiSO_4$ electrolyte constant load scenario, displacement and voltage output

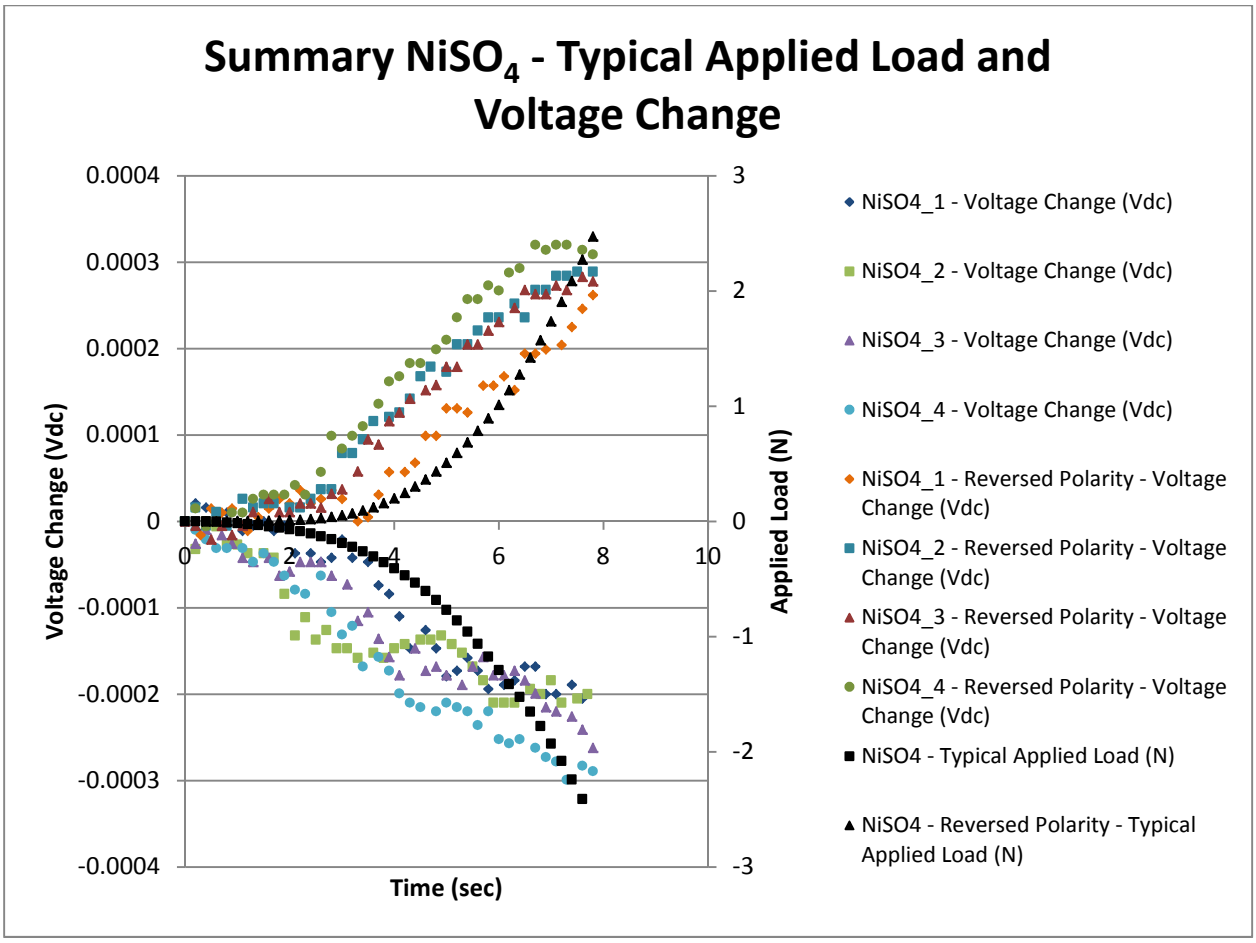

Figure 30. Summary of normal and reversed polarity $NiSO_4$ electrolyte constant load scenario, load and voltage change

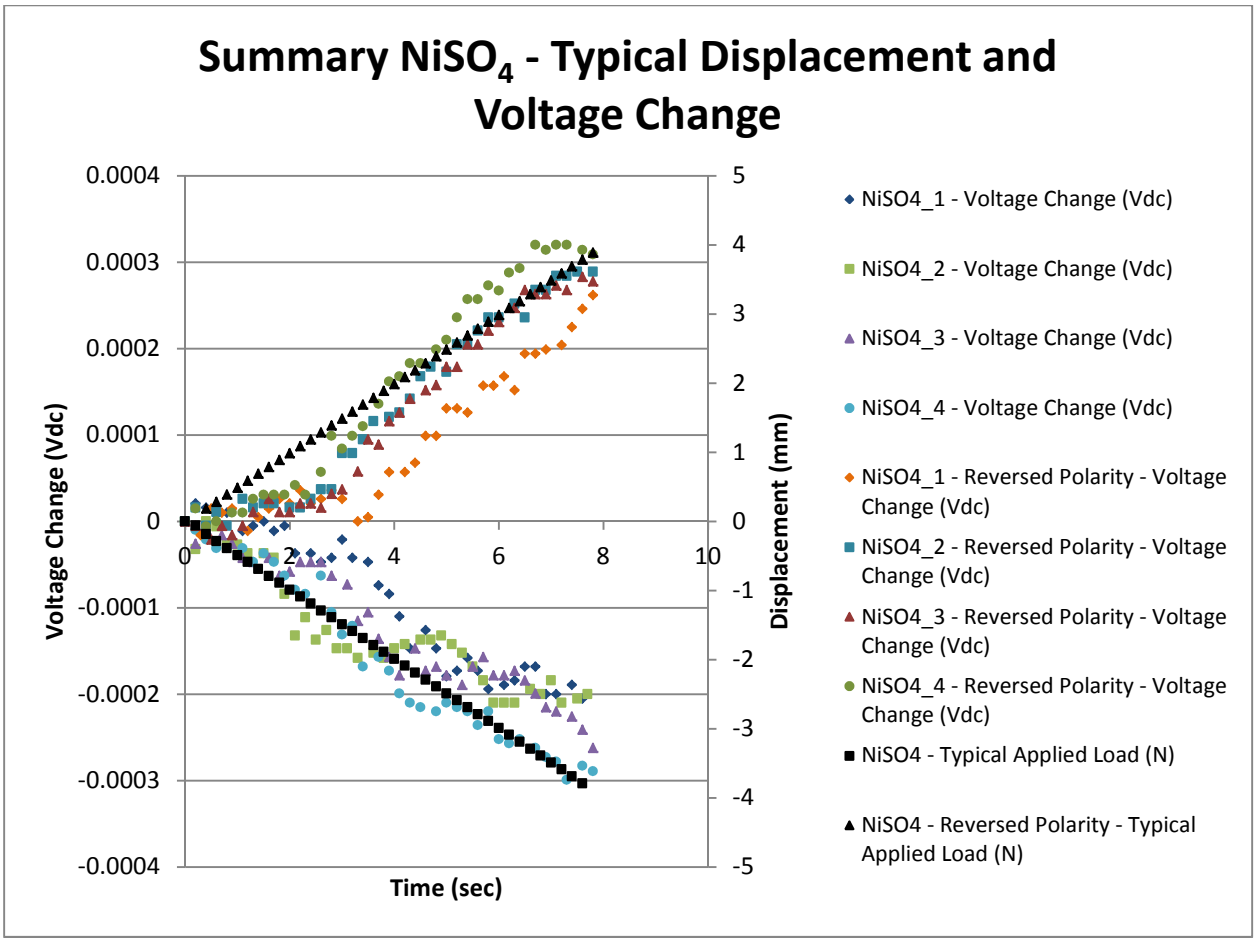

Figure 31. Summary of normal and reversed polarity $NiSO_4$ electrolyte constant load scenario, displacement and voltage change

From Figures 30 & 31, it can be seen that there was a maximum voltage change of .320 mV and -.299 mV for reversed and normal polarity respectively. Again looking at the difference between voltage change (Figures 30 and 31) and the raw voltage output (Figures 29 and 30) it is interesting that the raw voltage output may drift from test run to test run but the voltage change stays fairly constant. The individual data sets can be found in Figures 132-163 in Appendix D, reveals that the voltage response of the $NiSO_4$ follows more of the shape associated with a higher order polynomial.

DI Water Constant Results

The final liquid that was evaluated was DI water, for its availability and limited safe use instructions. Figures 32-35 show the summary of the DI water trials for a constantly increasing load up to 2.5 N.

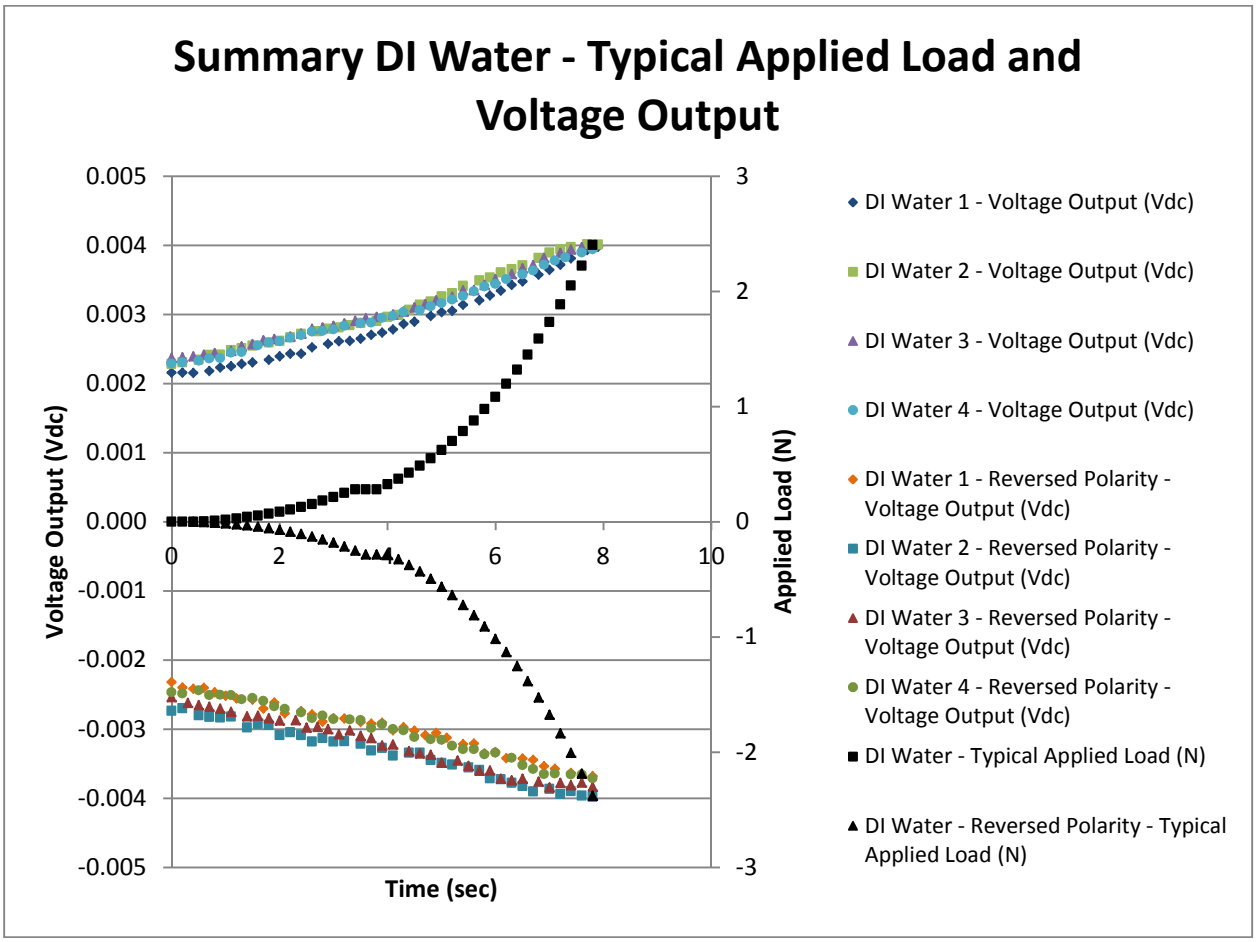

Figure 32. Summary of normal and reversed polarity DI water electrolyte constant load scenario, load and voltage output, note minimal variation of voltage data from test run to test run

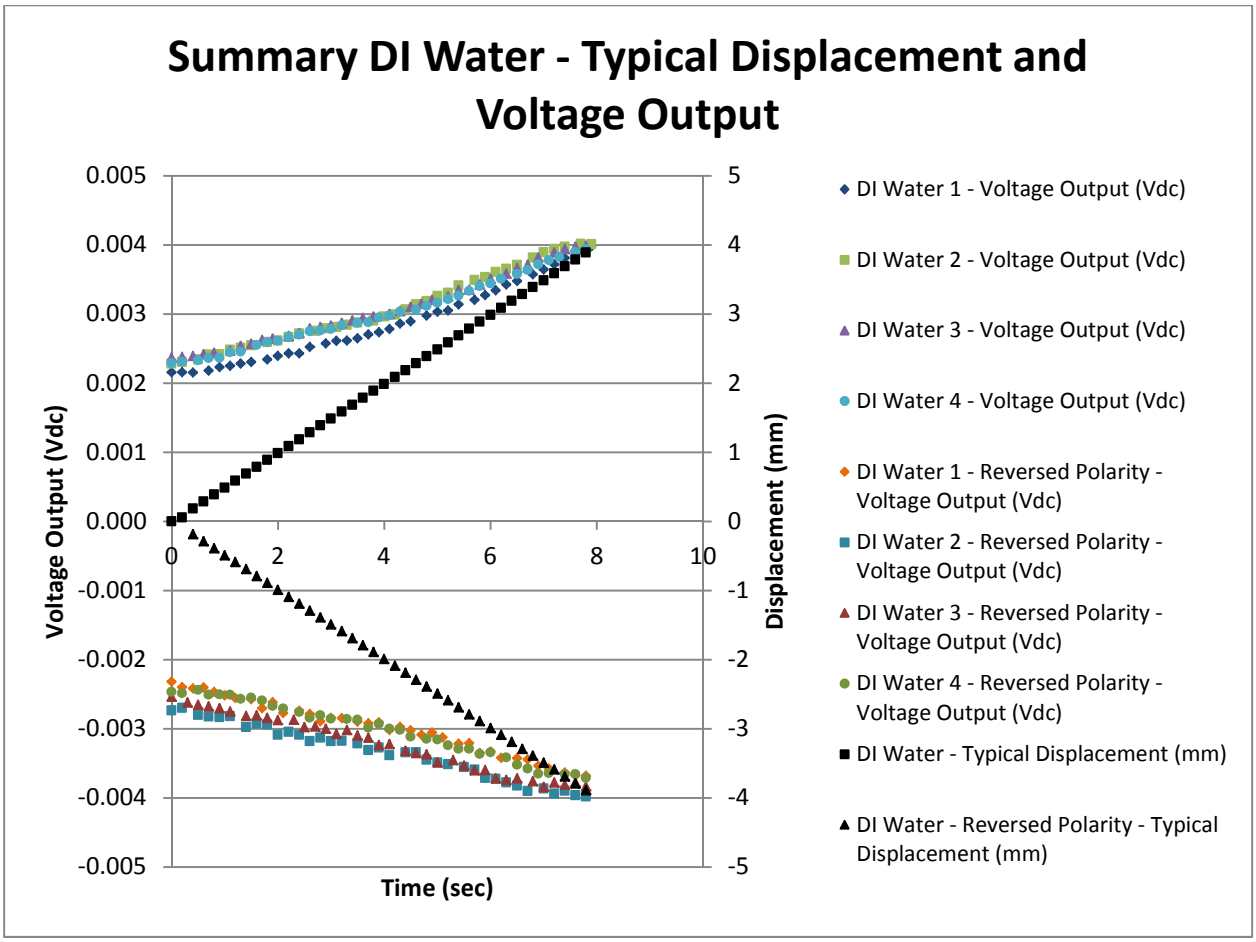

Figure 33. Summary of normal and reversed polarity DI water electrolyte constant load scenario, displacement and voltage output

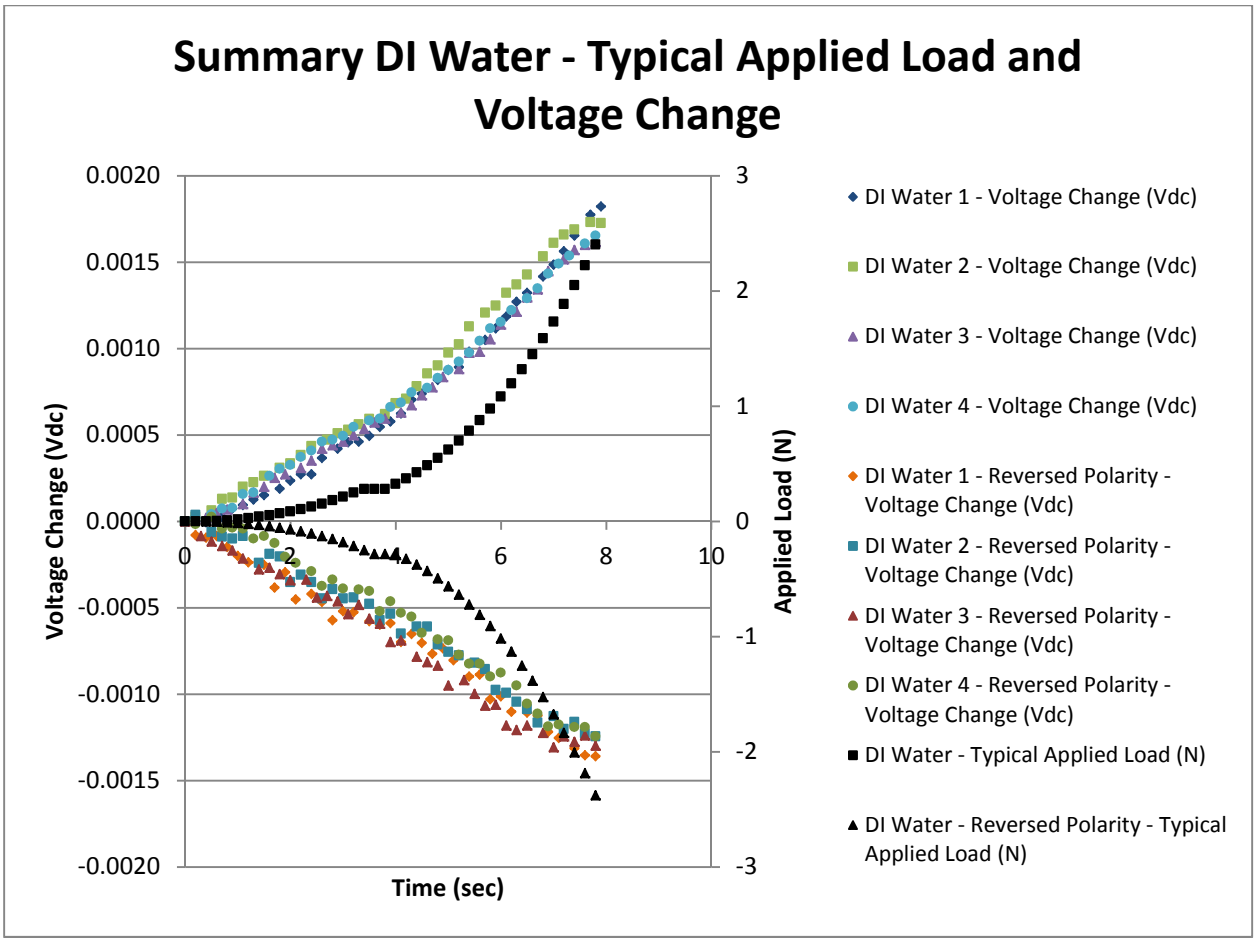

Figure 34. Summary of normal and reversed polarity DI water electrolyte constant load scenario, load and voltage change, note almost identical voltage change from test run to test run and almost complete reversibility

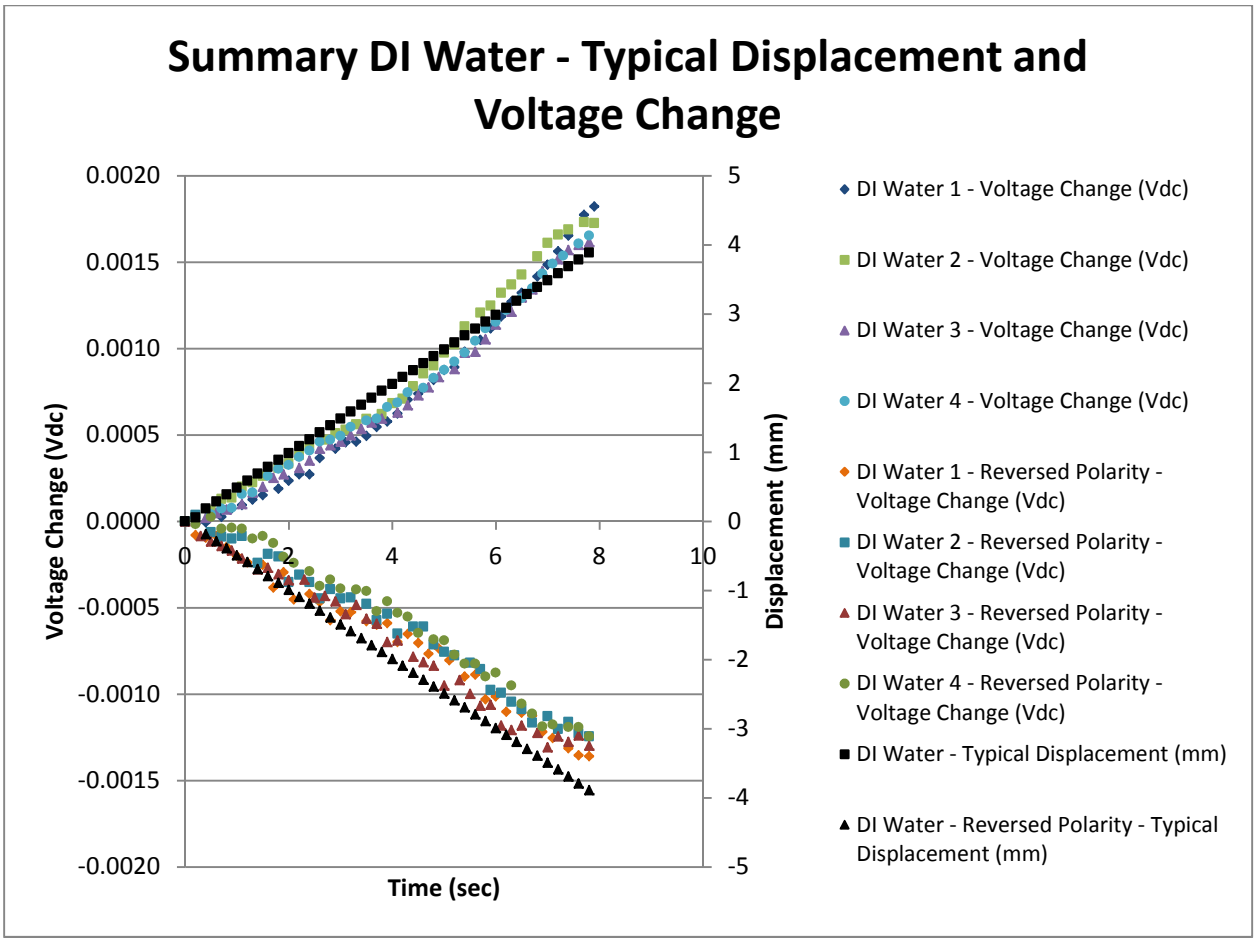

Figure 35. Summary of normal and reversed polarity DI water electrolyte constant load scenario, displacement and voltage change

Surprisingly the DI water had the best response out of the 4 liquids tested with a moderately large voltage change of 1.822mV and -1.359 mV for normal and reversed polarity, respectively. Only a very small distribution of raw voltage output and voltage changes were observed from test runs 1-4 and 5-8. Figures 164-195 Appendix E, show the individual experimental results for the DI water.

$NiCl_2$ Constant Compression Results

There was question as to whether force was an accurate metric for correlation to voltage output of IPMCs in a 3 point bend scenario since force was applied by displacing the center of the clamped membrane. In order to quantify the correlation of force to voltage response of IPMCs, an additional "control" experiment was performed where the membrane was compressed

across it's thickness. An electrolyte that showed a high sensitivity (large voltage change) was necessary in order to allow for the best chance of obtaining a measureable result under this loading scenario. $NiCl_2$ was chosen as the electrolyte since it exhibited a large voltage output and the sample was affixed in the test rig with an alignment pin in place to prevent the membrane from bending. The setup can be seen in Figure 36 without the probe and Figure 37 with the probe used to apply load.

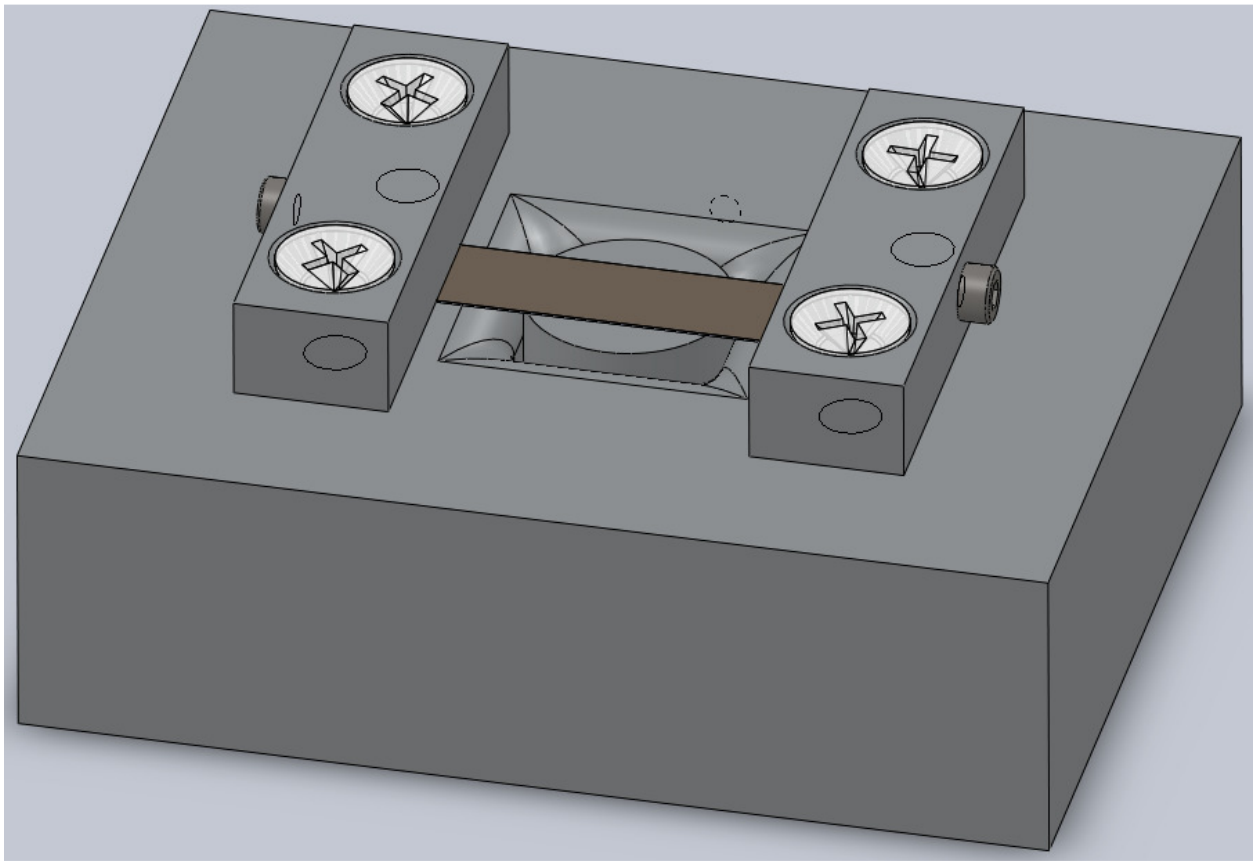

Figure 36. $NiCl_2$ Compress test setup base with alignment pin

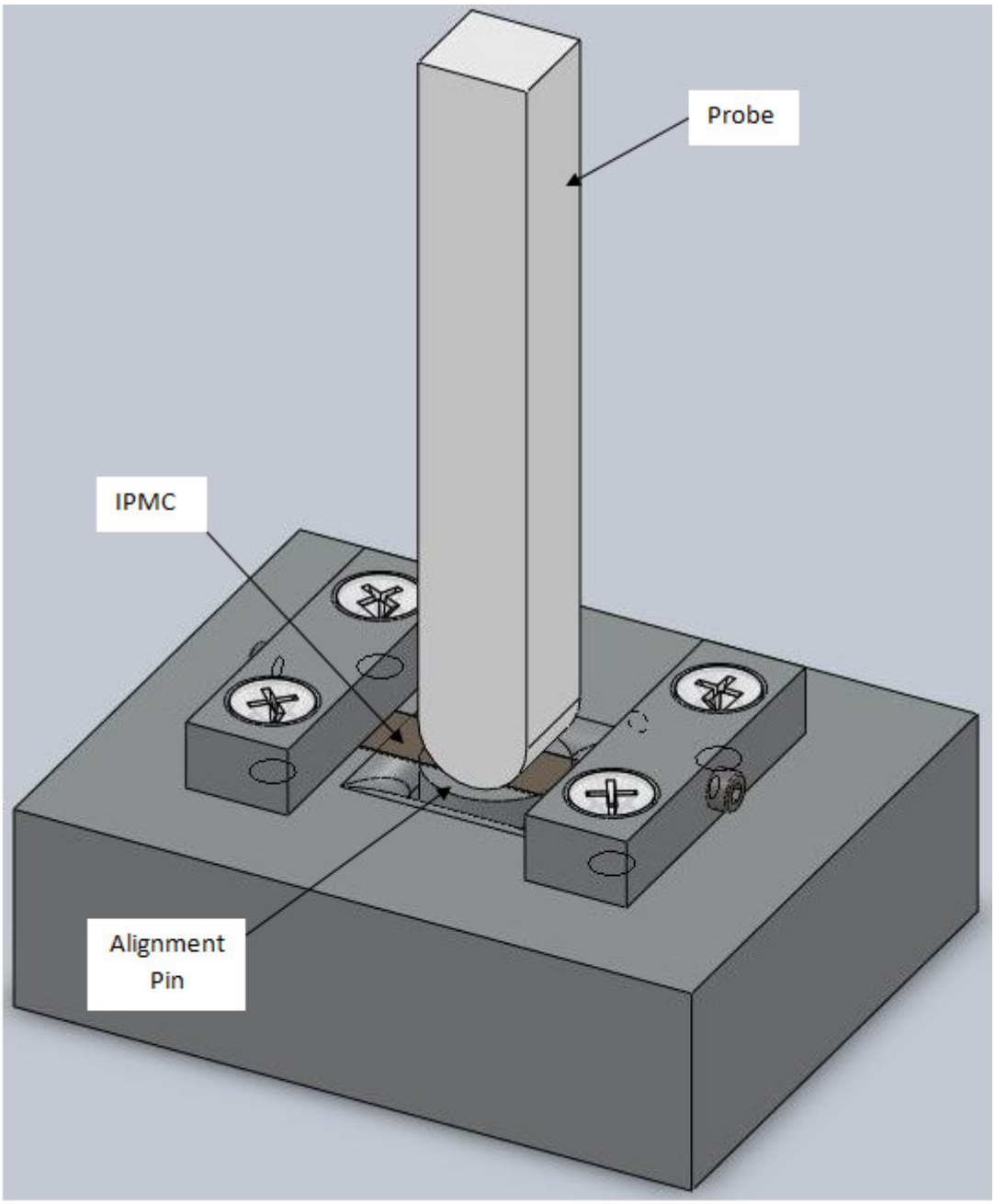

Figure 37. $NiCl_2$ Compress test setup

The same constant and cyclic profiles were then run performed with the summary of the constant data displayed below in Figures 38-41.

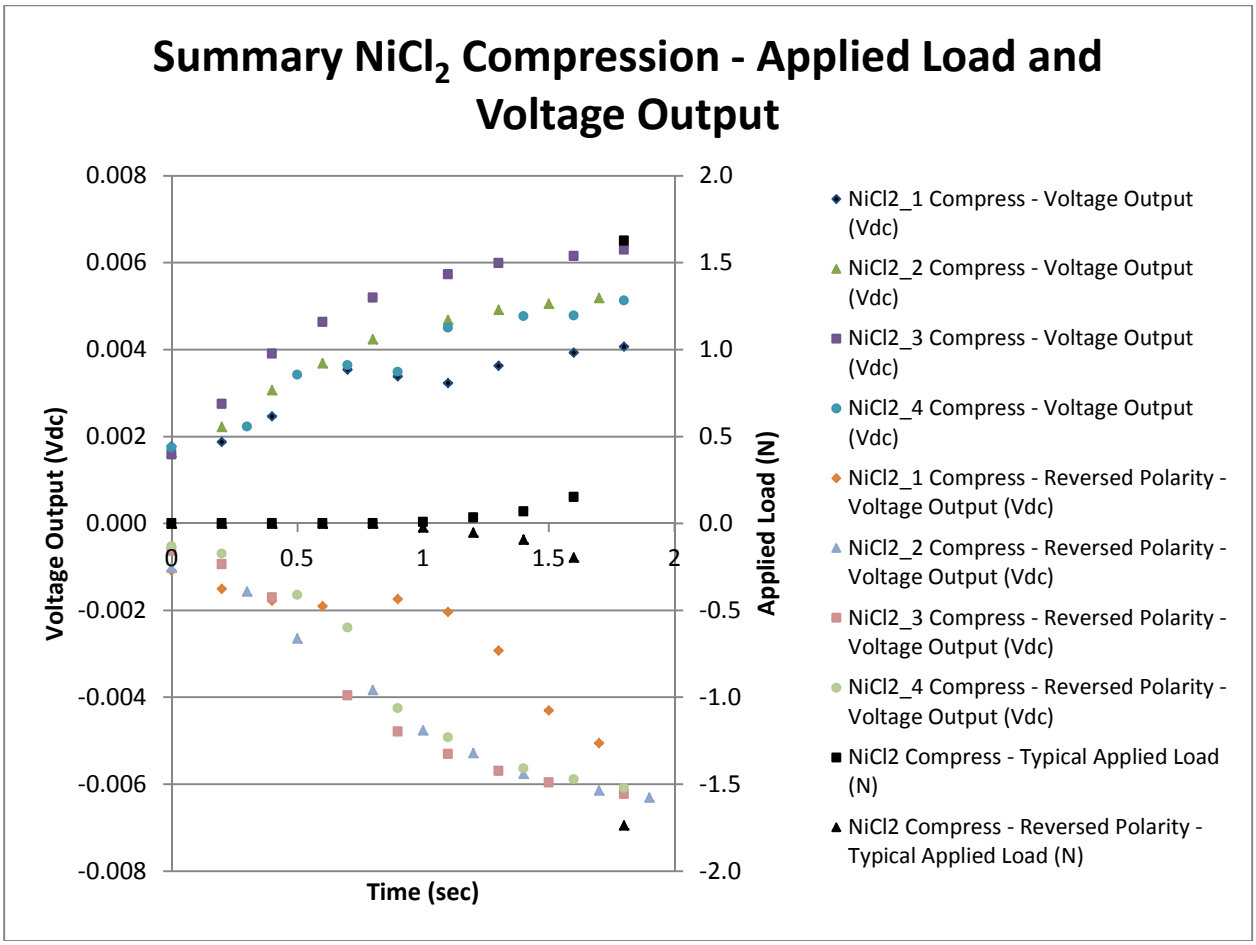

Figure 38. Summary of normal and reversed polarity $NiCl_2$ electrolyte constant compression load scenario, load and voltage output

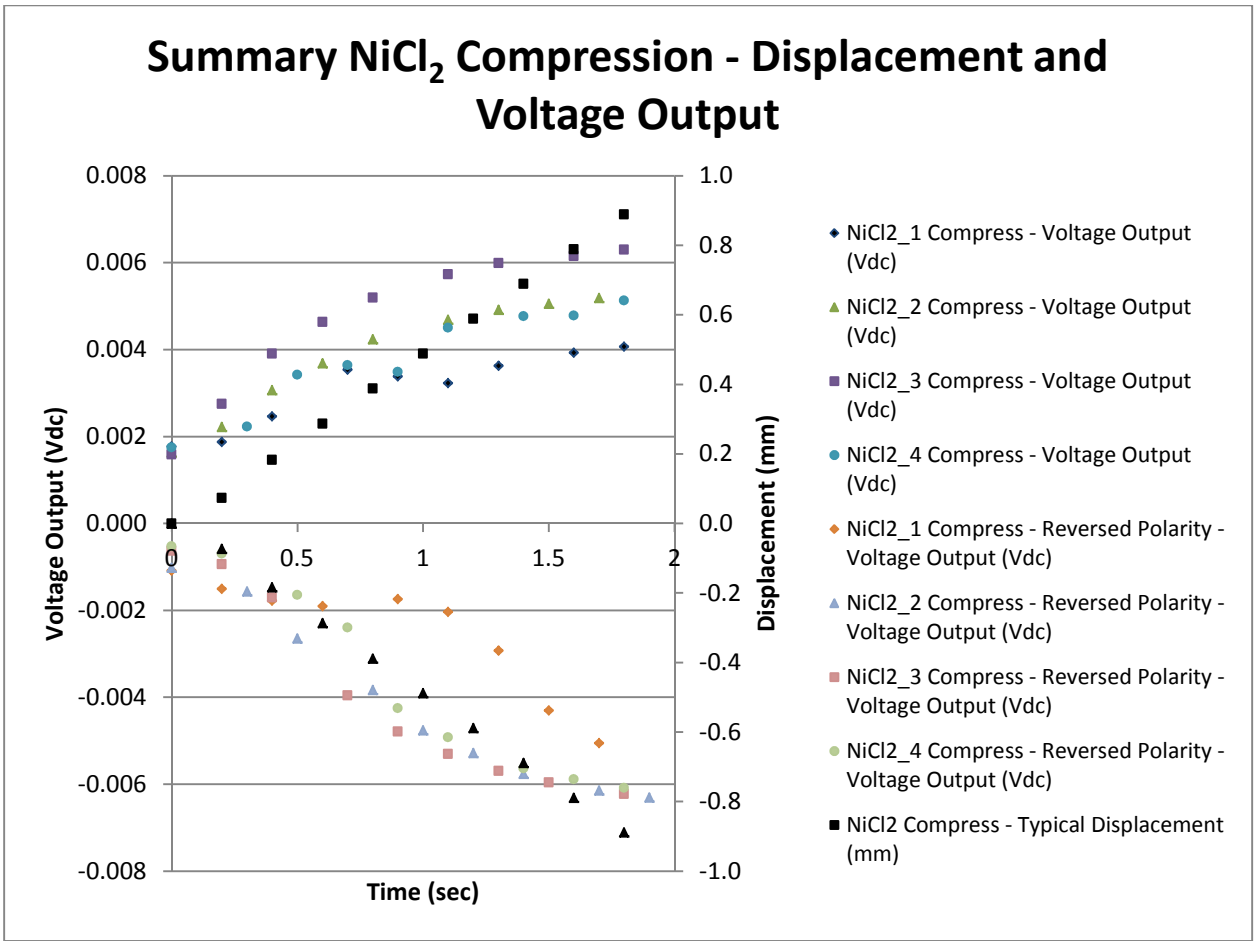

Figure 39. Summary of normal and reversed polarity $NiCl_2$ electrolyte constant compression load scenario, displacement and voltage output

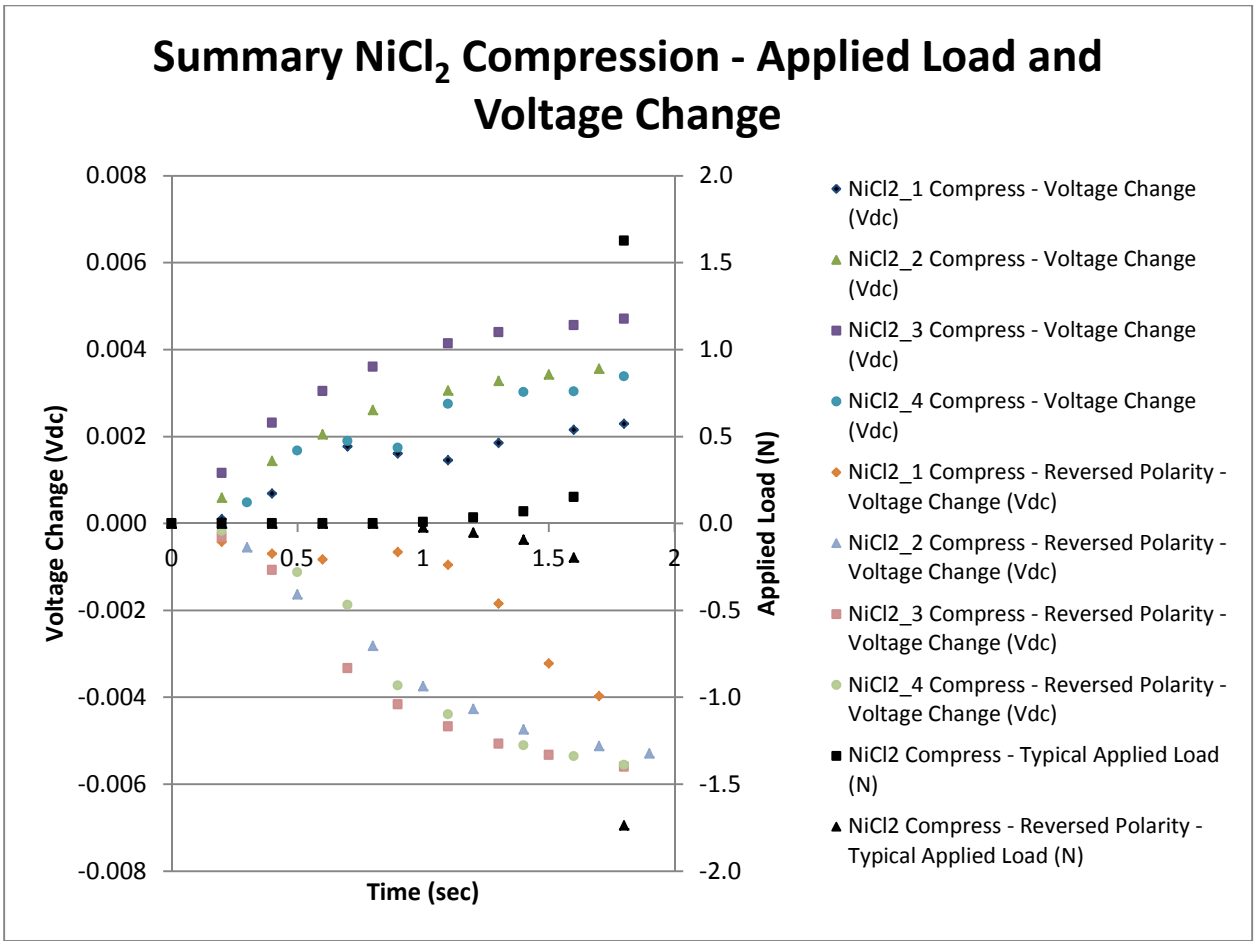

Figure 40. Summary of normal and reversed polarity $NiCl_2$ electrolyte constant compression load scenario, load and voltage change, note large magnitude of voltage change compared to the other constant data

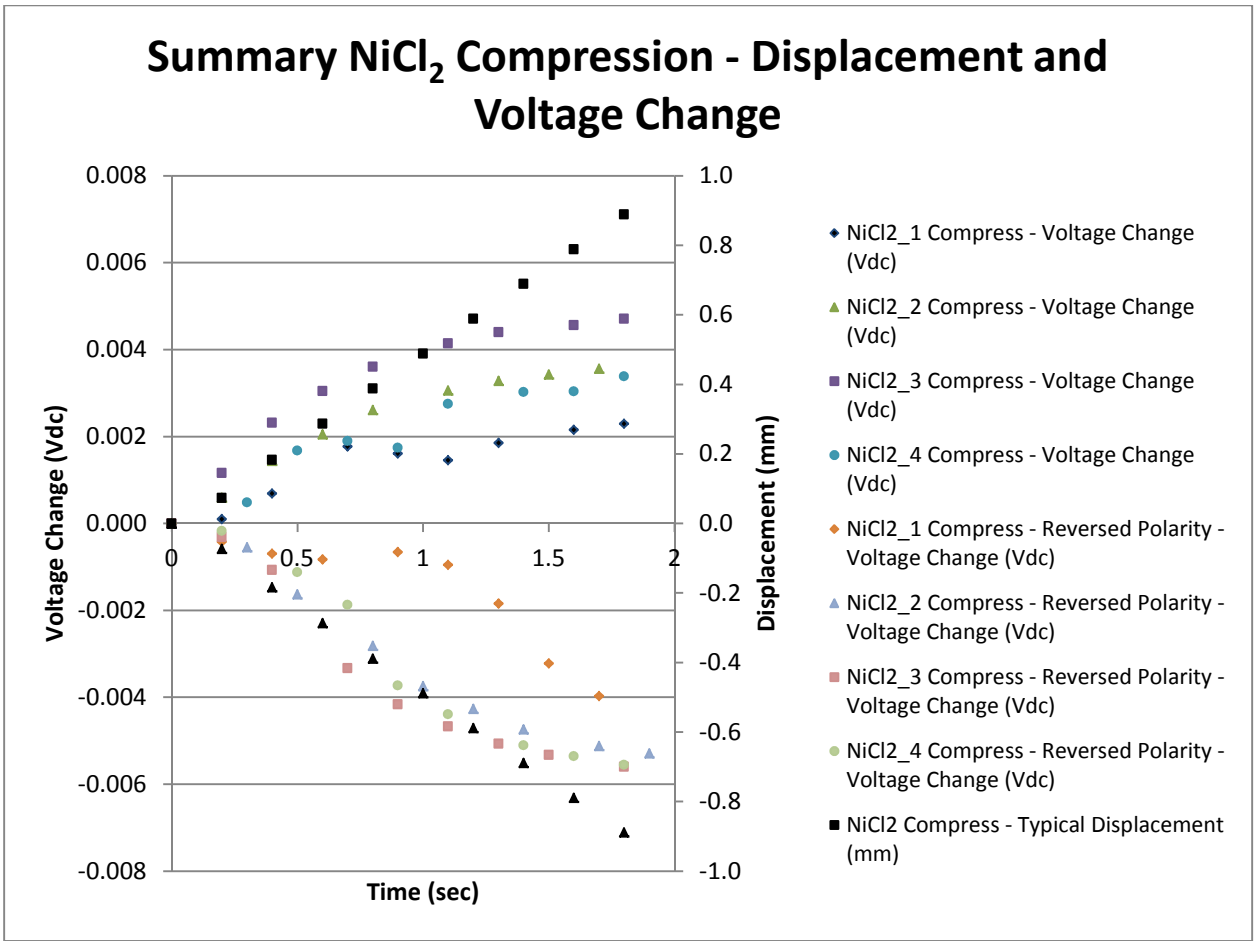

Figure 41. Summary of normal and reversed polarity $NiCl_2$ electrolyte constant compression load scenario, displacement and voltage change

Interestingly, the $NiCl_2$ compression sample had the highest voltage changes with maximum recorded voltages of 4.714 mV and -5.595 mV for normal and reversed polarity respectively. The voltage data, unfortunately, has more variation test run to test run than the other scenarios tested. The individual trial results are displayed in Figures 196-227 in Appendix F.

A comparison of all 4 of the liquids tested can be seen in Figures 42-45. These figures show the 4 normal and 4 reversed polarity runs for each liquid. The scale of the outputs, distribution of the data and side of the horizontal axis that the data appears (normal or reversed polarity), is of particular interest and could be an area of future research which will be addressed in detail in the future work section.

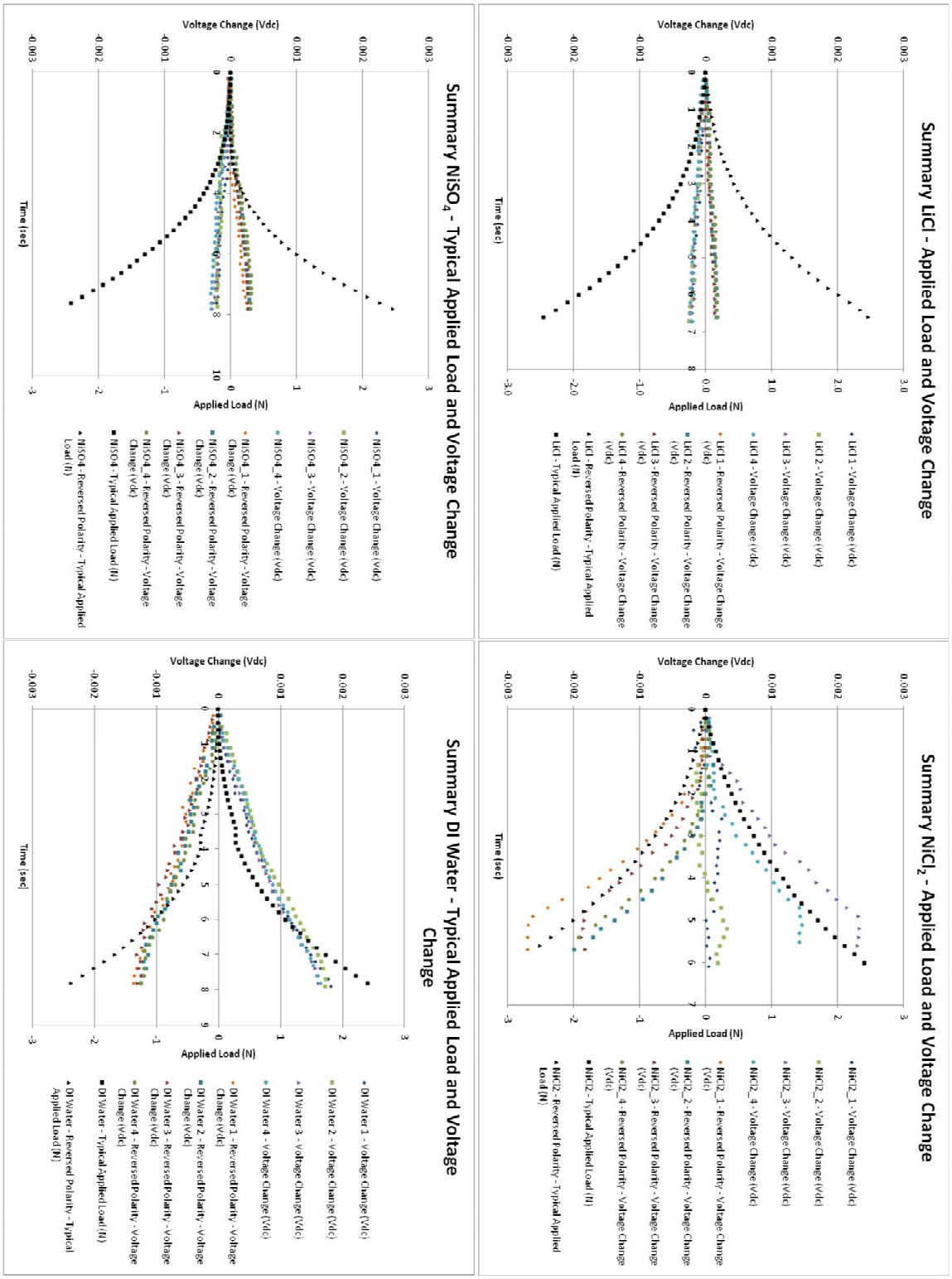

Figure 42. Summary of normal and reversed polarity all electrolytes constant load scenario, load and voltage change, note large sensitivity of $NiCl_2$ and DI water compared to LiCl and $NiSO_4$

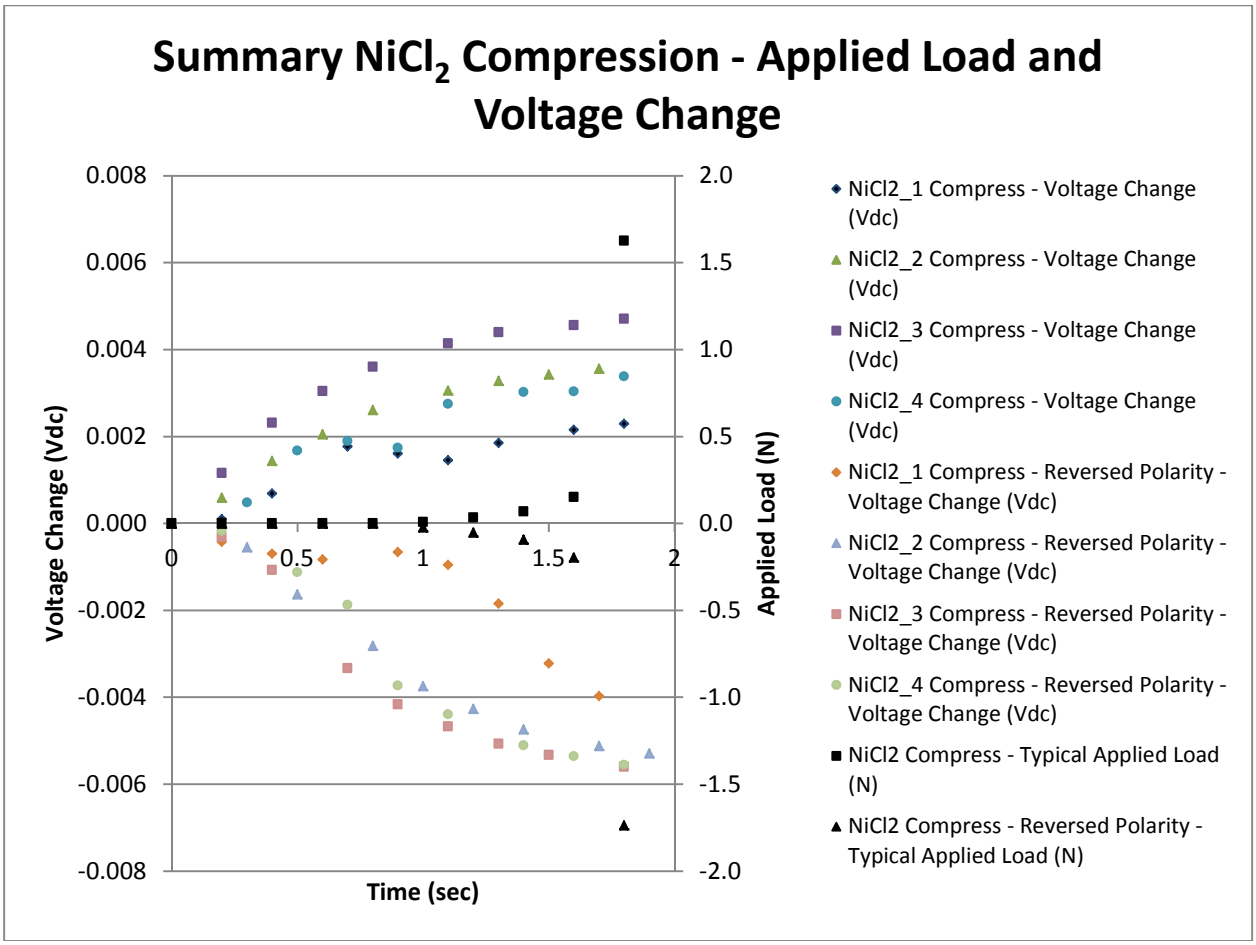

Figure 43. Summary of normal and reversed polarity $NiCl_2$ electrolyte constant compression load scenario, load and voltage change, note largest sensitivity compared with summary in previous figure

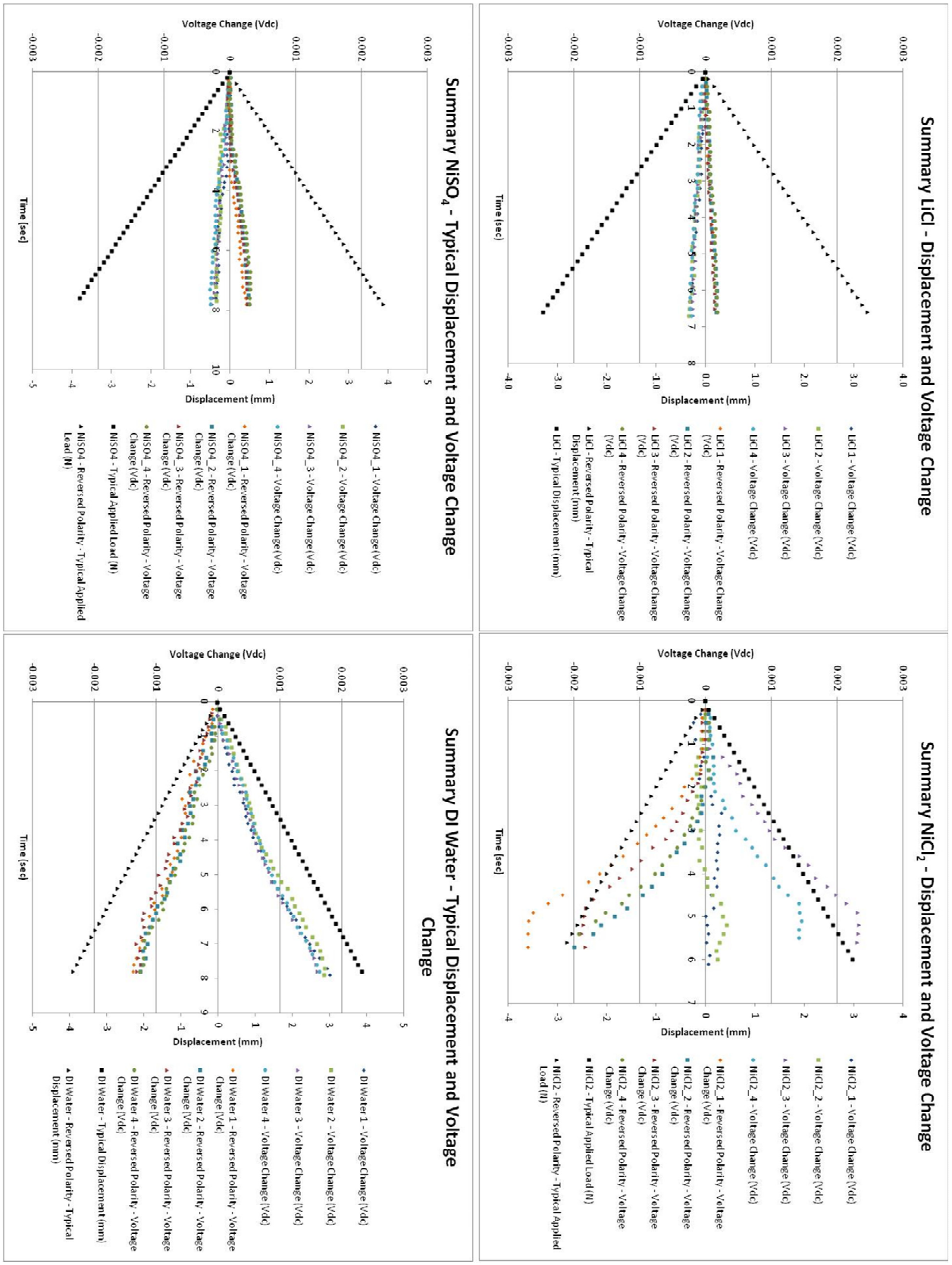

Figure 44. Summary of normal and reversed polarity all electrolytes constant load scenario, displacement and voltage change

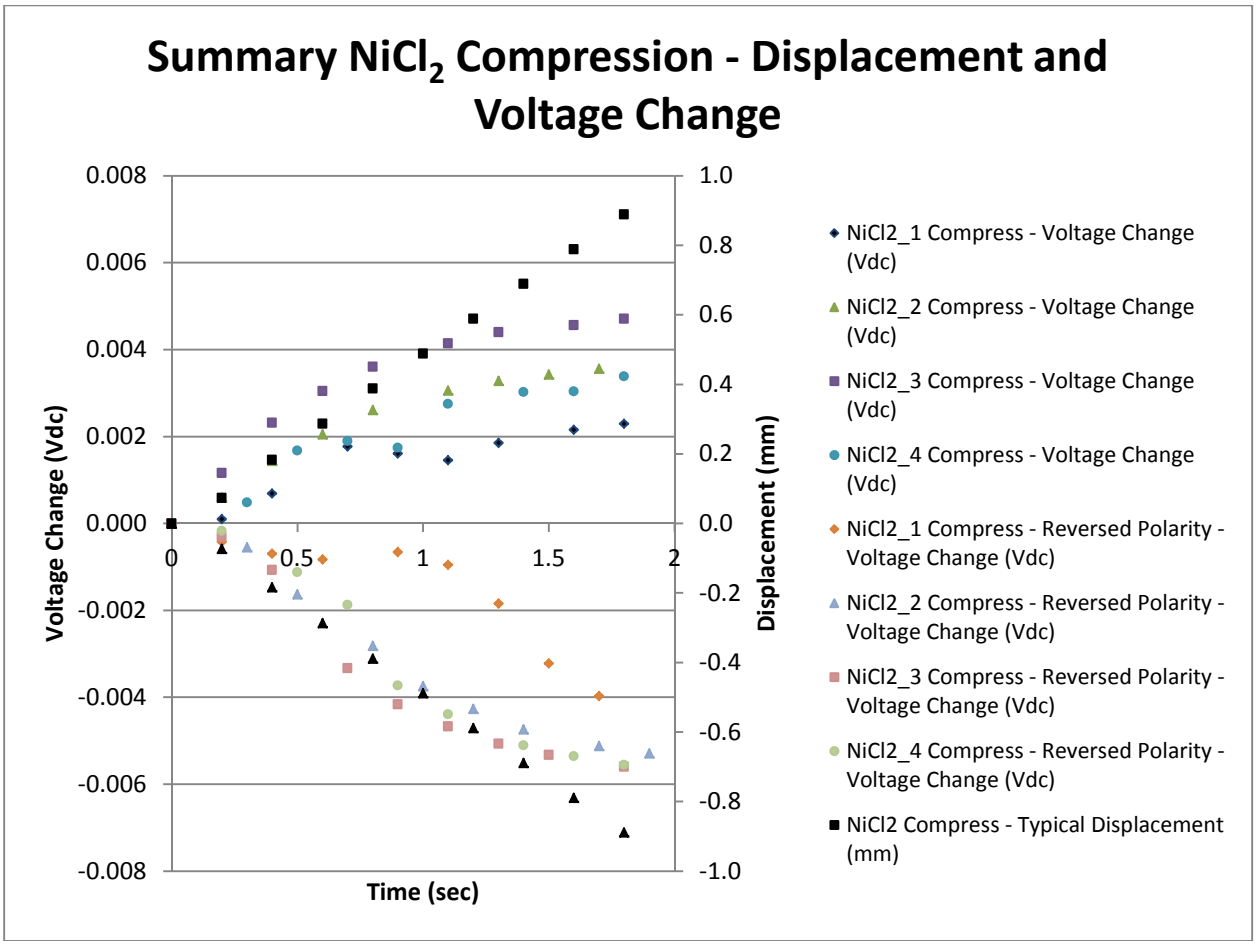

Figure 45. Summary of normal and reversed polarity $NiCl_2$ electrolyte constant compression load scenario, displacement and voltage change

The cyclic data was formatted the same way that the constant data was with voltage on the left vertical axis and force or displacement on the right vertical axis.

LiCl Cyclic Results

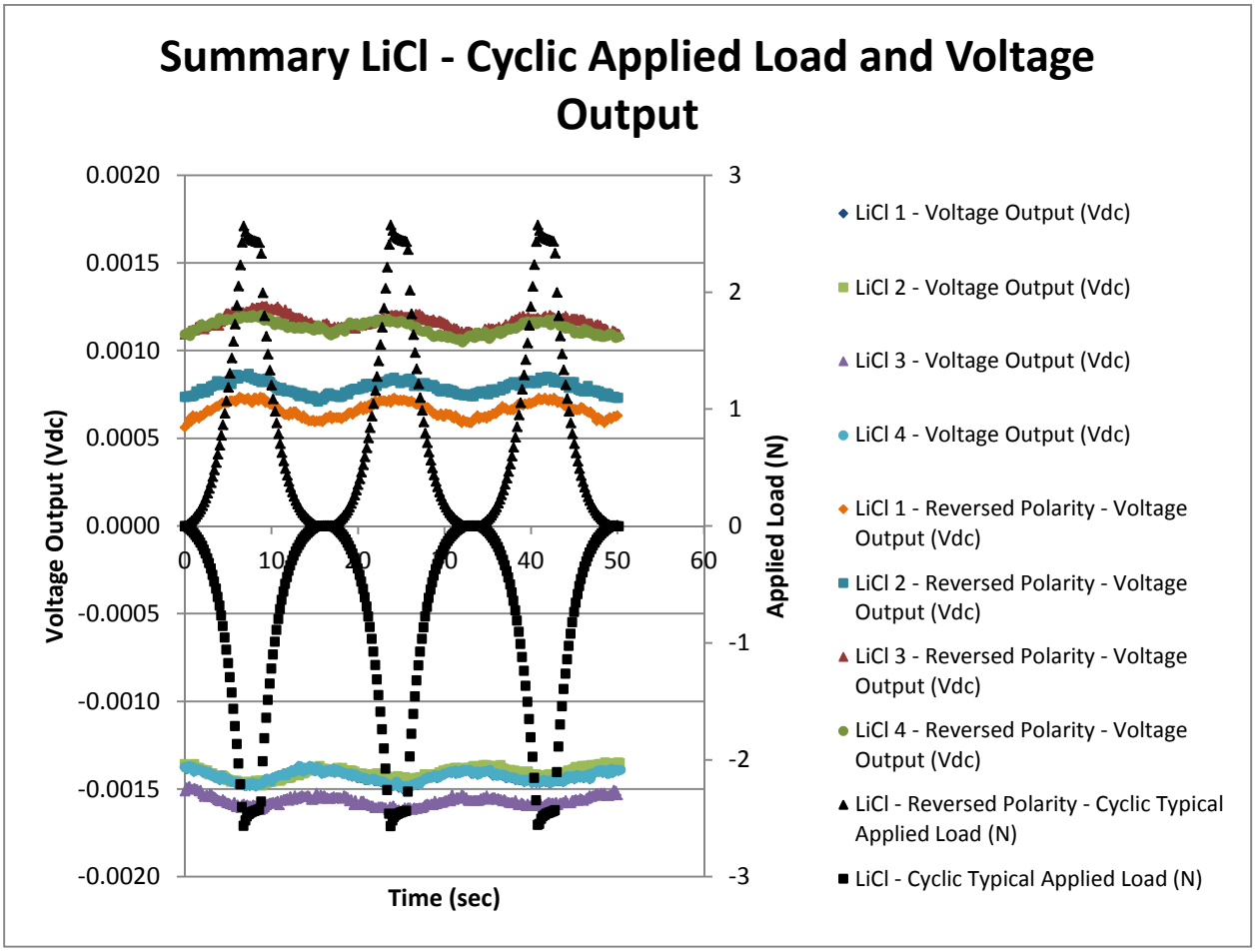

Figure 46. Summary of normal and reversed polarity LiCl electrolyte cyclic load scenario, load and voltage output, note sinusoidal response of voltage output

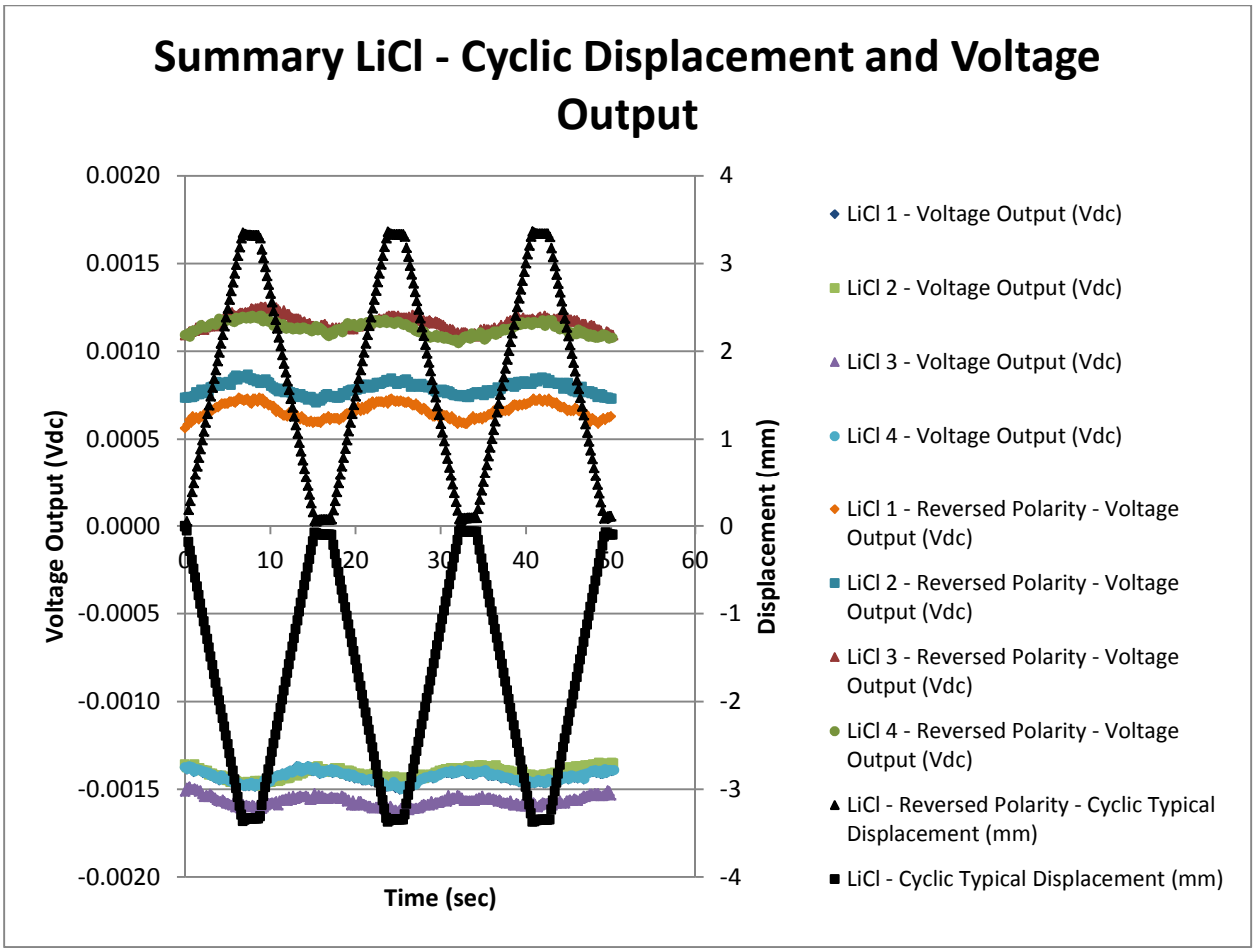

Figure 47. Summary of normal and reversed polarity LiCl electrolyte cyclic load scenario, displacement and voltage output

$NiCl_2$ Cyclic Results

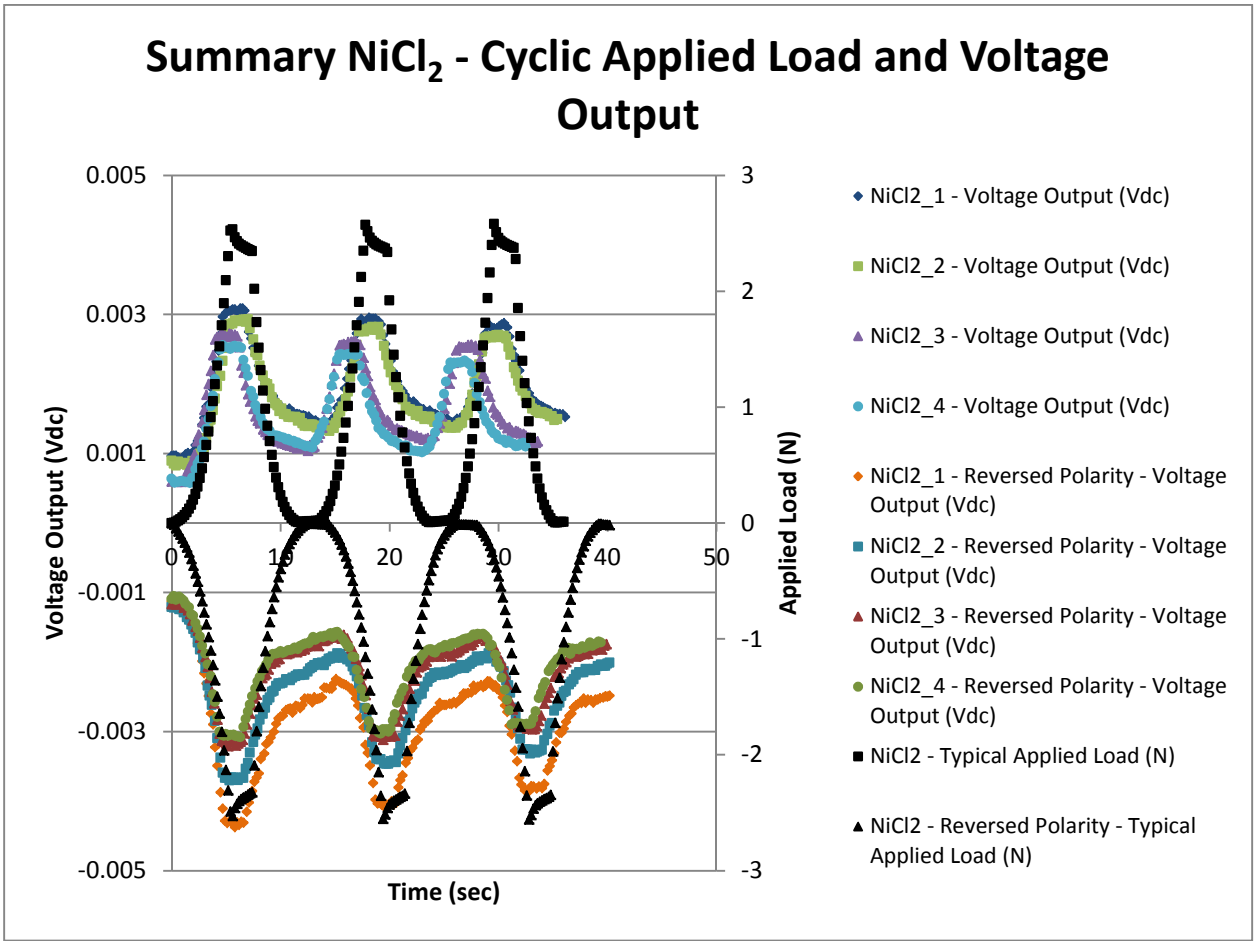

Figure 48. Summary of normal and reversed polarity $NiCl_2$ electrolyte cyclic load scenario, load and voltage output, note difference in voltage output slope with removal of load as opposed to application of load

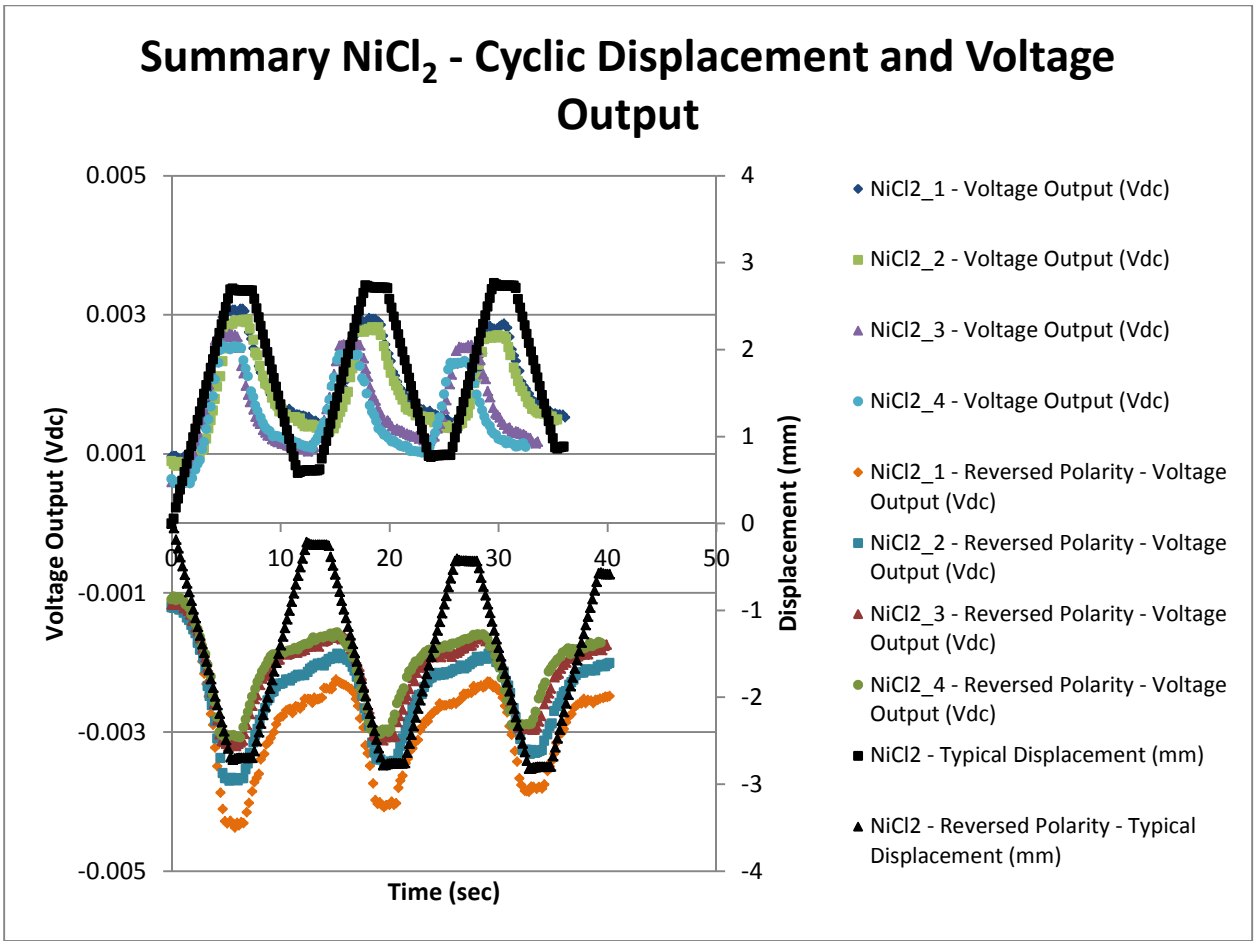

Figure 49. Summary of normal and reversed polarity $NiCl_2$ electrolyte cyclic load scenario, displacement and voltage output

$NiSO_4$ Cyclic Results

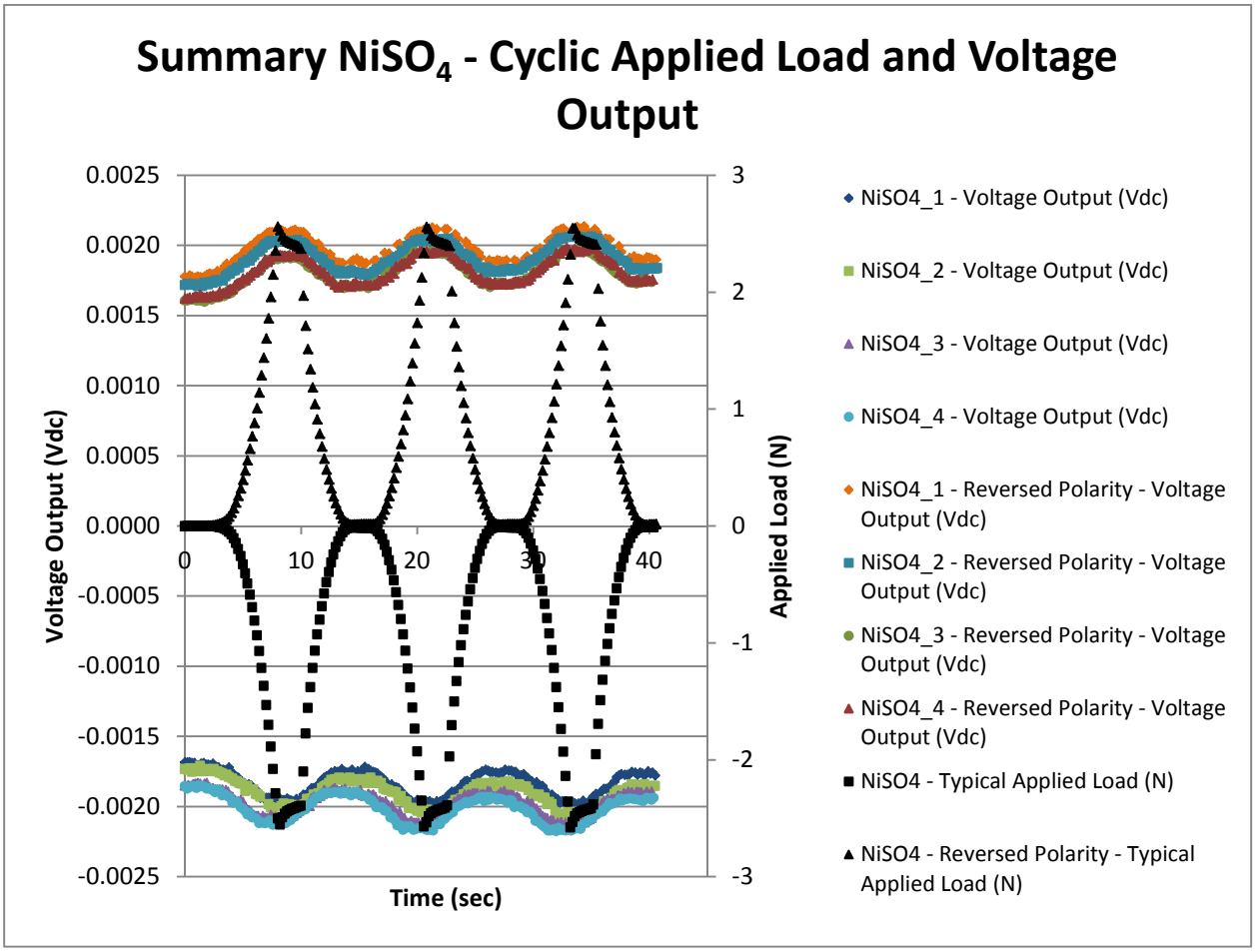

Figure 50. Summary of normal and reversed polarity $NiSO_4$ electrolyte cyclic load scenario, load and voltage output, note sinusoidal response with slightly higher voltage change than LiCl

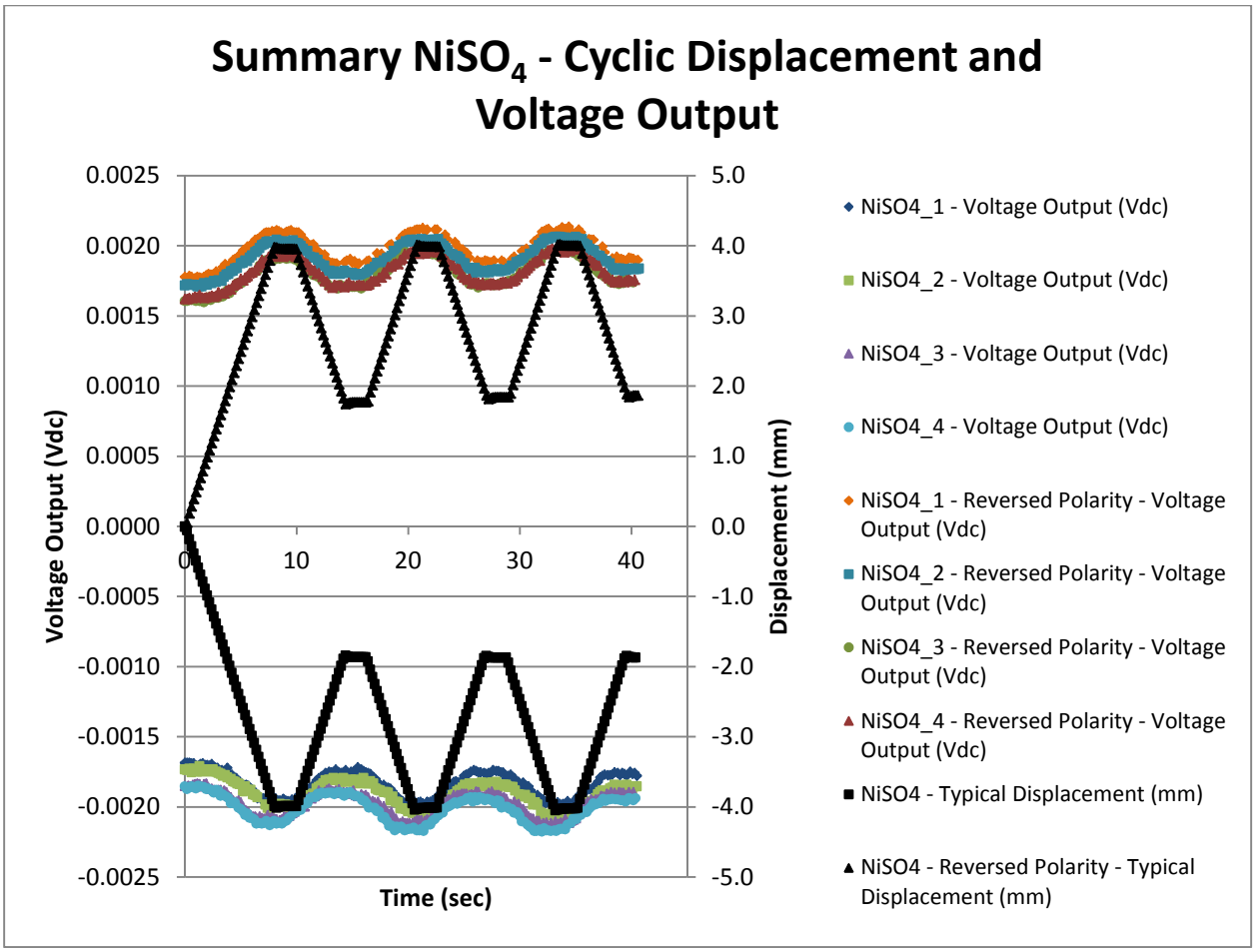

Figure 51. Summary of normal and reversed polarity $NiSO_4$ electrolyte cyclic load scenario, displacement and voltage output

DI water Cyclic Results

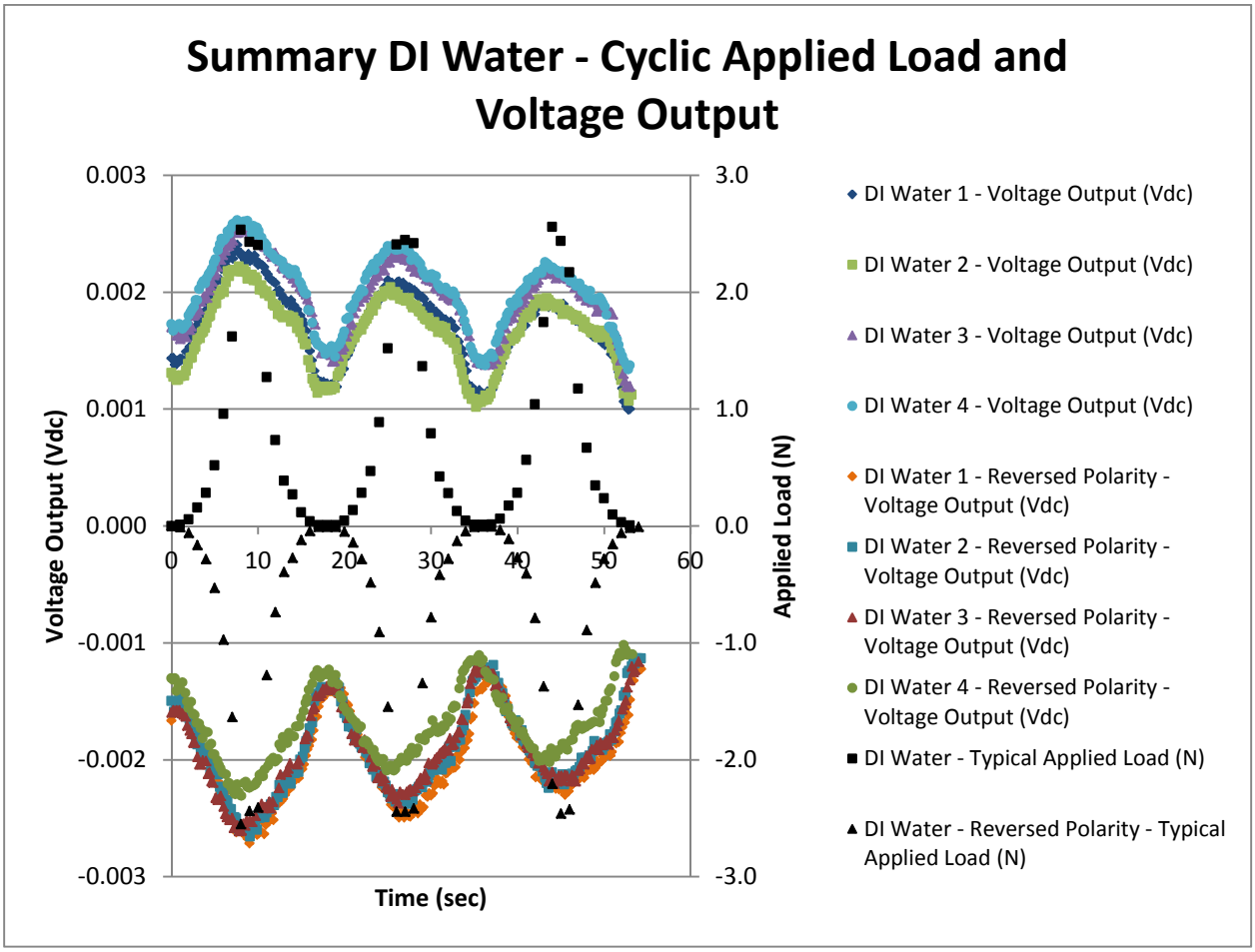

Figure 52. Summary of normal and reversed polarity DI water electrolyte cyclic load scenario, load and voltage output, note good sensitivity but slow reaction to load based on slopes of voltage output

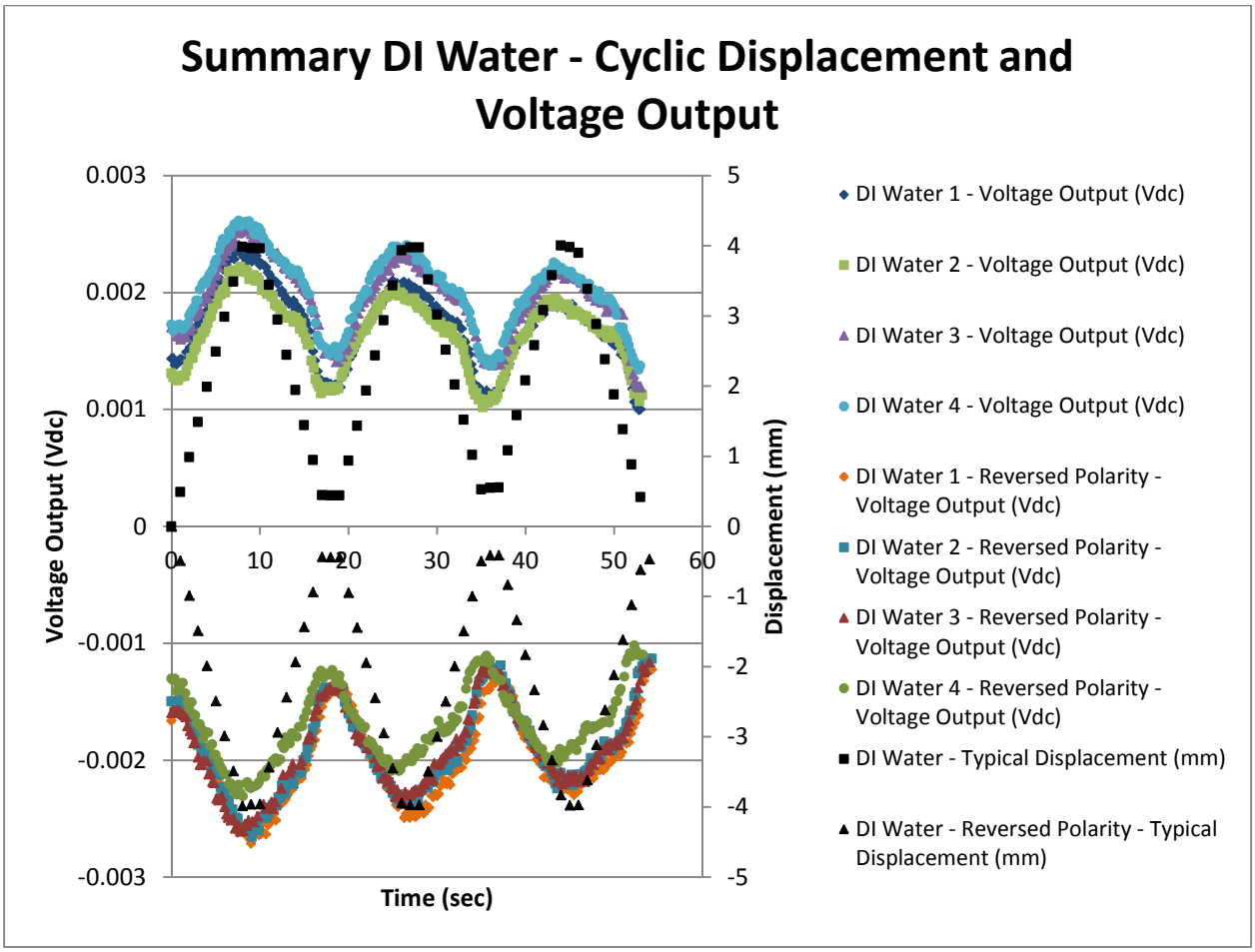

Figure 53. Summary of normal and reversed polarity DI water electrolyte cyclic load scenario, displacement and voltage output

The differing response in the 4 liquids is evident from Figures 46-53. The LiCl would appear to have the smallest output in comparison to the other liquids for cyclic testing and a good amount of noise in the data. The $NiSO_4$ was only markedly better with a slightly higher output. The $NiCl_2$ and DI water had the greatest response with the $NiCl_2$ being possibly slightly better due to the decreased time it took to return to equilibrium, evident in the shape of the voltage curves. Interestingly, the LiCl and the $NiSO_4$ have a mirrored response to that of the $NiCl_2$ and DI water. The data for the $NiCl_2$ compress "control" experiment is displayed below in Figures 54-55.

$NiCl_2$ Compress Cyclic Results

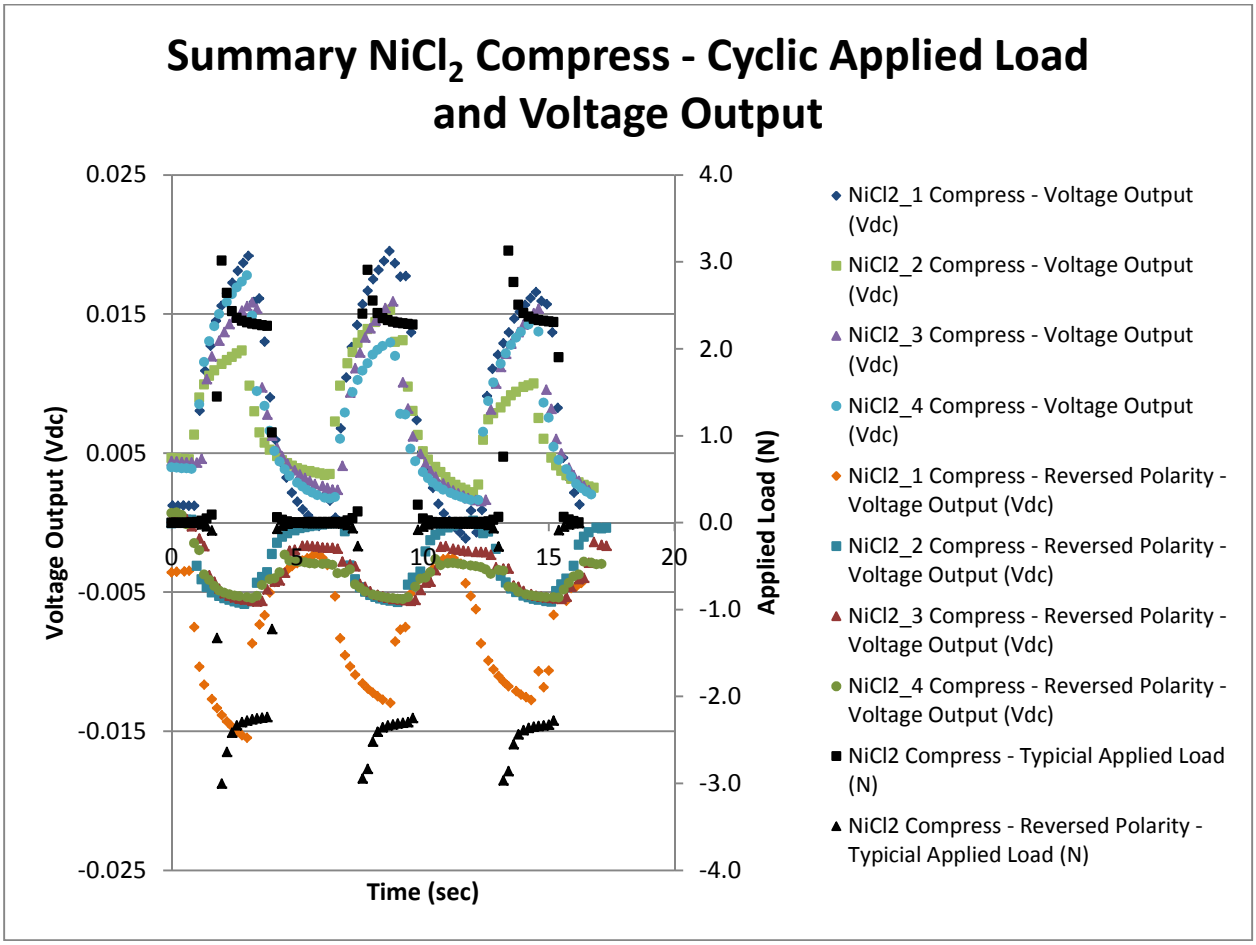

Figure 54. Summary of normal and reversed polarity $NiCl_2$ electrolyte cyclic compression load scenario, load and voltage output, note sensitivity (large voltage change) and fast response time (slopes of voltage output)

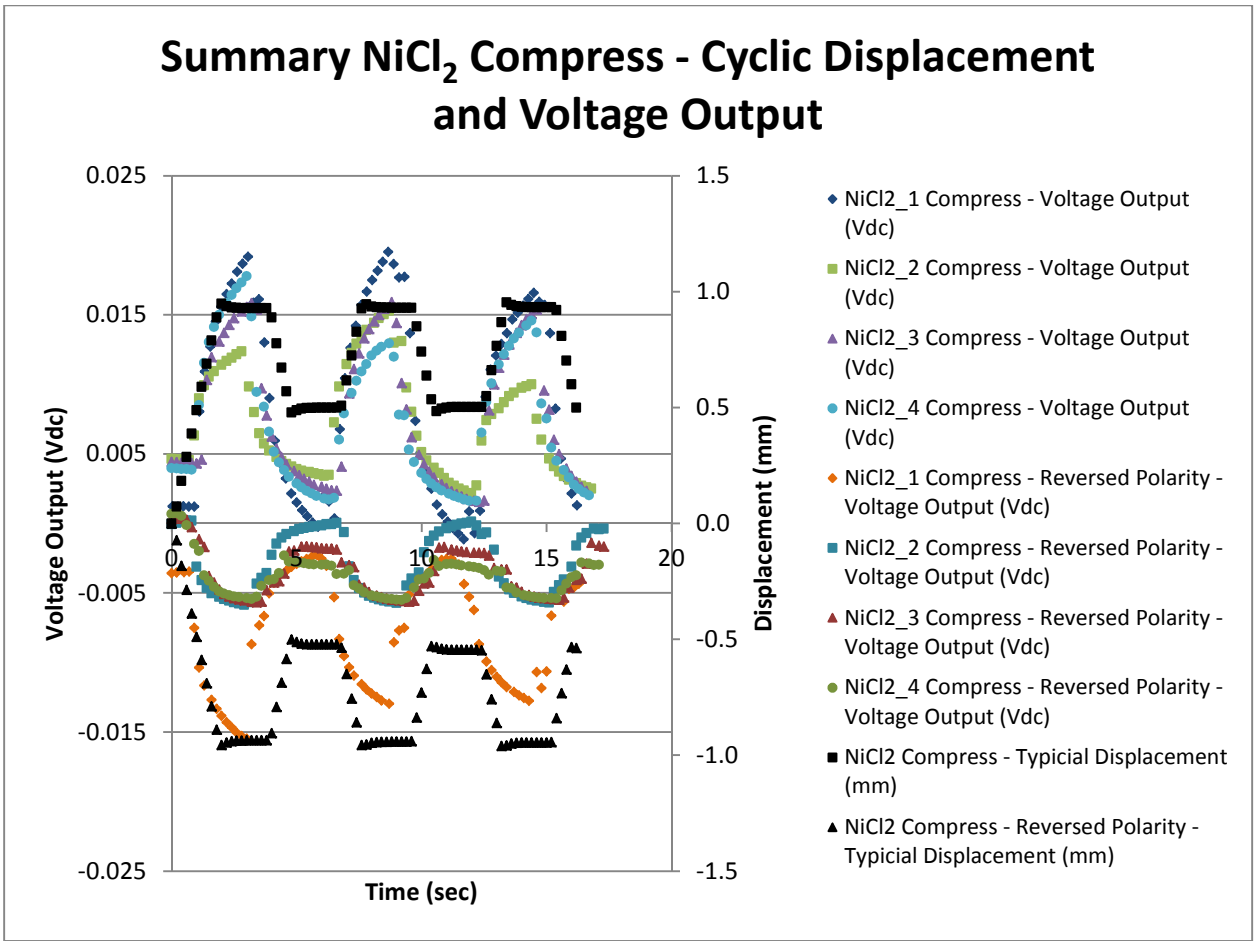

Figure 55. Summary of normal and reversed polarity $NiCl_2$ electrolyte cyclic compression load scenario, displacement and voltage output

A comparison of all the cyclic runs, including the $NiCl_2$ compress comparison experiment is displayed in Figures 56-59.

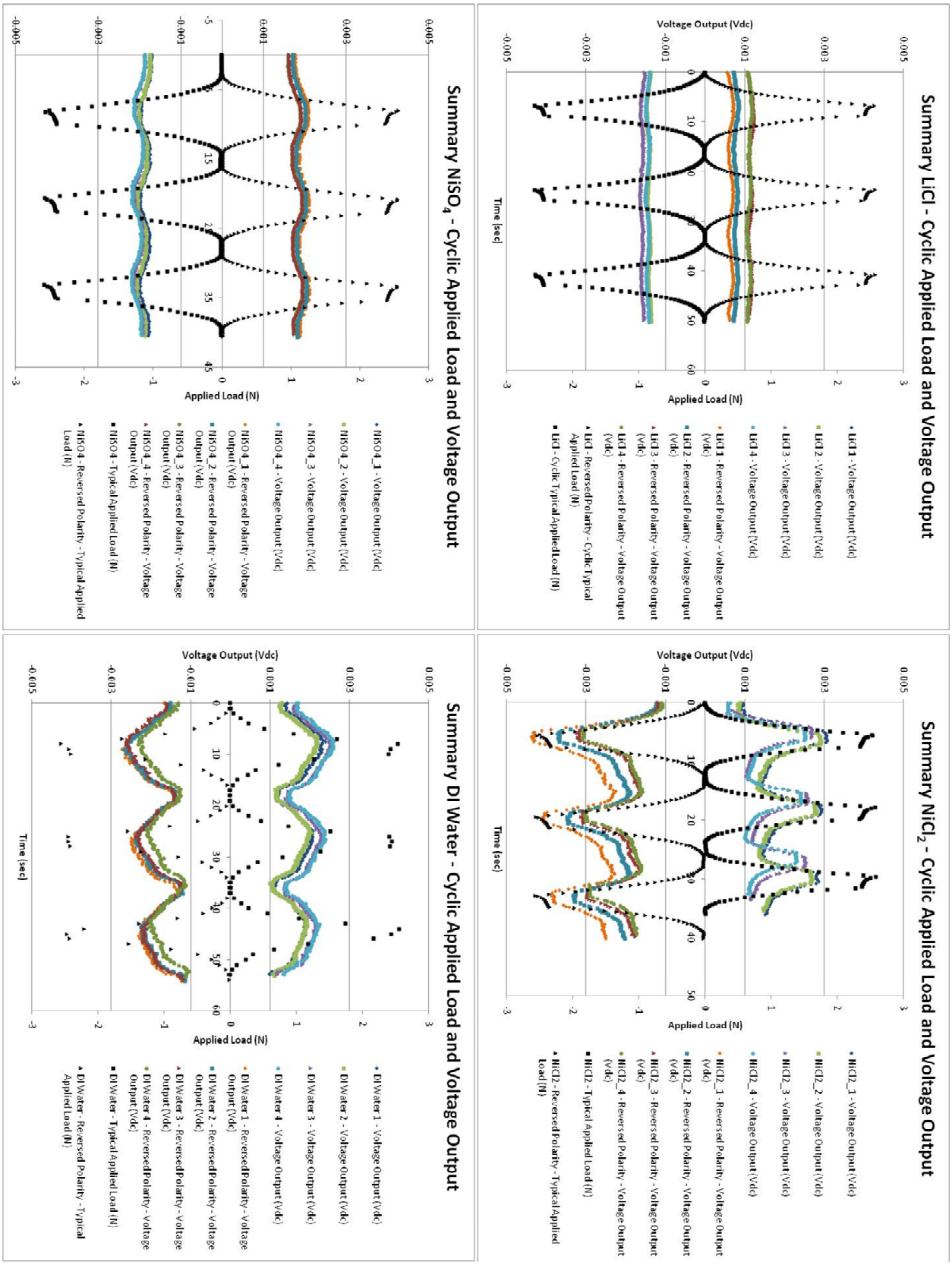

Figure 56. Summary of normal and reversed polarity all electrolytes cyclic load scenario, load and voltage output

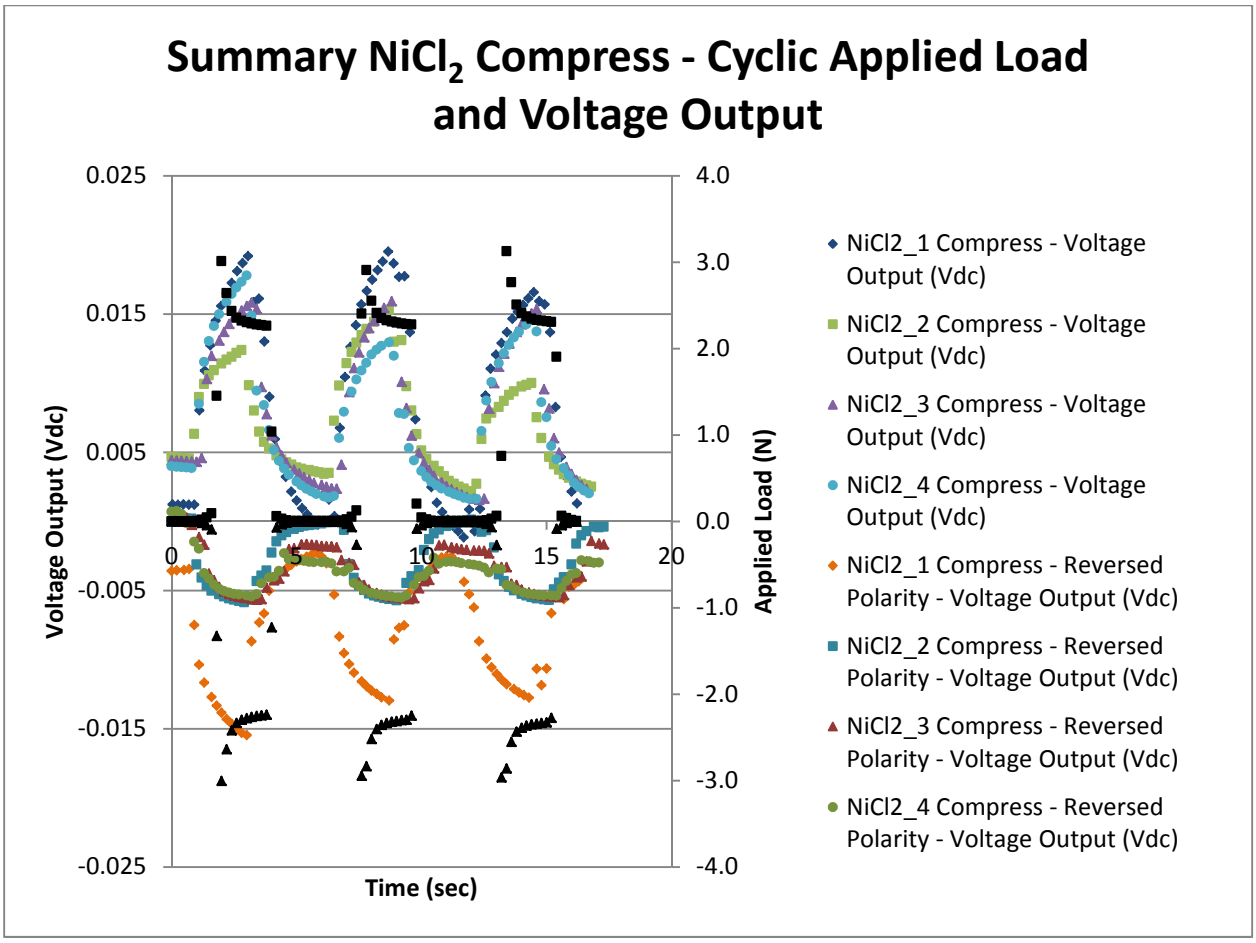

Figure 57. Summary of normal and reversed polarity $NiCl_2$ electrolyte cyclic compression load scenario, load and voltage output

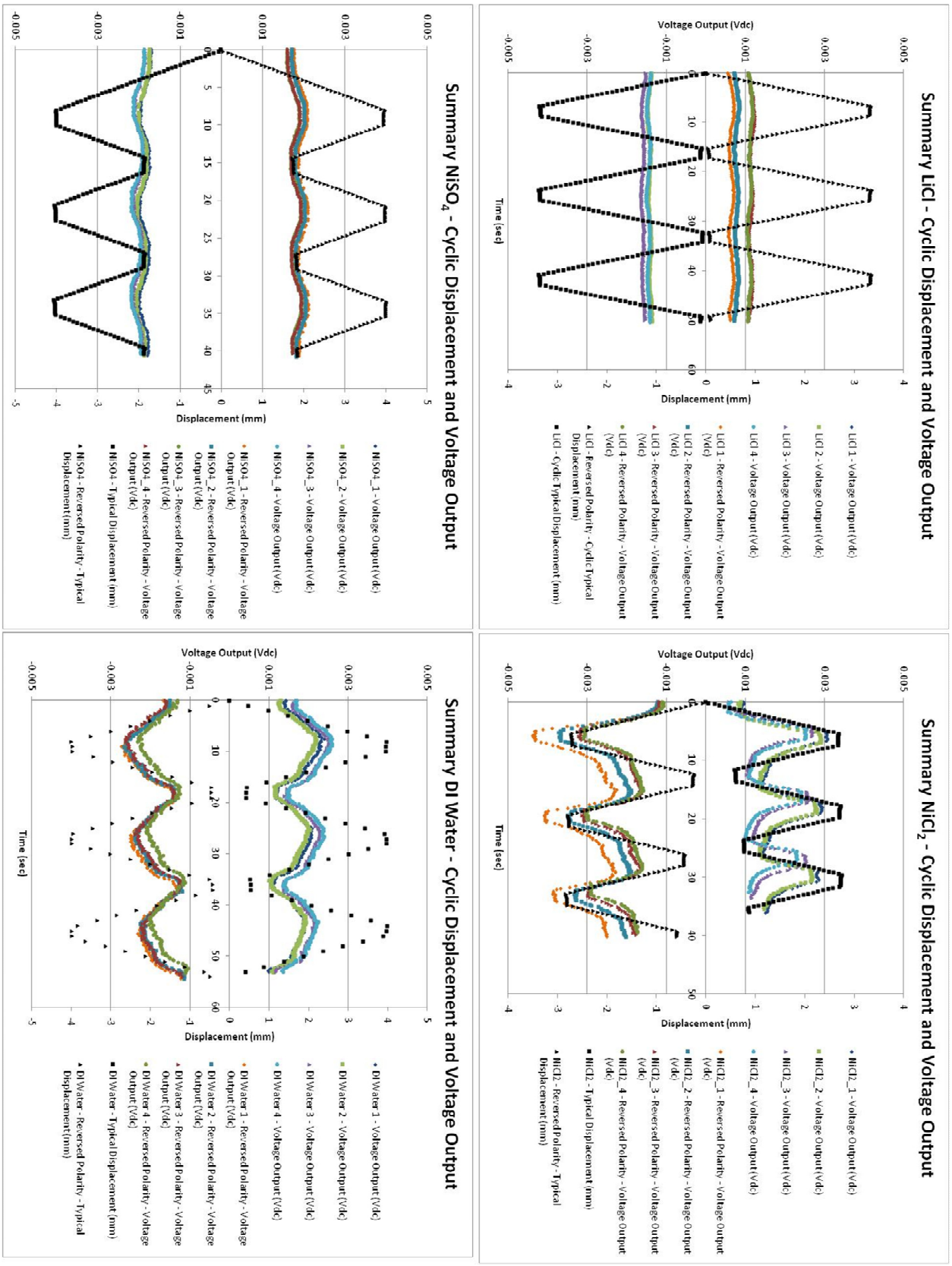

Figure 58. Summary of normal and reversed polarity all electrolytes cyclic load scenario, displacement and voltage output

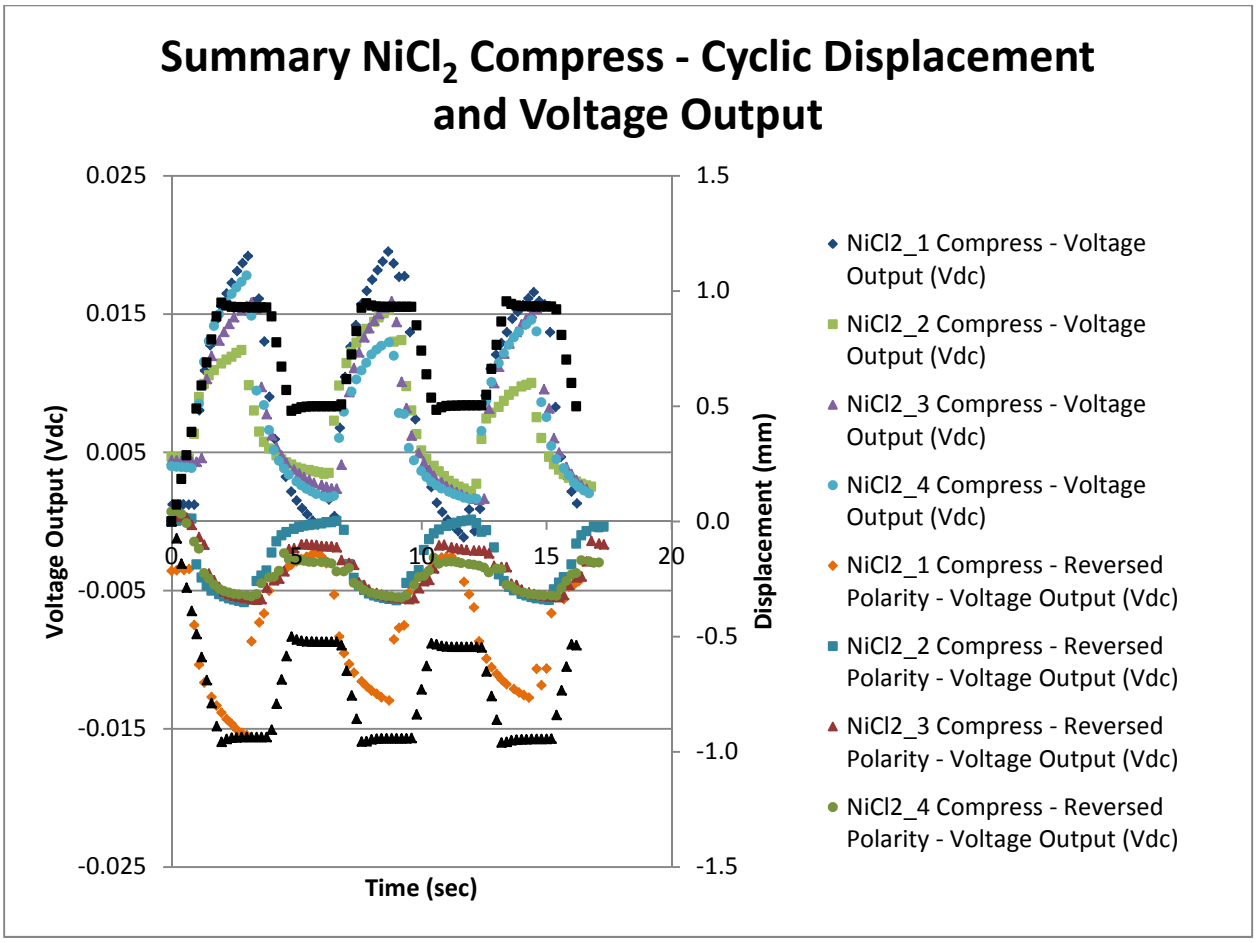

Figure 59. Summary of normal and reversed polarity $NiCl_2$ electrolyte cyclic compression load scenario, displacement and voltage output

Table 1 displays a summary of the results of all the electrolytes tested. It shows the characteristics of each and the positive and negative aspects. Looking at this it is easy to see which electrolyte yields the highest sensitivity, which ones are repeatable and the reversibility of each.

Electrolytes

- LiCl – least sensitive, good repeatability, and reversible response
- $NiCl_2$ – great sensitivity, worst repeatability and reversible response
  - Repeatability possibly mitigated by incubation time
- $NiSO_4$ – lower sensitivity, good repeatability, and almost completely reversible response
- DI water – great sensitivity, good repeatability, reversible response
  - It's just WATER!

Table 1. Summary of Electrolyte Results

Discussion

The ultimate research goal, a composite tactile sensor, could not be pursued until sufficient data on the characterization of IPMCs as tactile sensors was available. The only data that was found to exist was in the form of displacement and voltage output; usually in terms of tip deflection where a strip of IPMC was clamped at one end while the other end was deflected. This raises the question of why data that correlates force applied to the material and resulting voltage does not exist?

The test rig for clamping the samples to achieve a 3-point bend scenario was utilized and immersed in the electrolyte in a 3 liter beaker. Since both ends of the IPMC are clamped the scenario could be approximated as a dual cantilever beam. Comparing the axial strain the IPMC experienced (~.05%) with the stress strain curve for Nafion® [22], it was determined that within

a tolerable margin of error, that the testing performed here was within the linear elastic region of the material.

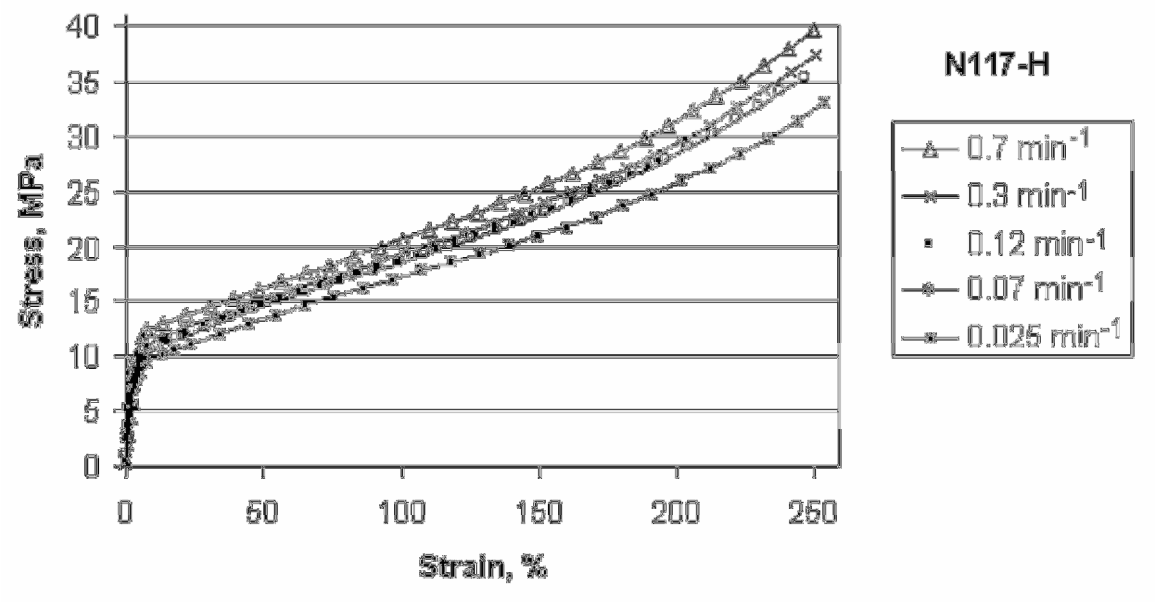

Figure 60. Stress – Strain curve of Nafion® N117-H [22]

Since the IPMC is clamped at both ends and a load is being applied at the center of the membrane, a complex loading scenario exists and the strain the membrane experiences is assumed to be completely axial. The strain can be determined by simplifying the scenario to a simple right angle triangle seen in Figure 61, where l_0 is the original length of the IPMC, d is the displacement of the center of the IPMC and l_f is the final length of the IPMC at the peak load of 2.5 N.

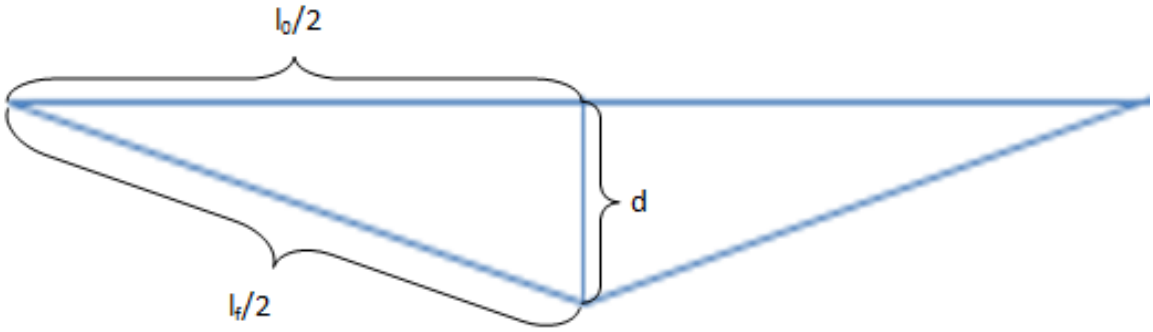

Figure 61. Strain scenario modeled as right angle triangle

The complexity of the loading scenario outlined here may explain why sufficient data on the characterization of IPMCs as tactile sensors did not exist. It also aids in revealing the need for data that conclusively correlates force input and voltage output of IPMCs before the previously intended investigation of a "composite" tactile sensor could be continued.

Data was collected characterizing IPMCs in the presence of four different electrolytes: 1M LiCl, 1M $NiCl_2$, 1M $NiSO_4$, and DI water. The samples were clamped at either end between the top electrodes and bottom base electrode (Figure 19). Voltage was collected for normal and reversed polarity to determine if indeed one side of the IPMC was more sensitive than the other. This was done by moving the Instron® cross head at a rate of 30 mm/min up to a load of 2.5 N, and by applying and removing a 3 cycle cyclic load at a rate of 30 mm/min with 2 second holds at 2.5 N and 0 N. The load was applied at the center of the material using a probe that was slightly wider than the IPMC to ensure the entire width received the same loading. Since the load was applied over an area and in a "double cantilevered beam" scenario, a unit load such as bending strength would be an appealing metric. Due to the complex loading scenario presented by the dual clamped ends, the visco-elastic nature of the Nafion®, and the IPMC being a composite material (the platinum on either side of the Nafion®), doing this could add unnecessary error to the data. For this reason, the results are reported in terms of applied load, along with displacement and voltage output.

The magnitude of the outputs and distribution of the data tells us much about the viability of the liquids for use with IPMCs as tactile sensors. The most optimal scenario would yield the following responses: a large voltage swing with an instantaneous voltage response due to force input, the same starting and stopping voltage (no hysteresis) and no variability from test to test (good repeatability).

The LiCl constant data displayed little variation between test runs but a very small magnitude in voltage output. The normal polarity had a negative voltage response and the reversed polarity had a positive one. The fact that this liquid and the $NiSO_4$ showed this type of response while the $NiCl_2$ and DI water had the opposite response is particularly interesting and merits future research. One possible reason for this response is due to anion effects and the different diffusivities of these ions. Diffusivity, commonly known as the diffusion coefficient, is a constant used to describe mass transport through atomic motion [24]. Diffusion in ionic compounds is much more complicated than that in metals and the diffusivities of oppositely charged ions must be taken into account. Also, diffusion in polymers happens more readily in amorphous regions rather than crystalline, making Nafion® a complex system from a diffusivity perspective [24]. Not surprisingly, the exact role that cations and anions play in the operation of IPMCs and the effect their diffusivities have on this operation is not well understood. Though there are many models and governing equations that exist in the literature, their particular roles and the magnitude of their contribution should be further investigated. When speaking of repeatability from the data presented here, LiCl performs adequately since it exhibits a measurable voltage response due to mechanical deformation with little variation between test runs.

Like the LiCl, the $NiSO_4$ constant data shows a negative voltage response for normal polarity and a positive voltage in the reversed configuration. The voltage output is quite similar in scale to the LiCl, with an overall peak voltage somewhere in between the voltage response observed for the LiCl and $NiCl_2$. The voltage output is just slightly higher (max of approximately +/- .3 mV) than that of the LiCl, but has a slightly higher variation in voltage data from run to run; but still less variation than that for the $NiCl_2$ test runs. The small magnitude of

the voltage output and polynomial response seen in Figures_ Appendix_ are curious and should be further investigated. An interesting note about the $NiSO_4$ however, is that one side of the membrane does not appear to be drastically more sensitive than the other evident in the summary in Figures 56 and 58. The two different distributions (for normal and reversed polarity) are nearly mirror images of each other across the horizontal axis exhibiting an almost completely reversible response. This appears to be a contradiction of the data presented by [9], Shahinpoor et. al. Figure 62, from Shahinpoor, shows the response characterized by collecting the voltage output of a membrane face up and face down as a result of a change in displacement.

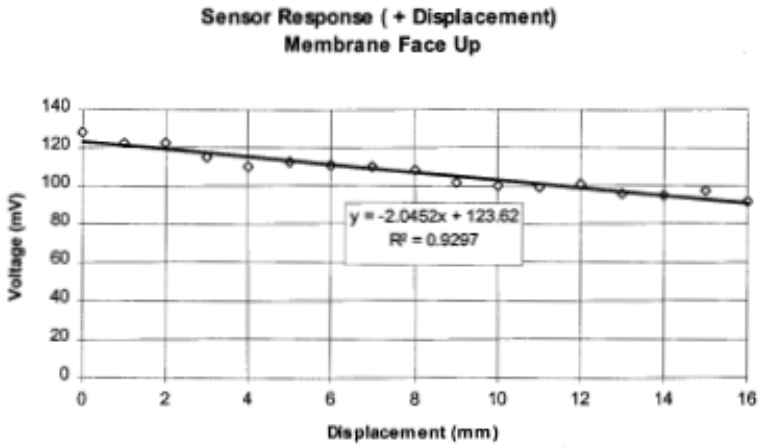

Figure 3. IPMC film sensor response for positive displacement input.

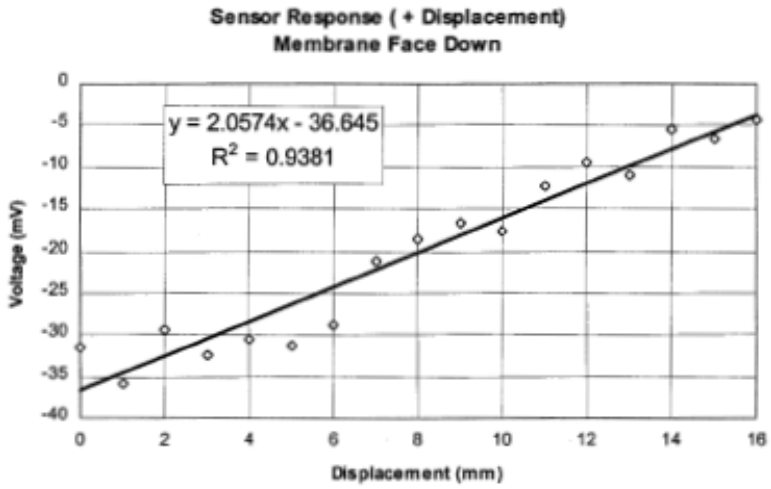

Figure 62. Displacement and voltage response of IPMC showing membrane side sensitivity [9]

As seen in Figure 62, Shahinpoor et. al [9] suggests the material has a much greater response on the "face up" side as opposed to the "face down" side, suggesting that there may indeed be a more sensitive side of the membrane. According to the data obtained for this thesis, the change in output due to membrane face would appear to depend on the electrolyte of choice. Shahinpoor et. al [9] does not seem to specify which liquid is being tested in Figure 62 and therefore, it is difficult to draw a concrete conclusion on whether or not one side of the membrane being more sensitive than the other is a basic property of IPMCs or dependent on the electrolyte. The idea that a membrane may have the same sensitivity independent of loading direction is an attractive

conclusion, illustrating the possibility of achieving complete reversibility from an IPMC sensor. Reversibility would greatly increase the feasibility of IPMCs as tactile sensors since their response could be more easily predicted and even tailored depending on the type of electrolyte chosen.

The $NiCl_2$ had the largest voltage output which would make it attractive from an ease of sensing standpoint (good sensitivity). The voltage data, unfortunately, had the largest variation from trial to trial compared to all of the data collected for each electrolyte. The variability could be a result of many factors, one being incubation time or time that the membrane is kept in the electrolyte prior to testing. Further research should be done to determine the effect of incubation time on membrane response. More specifically, membranes should be immersed in a particular electrolyte and tested similarly to the experiments presented here at different points in time, e.g. 1 hour, 2 hours, etc. These tests would quickly determine if the noise observed by the $NiCl_2$ sample was due to the liquid itself or simply not allowing the sample ample time in the electrolyte prior to testing. The fact that the first two runs of the $NiCl_2$ sample are drastically different than the remaining six and that the last three runs are almost completely identical would suggest that insufficient time to reach equilibrium (or incubation time) is most likely the cause of the noise.

The scale of the $NiCl_2$ voltage output in comparison with the LiCl is quite intriguing. Figures 63 and 64 show the ionic radius for a few common ions.

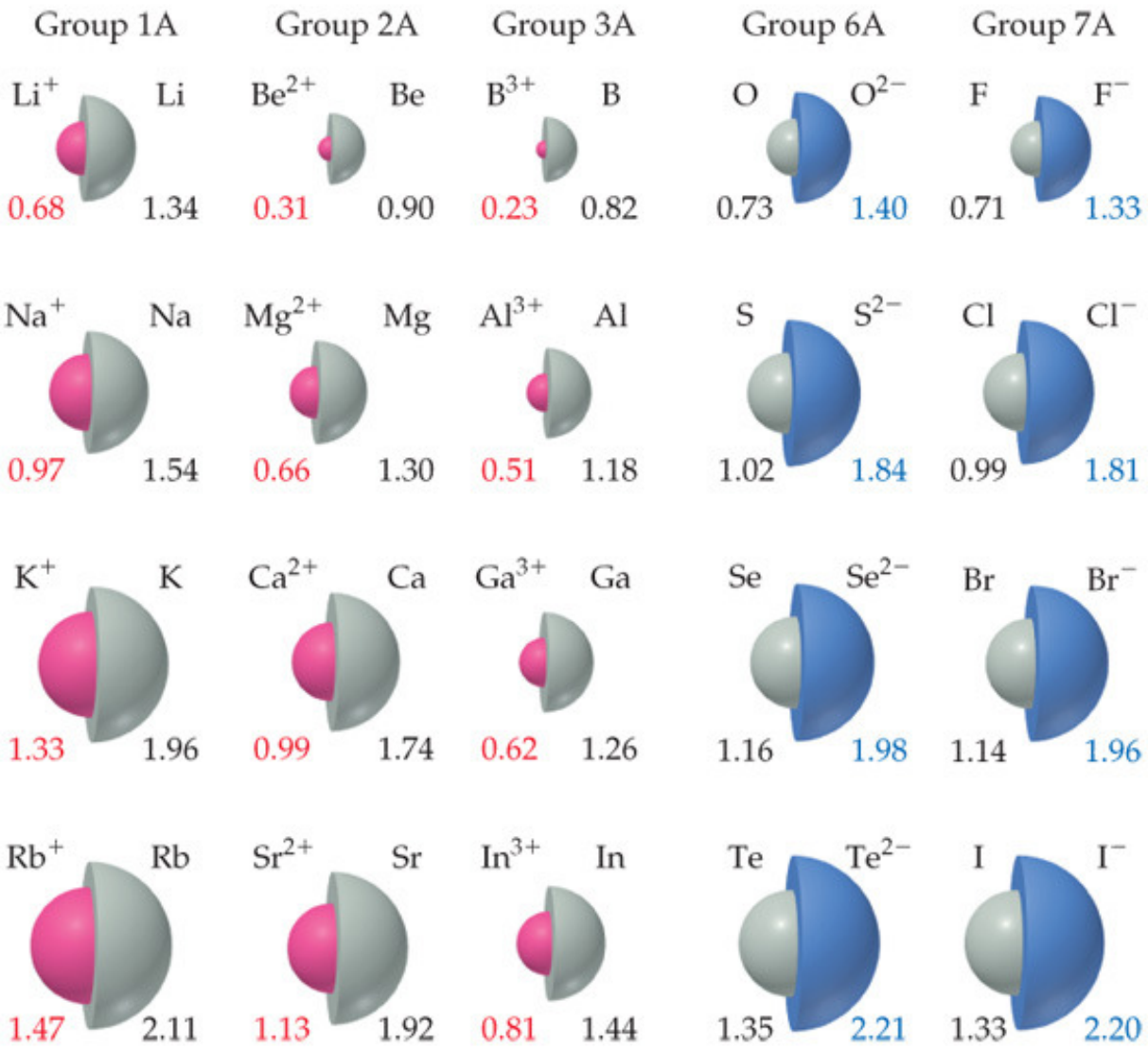

Figure 63. Ionic radii for common ions and their corresponding atomic radii (Å) [23].

Cation	Ionic Radius (nm)	Anion	Ionic Radius (nm)
Al^{3+}	0.053	Br^{-}	0.196
Ba^{2+}	0.136	Cl^{-}	0.181
Ca^{2+}	0.100	F^{-}	0.133
Cs^{+}	0.170	I^{-}	0.220
Fe^{2+}	0.077	O^{2-}	0.140
Fe^{3+}	0.069	S^{2-}	0.184
K^{+}	0.138		
Mg^{2+}	0.072		
Mn^{2+}	0.067		
Na^{+}	0.102		
Ni^{2+}	0.069		
Si^{4+}	0.040		
Ti^{4+}	0.061		

Figure 64. Ionic Radii for Several Cations and Anions (for a Coordination Number of 6) [24].

Paying particular attention to Li^{+} and Ni^{2+}, it is clear that they have almost the same size ionic radius. The only difference between LiCl and $NiCl_2$ is the extra Cl^{-}, for the Ni salt. More than likely, the large increase in magnitude of the $NiCl_2$ output is due to anion effects. Generally, anion effects are ignored in the literature when talking about IPMCs and their operation. K. Farinholt and D. Leo [20] offer insight into the effects that different ionic species play on charge sensing in IPMCs. K. Farinholt and D. Leo [20] offer a model based on two field equations

$$\mathbf{E} = \frac{\mathbf{D}}{\mathscr{K}_e} = -\nabla\phi \quad , \quad \nabla \cdot \mathbf{D} = \rho = F(C^+ - C^-)$$

, and a continuity equation

$$\nabla \cdot \mathbf{J} = -\frac{\partial C^+}{\partial t} \quad \text{where} \quad J = -d\left(\nabla C^+ + \frac{C^+ F}{RT}\nabla\phi + \frac{C^+ \Delta V}{RT}\nabla \mathbf{p}\right) + C^+ \mathbf{v}$$

(previously introduced by Nemat-Nasser and Li, 2000) [20]. The terms of interest are: E, electric field (V/m), D, electric displacement (C/m^2), ρ, charge density (C/m^3), F, Faraday's constant-96,487 (C/mol), C^+ and C^-, cation and anion concentration (mol/m^3), J, current flux density (A/m^2), and d, diffusion coefficient (m^2/s). From these, it is clear that the anion and cation along with their

diffusivities play a role in the operation of IPMCs, being that they are ionic conductors. While full understanding of these equations is not necessary for the work presented here, they do speak to possible reasons for the difference in magnitude of the LiCl and $NiCl_2$ voltage outputs and open the door for future work. With that in mind the data suggests, that the anion may play a large role in how IPMCs react to a mechanical deformation and why metal salts like LiCl, NaCl and the like, with a 1:1 ratio of cation to anion, are the most common reported. The complexity added due to anion effects when using the $NiCl_2$ may be tolerable since the voltage output is increased by almost an order of magnitude. The increased magnitude of the voltage output when using $NiCl_2$ yields a more sensitive response. $NiCl_2$ and other metal salts with a ratio of anion to cation different than 1:1 would be an interesting area for future research.

The DI water surprisingly responded better than any of the other three liquids discussed here with limited drawbacks. One drawback is that it also displays an increased sensitivity on one side (not a completely reversible response). In this case, the normal polarity side has a slightly higher output than the reversed polarity side. The grouping of voltage data however, is extremely tight with the four runs per polarity almost completely identical. This is extremely exciting and shows great promise for actual implementation of these materials as sensors. The idea that these materials could be utilized with something as safe as water facilitating their response is potentially revolutionary for the field.

The $NiCl_2$ compression test is perhaps the most promising of any of the data presented. It was previously thought that in order to achieve a measurable voltage output, a significant bending radius of the material was necessary. The compression of the IPMC across it's thickness in the presence of the $NiCl_2$ electrolyte and the size of the voltage output data suggests significant bending is not necessary. Not only is the voltage output measurable, it has a higher

magnitude, 4.714 mV and -5.595 mV (good reversibility), than any of the other runs for the bending scenario. This is extremely important for IPMCs as tactile sensors as it could significantly reduce the necessary foot print for an actual sensor. Specifically, IPMCs could be scaled down much smaller than would have been previously thought possible under a bending operation. The data displays a slightly larger spread than under the bending scenario, but this is to be expected with the rate at which the load was applied (30 mm/min) for the small distance the material was compressed (~.9mm). Obtaining a measurable voltage response under this type of loading scenario and the speeds of application is even more beneficial than the sensitivity observed since it shows promise for a quick response time.

The decreased variation in the $NiCl_2$ data as time increased, would suggest that each liquid may have a necessary incubation, or equilibrium time. For every liquid there may be inherent tradeoffs, or more simply, just certain protocols to follow, such as allowing the material adequate time to equilibrate. In summary, the LiCl and $NiSO_4$ displayed better repeatability than the $NiCl_2$ with a constantly increasing load. From an accuracy standpoint, that would put them higher on the list for use with IPMCs as sensors. The DI water, however, shows better consistency and a higher output meaning more accurate and sensitive response. These results would suggest that, of the liquids tested for a constant force input, the DI water performed the best since it exhibited a measureable and fairly consistent response due to a constantly increasing force input. With DI water as the "ionic" liquid, IPMCs are looking promising as materials for precision tactile sensing.

The cyclic data, which was evaluated to determine the feasibility of IPMCs as "simple" binary touch sensors, as proposed by L.D. Harmon [21], gives us another piece of the puzzle. Insight into the cyclic repeatability of the material and which of the electrolytes tested yield the

best results can be realized by the data presented here. The shape of the voltage output due to the applied load, also provides insight into the rise and fall time response of the material, concerning each liquid.

Similar to the constant data, the LiCl cyclic data displayed the same positive voltage response for reversed polarity and negative voltage response for normal polarity. Again, the magnitude of the output was small in comparison to $NiCl_2$ and DI water. As seen in Figure 56-59 along with Figures 228-243 Appendix G, the curve of the voltage output graphs for LiCl showed that it had a fairly quick response with the rise and fall being similar. Though the scale of the response was small, there was still a measurable change, validating LiCl as a usable liquid for the binary sensor scenario.

The $NiSO_4$ results, just like the LiCl results, were similar to the results found for a constantly increasing load, where the magnitude of the voltage output was small in comparison to the $NiCl_2$ and DI water and also had a negative voltage response for a normal polarity. The magnitude of the output was also slightly larger than that of the LiCl and only slightly noisier, just as in the $NiSO_4$ constant data. The magnitude of the binary grouping was again on the same scale as the LiCl, but did display a definite grouping for the 3 cycles and therefore is also feasible for the application as a "simple" binary touch sensor [21].

The $NiCl_2$ had a much higher magnitude of voltage output in comparison to the LiCl and the $NiSO_4$, which makes it attractive from a sensitivity standpoint. The voltage response also very closely follows the applied load imposed on the material. Looking closer at the graph (Figure 65), it can be seen that the rising slope as load is being applied is almost identical to the rising voltage slope resulting from this load.

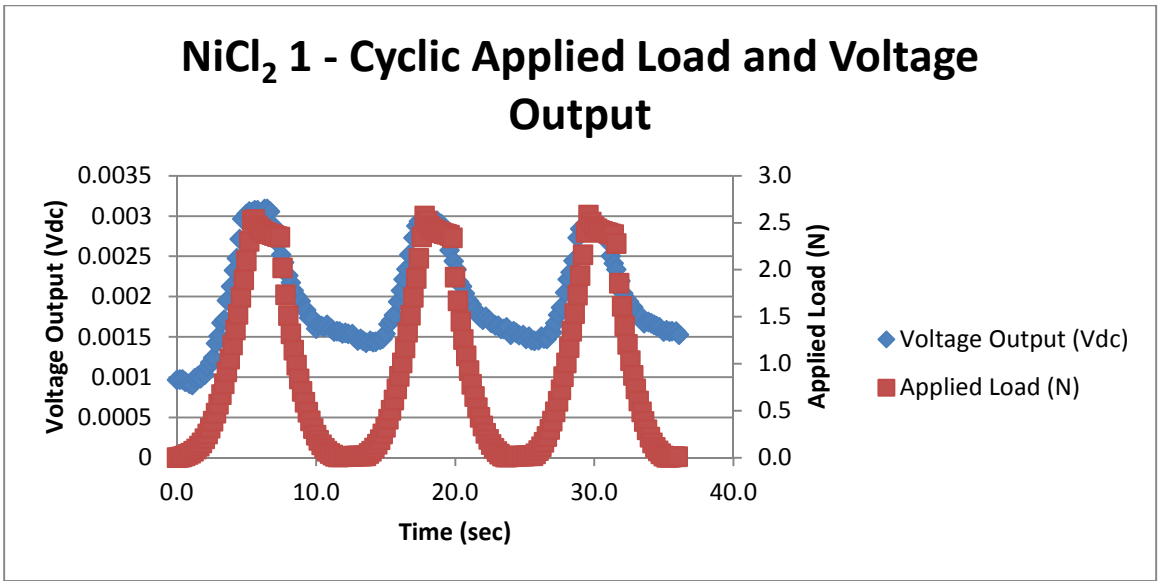

Figure 65. Comparison of applied load and resulting voltage slope for normal polarity $NiCl_2$ electrolyte cyclic load scenario

Interestingly though, the voltage slope as the load is being applied, differs from the slope as the load is being removed. This tells us that the material has a much faster and more accurate response as load is being applied, but that as the load is removed, the response is slower and perhaps less precise at very low levels of force. Since the 3 cycles had a very close maximum voltage output (small hysteresis), that was larger in magnitude than the LiCl and $NiSO_4$, $NiCl_2$ is an extremely promising electrolyte for binary sensing.

The DI water again exhibits an attractive response with a large magnitude of voltage output and tightly grouped data. The response time based on the slope of the voltage rise is slightly less than that of the $NiCl_2$. The fall time however is markedly slower than that of the $NiCl_2$ with more of a dome shape than concave down curve, which was observed for the $NiCl_2$ (Figure 66).

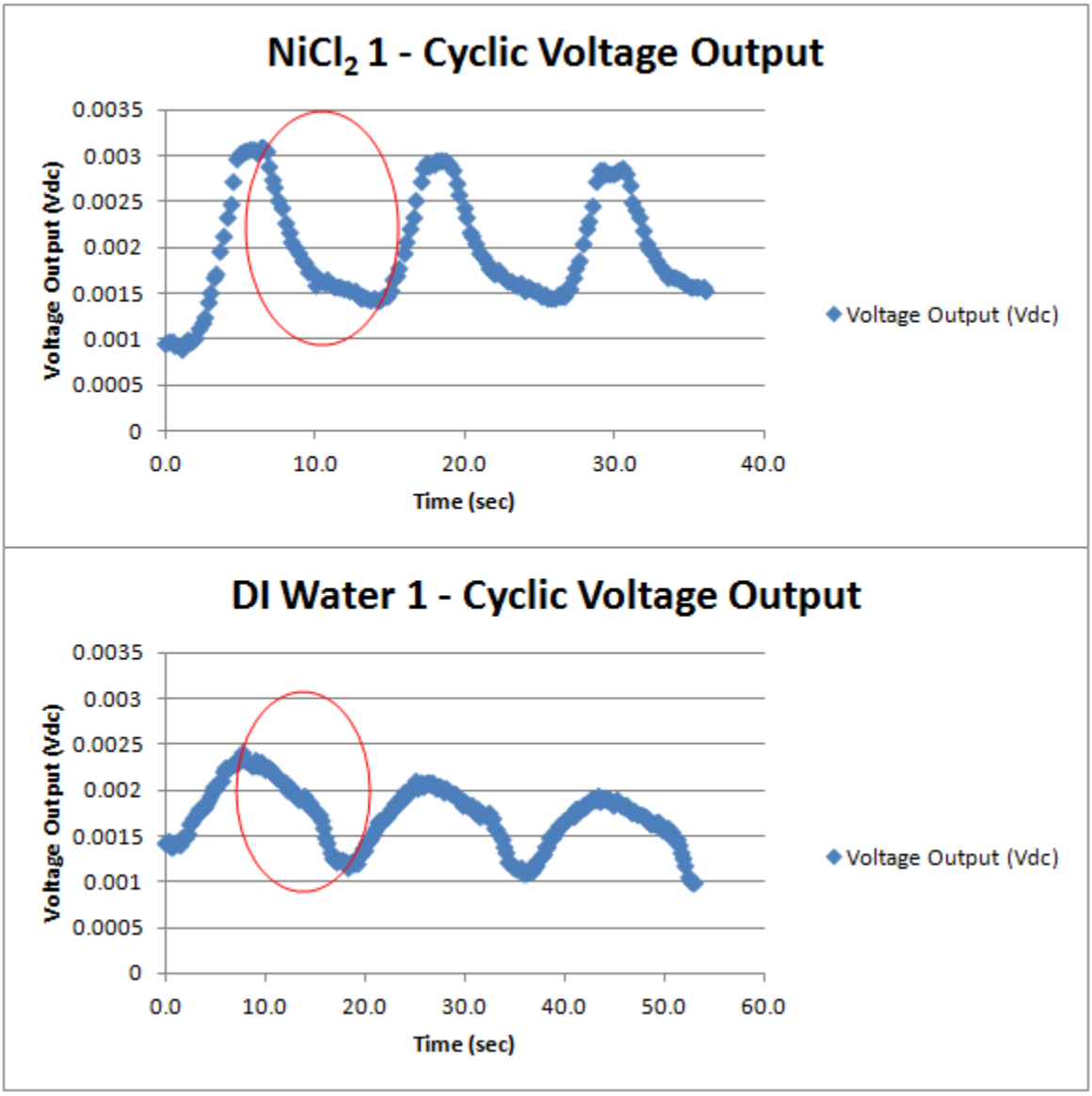

Figure 66. Comparison of $NiCl_2$ and DI water run 1 slope of voltage output due to removal of load

Looking at the DI water data from a maximum and minimum ("binary") perspective, it is clear that the magnitude of the output is not quite as large as that observed for $NiCl_2$, but still higher than that of the LiCl and $NiSO_4$. Not surprisingly, there exists a good deal of hysteresis with the DI water, a known drawback to IPMCs. However, the data grouping is concise and exhibits a definite measureable change for applied load and no applied load.

The $NiCl_2$ compression data, similar to the constant data, had a larger magnitude of voltage output than the other runs. The results also exhibited a decrease in maximum voltage

output as the run number increased, with a greater magnitude however, than the other cyclic runs. Though the magnitude of output decreased, the data became more tightly grouped (varied less from run to run). This could mean that the material is more sensitive to a necessary incubation time under this type of loading, or that some degree of initial cycling of the material is necessary for a more repeatable voltage response. Details of the further investigation of this material pre-treatment will be discussed in the future work section. The curve of the voltage output for both constant and cyclic loading scenarios look quite similar to the curve of a charging capacitor. As was mentioned earlier, IPMCs are said to be exhibit capacitive characteristics and could be the mechanism for this type of output and should also be further investigated.

The results for all of the liquids, show a much stronger correlation between the displacement of the material and the voltage output. Which could be a material property, but is more than likely the result of the input from the Instron®. Recall that, the load was applied at a rate of 30 mm/min, meaning the Instron® was being driven by a dimension change, not a force change due to the capabilities of the equipment. The voltage outputs more closely following the displacement is a good thing, it suggests that IPMCs may be sensitive to the form of mechanical stimulus imposed on them. If the experiment were repeated with equipment capable of inducing a force change with time, it is likely that the IPMC's voltage output would more closely resemble the force, rather than the displacement, and would be an excellent area for future research.

The difference in slopes of the voltage outputs and the applied loads and displacements for each electrolyte is to be expected, as it is well known that one of the drawbacks of IPMCs is their slow reaction time, since their voltage output results from the diffusion of ions. An averaging of the data may drastically clean up the response of the material and could be a useful tool in the implementation of control algorithms when utilizing this material as a precision tactile

sensor. The change in sign of the voltage due to difference in polarity of the measurement equipment means that these materials are not only capable of sensing small applied loads, but also the direction in which they are applied, illustrating the reversibility of the material.

Future Work

The future scope of this research and possible avenues of advancement is limited only by the imagination. Merely from a sensing perspective, IPMCs could find applications in a vast number of industries. In the bio-medical field, IPMCs could be used as an improvement of the tactile sensing ability of surgical robots or even as a prosthetic skin someday. One way of doing this could be using the IPMCs in a vertical array similar to Figure 67. The IPMC array, shown in Figure 67, could be used for applications where it is necessary to sense small forces. Material deformation and resultant electrical output would result from either vertical or transverse loading of the top edge.

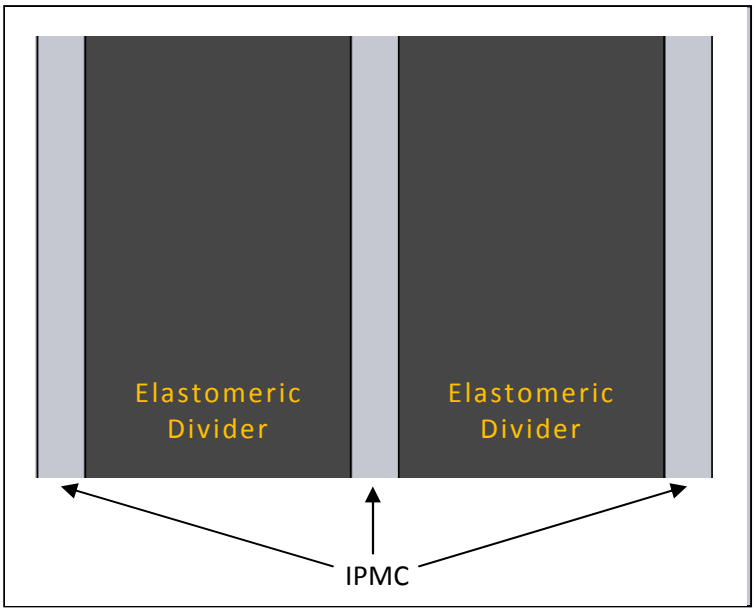

Figure 67. IPMC vertical tactile sensing array

In the environmental sector, they could be implemented as seismic activity sensors used to predict events like earthquakes and tsunamis for early warning systems. An aquatic

application might entail tidal and current change detection. In robotics, they could be used as a smart skin for humanoid robot design. Aerospace applications could utilize IPMC sensors as part of a closed loop system for optimal angle of attack, meaning the aircraft could sense the slightest changes in surrounding air conditions and continually adapt. These are just a few conceptual examples, the collected data shows progress towards these possibilities.

From the results, it is clear that the voltage data tends to more closely follow the displacement of the center of the membrane, as opposed to the force from that displacement. In order to determine whether the material can be conclusively correlated to force, a machine similar to the one used here should be setup to induce a force change with time in a similar manner to the displacement rate of 30 mm/min presented here.

It was also observed that the LiCl and $NiSO_4$ exhibited an opposite voltage response (in comparison to the $NiCl_2$ and DI water), when the voltage was read under normal polarity conditions (negative voltage output). It is believed that this could be due to anion effects but is un-clear whether or not this is indeed the case. This opposite response should be further characterized and investigated to determine its role in the operation of IPMCs as sensors.

In addition, the specific roles that the anion and cations play in the operation of IPMCs as sensors should be evaluated in great detail. The diffusivities of the individual ions and the effect diffusivity will have on the voltage response, particularly whether the longer diffusion time leads to a slower voltage response time, will likely determine the role that each plays on the voltage output. Specifically in reference to whether or not the difference in magnitude of the LiCl and $NiCl_2$ voltage outputs can be attributed to these diffusivities. Particular attention should be noted on how the different ions and their diffusivities could affect the slopes of the cyclic voltage data (response of the sensor).

In reference to the LiCl and $NiCl_2$ solutions, the obvious difference between the two is the molar ratio of cation to anion, where LiCl is a 1:1 and the $NiCl_2$ is a 1:2. Further investigation into this ratio and the effect it might have played on the difference in magnitude of the voltage outputs, would bring a greater understanding of the reason for the disparity in voltage outputs since it is generally reported that IPMCs attribute their voltage response (from mechanical deformation) to cation migration. Other ratios of cation to anion could also be investigated to gain a greater overall perspective of the effect these ratios might have on the voltage response of IPMCs.

Shahinpoor et. al [9] reported on the difference in sensitivity of the side of the membrane in which the deformation was being applied and suggested it as being a basic property of IPMCs. Since the results presented here suggest that this may be more dependent on the electrolyte chosen, further characterization of this claim should be investigated in depth to determine its validity. This is of relatively high importance as a completely reversible response from a sensor is a sought after property.

Looking closely at the summaries of the data, it becomes apparent that as time went on through testing, the voltage outputs seemed to decrease in magnitude, but became more tightly consolidated. The $NiCl_2$ appeared to most prominently exhibit this response. It is believed that this could be due to a necessary incubation time in the electrolyte not being met and should be evaluated to determine if one exists. A design of experiments (DOE) could be set up to test incubation time and its effect on the voltage output, both in magnitude and distribution. This is of high importance because an accurate and repeatable response is a necessity of any high quality sensor.

The $NiSO_4$ metal salt was evaluated to determine its feasibility for operation with IPMCs as sensors for the proposition of a non-chloride form of metal salt, which would hopefully mitigate the need for noble metals as electrodes. The magnitude of the voltage output was much smaller than that of its chloride counterpart. The response also resembled that of a higher order polynomial with a decaying amplitude. It is unknown why the sulfate form of the nickel salt responds in this way and could be why the chloride forms of metal salts are used over their sulfate counterparts and should be further investigated.

There is a great deal of further characterization to be performed on the liquids presented here and the role they play on IPMCs as sensors. The scale and distribution of their voltage outputs and the sign of their response (negative or positive across the horizontal axis) will need extensive validation for IPMCs and their applications as tactile sensors to be fully realized.

The compression of the IPMC across its thickness in the presence of the $NiCl_2$ electrolyte begins to challenge the previous understanding that IPMCs attribute their voltage output to the bending radius of the material. Other metal salts should be evaluated in this loading scenario along with a characterization of incubation time of the material in these liquids. The data presented on this topic is of great curiosity along with great excitement of what it could mean from a packaging perspective for this material in sensing applications.

In addition to further investigation of the trends the data displays, basic material properties of the IPMCs themselves is a large area for future work. An accurate Young's Modulus would be very beneficial for proper modeling of the material. This may not be obtainable though. There is no standardized recipe for the construction of IPMCs and therefore one batch of IPMCs to the next could have greatly different plating thicknesses and diffusion depths depending on the method used for electrode deposition. The electroding process itself

and the possible resulting sensitization to the Nafion® could yield vastly different material stiffness.

Other metals such as nickel and cobalt could be evaluated for the use as electrodes to replace the expensive noble metal Pt on the Nafion®. Pt is extremely expensive and a suitable replacement would greatly reduce the cost of IPMCs and increase their viability as sensors. Pt is also highly conductive and the determination of how large a role conductivity plays on the performance of IPMCs would also be a valuable study.

Along with other metals as electrode materials, the electrodes and their surface condition is another area of apparent debate. M. Shahinpoor and K. J. Kim [2] and Punning et. al. [17], have contradicting ideas on the condition of the electrode and how it affects the operation of IPMCs. From an actuation perspective, one side argues that a thicker more highly conductive electrode yields a larger tip displacement with a smaller voltage requirement. On the other hand, some suggest that the thicker the electrode the stiffer the material and therefore the higher the necessary voltage for actuation (or in terms of sensing, the higher the required force input for voltage output). In either case, there is data to support the claims, suggesting something is possibly being overlooked. In terms of sensing, the role that the thickness of the plating, penetration depth into the Nafion® and degree of fractionation effect the voltage output is unknown and should be further investigated.

Conclusion

The overall objective of the research presented was to evaluate IPMCs as precision tactile sensors. The goal was to determine if a measureable voltage change could be observed in response to a small force input. Two load profiles were implemented to evaluate the voltage response of IPMCs due to a small force input. A constant rate increase of 30 mm/min up to a

load of 2.5 N along with a 3 cycle cyclic load of 2.5 N applied and removed at the same 30 mm/min rate with 2 second holds and 0 N and 2.5 N. Normal and reversed polarity voltage profiles were collected to correlate with literature sources for determining if one side of the membrane was more sensitive than another. Characterization of the sensitivity of each side of the IPMC was done partly by characterizing four different electrolytes (LiCl, $NiCl_2$, $NiSO_4$, and DI water) and their applicability to this application. The IPMCs were fixtured in a 3 point bend scenario by clamping both ends and deflecting the center of the membrane using an Instron® tensile testing machine. The applied load and displacement along with the voltage output resulting from this input (all with respect to time in seconds) were collected.

The results showed that the IPMC did indeed result in a measureable change resulting from a small force input. Each liquid evaluated resulted in measureable voltage changes confirming their applicability for sensing. The results however showed much more than just their justification for use with IPMCs as sensors. The distribution of the data and resulting trends open the door to a plethora of future research. The LiCl had a fast response time, evident from the sinusoidal cyclic response of the voltage output. The $NiSO_4$ exhibited a very similar response with a slightly larger voltage output, but also an increase in hysteresis. The $NiCl_2$ displayed a very large voltage output, but a good deal of hysteresis and less of a sinusoidal response (smaller voltage slope upon removal of the load) than the LiCl and $NiSO_4$. The DI water had the tightest grouping of data for the constant scenario and the smallest amount of hysteresis under cyclic loading conditions along with a large voltage change (good sensitivity). The cyclic response, however, was the least sinusoidal of any of the 4 liquids tested with a slow voltage response as the load was removed.

The compression across the membranes thickness in the presence of the $NiCl_2$ salts greatly strengthened the validity of force to voltage characterization of the IPMCs as tactile sensors. This control experiment, however, raises some question as to exactly what the activation mechanisms are for the voltage output of the material due to mechanical input. The scale of the voltage output was much higher than expected for this type of loading scenario and shows even more promise for IPMCs as precision tactile sensors.

The purpose of the research presented here, was to determine the viability of IPMCs as precision tactile sensors. To aid in this, the characterization of different electrolytes and the effect each liquid had on the material under this type of application was also performed. The data collected, proves the feasibility of using IPMCs as tactile sensors and, with continued research, IPMCs could be used as precision tactile sensors in the near future.

References

[1] Sia Nemat-Nasser, “Electrochemomechanics of Ionic Polymer-Metal Composites,” in *Springer Handbook of Experimental Solid Mechanics, Sharpe* ed. New York, Springer Science+Business Media, 2008, ch. *8*, sec. *8.1,2,5*, pp. *187–199.*

[2] M. Shahinpoor and K. J. Kim. “Ionic Polymer-metal composites: I. Fundamentals.” Smart Materials And Structures, vol. 10, pp. 819-829, Aug. 2001.

[3] Yoseph Bar-Cohen et al. “Characterization of the Electromechanical Properties of EAP materials,” in *Proc. EAPAD, SPIE's Annu. Int. Symp. on Smart Structures and Materials*, Newport CA, 5-8 March, 2001, Paper No. 4329-43.

[4] ASM International, “Bath Composition and Characteristics,” in *Electroless Nickel Plating,* Materials Park, OH, ASM International, 2011.

[5] Wikipedia. (2011, April 12). *Ion Implantation Networks* [Online]. Available: http://en.wikipedia.org/wiki/Ion_implantation

[6] Yoseph Bar-Cohen et al. (2011, May). *Characterization of the Electromechanical Properties of Ionomeric Polymer-Metal Composites (IPMC)* [Online]. Available: http://trs-new.jpl.nasa.gov/dspace/bitstream/2014/11866/1/02-0550.pdf

[7] Matthew D. Bennett and Donald J. Leo. "Electrolytes as stable solvents for ionic polymer transducers." *Sensors and Actuators A,* vol. 115, pp. 79-90, May 2004.

[8] K.J. Kim. "Ionic Polymer-Metal Composites as a New Actuator and Transducer Material" in *Electroactive Polymers for Robotic Applications*, 1st ed,, vol. 1. K.J. Kim and S. Tadokoro, Ed. London: Springer-Verlag, 2007, pp. 153-164.

[9] M. Shahinpoor et. al. "Ionic Polymer-Metal Composites (IPMC) As Biomimetic Sensors and Actuators-Artificial Muscles." in *Proc. of SPIE's 5th Annu. Int. Symp. on Smart Structures and Materials*., San Diego., CA, 1998, pp. 1-21.

[10] N. Maalej et. al "A Conductive Polymer Pressure Sensor." in *IEEE Engineering in Medicine & Biology Society 10th Annu. Int. Conf.*, 1988.

[11] N. Maalej et. al "A Conductive Polymer Pressure Sensor Array." in *IEEE Engineering in Medicine & Biology Society 10th Annu. Int. Conf.*, 1989.

[12] Masato Suzuki et. al. "Development of Tactile Sensor Using Thin Film Made of Poly-Urethane And Its Characterization." in *World Automation Congr.*, Suita, Osaka, Japan 2010.

[13] Pen-Cheng Wang et. al. "Fabrication and Characterization of All-Polymer Pressure Sensors Integrated with Transduction Modules Based on Conducting Polymers." in *Microsystems*

Packaging Assembly and Circuits Technology Conf. (IMPACT) 5th Int., 2010, Taipei, Taiwan, pp. 1-4.

[14] G. Kofod and Sommer-Larsen, "Finite-Eleasticity Models of Actuation," in Dielectric Elastomers as Electromechanical Transducers: Fundamentals, Materials, Devices, Models and Applications of an Emerging Electroactive Polymer Technology, F. Carpi, et al., Eds., ed: Elsevier, 2008.

[15] ELNA America Inc. (2011, Aug 1). *Introduction to Aluminum Electrolytic Capacitors*[Online]. Available: http://www.elna-america.com/tech_al_principles.php

[16] Andres Punning et. al. "A self-Sensing ion conducting polymer metal composite (IPMC) actuator." in *Sensors and Actuators A,* vol. 136, pp. 656-664, July 2006.

[17] A. Punning et. al. "Surface resistance experiments with IPMC sensors and actuators." in *Sensors and Actuators A,* vol. 133, pp. 200-209, November 2005

[18] C. Bonomo, L. Fortuna, P. Giannone and S. Graziani, "A method to characterize the deformation of an IPMC sensing membrane," *Sensors and Actuators A,* Vols. 123-124, pp. 146-154, 2005.

[19] J. K. Park, J. Spano, R. B. Moore and S. Wi, "Counterion motions and thermal ordering effects in perfluorosulfonate ionomers probed by solid-state NMR," *Polymer,* vol. 50, pp. 5720-5727, 2009.

[20] K. Farinholt and D. J. Leo, "Modeling of electromechanical charge sensing in ionic polymer transducers," *Mechanics of Materials,* vol. 36, pp. 421-433, 2004.

[21] L. D. Harmon, "Automated Tactile Sensing," *The International Journal of Robotics Research,* vol. 1, no. 2, pp. 3-32, 1982.

[22] Dan Liu, "Durability Study of Proton Exchange Membrane Fuel Cells via Experimental Investigations and Mathematical Modeling," Ph.D. dissertation, Dept. Macromolecular Sci & Eng, Virginia Poly-tech, Blacksburg, 2006

[23] Pearson, "TABLES FROM THE TEXTBOOK," Pearson, 2011. [Online]. Available: http://wps.pearsoncustom.com/wps/media/objects/3033/3106029/fg07_07.jpg. [Accessed 21 May 2012].

[24] J. W. D. Callister, "FUNDAMENTALS OF MATERIALS SCIENCE AND ENGINEERING," John Wiley & Sons, Inc., Utah, 2001.

[25] K. Oguro, "Preparation Procedure Ion-Exchange Polymer Metal Composites (IPMC) Membranes," JPL Nasa, [Online]. Available: http://ndeaa.jpl.nasa.gov/nasa-nde/lommas/eap/IPMC_PrepProcedure.htm. [Accessed September 2012].

Appendices

Appendix A

Preparation of Chemicals for Material Production

Preparation of 2 N HCl

$$2\ \frac{\text{mol}}{\text{Liter}} \qquad 36.5\ \frac{\text{g}}{\text{mol}}\ \text{MW} \qquad 38\% \quad \text{Assay}$$

Find number of grams required

$$36.5\ \frac{\text{g}}{\text{mol}}\ \text{x}\ \ 2\ \frac{\text{mol}}{\text{L}}\ \text{x}\ \ 1\ \ \text{L}\ \ =\ \ 73\ \ \text{g}\ \ \text{HCL required}$$

FW — Normality — Soln Amnt

Correct for Impure Stock

$$1.19\ \frac{\text{g}}{\text{mL}}\ \text{x}\ \ 0.38\ \ =\ \ 0.4522\ \frac{\text{g HCl}}{\text{mL}}$$

SG — Assay

$$\frac{73\ \ \text{g HCl}}{0.4522\ \ \text{g HCl/mL}}\ =\ 161.43\ \ \text{mL HCl}$$

The calculations above were performed to determine the amount of water that needed to be added to 38% stock solution of hydrochloric acid. 2 N means 2 moles of solute per liter of solution. Hydrochloric acid has a molecular weight of 36.5 g/mol and the stock solution is 38% pure. Multiplying the molecular weight of stock solution by the normality required and amount of total solution required, yields the amount in grams of hydrochloric acid required. Correcting for the fact that the stock is not 100% pure, a multiplication of the specific gravity and purity of stock (in percent where 38% is .38) gives the amount in grams of HCl per milliliter of solution.

Taking the previously calculated amount in grams of HCl required and dividing it by the amount in g/mL that our stock solution contains yields the amount in milliliters of stock HCl that must be added to water. The amount of water is determined by taking the previously input amount of 2 N solution that is required and subtracting from it the amount of HCl that is required. In this case, 161.43 mL was subtracted from 1000 mL. So for 1 L of a 2 N solution of HCl, 161.43 mL of HCl was added to 838.57 mL of DI water.

Preparation of 5% NH_4OH

5 mL of NH_4OH stock was added to 95 mL of DI water

Preparation of Platinum Ammine Complex

A tetraammineplatinum(II) chloride hydrate 98%, was purchased from Sigma-Aldrich (Cat. # 275905-1G) as the source of platinum. The recipe specifies needing >3 mg of Pt/cm^2 of membrane and 2 mg of Pt/mL of water. This implies the requirement of 93 mL of Pt solution for a 5 cm by 6 cm sized membrane. To comply with these specifications, 3.1 mg of Tetraammineplatinum(II) chloride hydrate per cm^2 was assumed necessary so 186 mg of the Tetraammineplatinum(II) chloride hydrate was added to 93 mL of DI water.

Preparation of .1 N HCl

$$0.1 \ \frac{\text{mol}}{\text{Liter}} \qquad 36.5 \ \frac{\text{g}}{\text{mol}} \ \text{MW} \qquad 38\% \quad \text{Assay}$$

Find number of grams required

$$36.5 \ \frac{\text{g}}{\text{mol}} \ \text{x} \ \ 0.1 \ \frac{\text{mol}}{\text{L}} \ \text{x} \ \ 0.5 \ \ \text{L} \ = \ 1.825 \ \ \text{g} \ \ \text{HCL required}$$

FW Normality Soln Amnt

Correct for Impure Stock

$$1.19 \frac{g}{mL} \times \underset{\text{Assay}}{0.38} = 0.4522 \frac{g\ HCl}{mL}$$

SG

$$\frac{1.825}{0.4522} \frac{g\ HCl}{g\ HCl/mL} = 4.04 \text{ mL HCl}$$

The calculations above were performed to determine the amount of water that needed to be added to 38% stock solution of hydrochloric acid to achieve .1 N. Multiplying the molecular weight of stock solution by the normality required and amount of total solution required, yields the amount in grams of hydrochloric acid required. Correcting for the fact that the stock is not 100% pure, a multiplication of the specific gravity and purity of stock (in percent where 38% is .38) gives the amount in grams of HCl per milliliter of solution. Taking the previously calculated amount in grams of HCl required and dividing it by the amount in g/mL that our stock solution contains yields the amount in milliliters of stock HCl that must be added to water. The amount of water is determined by taking the previously input amount of .1 N solution that is required and subtracting from it the amount of HCl that is required. In this case, 4.04 mL was subtracted from 500 mL. So, for 500 mL of a .1 N solution of HCl, 4.04 mL of HCl was added to 495.96 mL of DI water.

Preparation of 20% Hydrazine Hydrate Solution

$V_1C_1 = V_2C_2$

$(V_1) \times 0.55 = 35 \times 0.20$

$V_1 = 12.73$ mL of Hydrazine Stock

Add 12.73 mL of Hydrazine stock to 22.27 mL of DI water.

Preparation of 5% Hydroxylamine Hydrochloride Solution

$V_1C_1 = V_2C_2$

$(V_1) \times 0.10 = 50 \times 0.05$

$V_1 = 25.00$ mL of Hydroxylamine Stock

Add 25 mL of Hydroxylamine HCl stock to 25 mL of DI water.

Appendix B

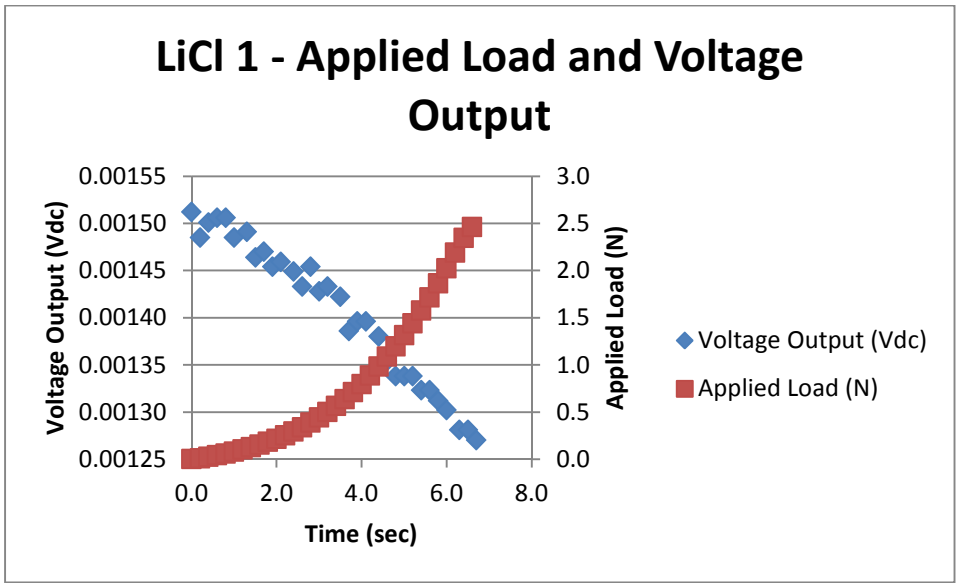

Figure 68

Trial 1 normal polarity LiCl electrolyte constant load scenario, load and raw voltage output

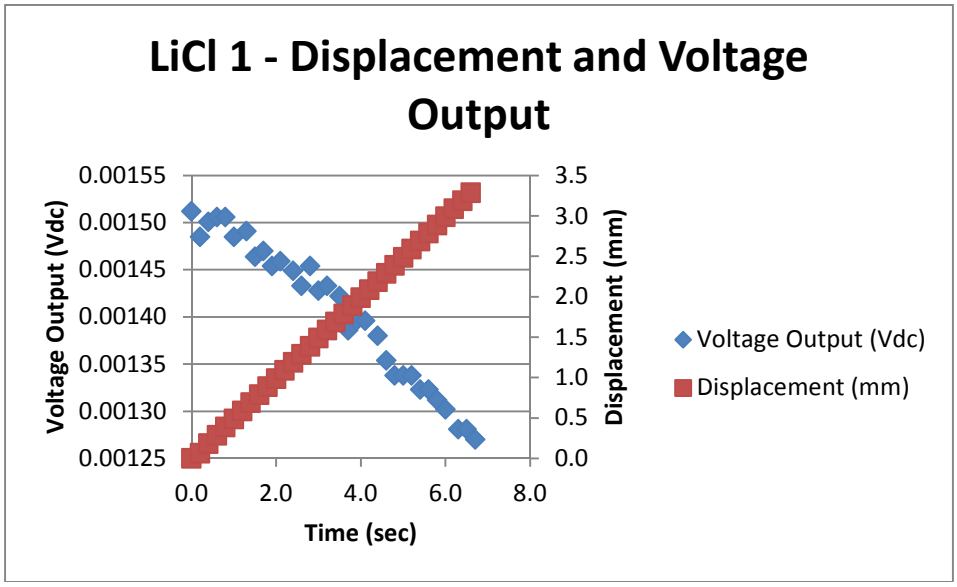

Figure 69

Trial 1 normal polarity LiCl electrolyte constant load scenario, displacement and raw voltage output

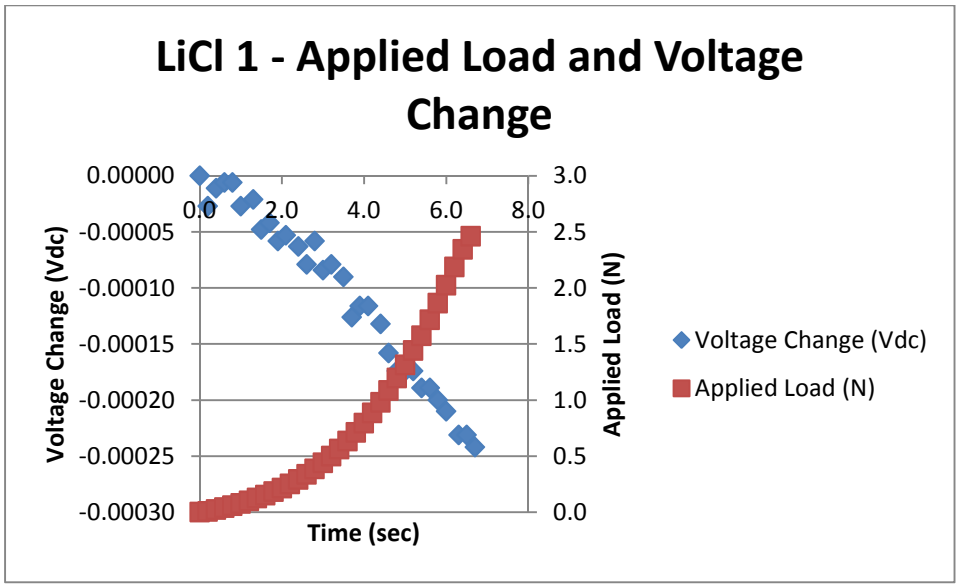

Figure 70
Trial 1 normal polarity LiCl electrolyte constant load scenario, load and voltage

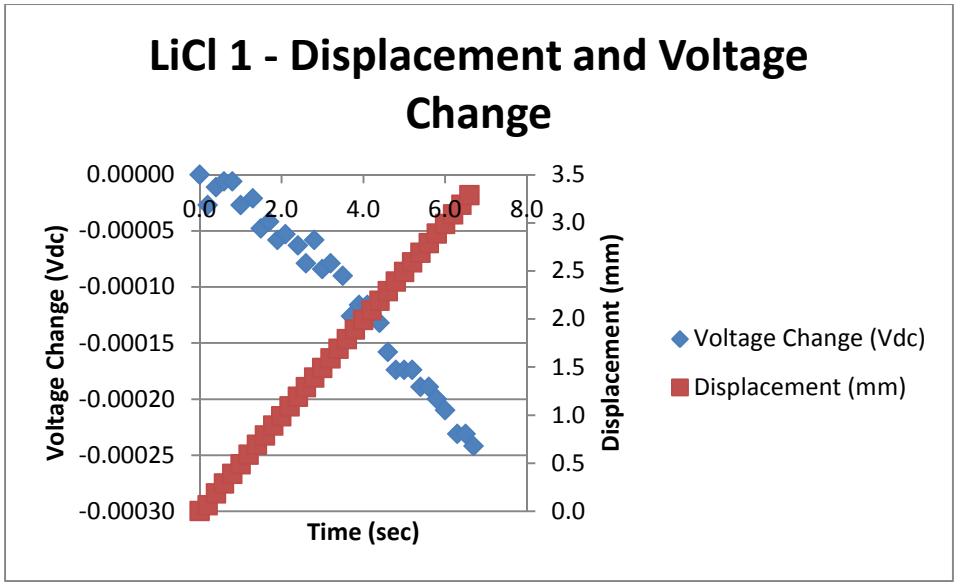

Figure 71
Trial 1 normal polarity LiCl electrolyte constant load scenario, displacement and voltage change

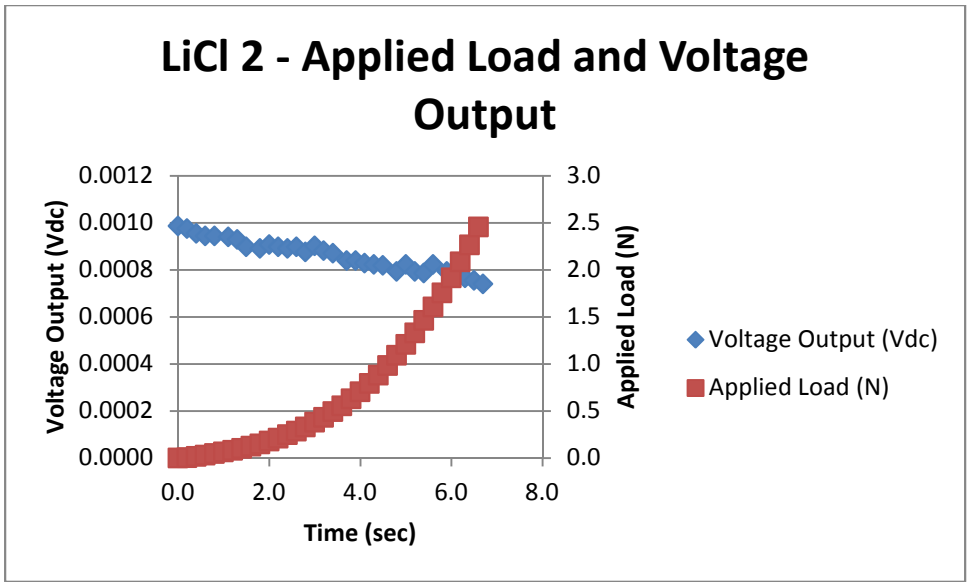

Figure 72

Trial 2 normal polarity LiCl electrolyte constant load scenario, load and raw voltage output

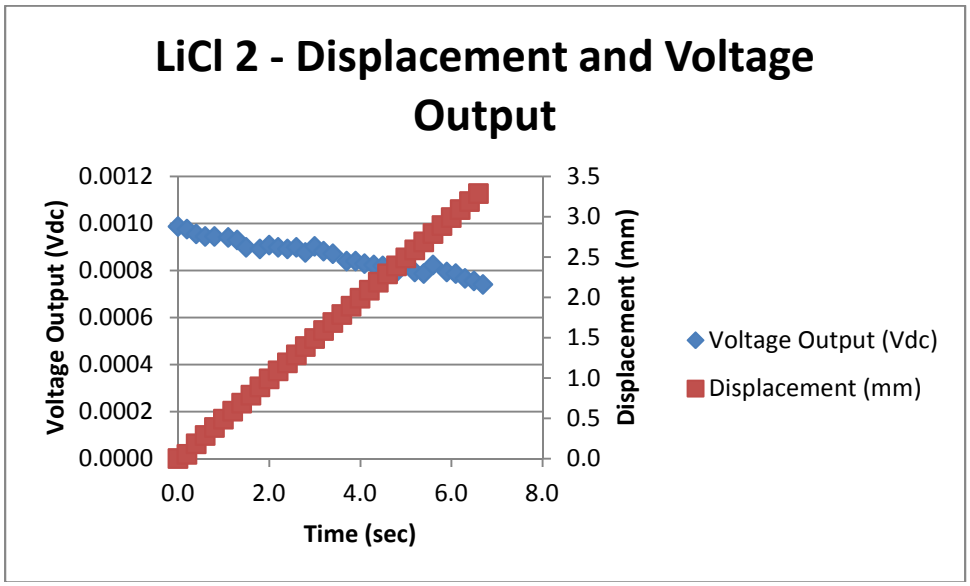

Figure 73

Trial 2 normal polarity LiCl electrolyte constant load scenario, displacement and raw voltage output

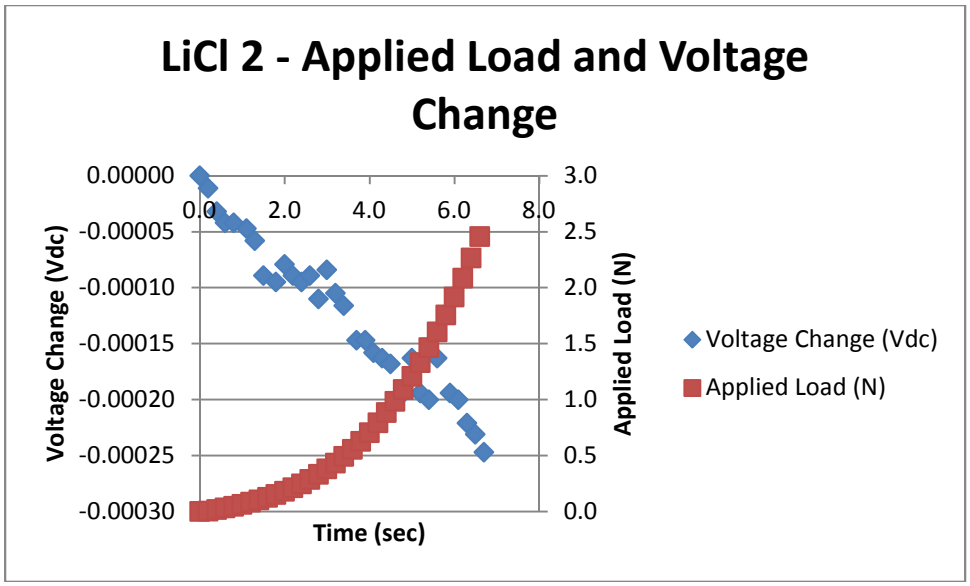

Figure 74
Trial 2 normal polarity LiCl electrolyte constant load scenario, load and voltage change

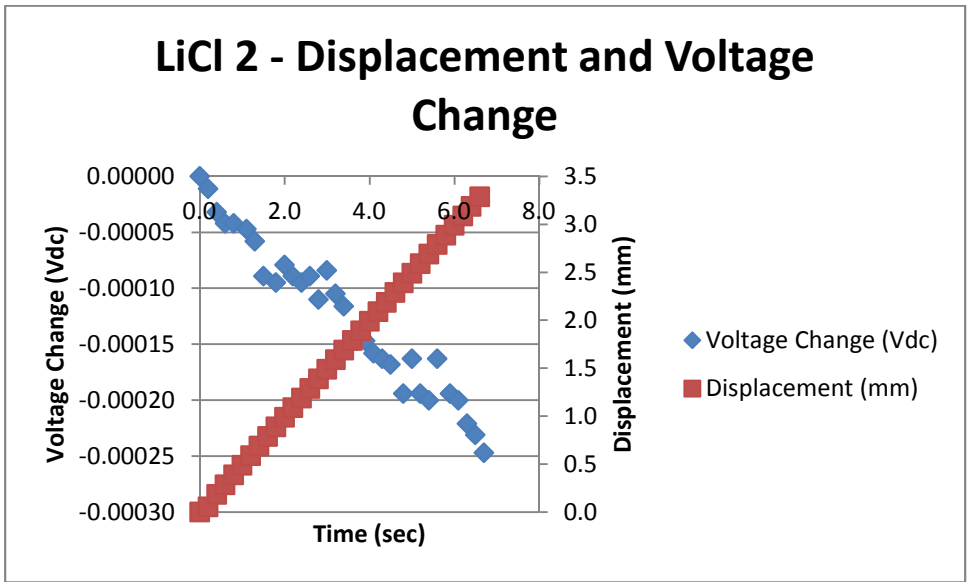

Figure 75
Trial 2 normal polarity LiCl electrolyte constant load scenario, displacement and voltage change

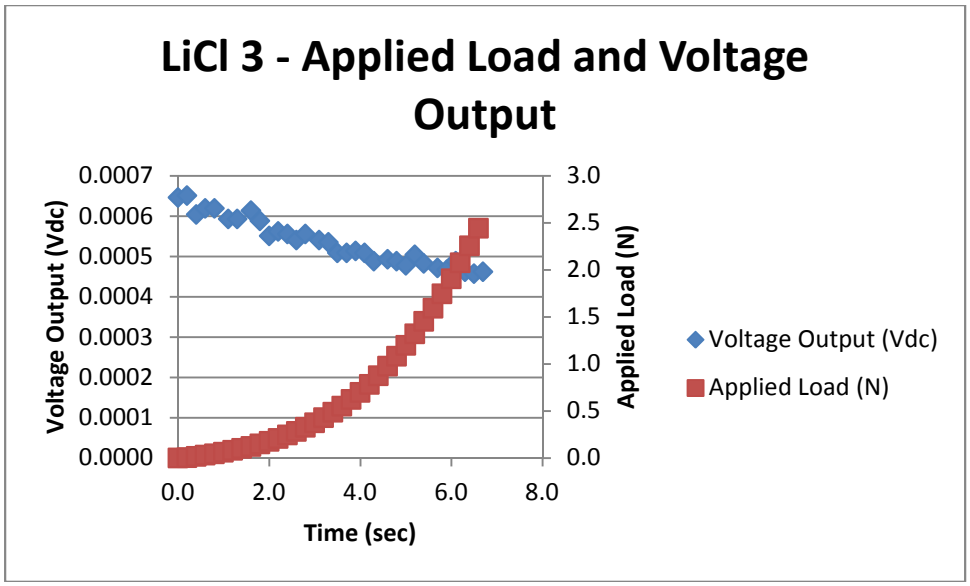

Figure 76
Trial 3 normal polarity LiCl electrolyte constant load scenario, load and raw voltage output

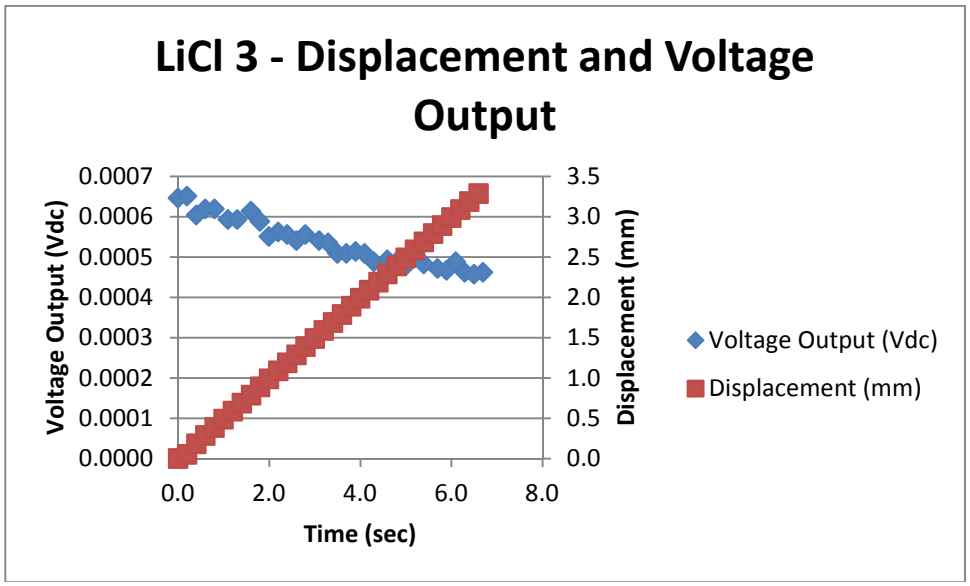

Figure 77
Trial 3 normal polarity LiCl electrolyte constant load scenario, displacement and raw voltage output

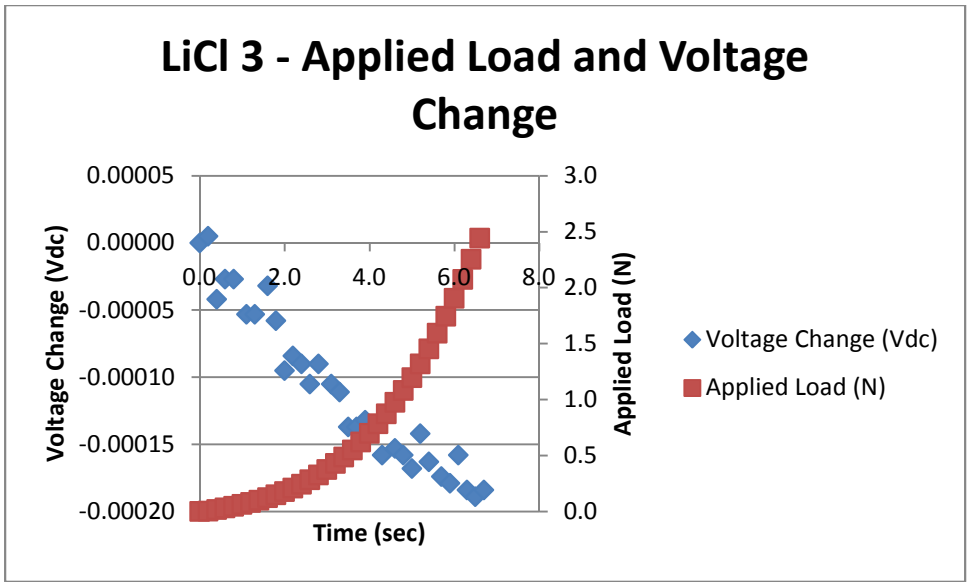

Figure 78
Trial 3 normal polarity LiCl electrolyte constant load scenario, load and voltage change

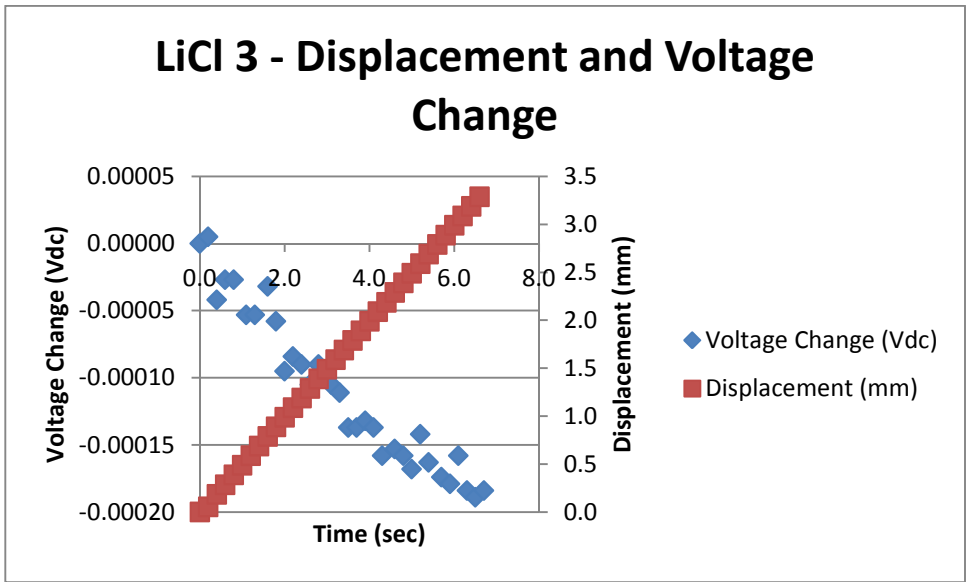

Figure 79
Trial 3 normal polarity LiCl electrolyte constant load scenario, displacement and voltage change

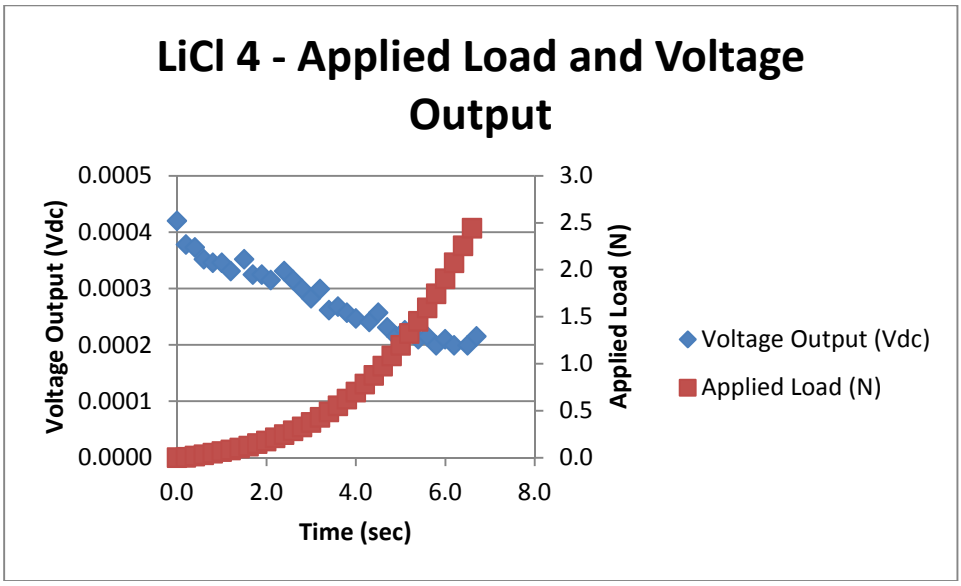

Figure 80

Trial 4 normal polarity LiCl electrolyte constant load scenario, load and raw voltage output

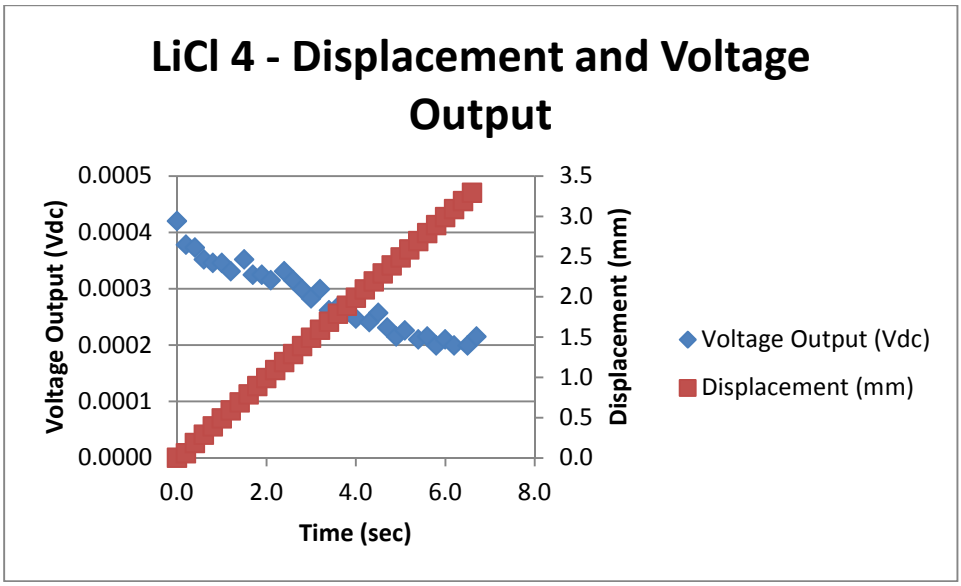

Figure 81

Trial 4 normal polarity LiCl electrolyte constant load scenario, displacement and raw voltage output

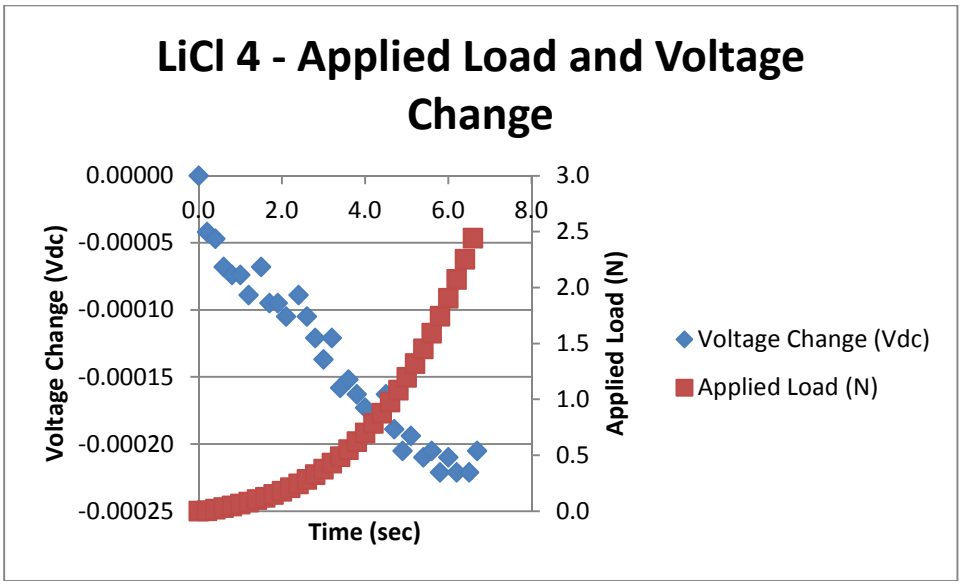

Figure 82
Trial 4 normal polarity LiCl electrolyte constant load scenario, load and voltage change

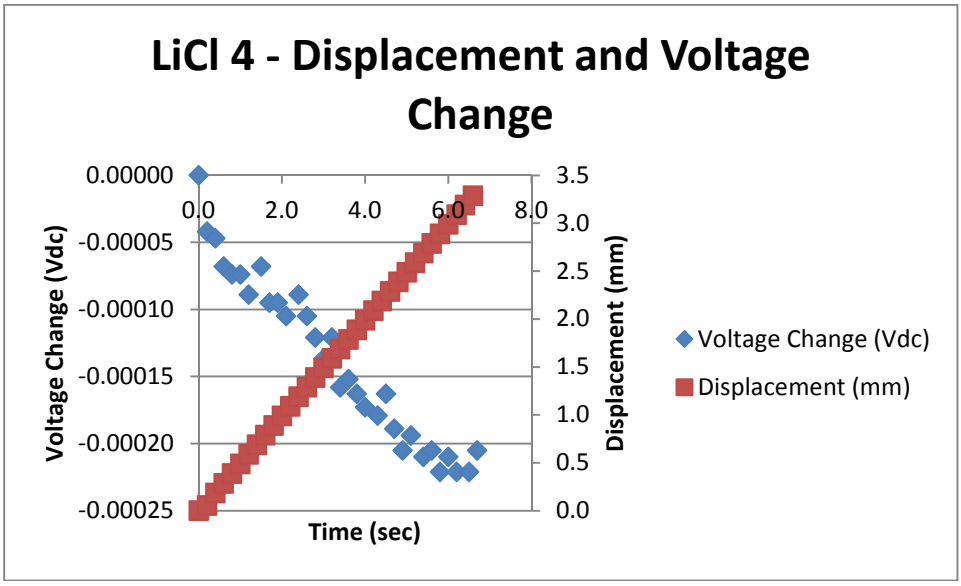

Figure 83
Trial 4 normal polarity LiCl electrolyte constant load scenario, displacement and voltage change

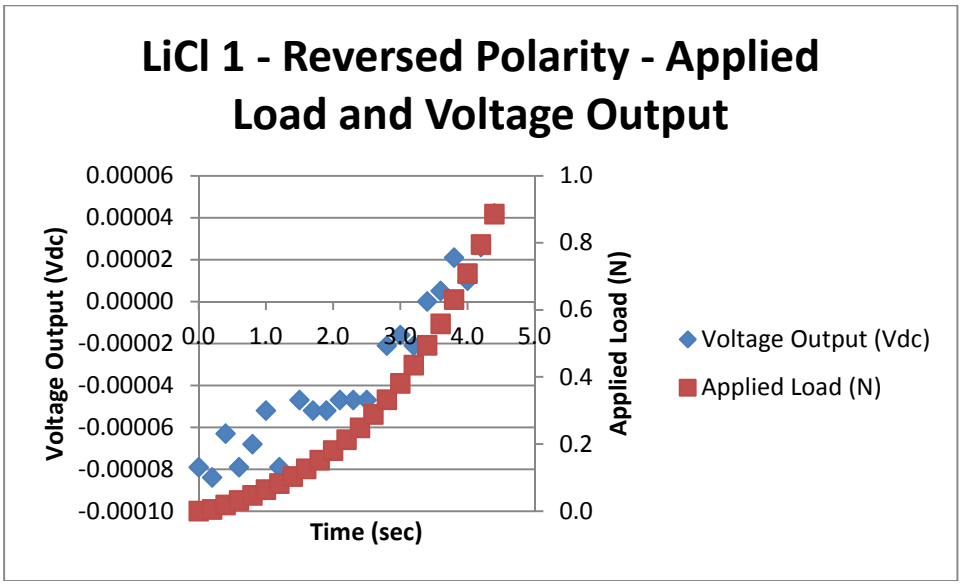

Figure 84

Trial 1 reversed polarity LiCl electrolyte constant load scenario, load and raw voltage output

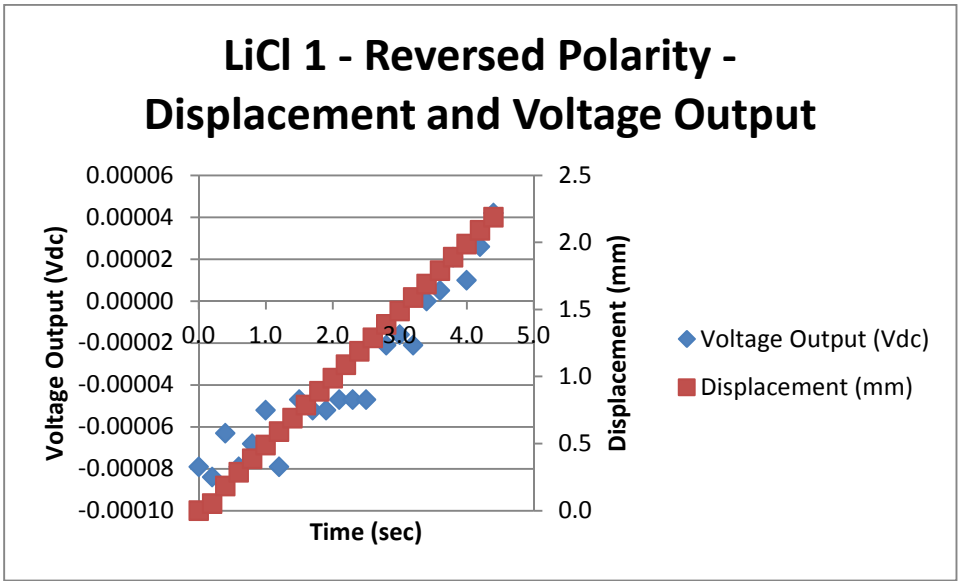

Figure 85

Trial 1 reversed polarity LiCl electrolyte constant load scenario, displacement and raw voltage output

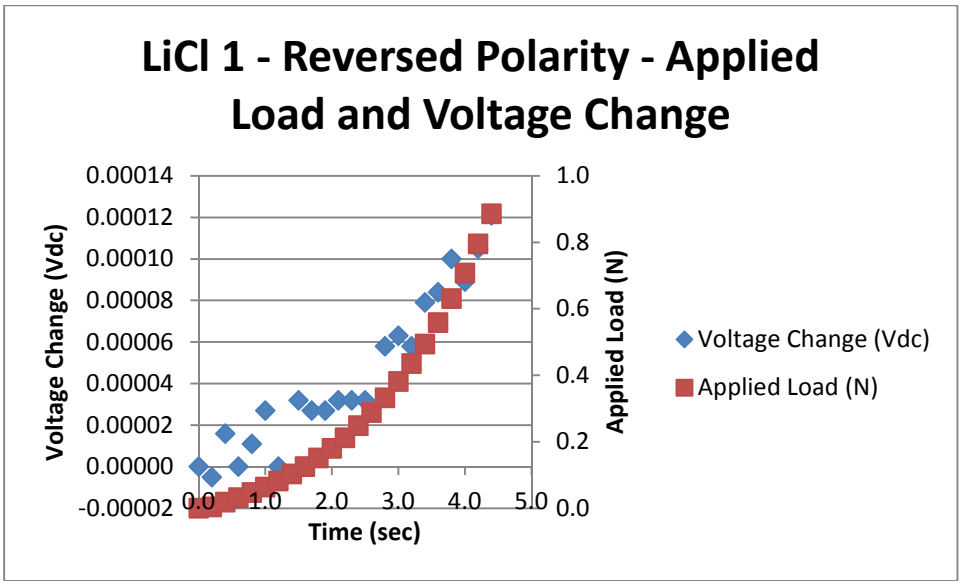

Figure 86

Trial 1 reversed polarity LiCl electrolyte constant load scenario, load and voltage change

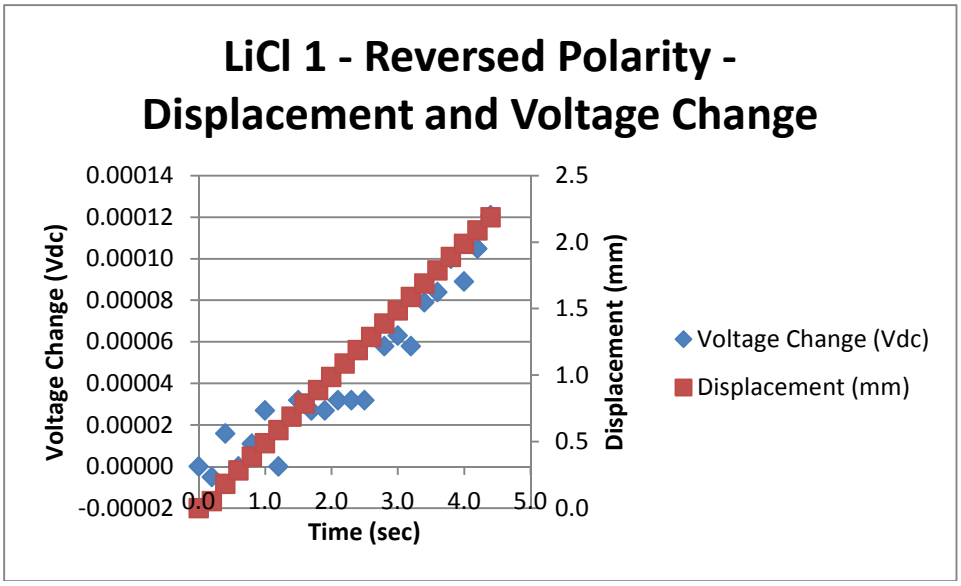

Figure 87

Trial 1 reversed polarity LiCl electrolyte constant load scenario, displacement and voltage change

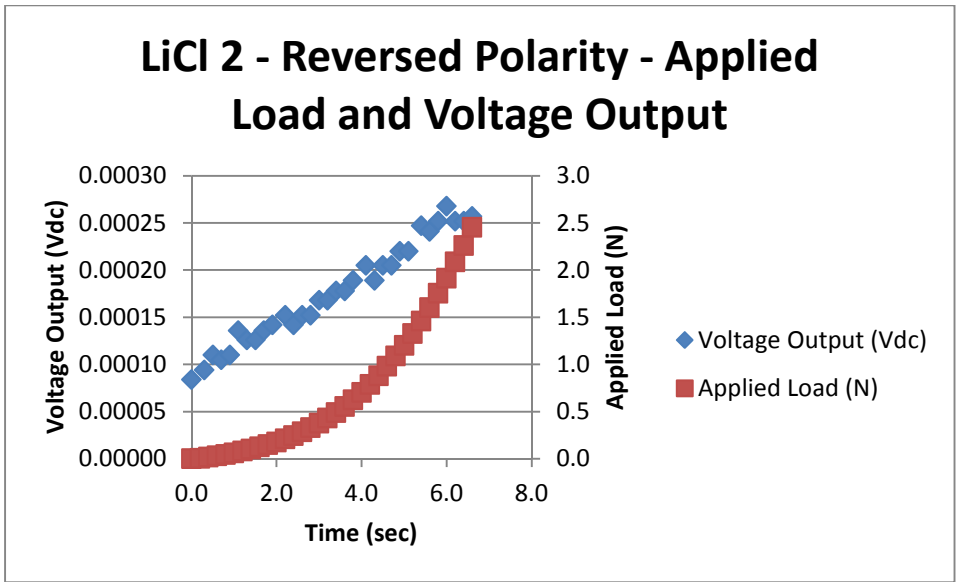

Figure 88
Trial 2 reversed polarity LiCl electrolyte constant load scenario, load and raw voltage output

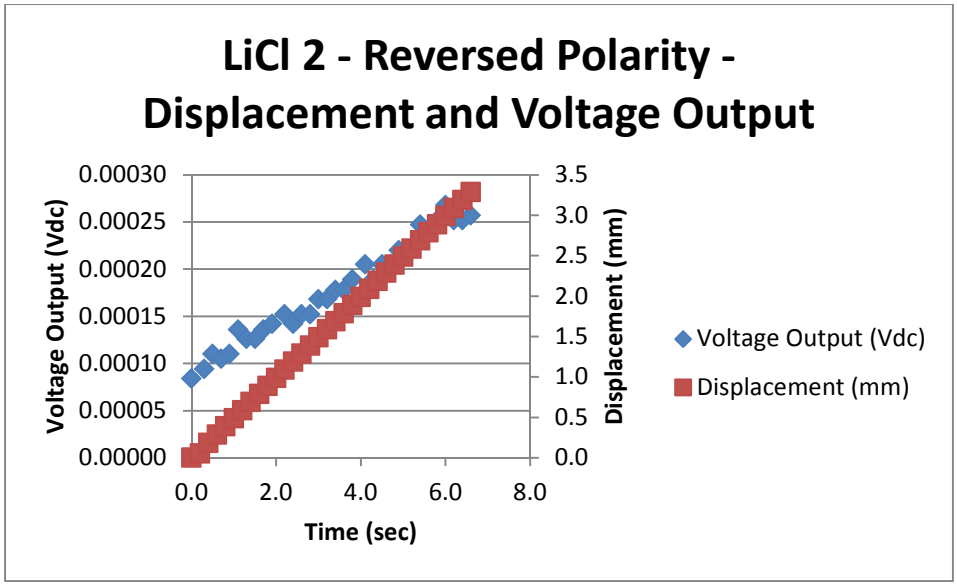

Figure 89
Trial 2 reversed polarity LiCl electrolyte constant load scenario, displacement and raw voltage output

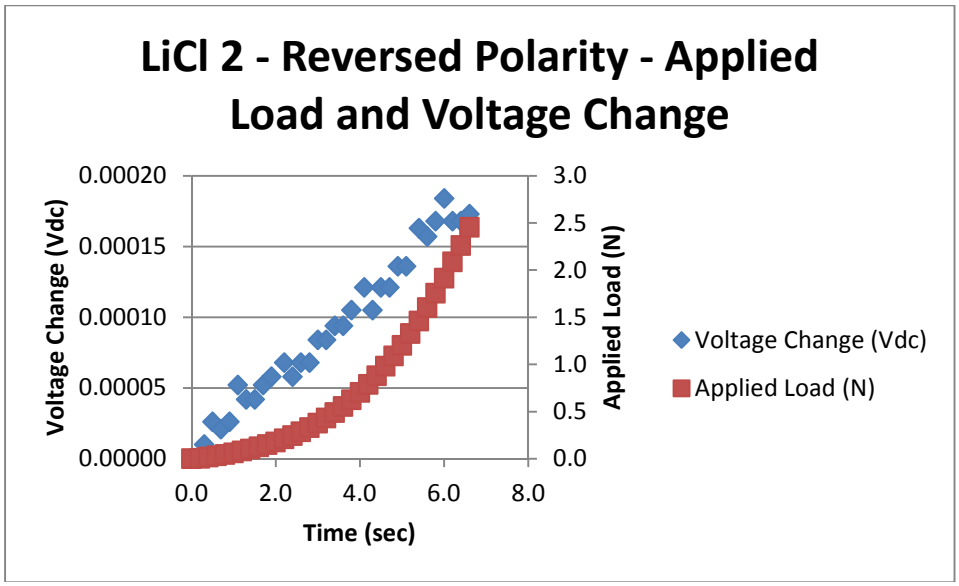

Figure 90
Trial 2 reversed polarity LiCl electrolyte constant load scenario, load and voltage change

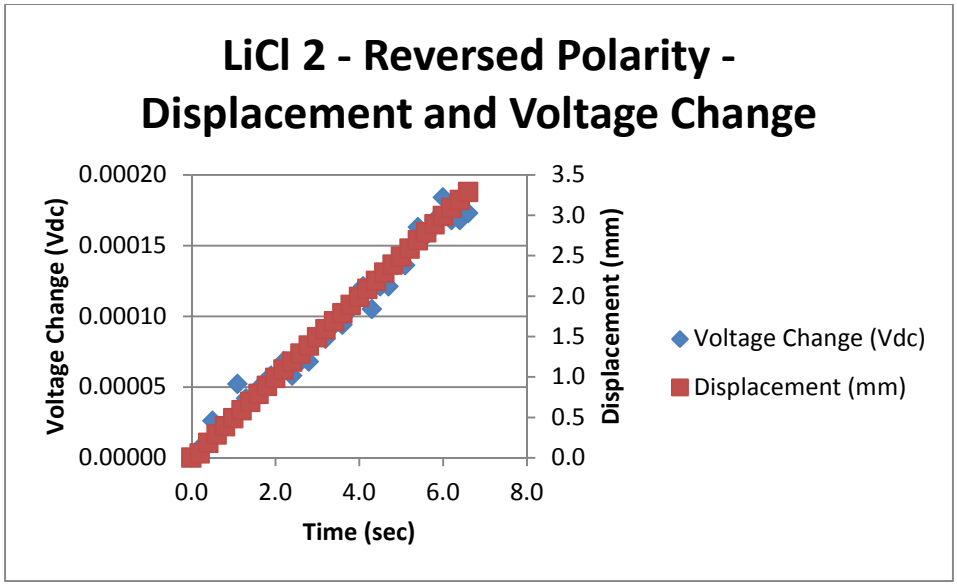

Figure 91
Trial 2 reversed polarity LiCl electrolyte constant load scenario, displacement and voltage change

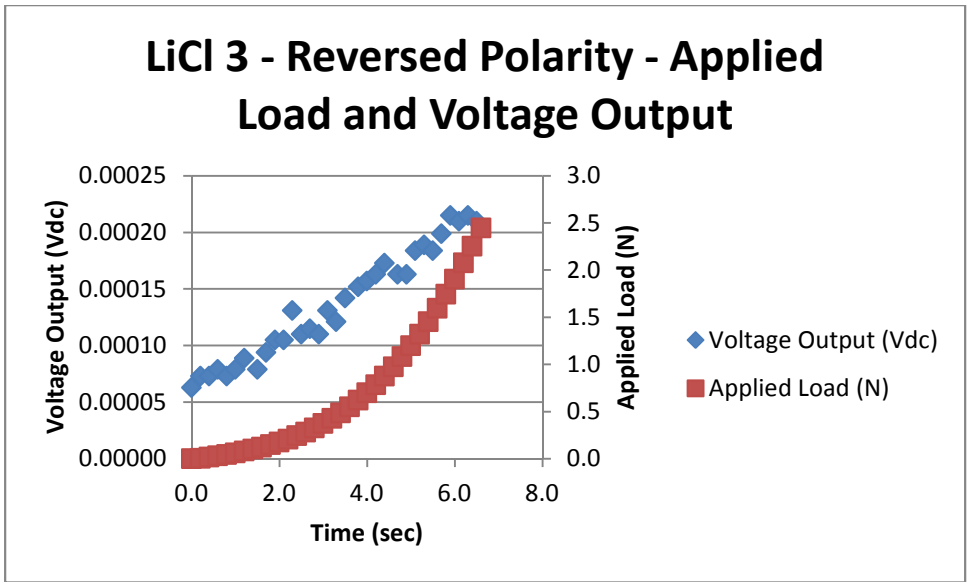

Figure 92
Trial 3 reversed polarity LiCl electrolyte constant load scenario, load and raw voltage output

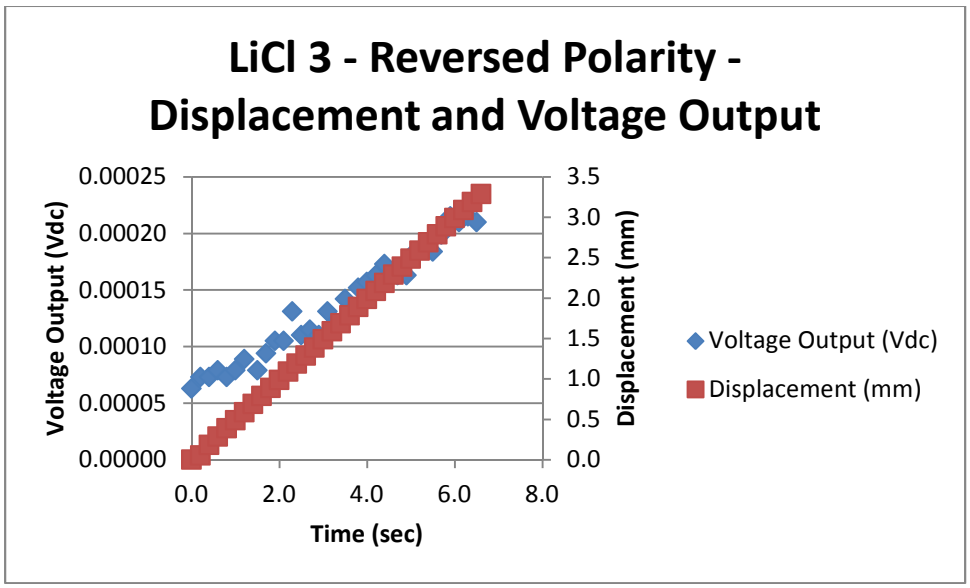

Figure 93
Trial 3 reversed polarity LiCl electrolyte constant load scenario, displacement and raw voltage output

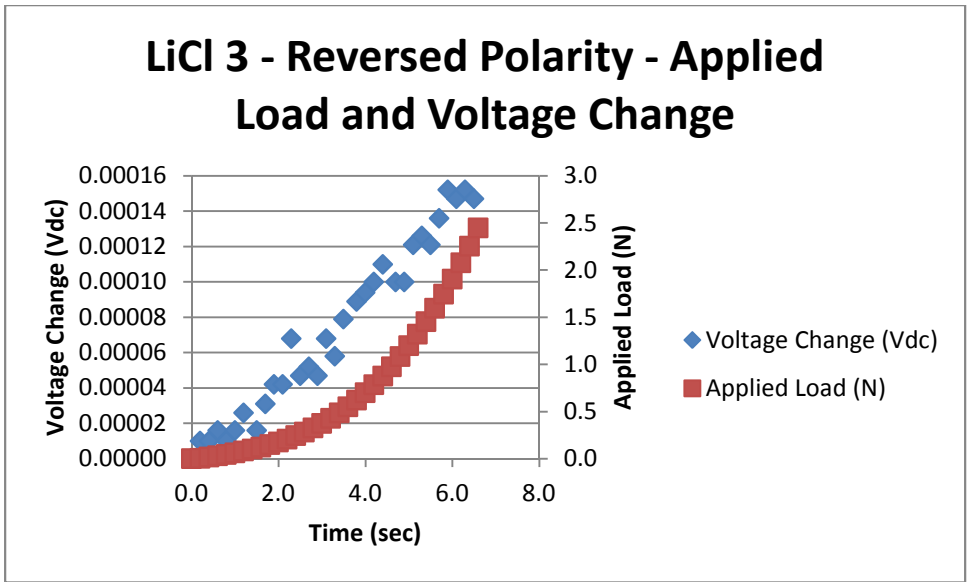

Figure 94
Trial 3 reversed polarity LiCl electrolyte constant load scenario, load and voltage change

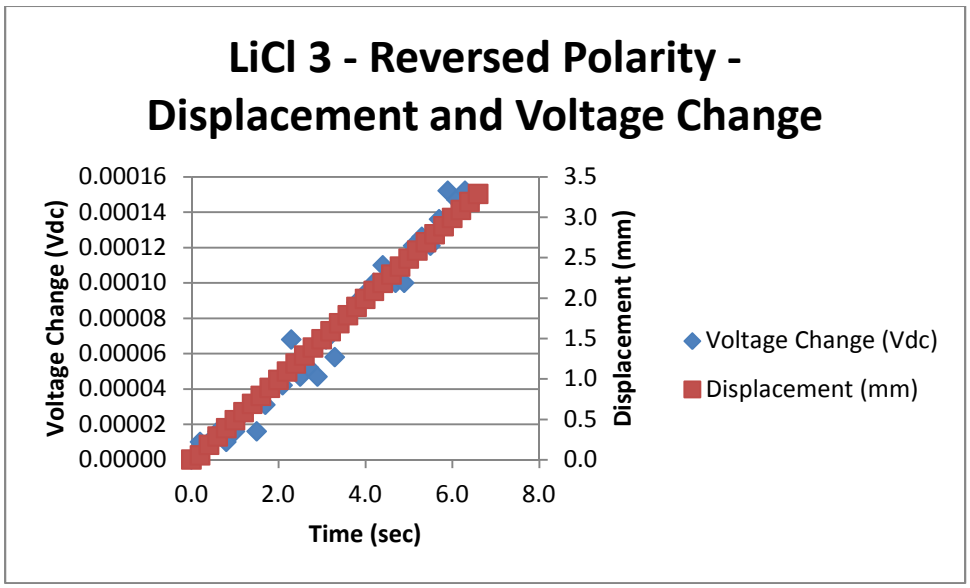

Figure 95
Trial 3 reversed polarity LiCl electrolyte constant load scenario, displacement and voltage change

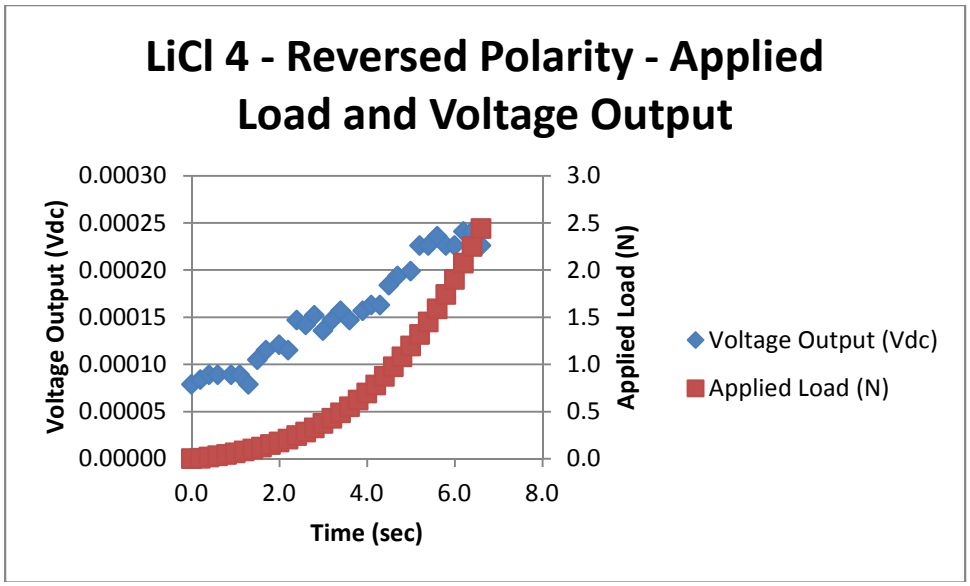

Figure 96

Trial 4 reversed polarity LiCl electrolyte constant load scenario, load and raw voltage output

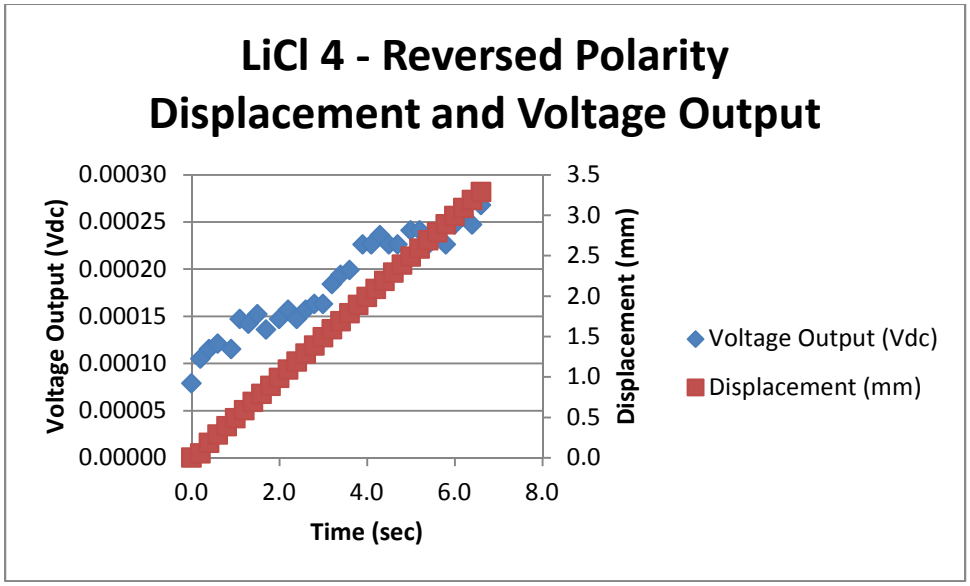

Figure 97

Trial 4 reversed polarity LiCl electrolyte constant load scenario, displacement and raw voltage output

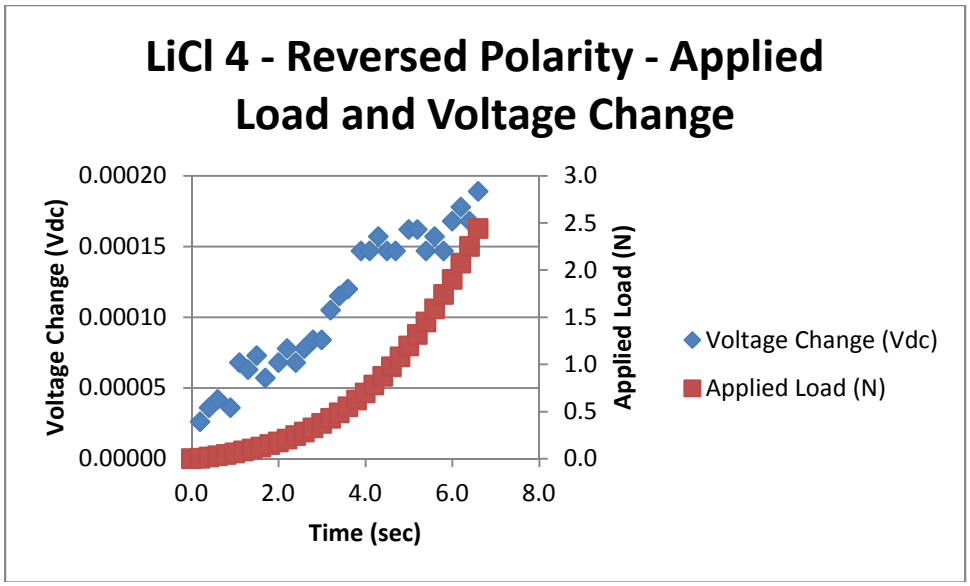

Figure 98
Trial 4 reversed polarity LiCl electrolyte constant load scenario, load and voltage change

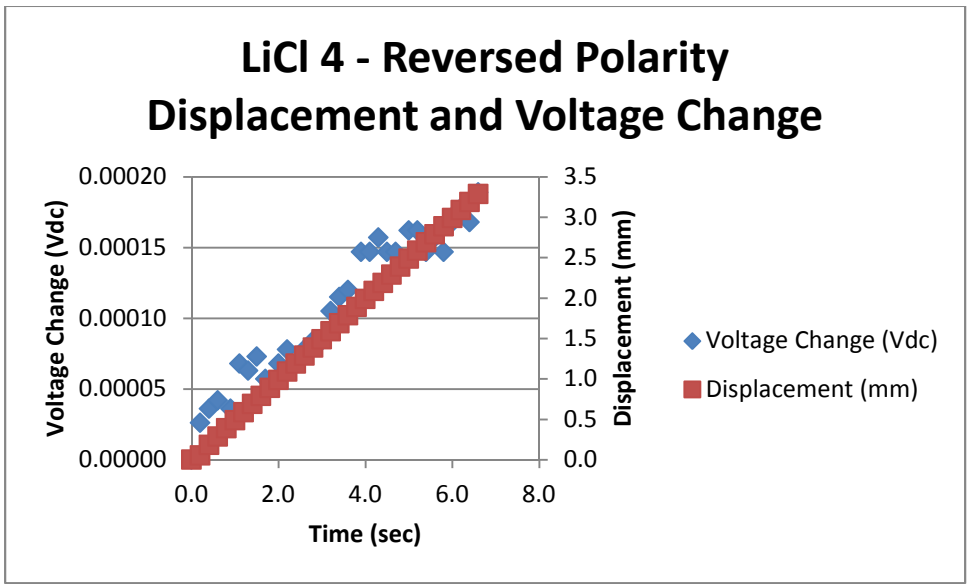

Figure 99
Trial 4 reversed polarity LiCl electrolyte constant load scenario, displacement and voltage change

Appendix C

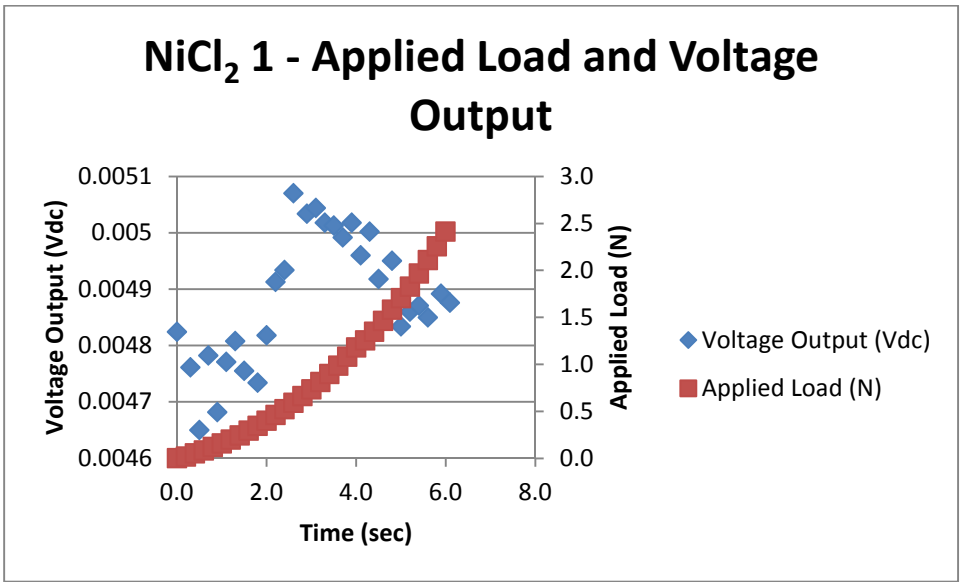

Figure 100

Trial 1 normal polarity $NiCl_2$ electrolyte constant load scenario, load and raw voltage output

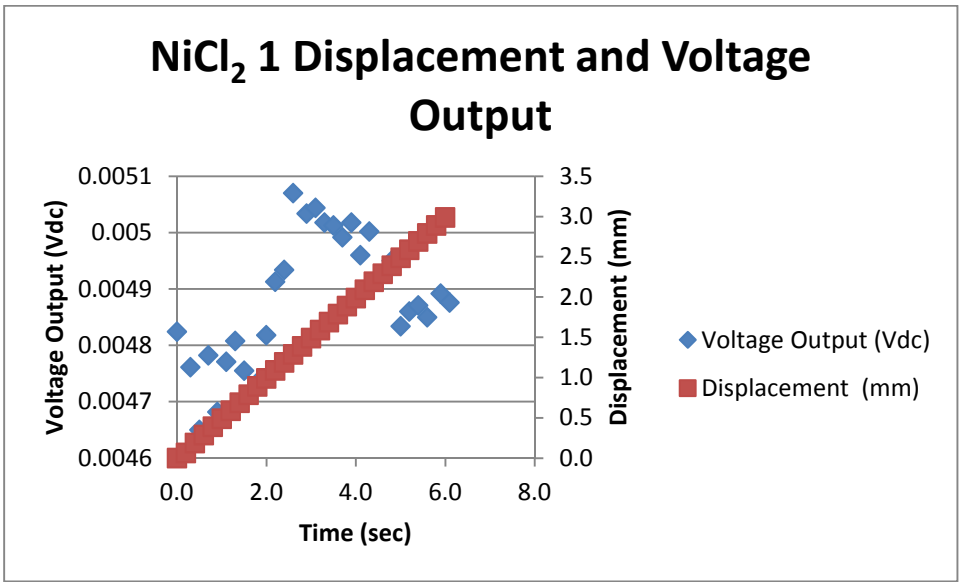

Figure 101

Trial 1 normal polarity $NiCl_2$ electrolyte constant load scenario, displacement and raw voltage output

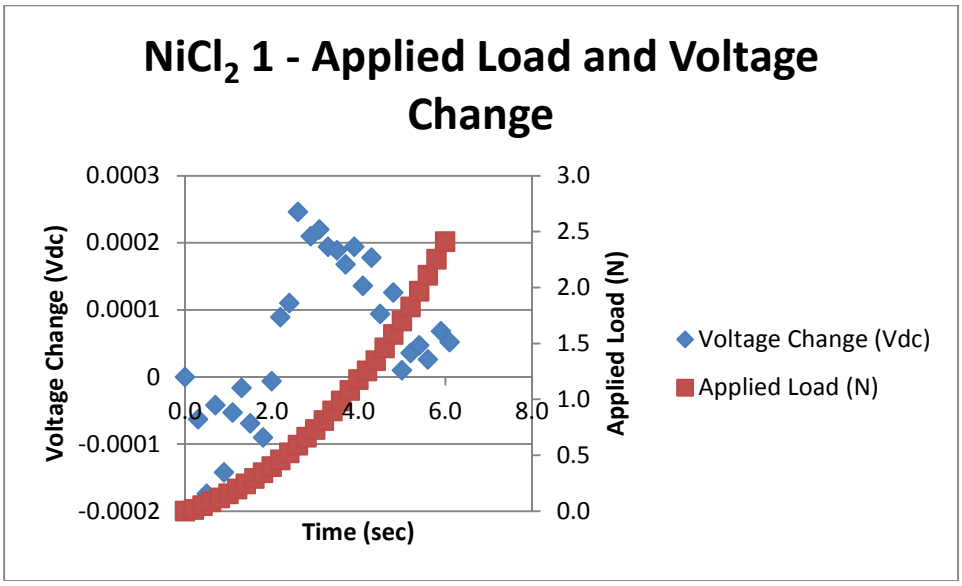

Figure 102

Trial 1 normal polarity $NiCl_2$ electrolyte constant load scenario, load and voltage change

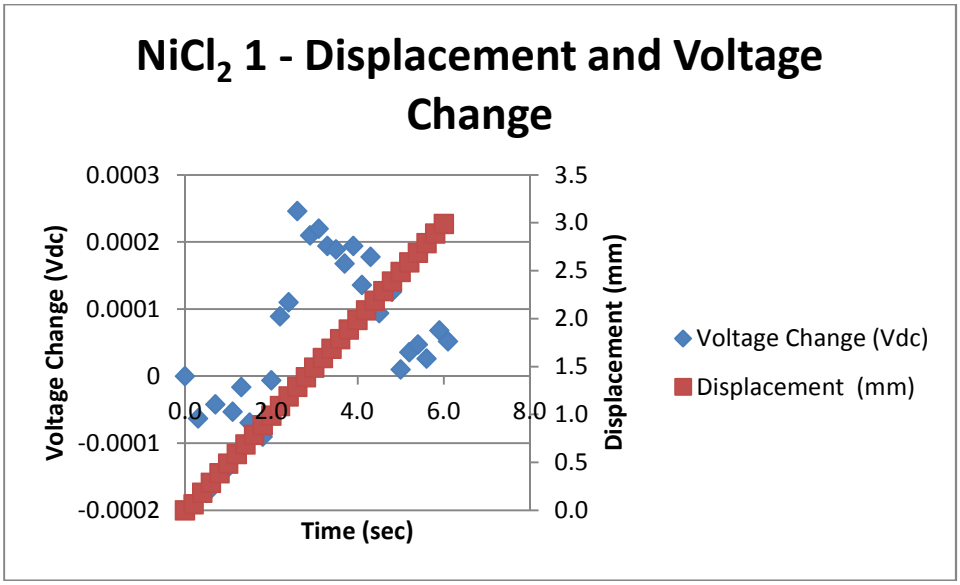

Figure 103

Trial 1 normal polarity $NiCl_2$ electrolyte constant load scenario, displacement and voltage change

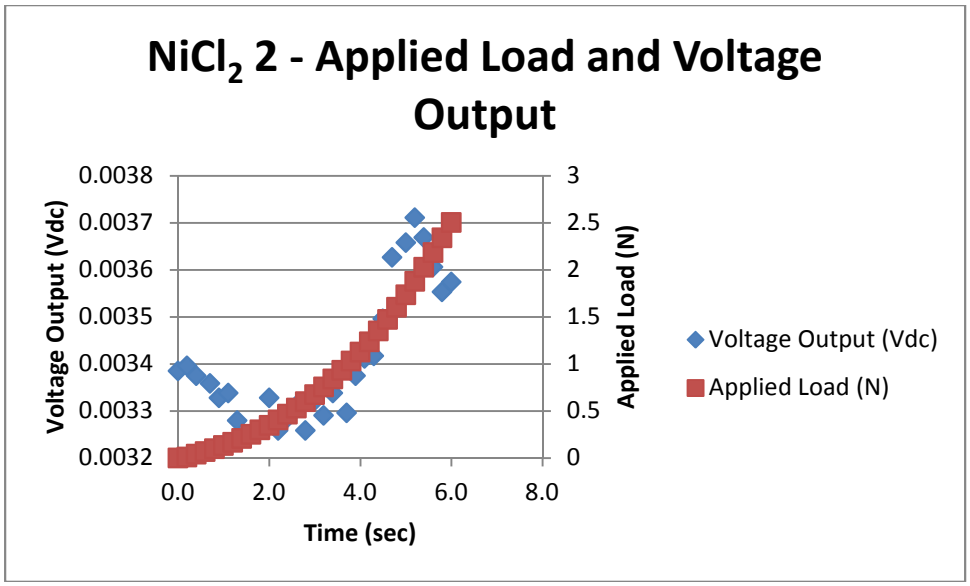

Figure 104

Trial 2 normal polarity $NiCl_2$ electrolyte constant load scenario, load and raw voltage output

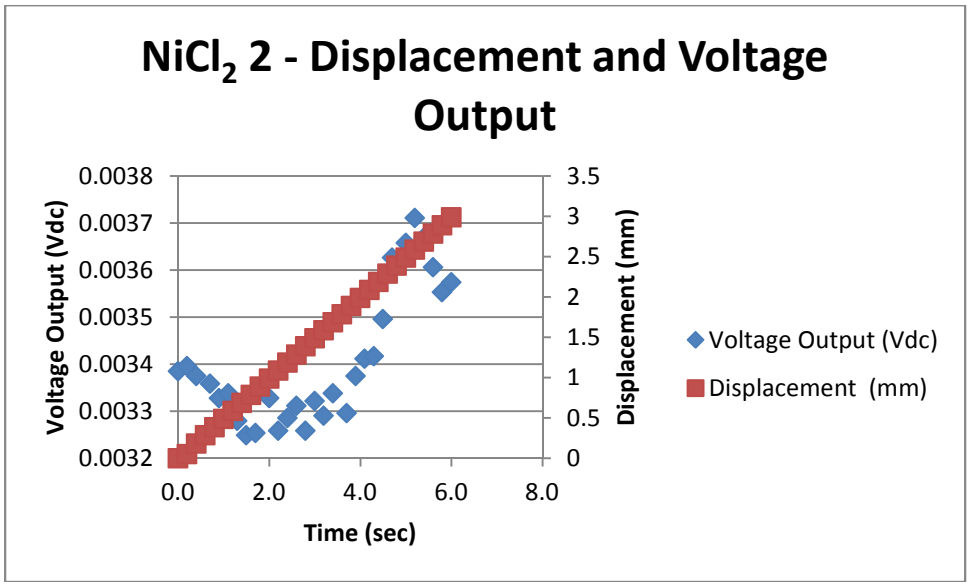

Figure 105

Trial 2 normal polarity $NiCl_2$ electrolyte constant load scenario, displacement and raw voltage output

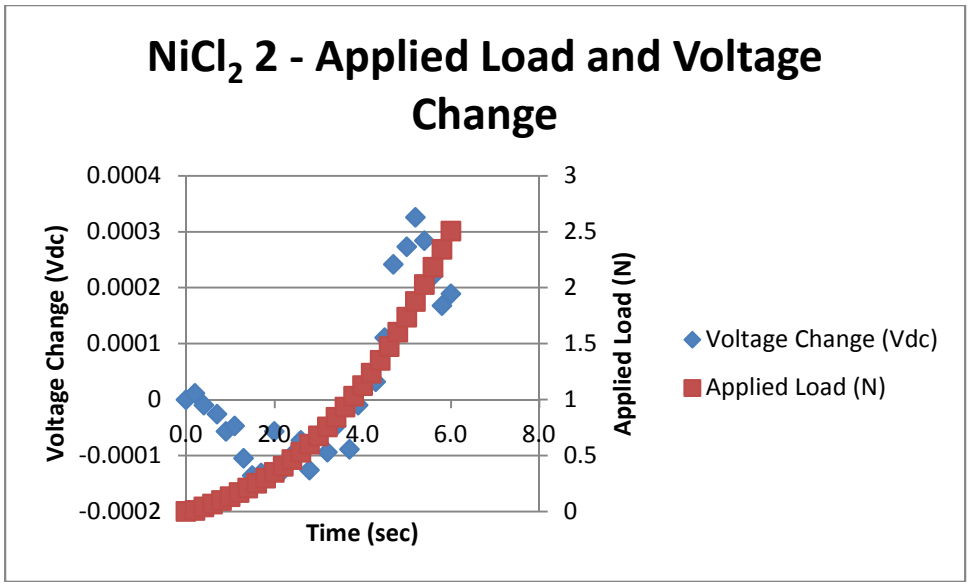

Figure 106

Trial 2 normal polarity $NiCl_2$ electrolyte constant load scenario, load and voltage change

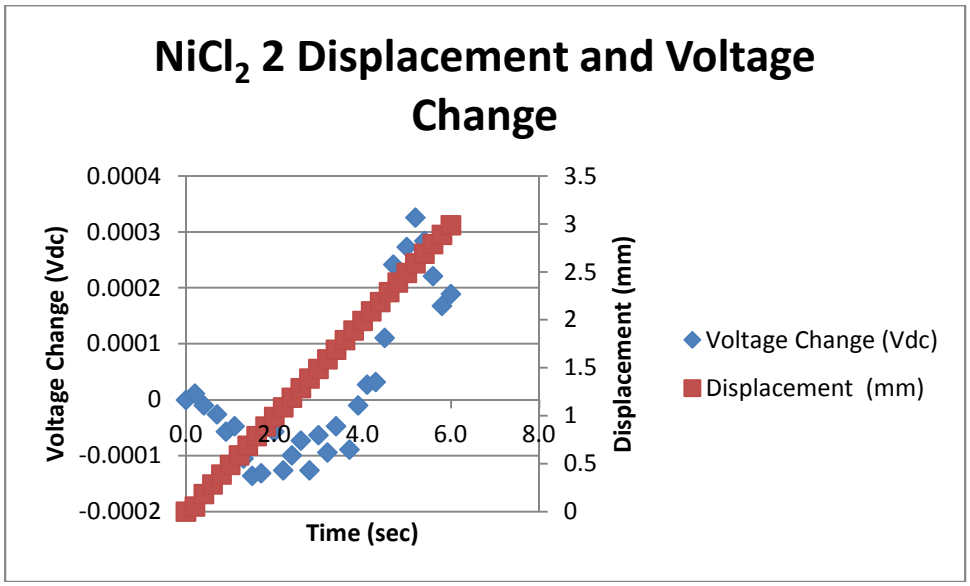

Figure 107

Trial 2 normal polarity $NiCl_2$ electrolyte constant load scenario, displacement and voltage change

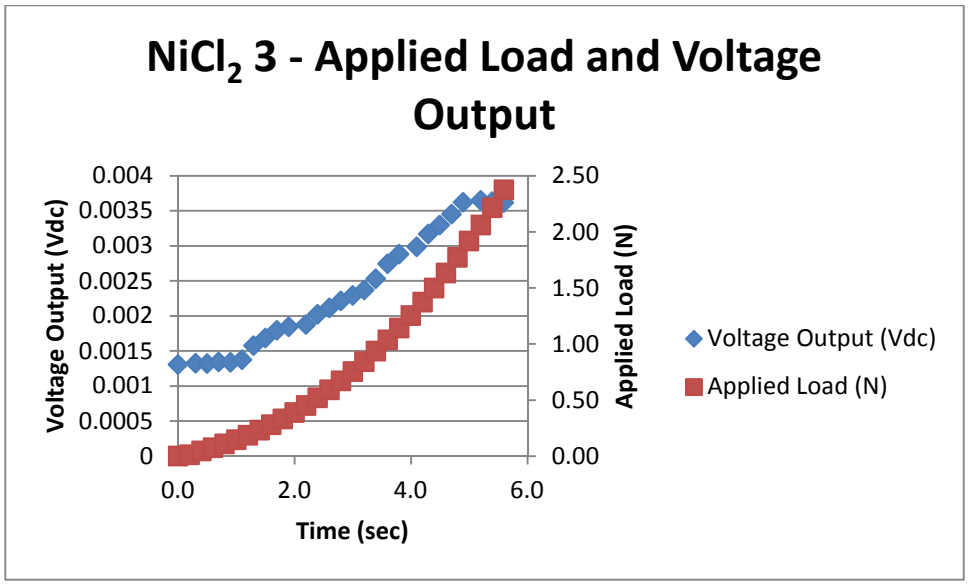

Figure 108

Trial 3 normal polarity $NiCl_2$ electrolyte constant load scenario, load and raw voltage output

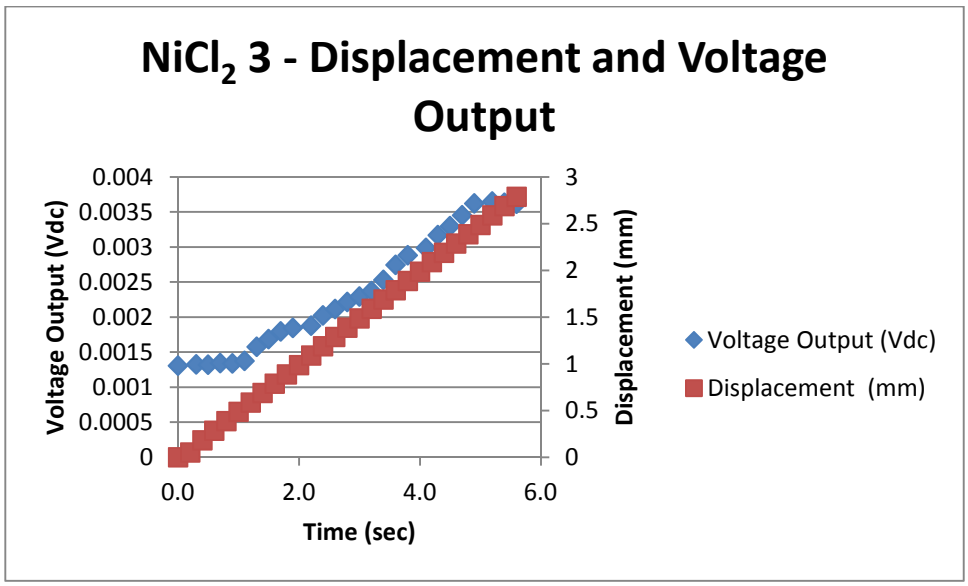

Figure 109

Trial 3 normal polarity $NiCl_2$ electrolyte constant load scenario, displacement and raw voltage output

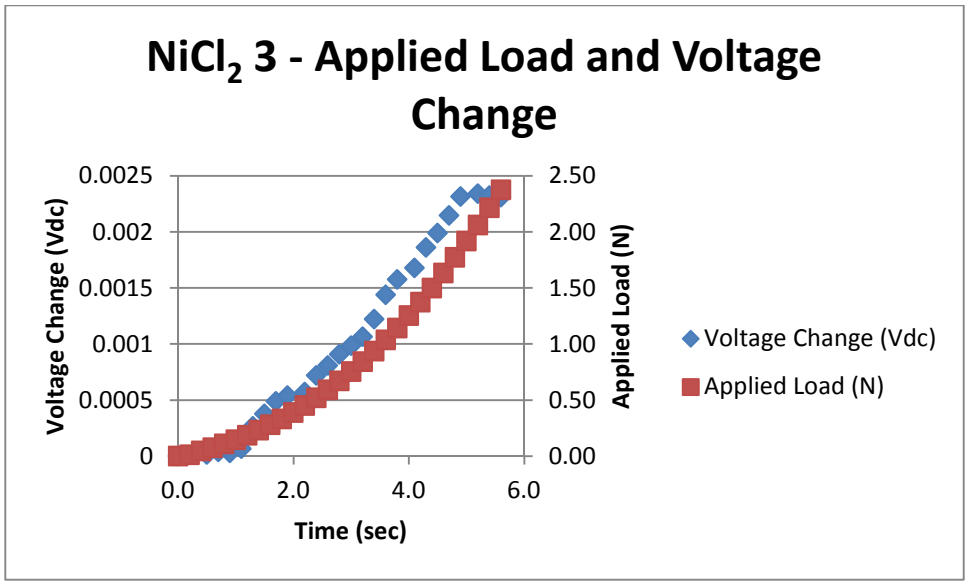

Figure 110

Trial 3 normal polarity $NiCl_2$ electrolyte constant load scenario, load and voltage change

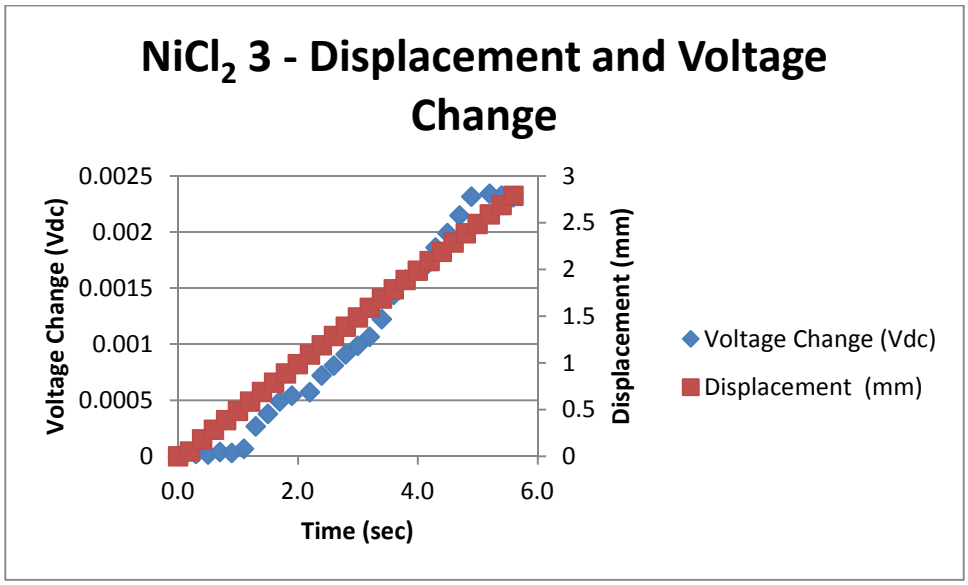

Figure 111

Trial 3 normal polarity $NiCl_2$ electrolyte constant load scenario, displacement and voltage change

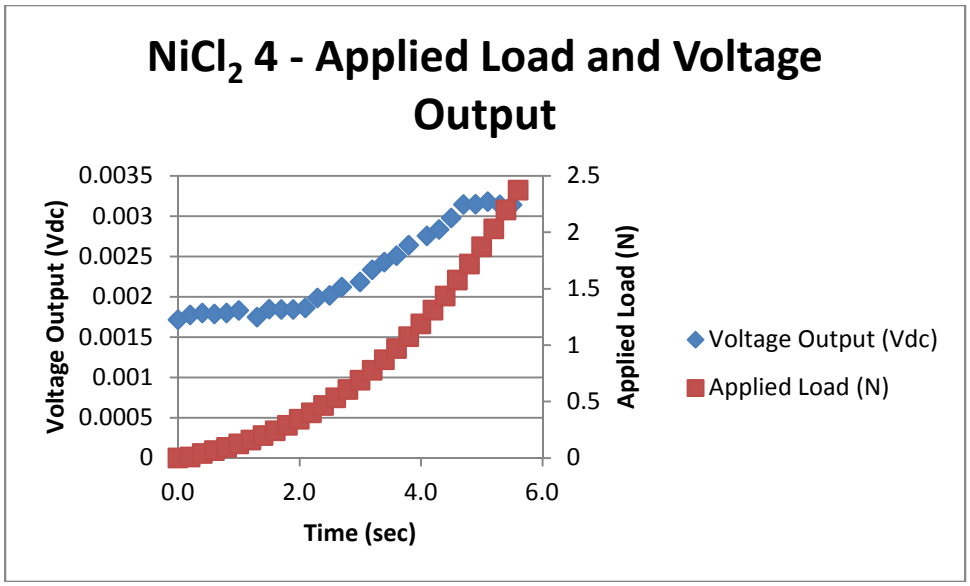

Figure 112

Trial 4 normal polarity $NiCl_2$ electrolyte constant load scenario, load and raw voltage output

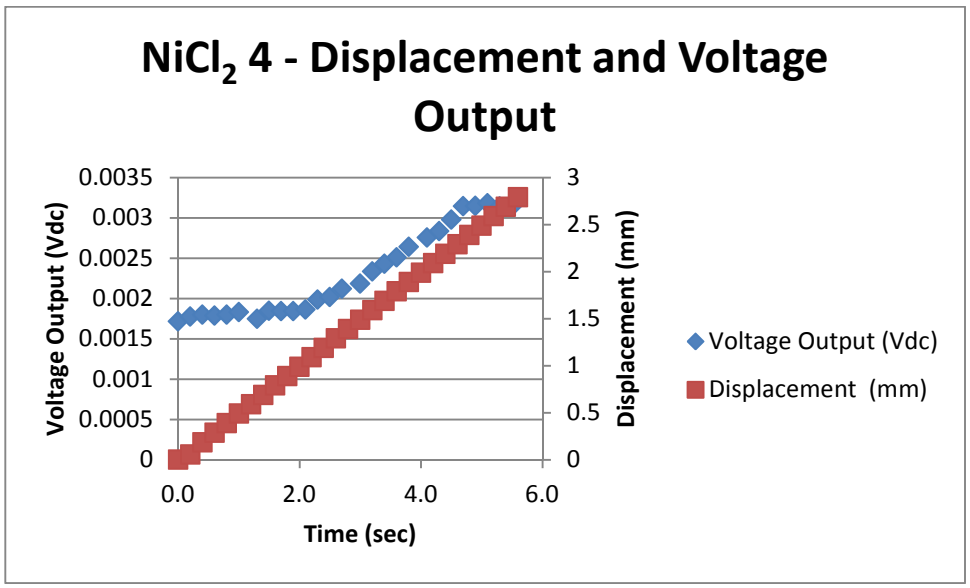

Figure 113

Trial 4 normal polarity $NiCl_2$ electrolyte constant load scenario, displacement and raw voltage output

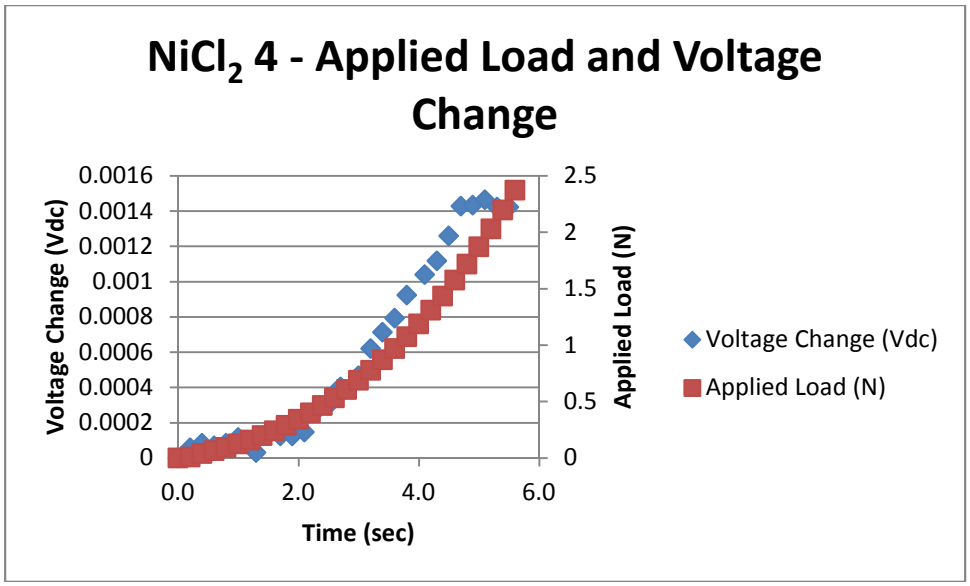

Figure 114

Trial 4 normal polarity $NiCl_2$ electrolyte constant load scenario, load and voltage change

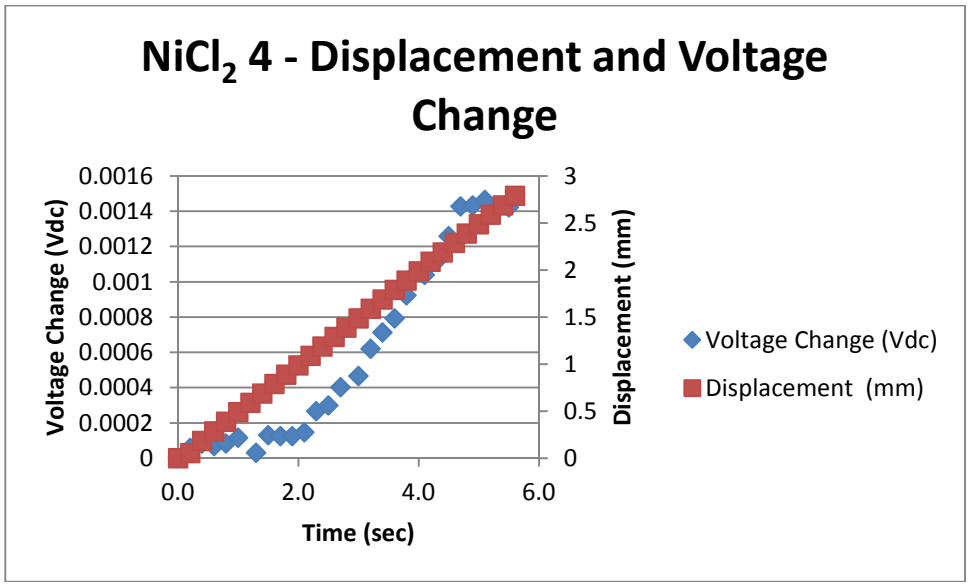

Figure 115

Trial 4 normal polarity $NiCl_2$ electrolyte constant load scenario, displacement and voltage change

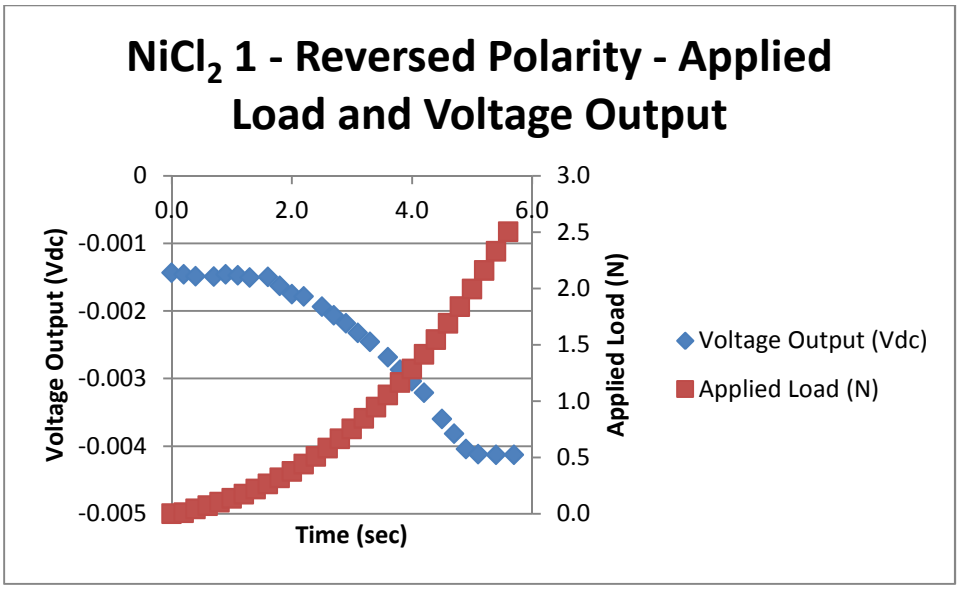

Figure 116

Trial 1 reversed polarity $NiCl_2$ electrolyte constant load scenario, load and raw voltage output

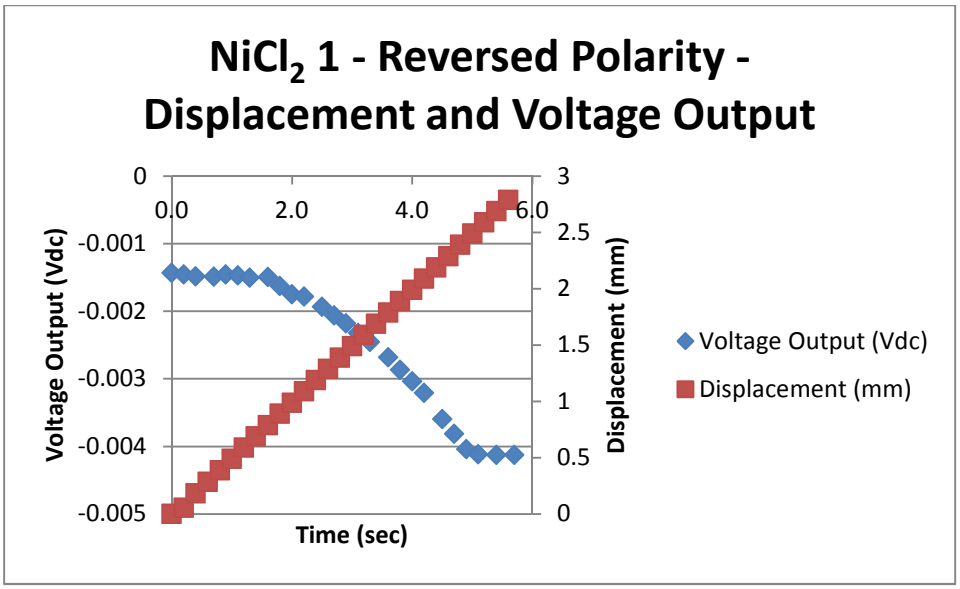

Figure 117

Trial 1 reversed polarity $NiCl_2$ electrolyte constant load scenario, displacement and raw voltage output

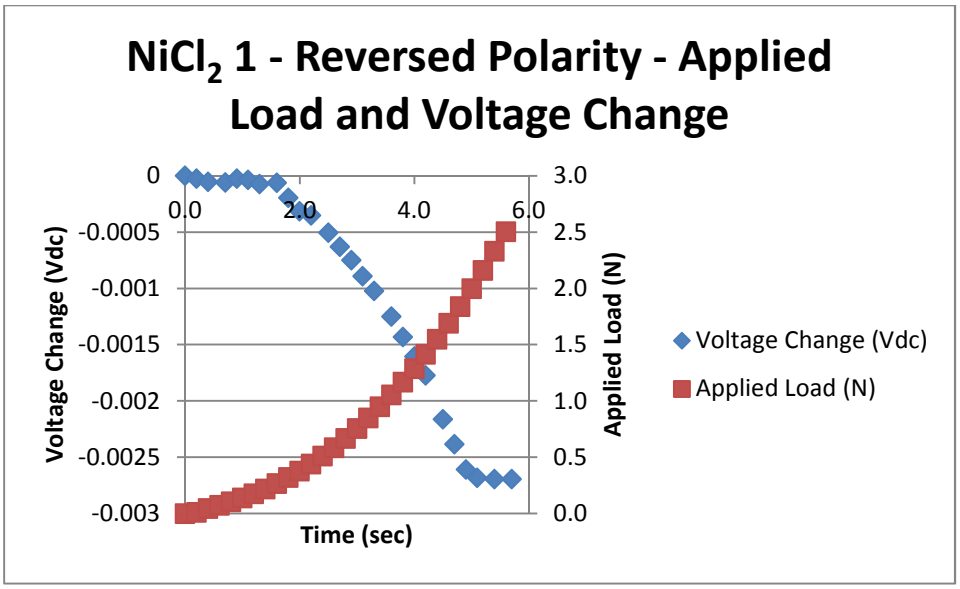

Figure 118

Trial 1 reversed polarity $NiCl_2$ electrolyte constant load scenario, load and voltage change

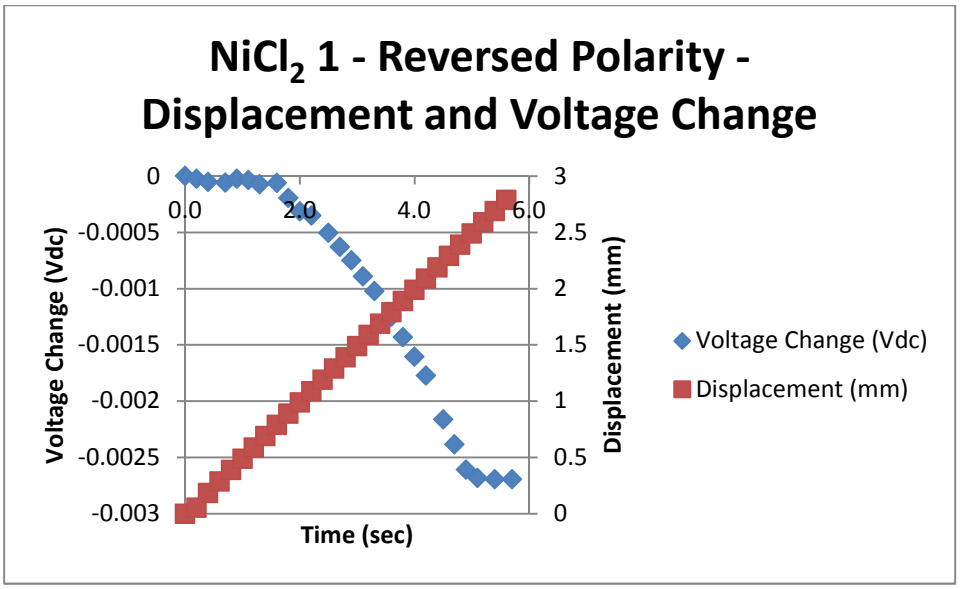

Figure 119

Trial 1 reversed polarity $NiCl_2$ electrolyte constant load scenario, displacement and voltage change

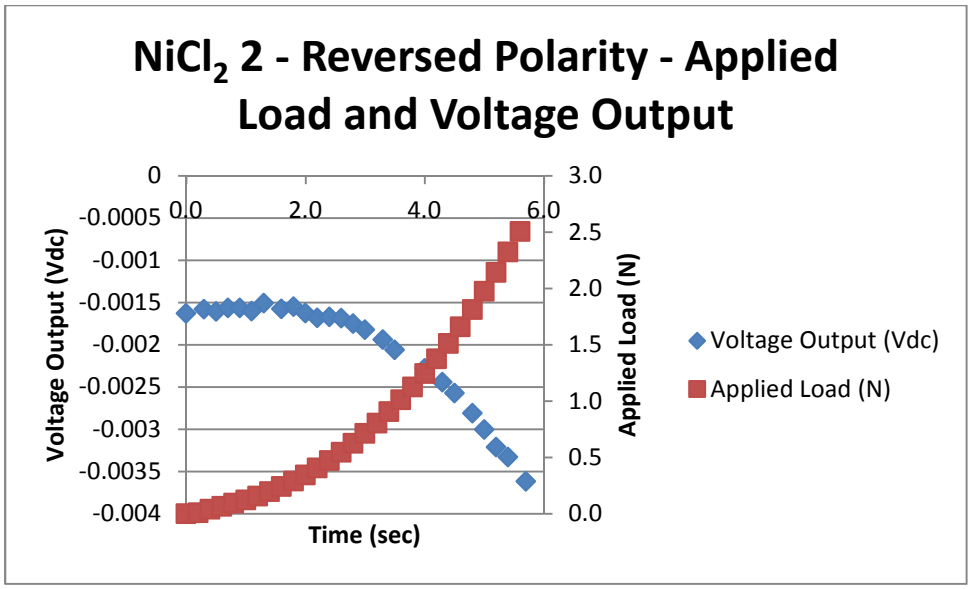

Figure 120

Trial 2 reversed polarity $NiCl_2$ electrolyte constant load scenario, load and raw voltage output

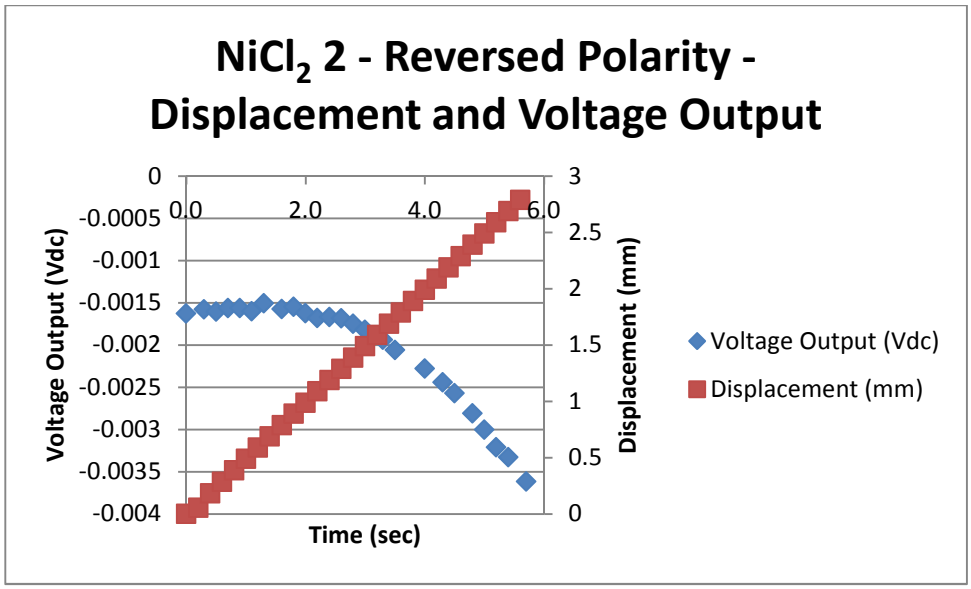

Figure 121

Trial 2 reversed polarity $NiCl_2$ electrolyte constant load scenario, displacement and raw voltage output

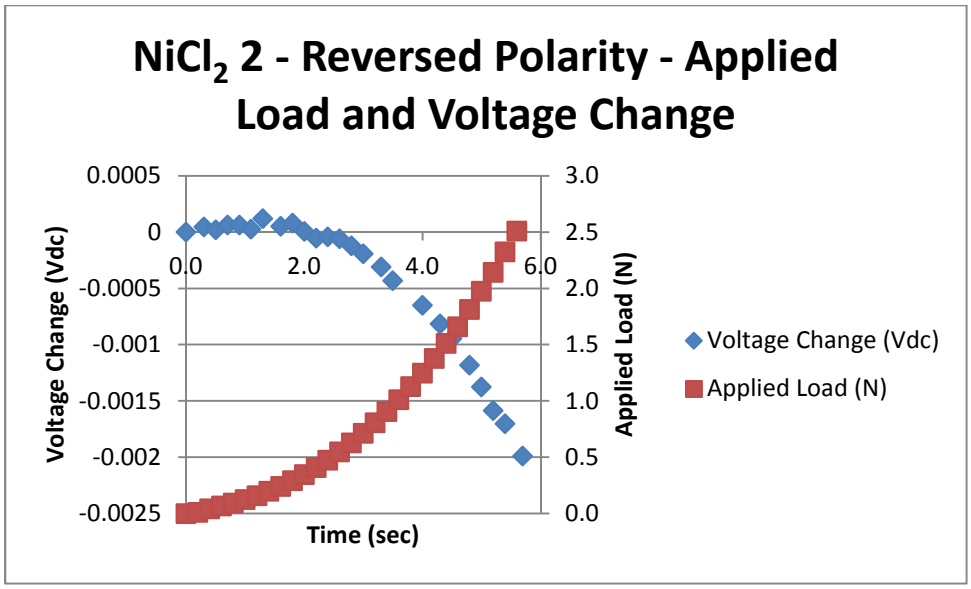

Figure 122

Trial 2 reversed polarity $NiCl_2$ electrolyte constant load scenario, load and voltage change

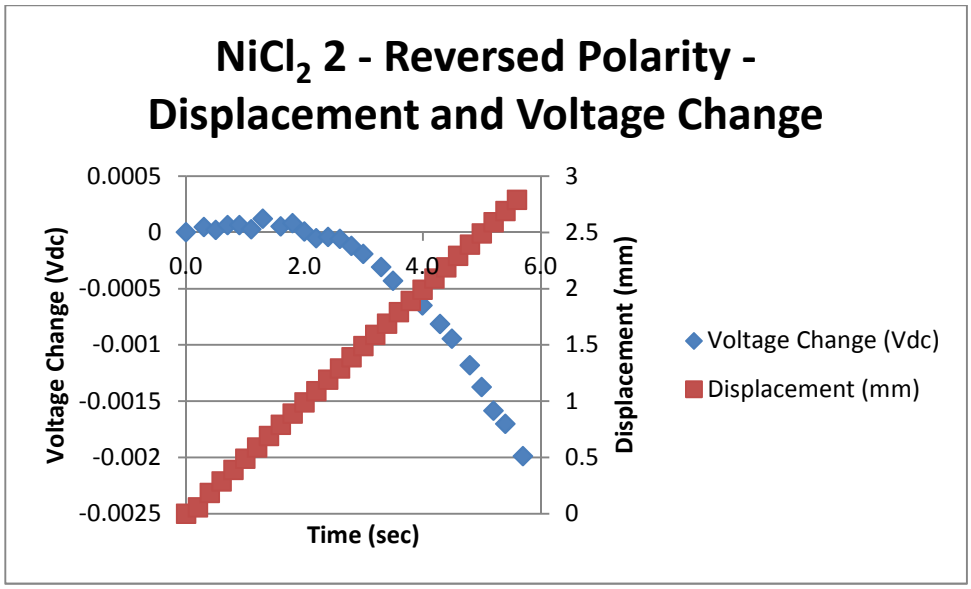

Figure 123

Trial 2 reversed polarity $NiCl_2$ electrolyte constant load scenario, displacement and voltage change

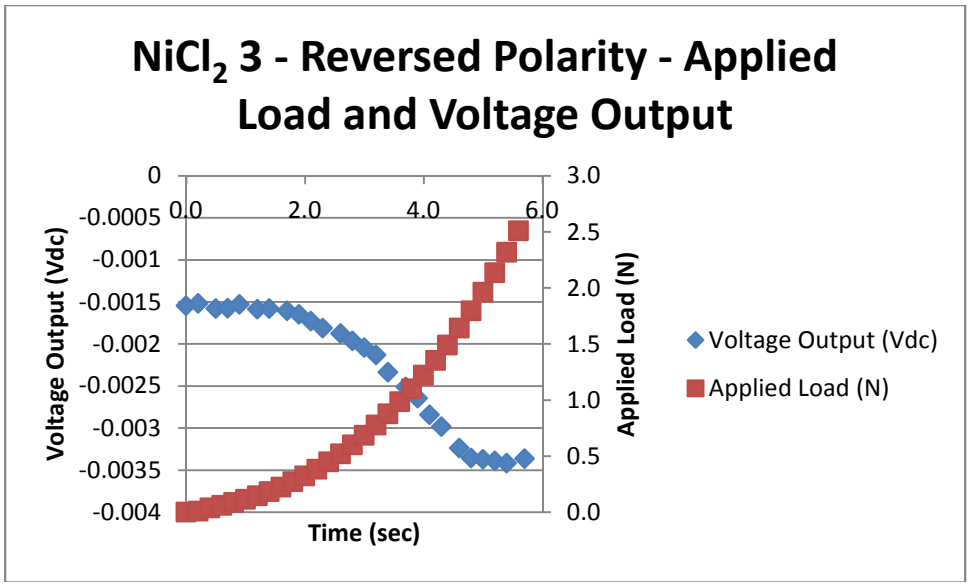

Figure 124

Trial 3 reversed polarity $NiCl_2$ electrolyte constant load scenario, load and raw voltage output

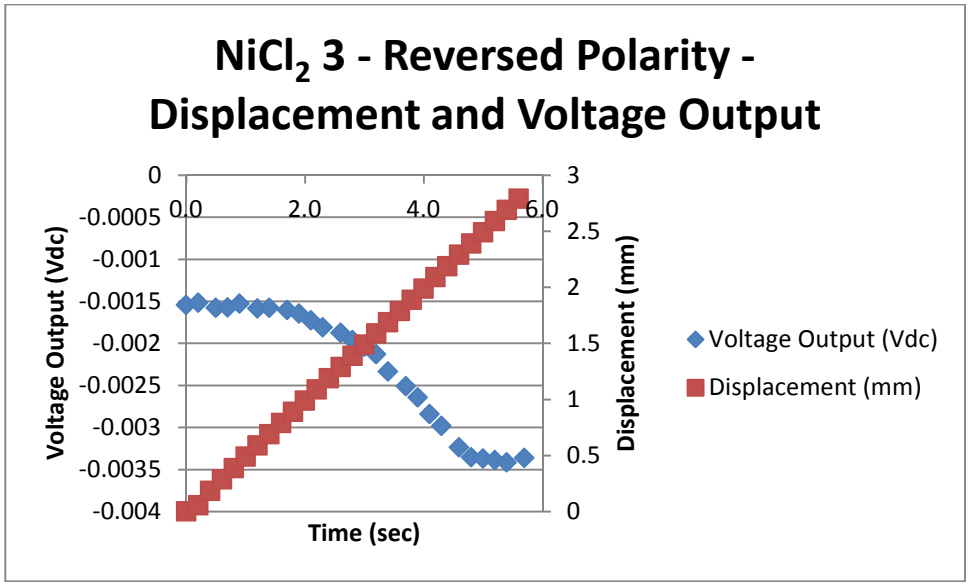

Figure 125

Trial 3 reversed polarity $NiCl_2$ electrolyte constant load scenario, displacement and raw voltage output

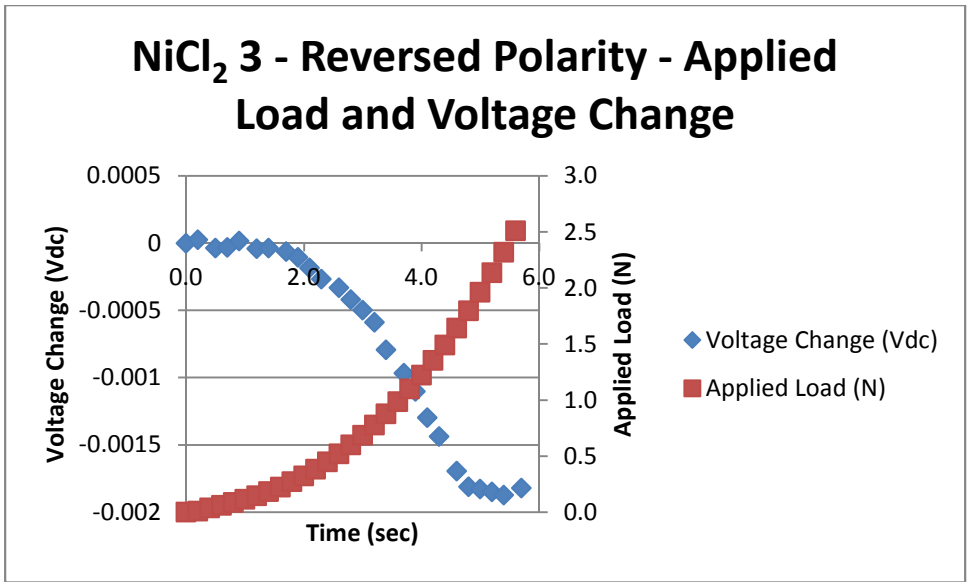

Figure 126

Trial 3 reversed polarity $NiCl_2$ electrolyte constant load scenario, load and voltage change

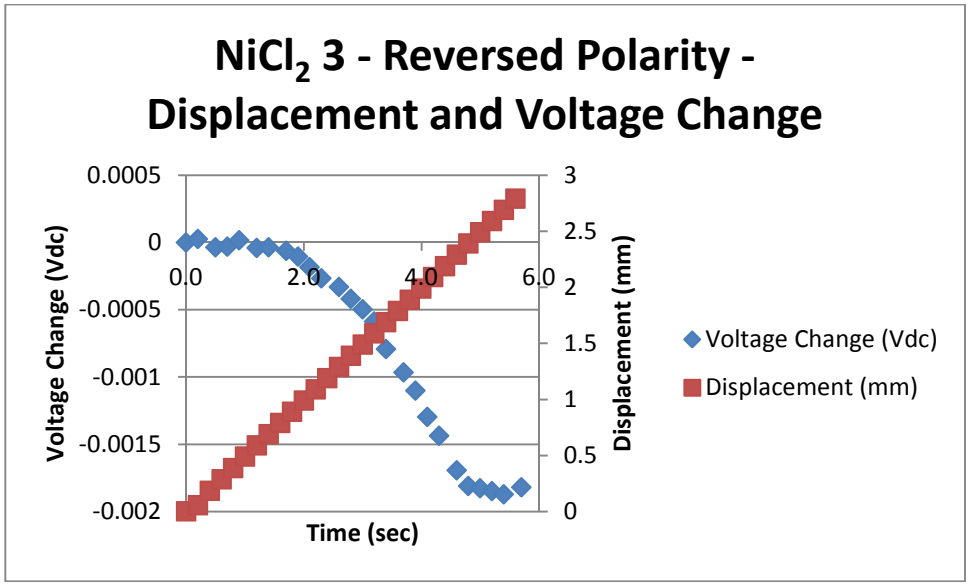

Figure 127

Trial 3 reversed polarity $NiCl_2$ electrolyte constant load scenario, displacement and voltage change

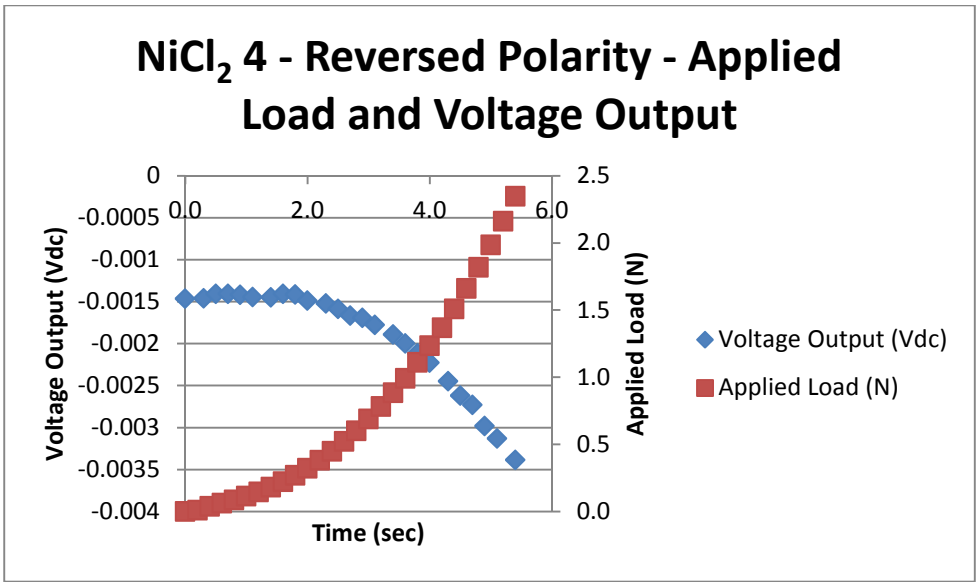

Figure 128

Trial 4 reversed polarity $NiCl_2$ electrolyte constant load scenario, load and raw voltage output

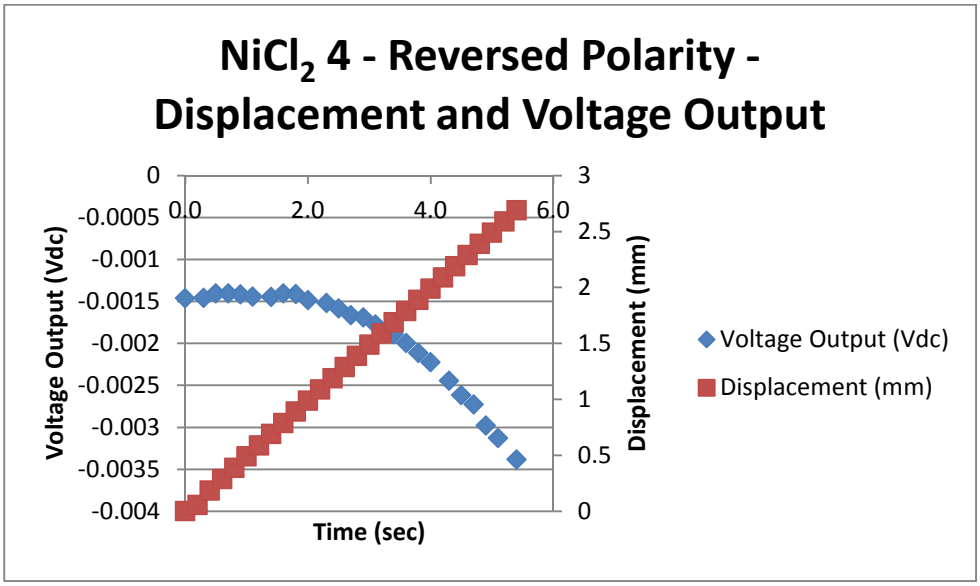

Figure 129

Trial 4 reversed polarity $NiCl_2$ electrolyte constant load scenario, displacement and raw voltage output

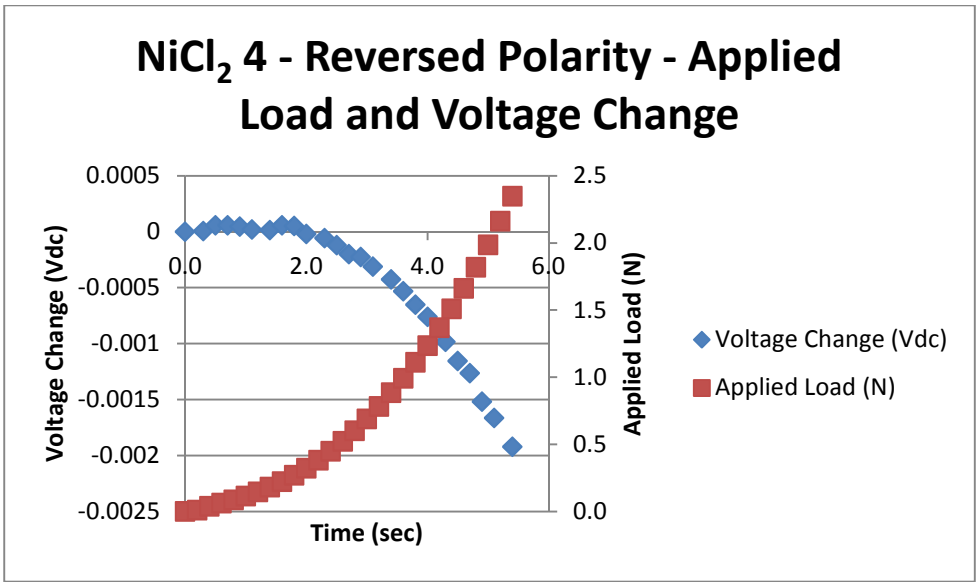

Figure 130

Trial 4 reversed polarity $NiCl_2$ electrolyte constant load scenario, load and voltage change

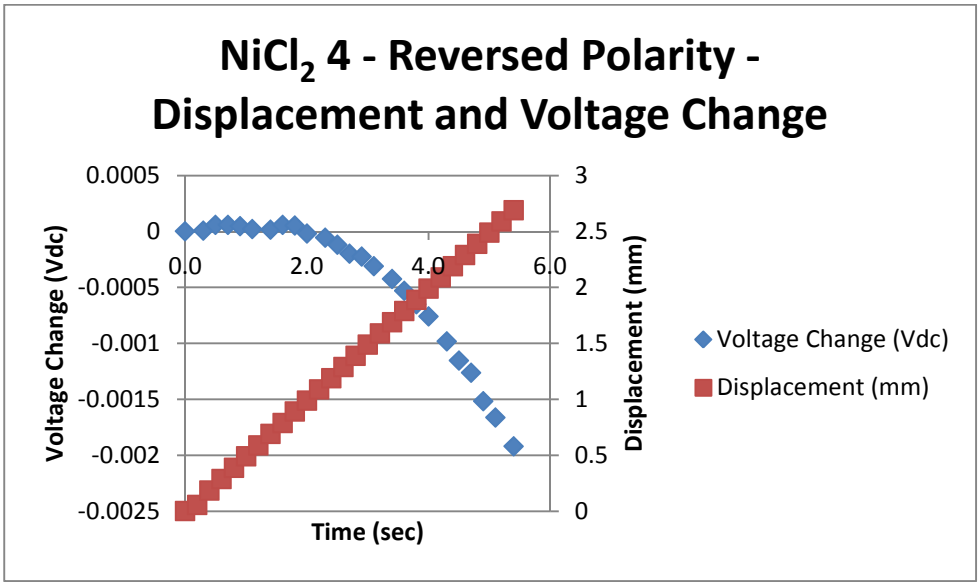

Figure 131

Trial 4 reversed polarity $NiCl_2$ electrolyte constant load scenario, displacement and voltage change

Appendix D

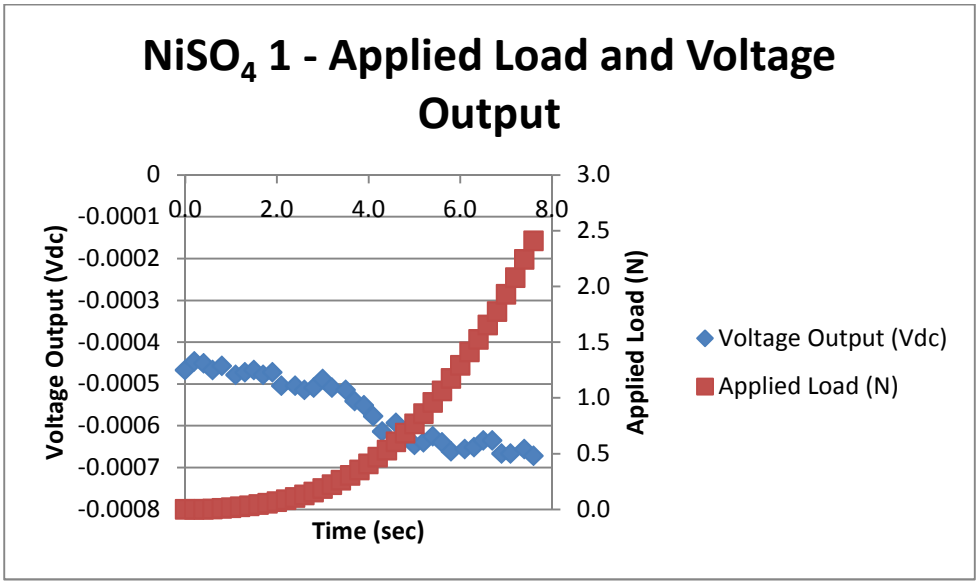

Figure 132
Trial 1 normal polarity $NiSO_4$ electrolyte constant load scenario, load and raw voltage output

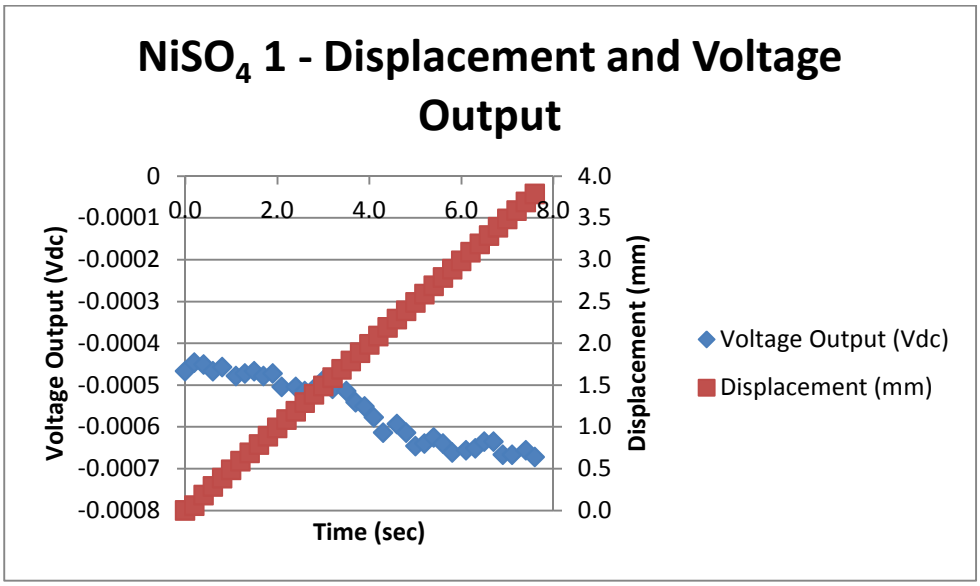

Figure 133
Trial 1 normal polarity $NiSO_4$ electrolyte constant load scenario, displacement and raw voltage output

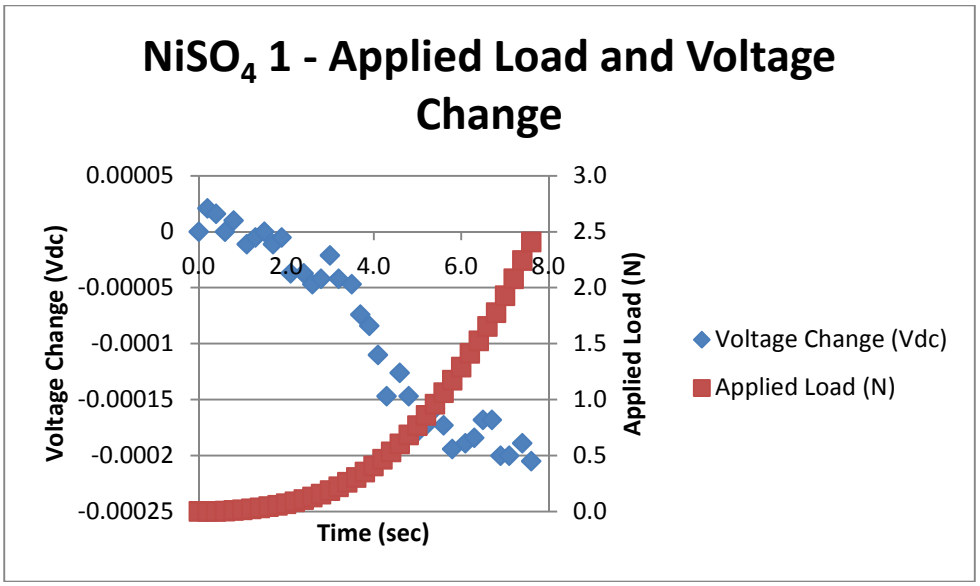

Figure 134

Trial 1 normal polarity $NiSO_4$ electrolyte constant load scenario, load and voltage change

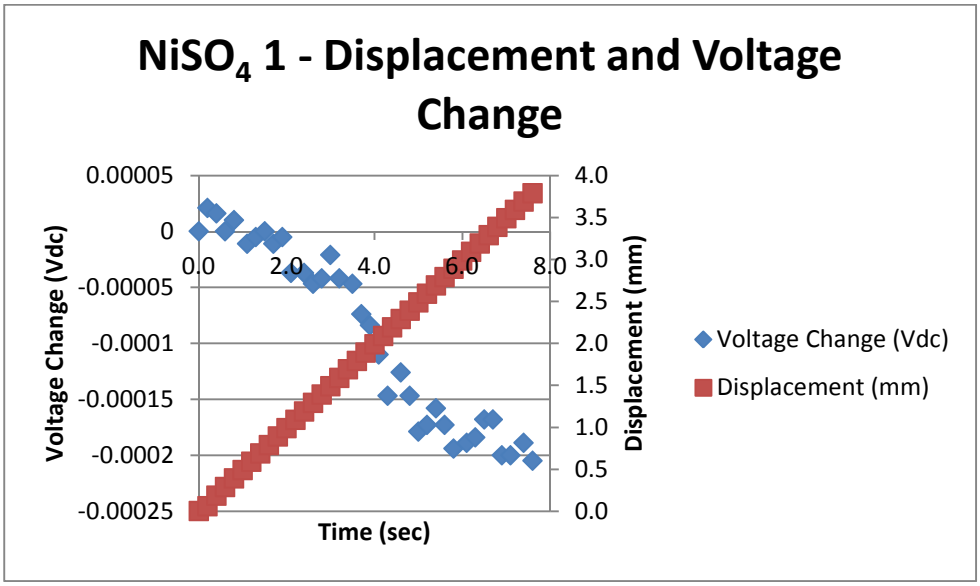

Figure 135

Trial 1 normal polarity $NiSO_4$ electrolyte constant load scenario, displacement and voltage change

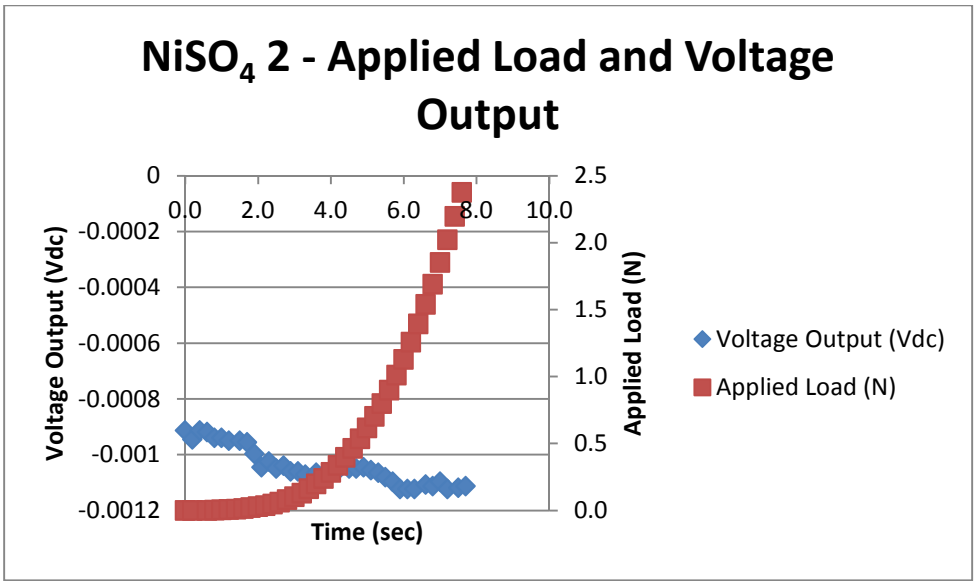

Figure 136

Trial 2 normal polarity $NiSO_4$ electrolyte constant load scenario, load and raw voltage output

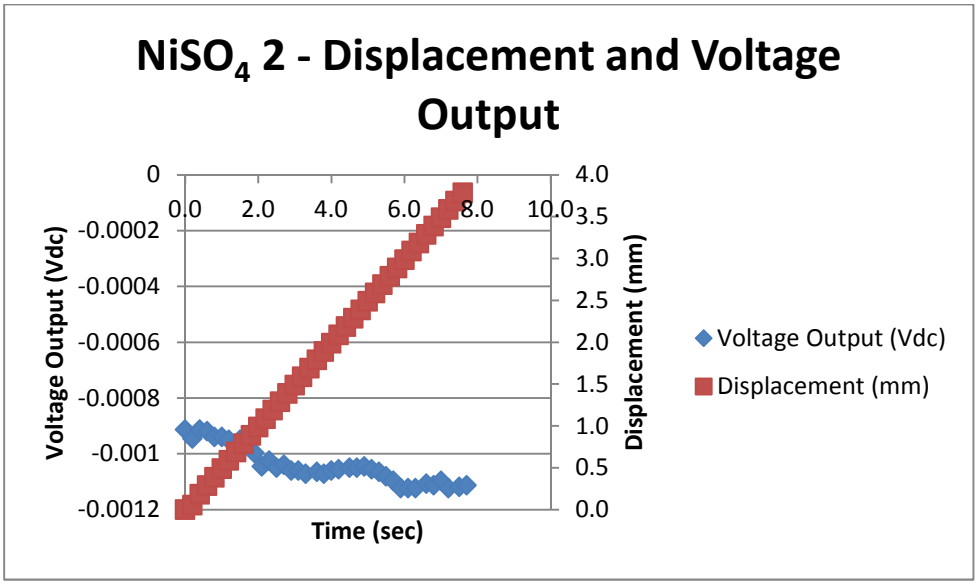

Figure 137

Trial 2 normal polarity $NiSO_4$ electrolyte constant load scenario, displacement and raw voltage output

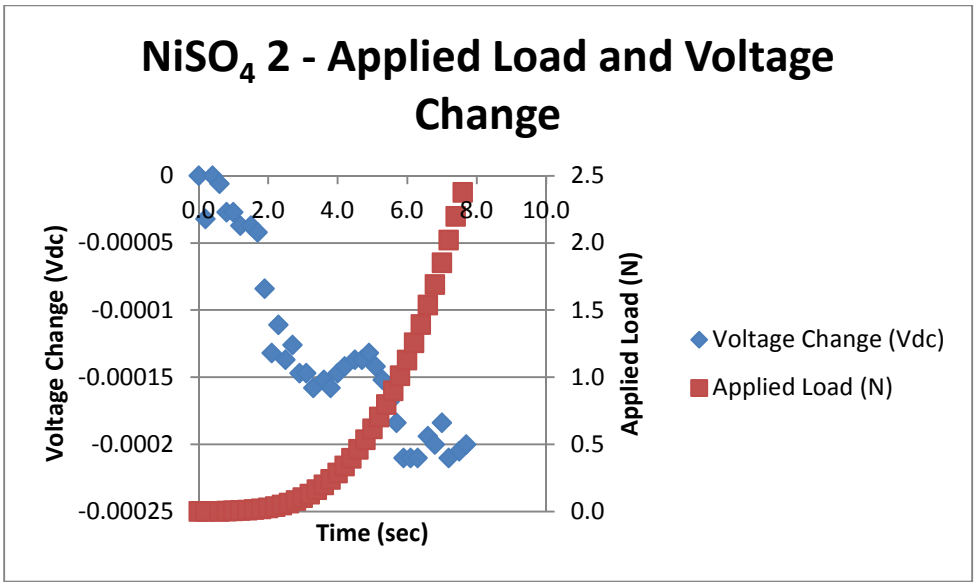

Figure 138

Trial 2 normal polarity $NiSO_4$ electrolyte constant load scenario, load and voltage change

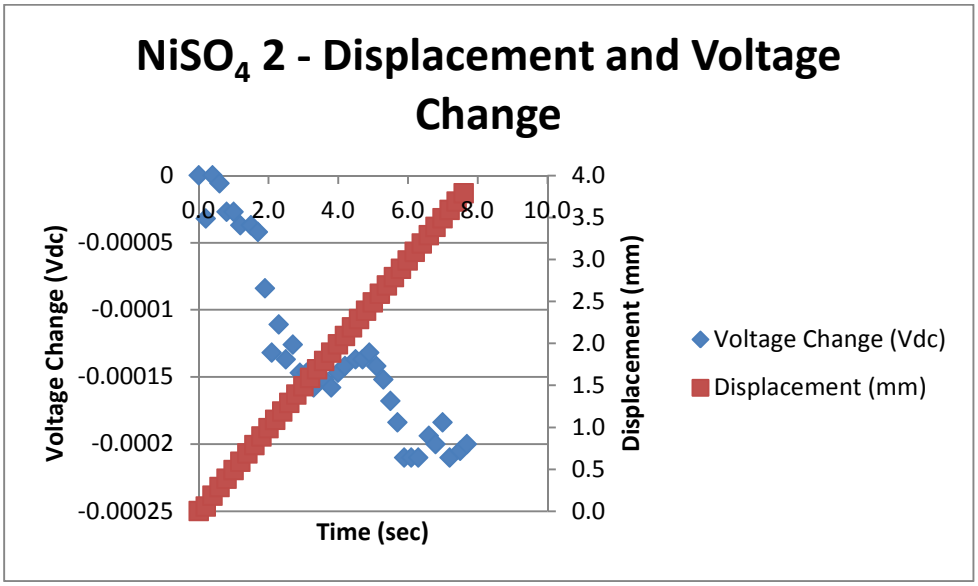

Figure 139

Trial 2 normal polarity $NiSO_4$ electrolyte constant load scenario, displacement and voltage change

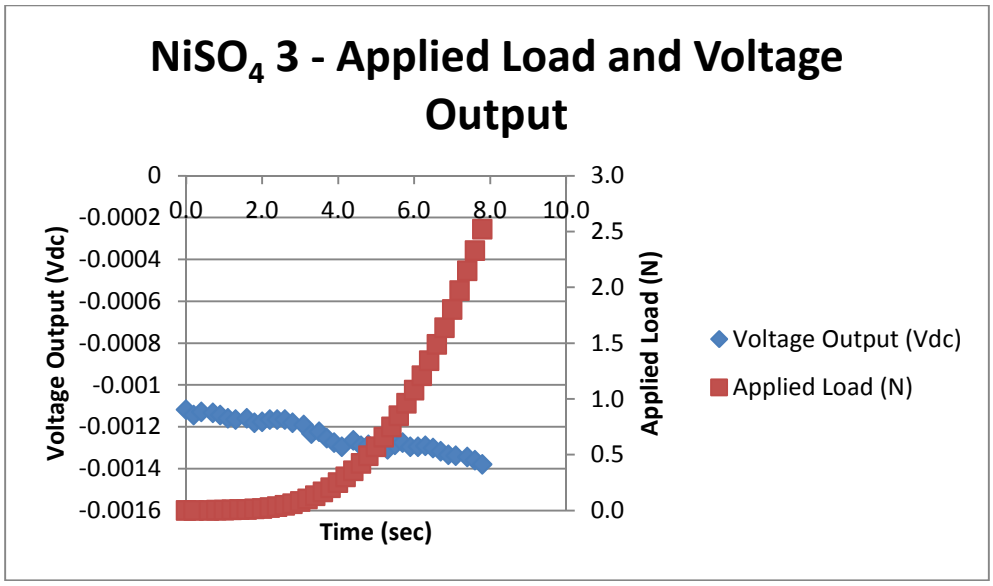

Figure 140

Trial 3 normal polarity $NiSO_4$ electrolyte constant load scenario, load and raw voltage output

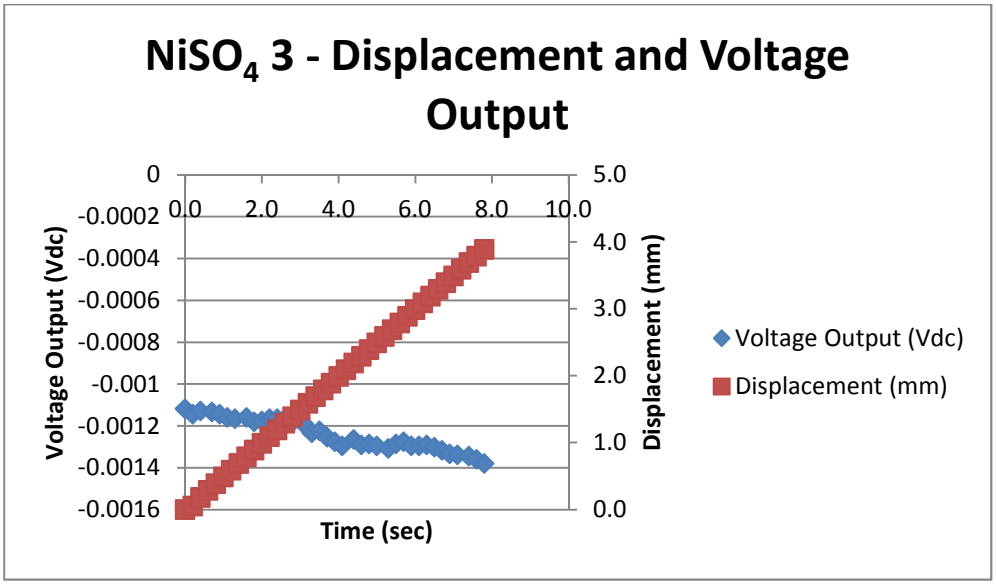

Figure 141

Trial 3 normal polarity $NiSO_4$ electrolyte constant load scenario, displacement and raw voltage output

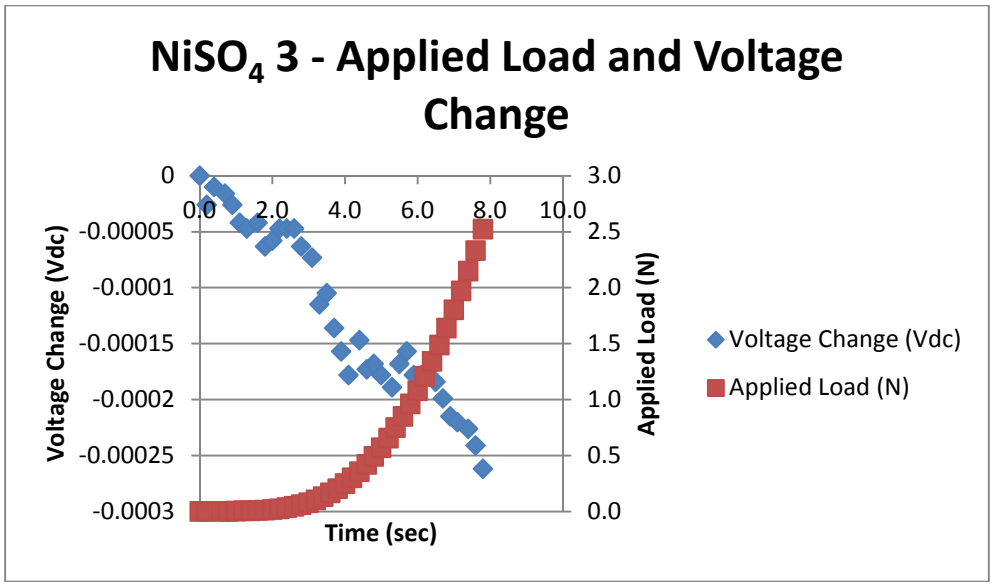

Figure 142
Trial 3 normal polarity $NiSO_4$ electrolyte constant load scenario, load and voltage change

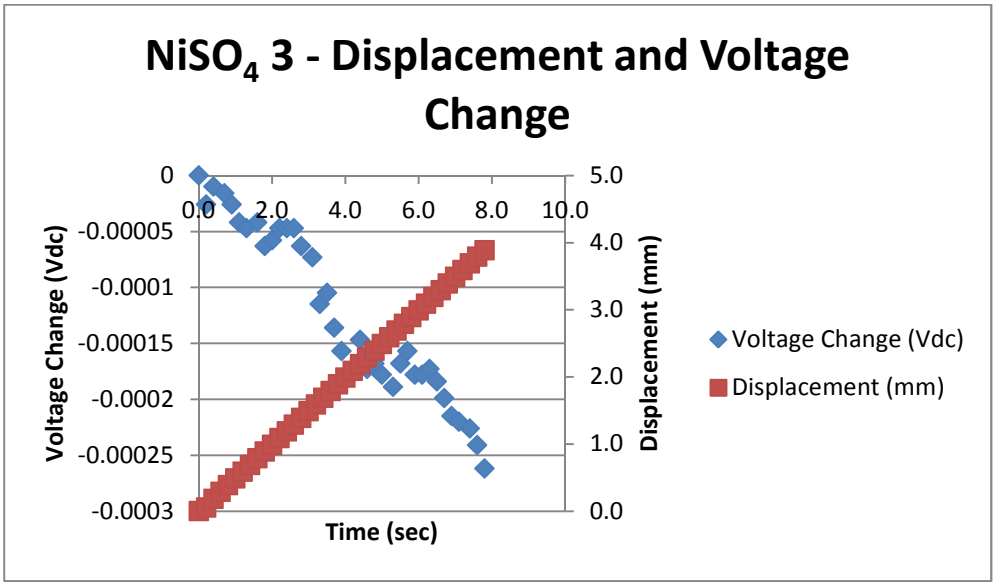

Figure 143
Trial 3 normal polarity $NiSO_4$ electrolyte constant load scenario, displacement and voltage change

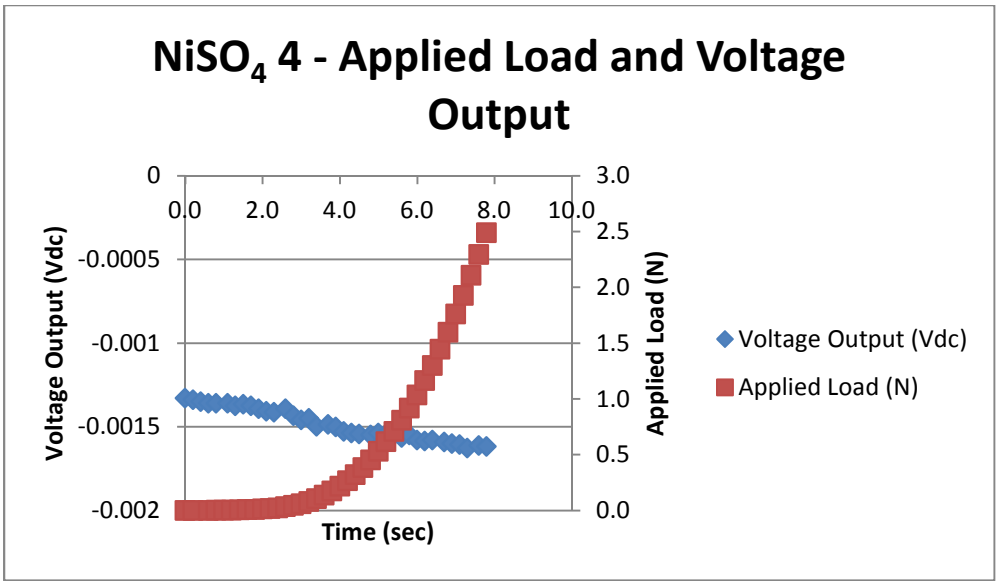

Figure 144

Trial 4 normal polarity $NiSO_4$ electrolyte constant load scenario, load and raw voltage output

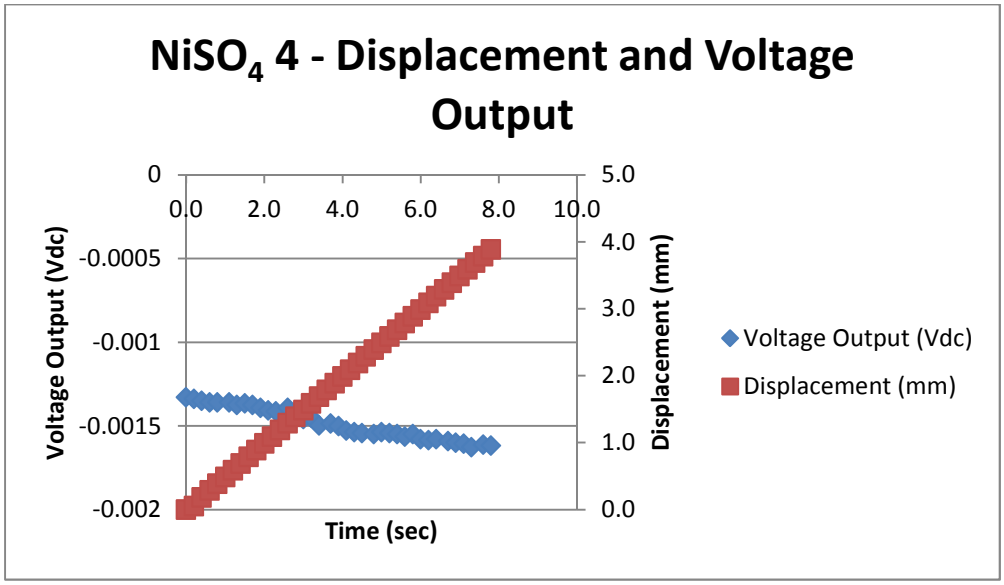

Figure 145

Trial 4 normal polarity $NiSO_4$ electrolyte constant load scenario, displacement and raw voltage output

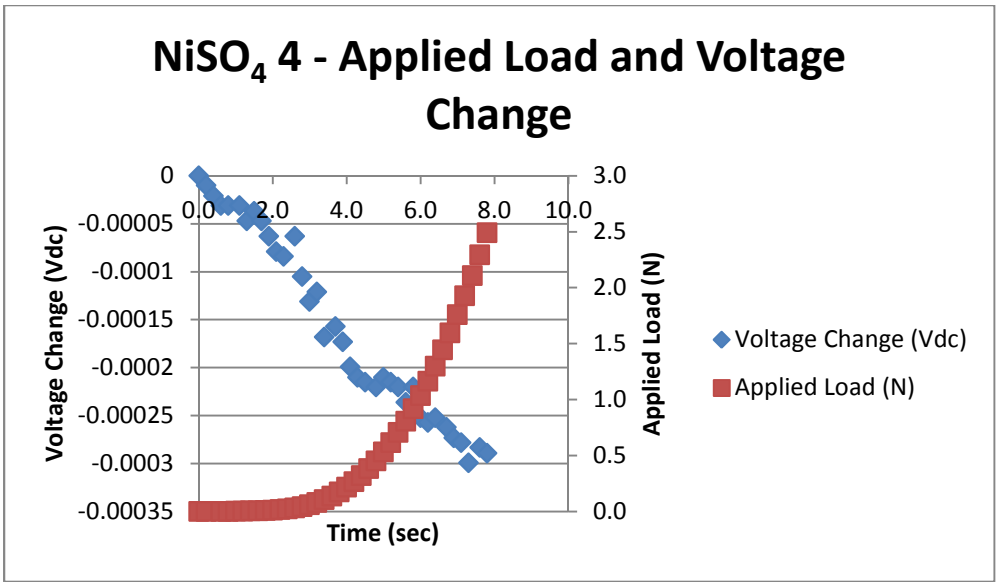

Figure 146

Trial 4 normal polarity $NiSO_4$ electrolyte constant load scenario, load and voltage change

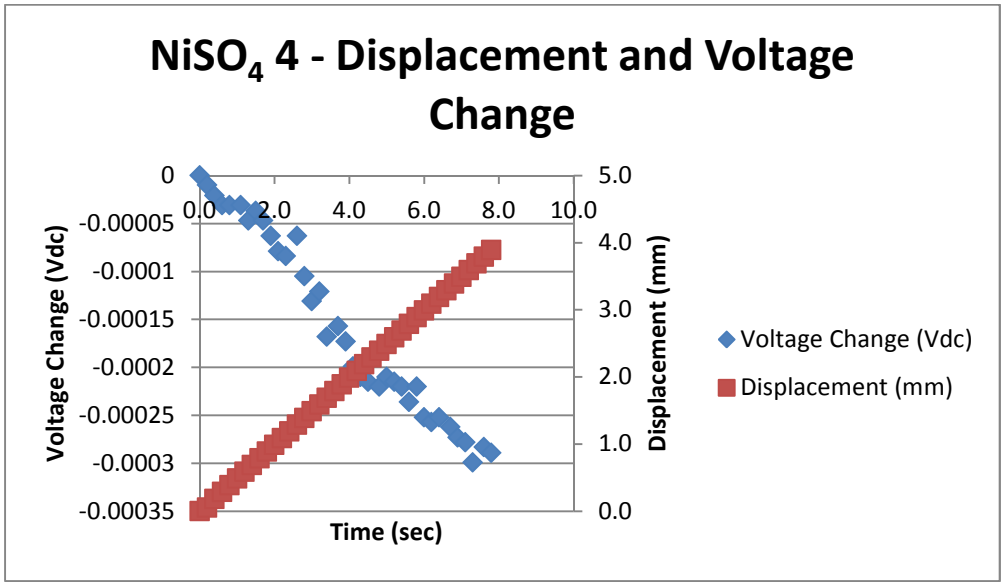

Figure 147

Trial 4 normal polarity $NiSO_4$ electrolyte constant load scenario, displacement and voltage change

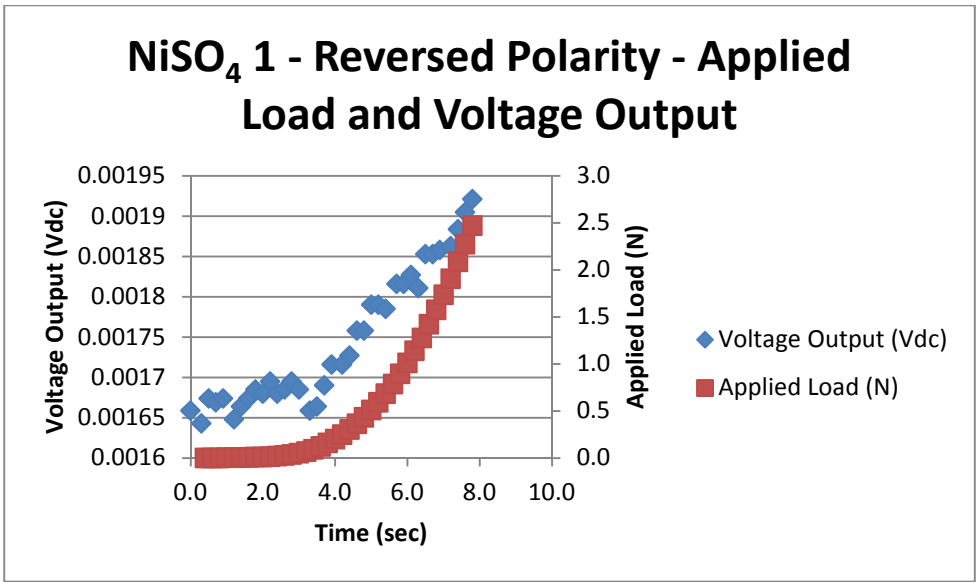

Figure 148
Trial 1 reversed polarity $NiSO_4$ electrolyte constant load scenario, load and raw voltage output

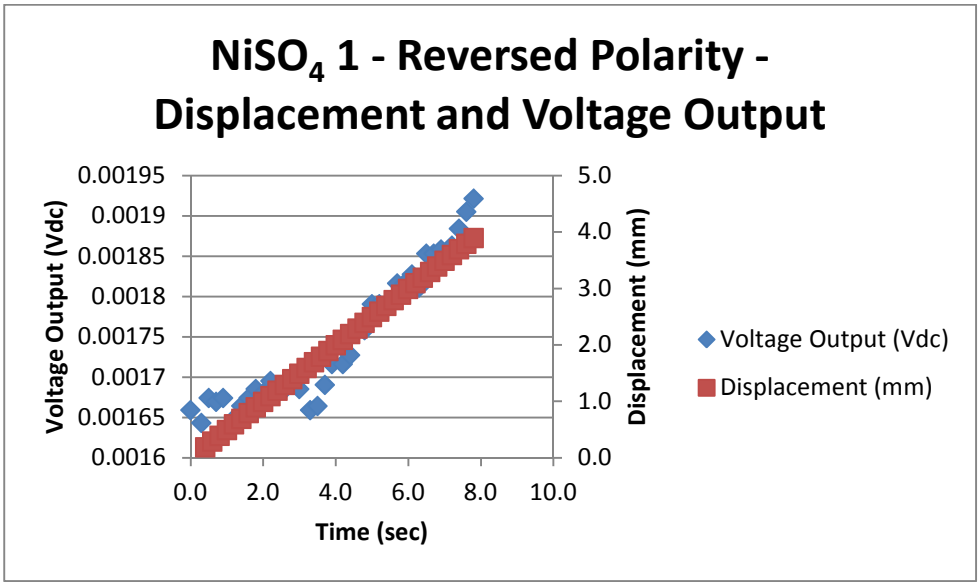

Figure 149
Trial 1 reversed polarity $NiSO_4$ electrolyte constant load scenario, displacement and raw voltage output

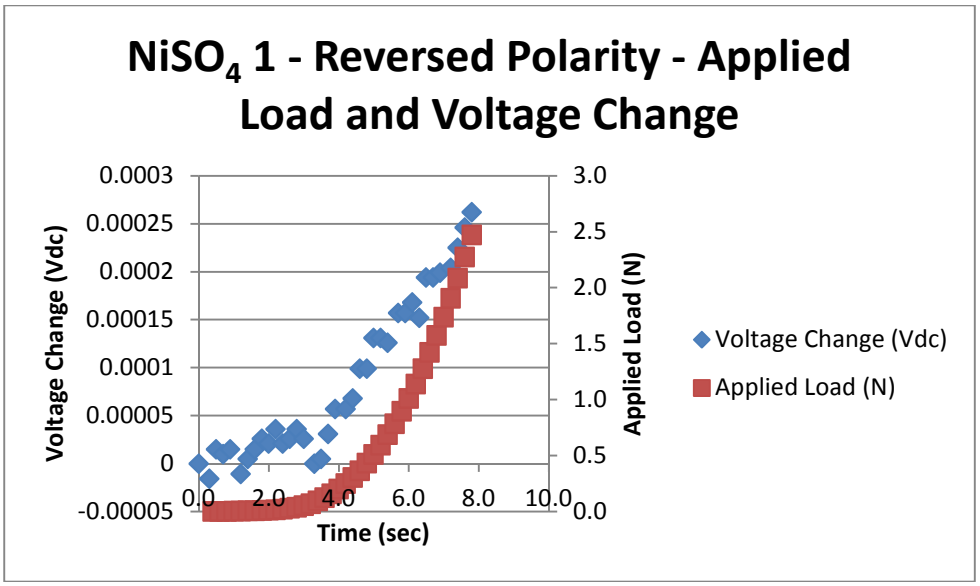

Figure 150

Trial 1 reversed polarity $NiSO_4$ electrolyte constant load scenario, load and voltage change

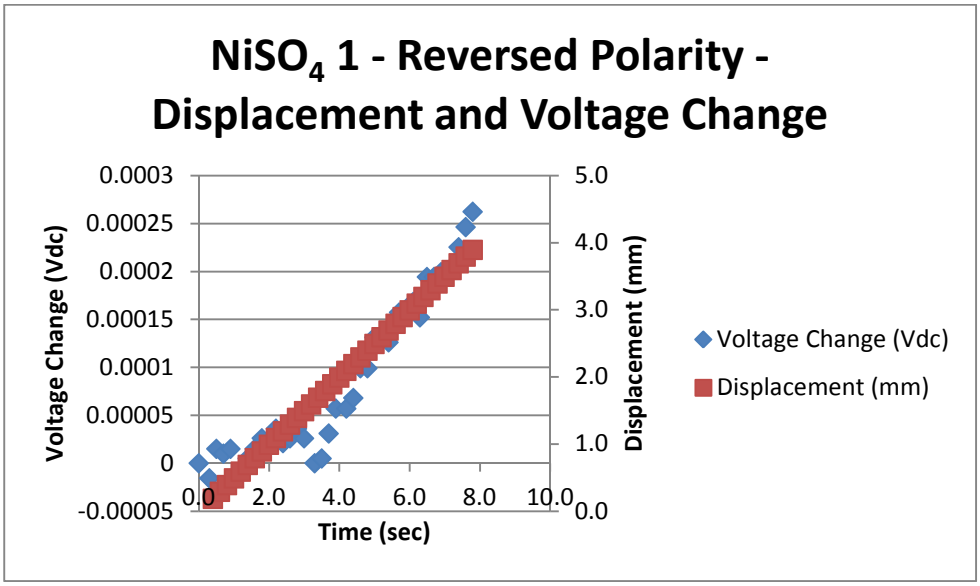

Figure 151

Trial 1 reversed polarity $NiSO_4$ electrolyte constant load scenario, displacement and voltage change

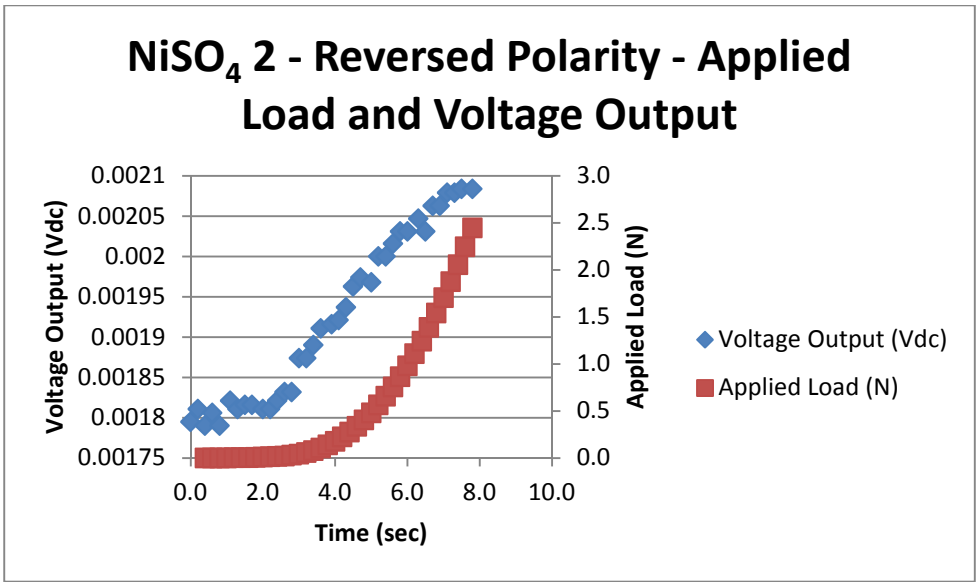

Figure 152
Trial 2 reversed polarity $NiSO_4$ electrolyte constant load scenario, load and raw voltage output

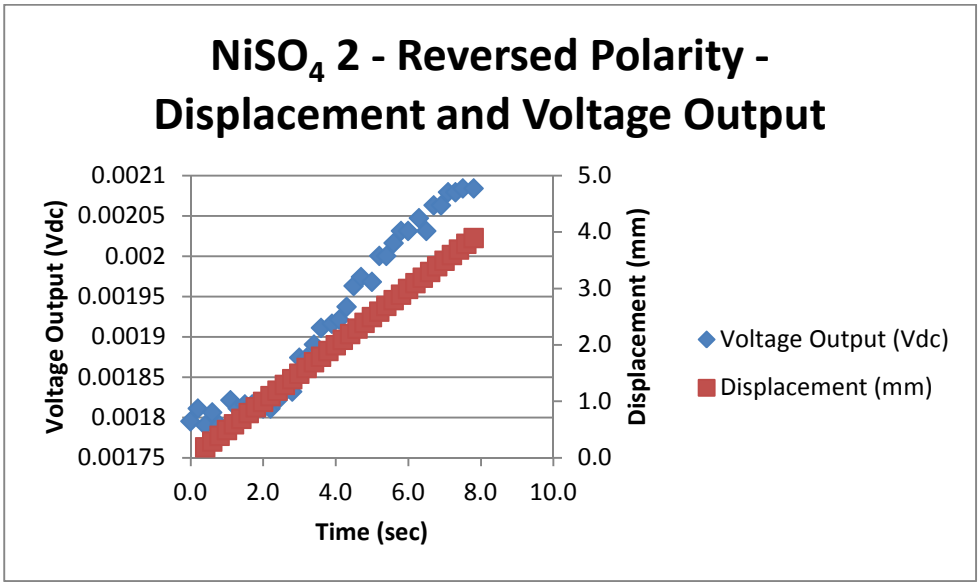

Figure 153
Trial 2 reversed polarity $NiSO_4$ electrolyte constant load scenario, displacement and raw voltage output

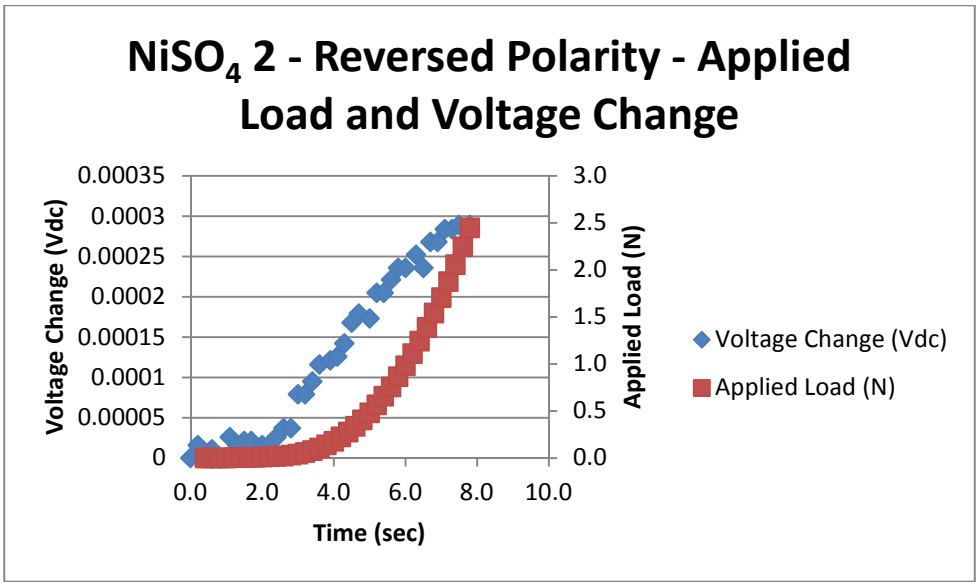

Figure 154

Trial 2 reversed polarity $NiSO_4$ electrolyte constant load scenario, load and voltage change

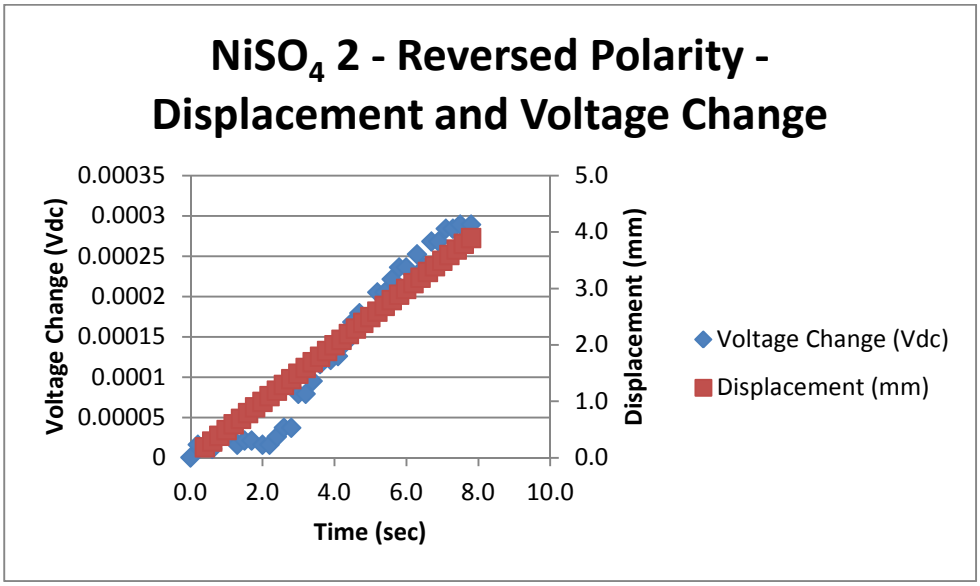

Figure 155

Trial 2 reversed polarity $NiSO_4$ electrolyte constant load scenario, displacement and voltage change

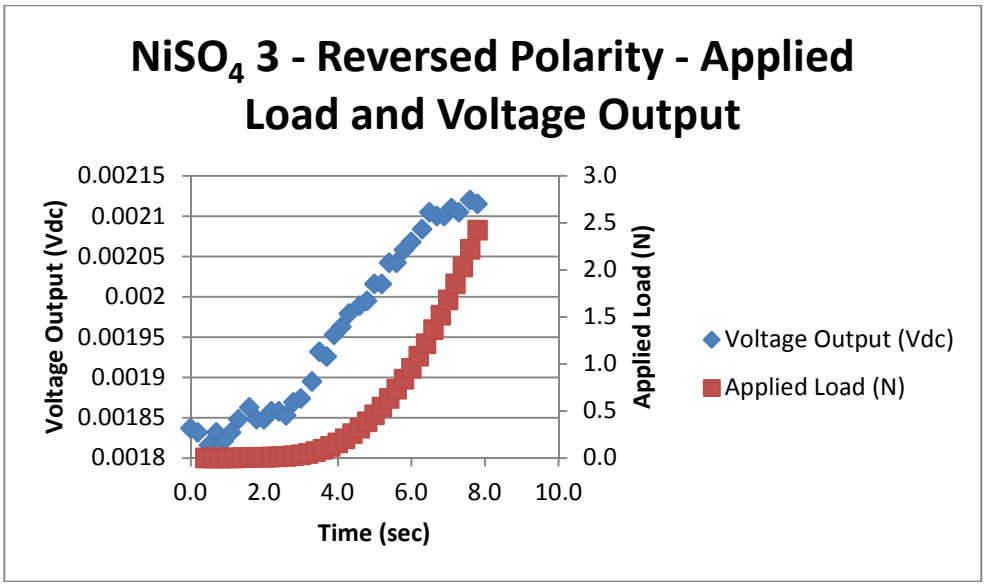

Figure 156
Trial 3 reversed polarity $NiSO_4$ electrolyte constant load scenario, load and raw voltage output

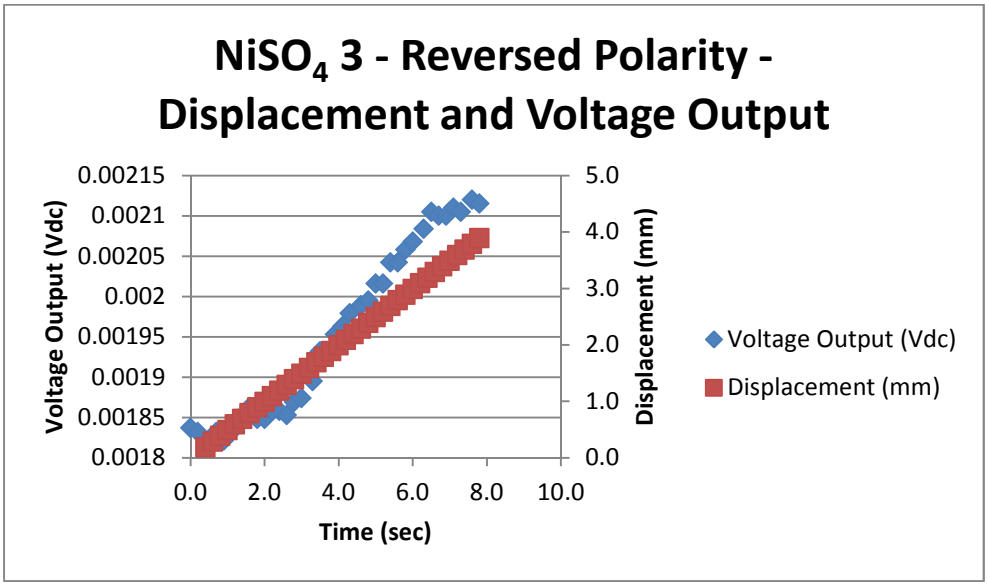

Figure 157
Trial 3 reversed polarity $NiSO_4$ electrolyte constant load scenario, displacement and raw voltage output

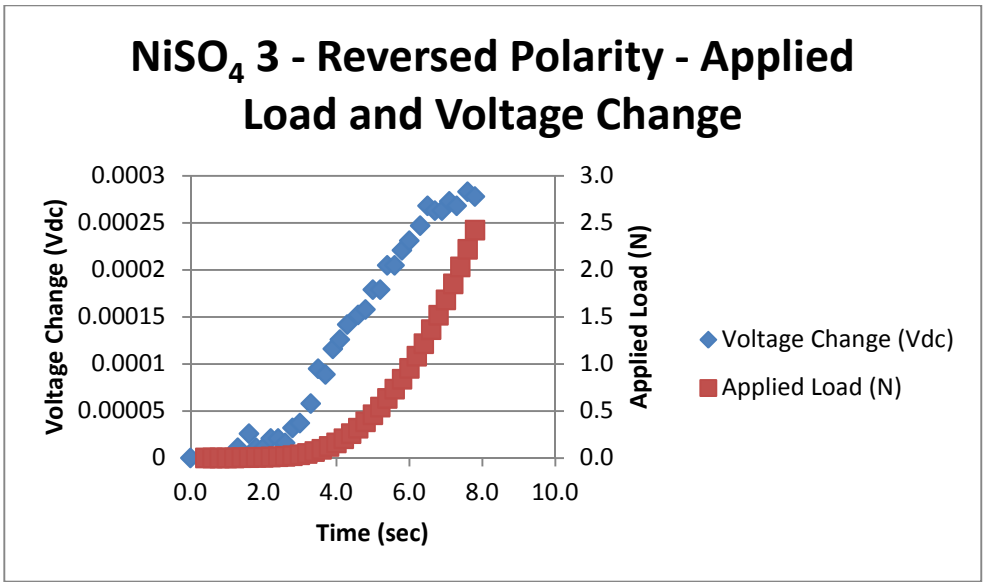

Figure 158

Trial 3 reversed polarity $NiSO_4$ electrolyte constant load scenario, load and voltage change

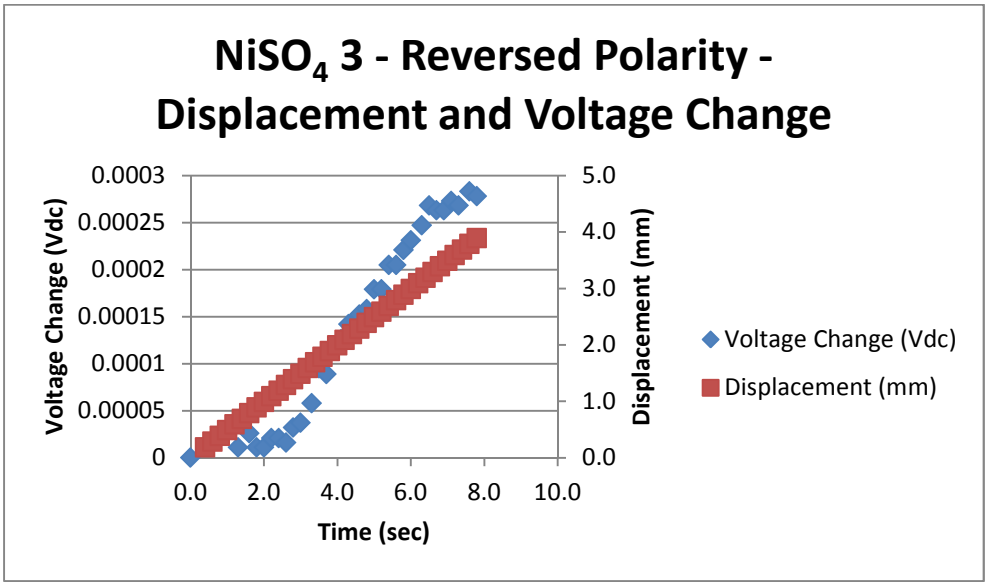

Figure 159

Trial 3 reversed polarity $NiSO_4$ electrolyte constant load scenario, displacement and voltage change

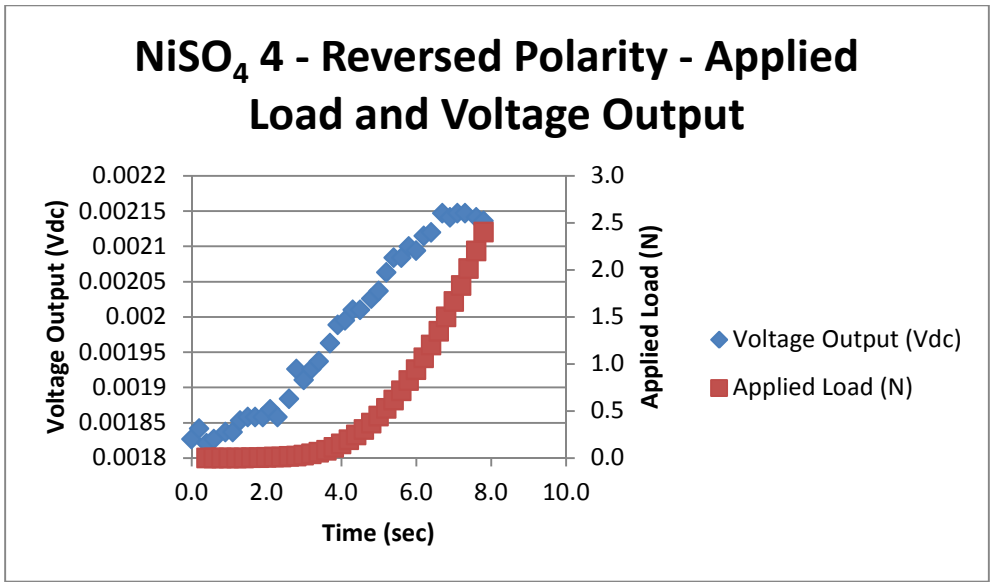

Figure 160

Trial 4 reversed polarity $NiSO_4$ electrolyte constant load scenario, load and raw voltage output

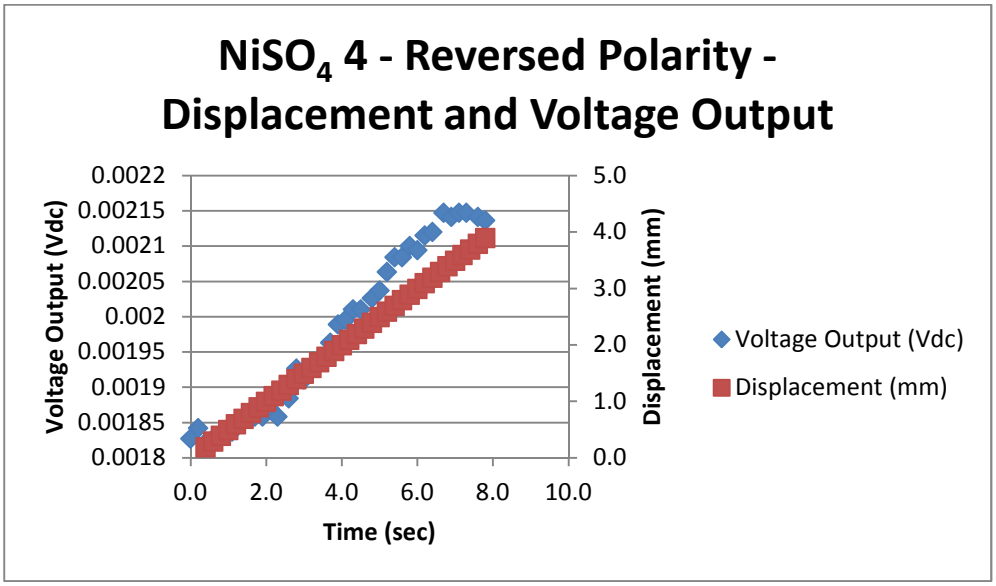

Figure 161

Trial 4 reversed polarity $NiSO_4$ electrolyte constant load scenario, displacement and raw voltage output

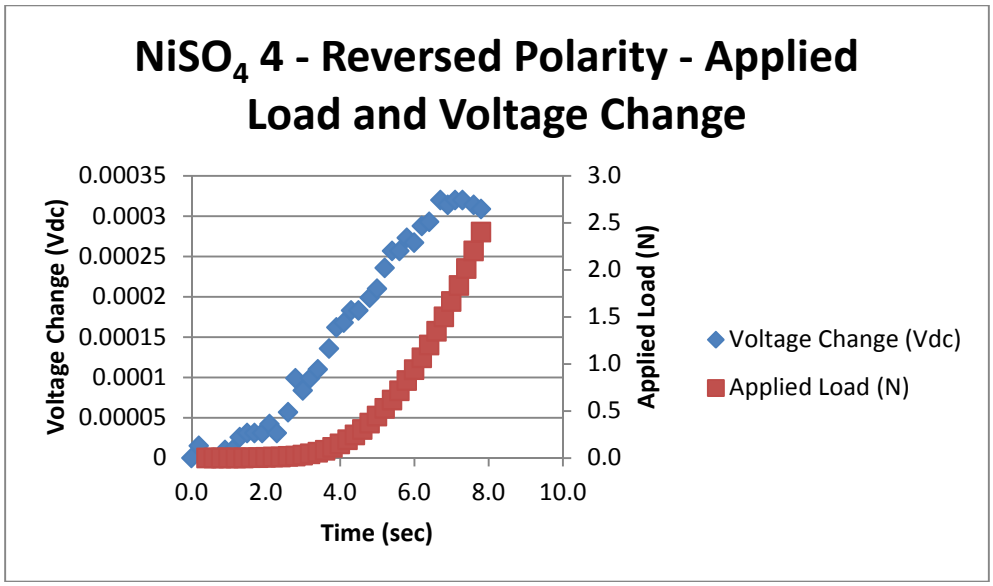

Figure 162

Trial 4 reversed polarity $NiSO_4$ electrolyte constant load scenario, load and voltage change

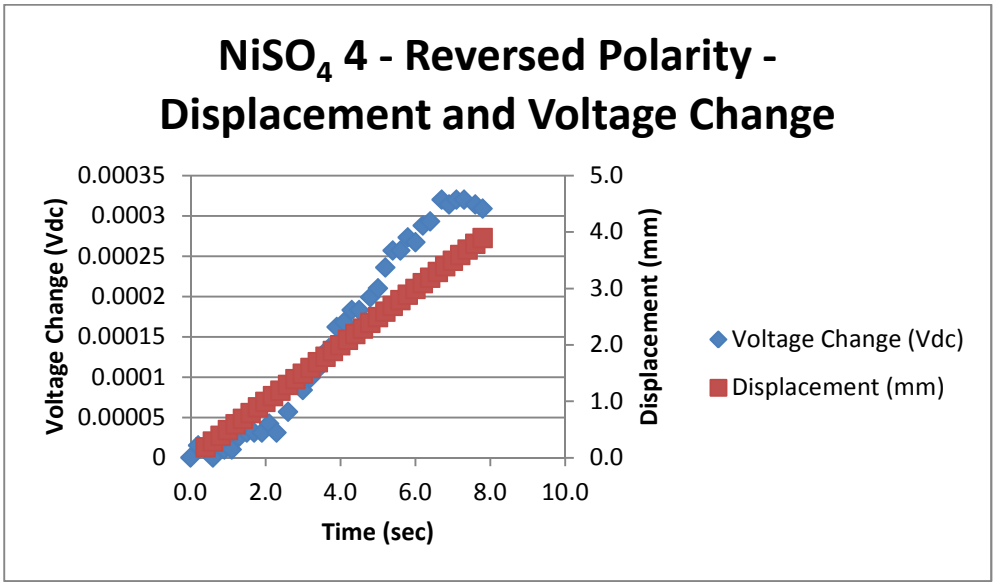

Figure 163

Trial 4 reversed polarity $NiSO_4$ electrolyte constant load scenario, displacement and voltage change

Appendix E

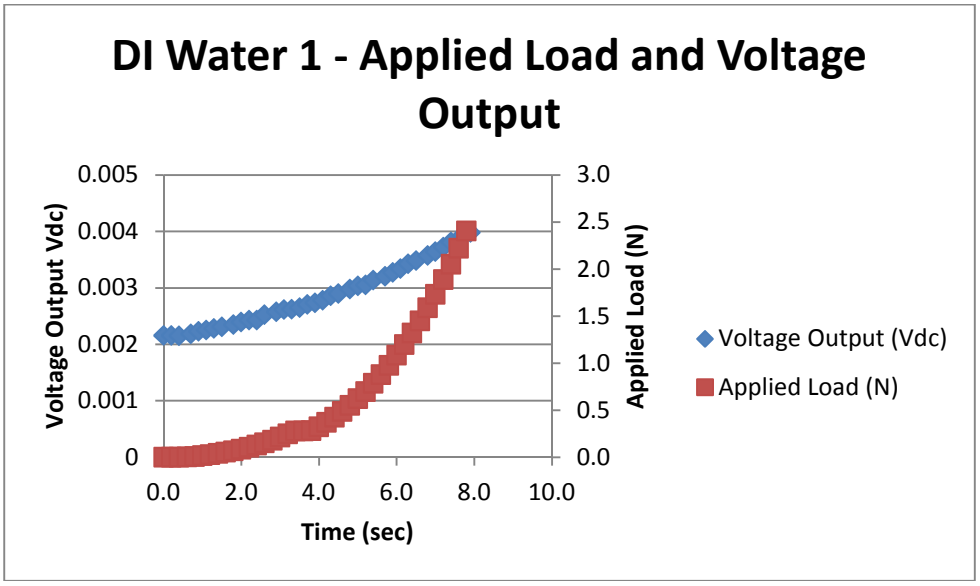

Figure 164

Trial 1 normal polarity DI water electrolyte constant load scenario, load and raw voltage output

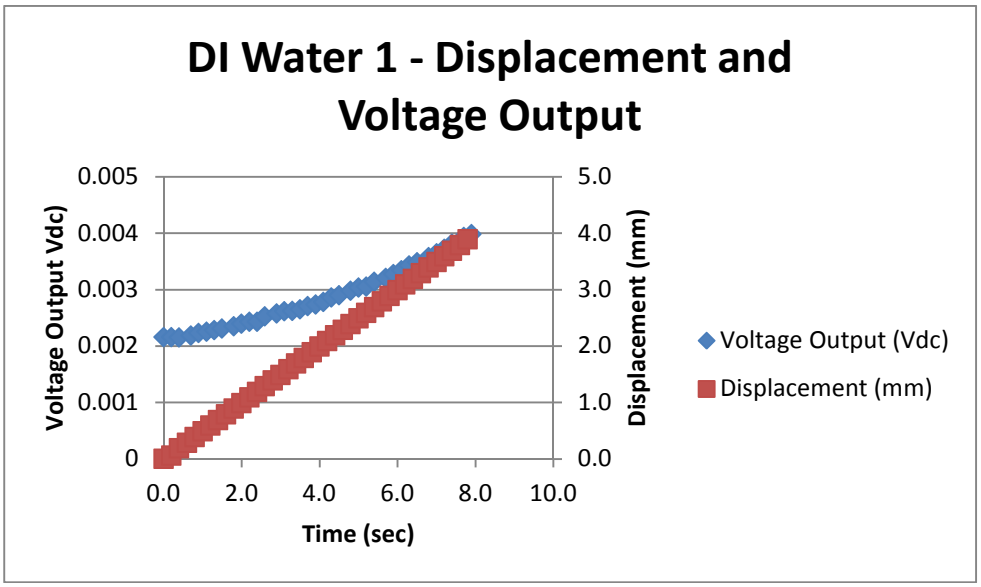

Figure 165

Trial 1 normal polarity DI water electrolyte constant load scenario, displacement and raw voltage output

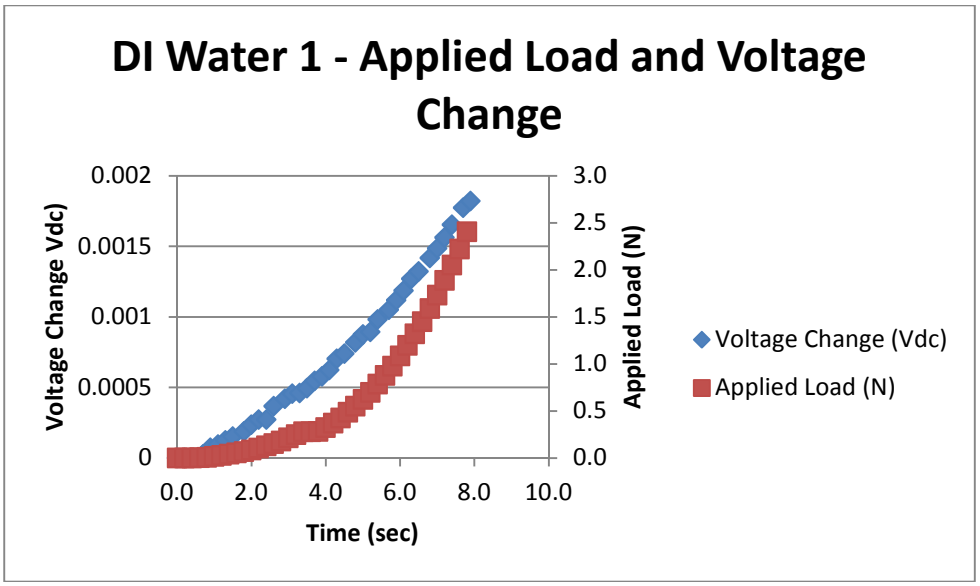

Figure 166

Trial 1 normal polarity DI water electrolyte constant load scenario, load and voltage change

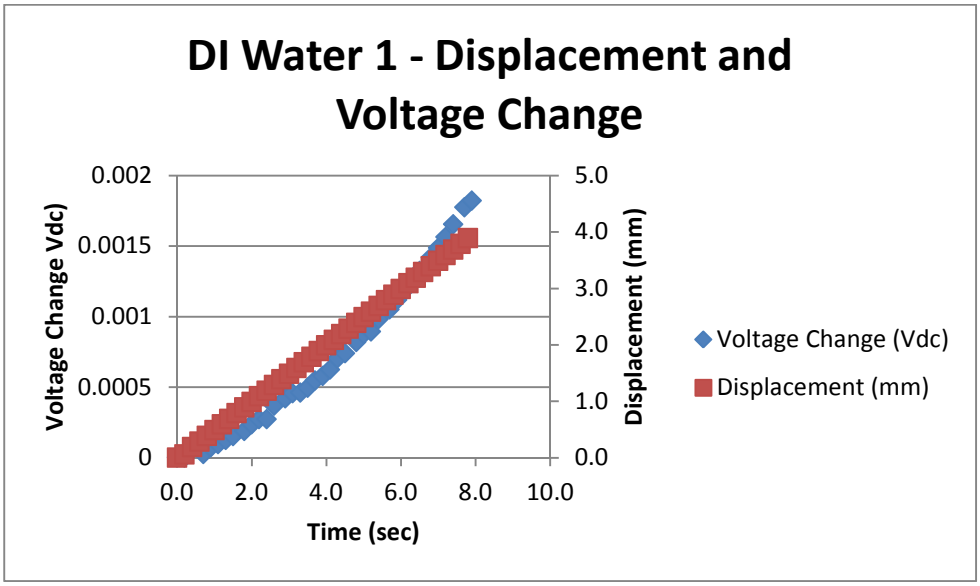

Figure 167

Trial 1 normal polarity DI water electrolyte constant load scenario, displacement and voltage change

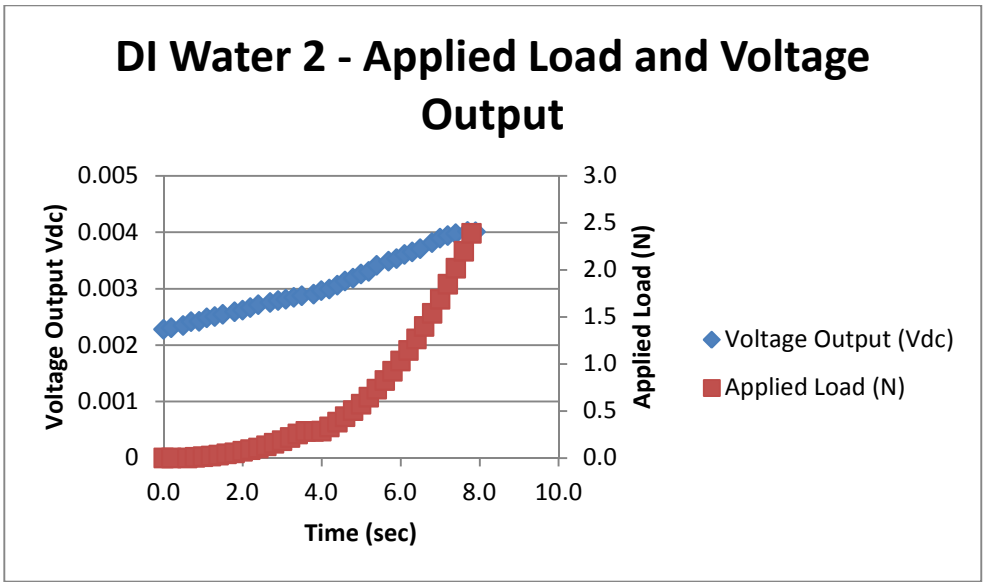

Figure 168

Trial 2 normal polarity DI water electrolyte constant load scenario, load and raw voltage output

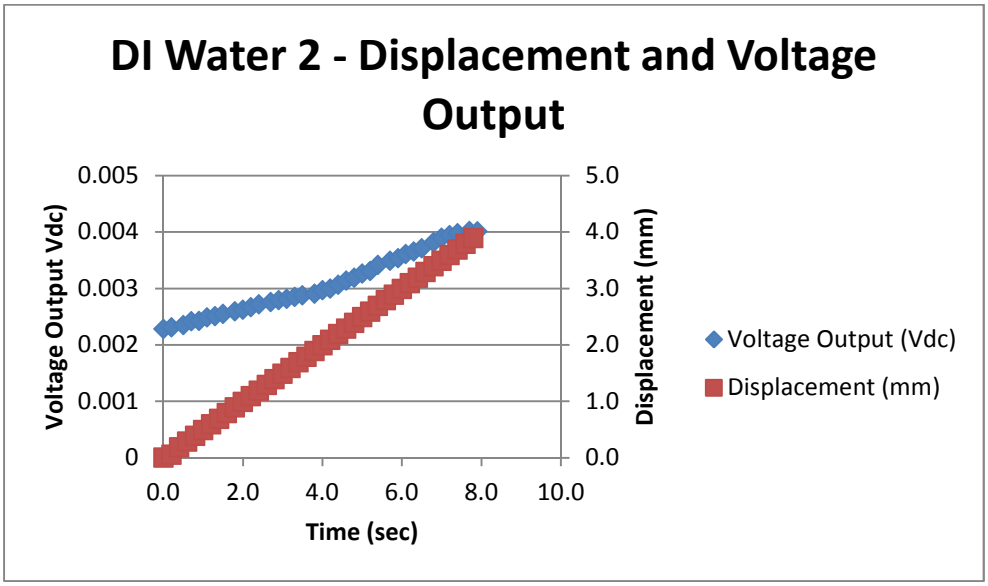

Figure 169

Trial 2 normal polarity DI water electrolyte constant load scenario, displacement and raw voltage output

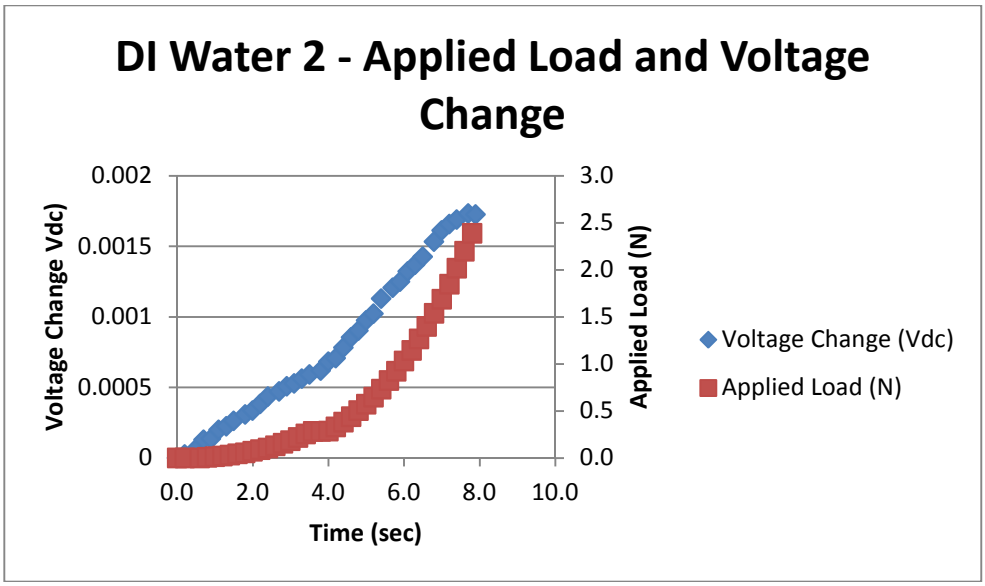

Figure 170

Trial 2 normal polarity DI water electrolyte constant load scenario, load and voltage change

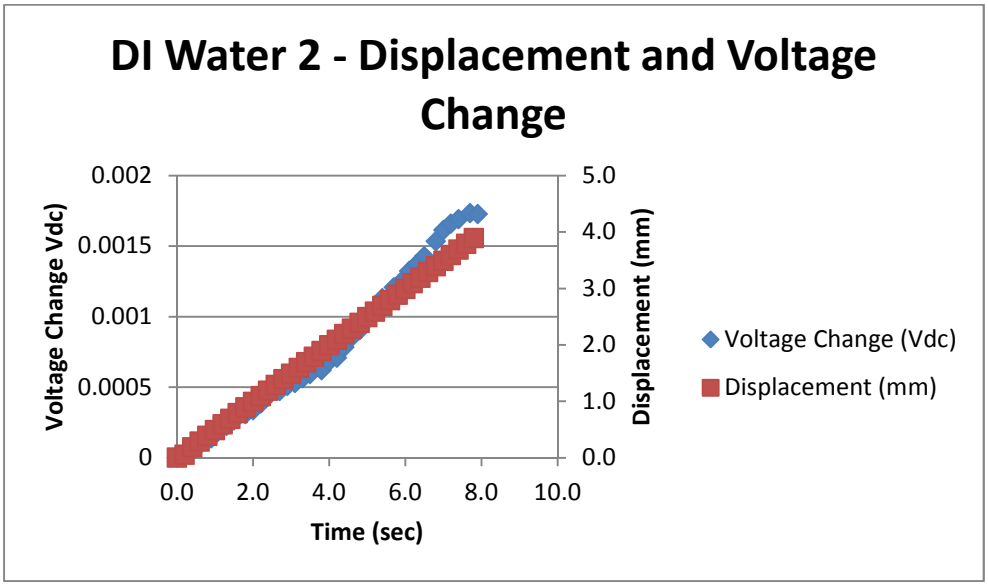

Figure 171

Trial 2 normal polarity DI water electrolyte constant load scenario, displacement and voltage change

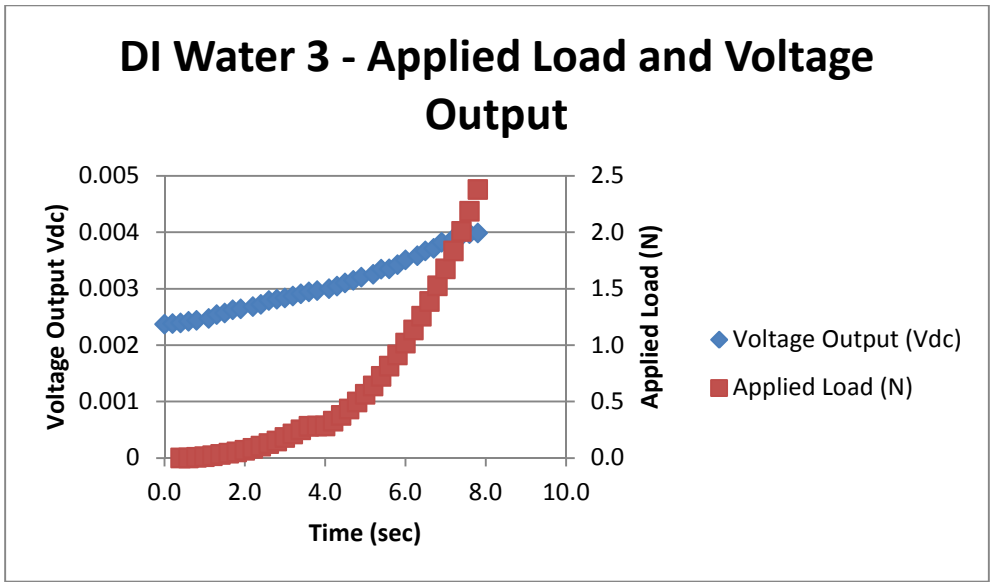

Figure 172
Trial 3 normal polarity DI water electrolyte constant load scenario, load and raw voltage output

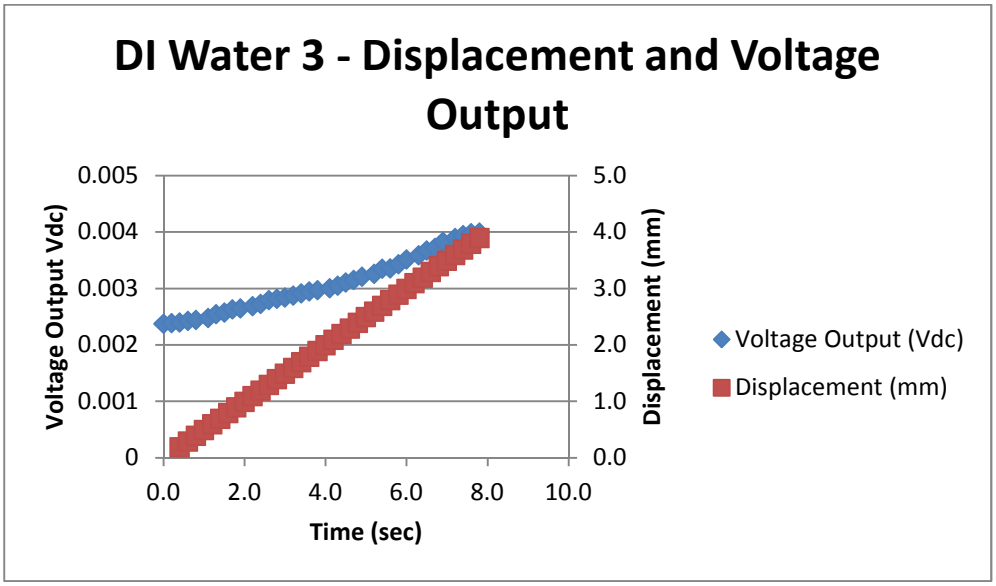

Figure 173
Trial 3 normal polarity DI water electrolyte constant load scenario, displacement and raw voltage output

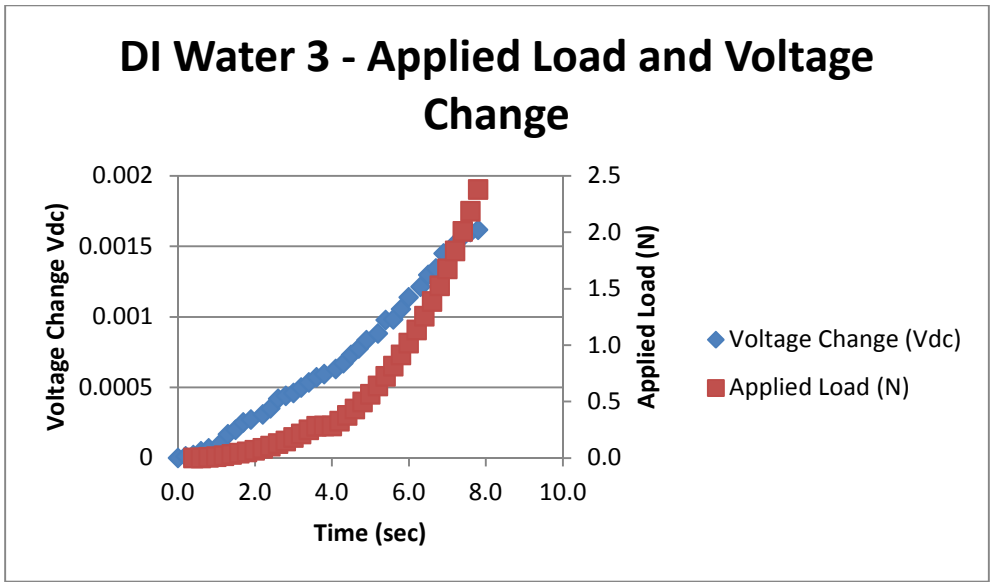

Figure 174

Trial 3 normal polarity DI water electrolyte constant load scenario, load and voltage change

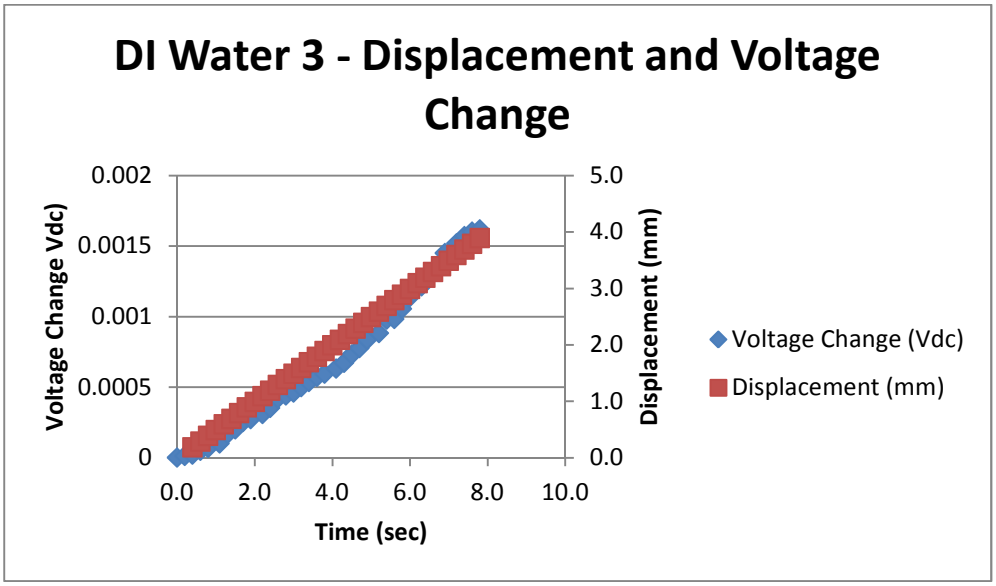

Figure 175

Trial 3 normal polarity DI water electrolyte constant load scenario, displacement and voltage change

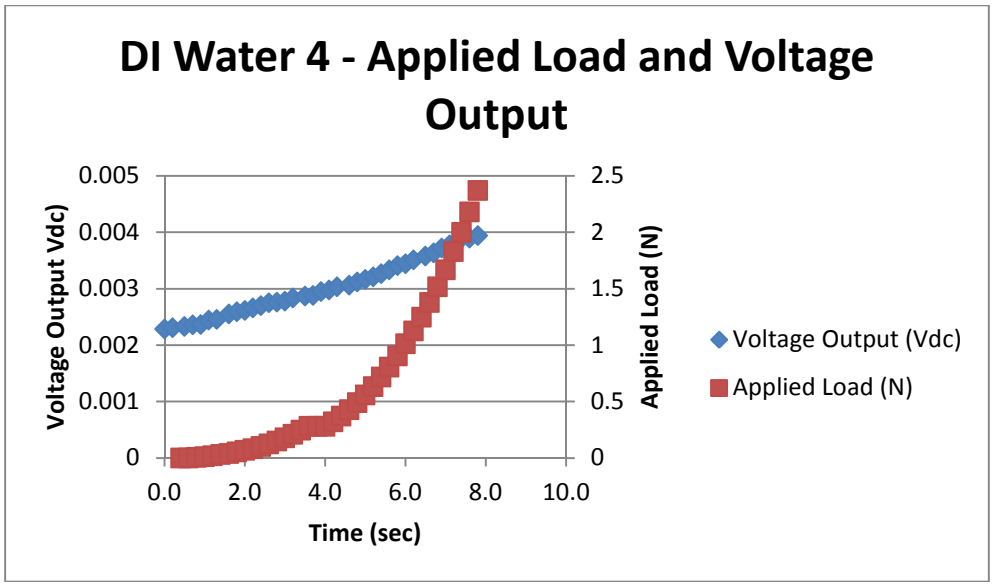

Figure 176
Trial 4 normal polarity DI water electrolyte constant load scenario, load and raw voltage output

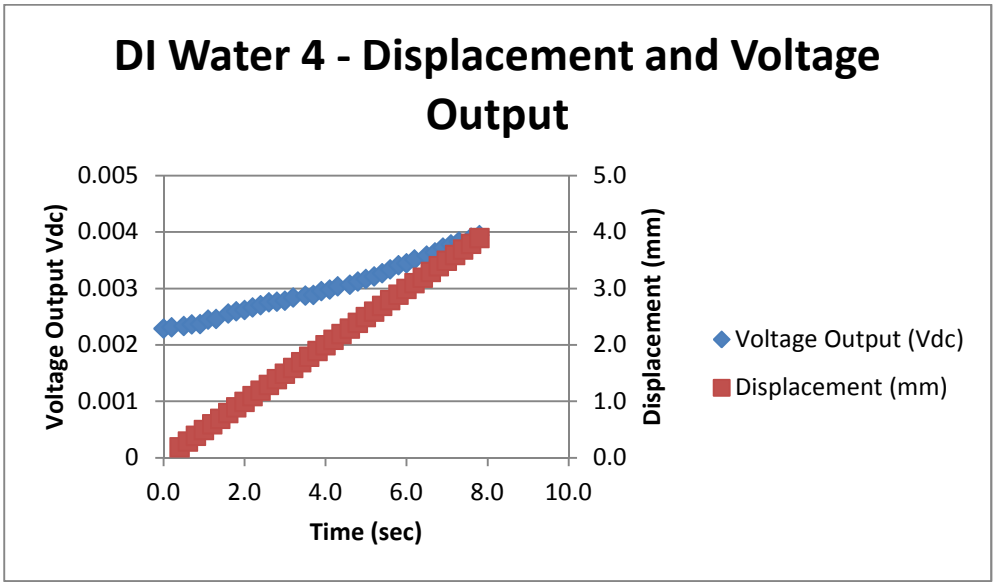

Figure 177
Trial 4 normal polarity DI water electrolyte constant load scenario, displacement and raw voltage output

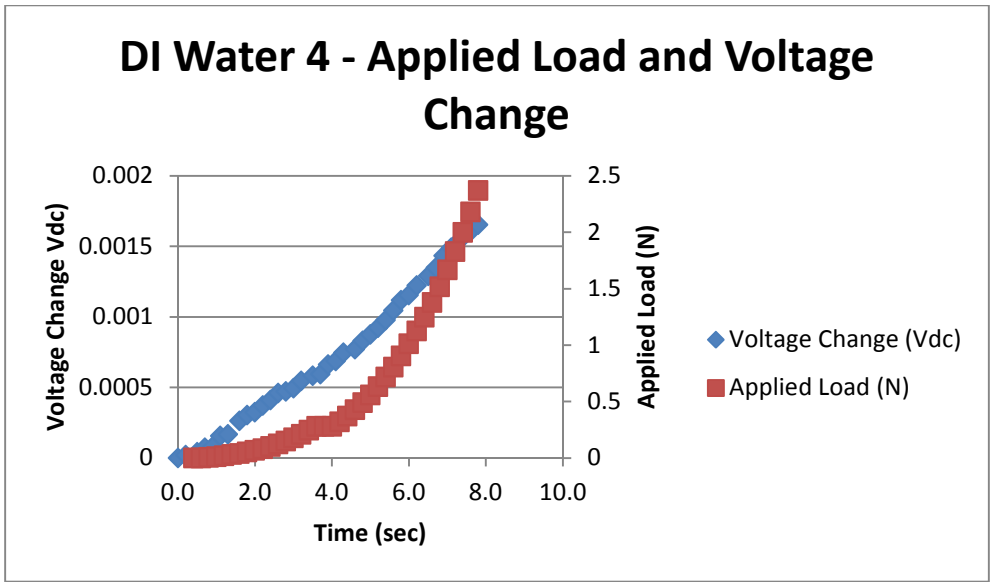

Figure 178

Trial 4 normal polarity DI water electrolyte constant load scenario, load and voltage change

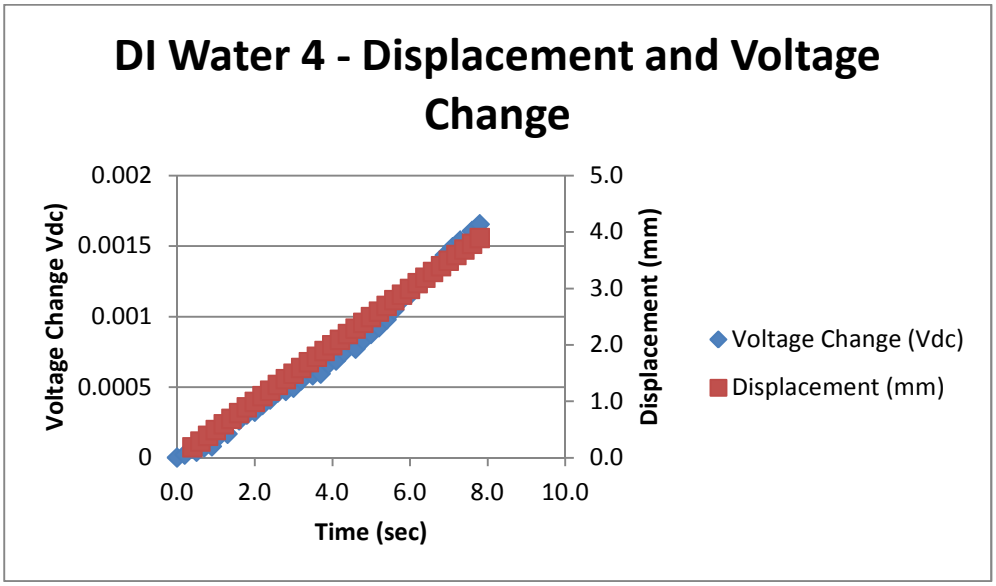

Figure 179

Trial 4 normal polarity DI water electrolyte constant load scenario, displacement and voltage change

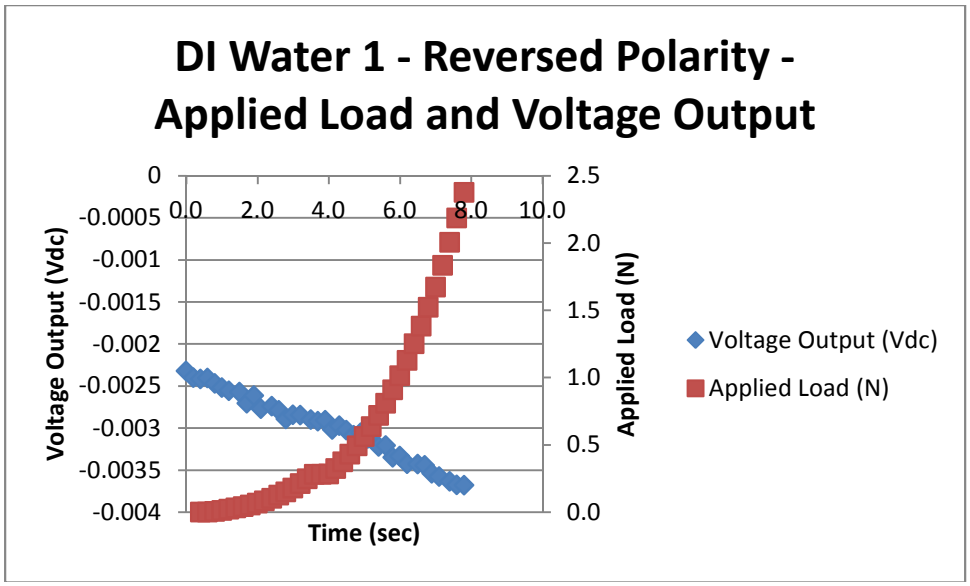

Figure 180

Trial 1 reversed polarity DI water electrolyte constant load scenario, load and raw voltage output

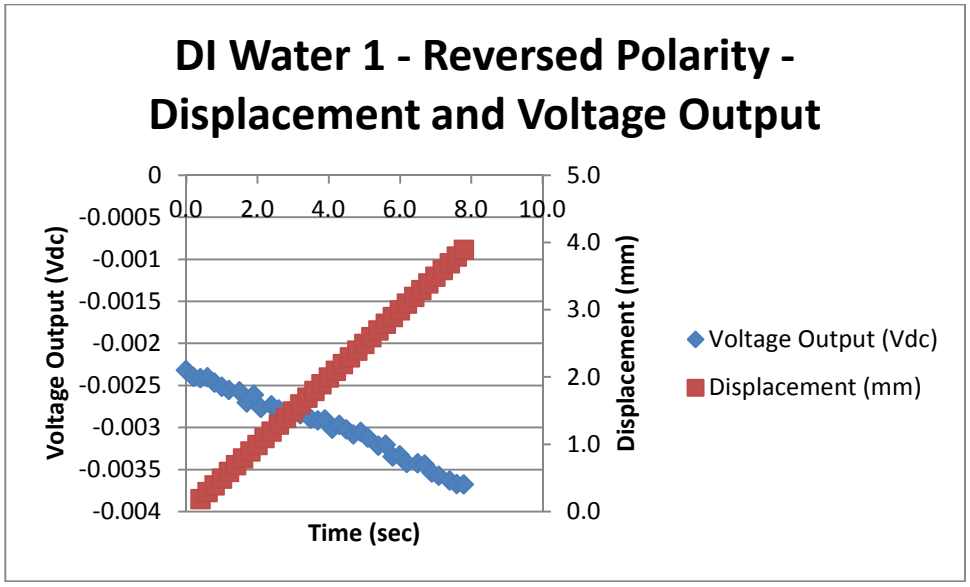

Figure 181

Trial 1 reversed polarity DI water electrolyte constant load scenario, displacement and raw voltage output

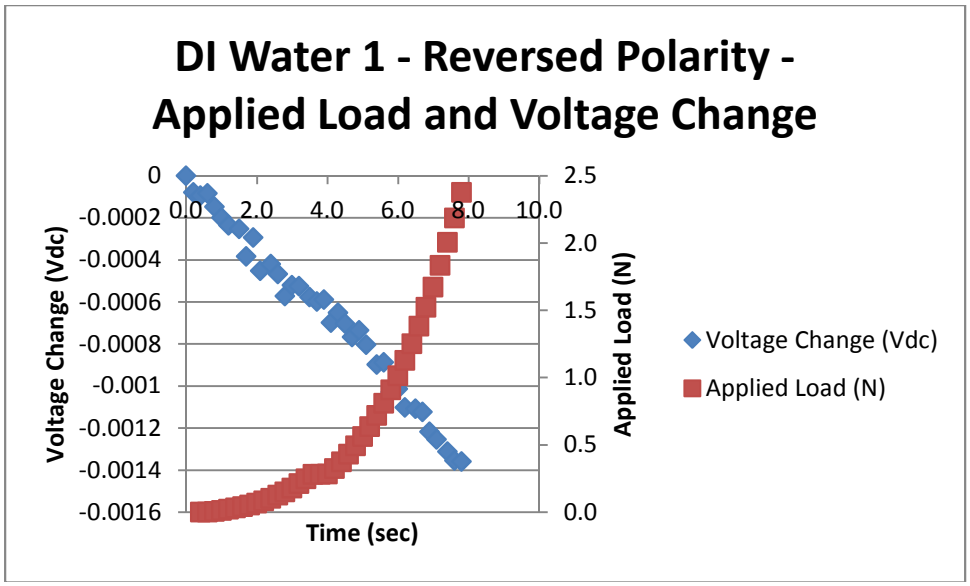

Figure 182
Trial 1 reversed polarity DI water electrolyte constant load scenario, load and voltage change

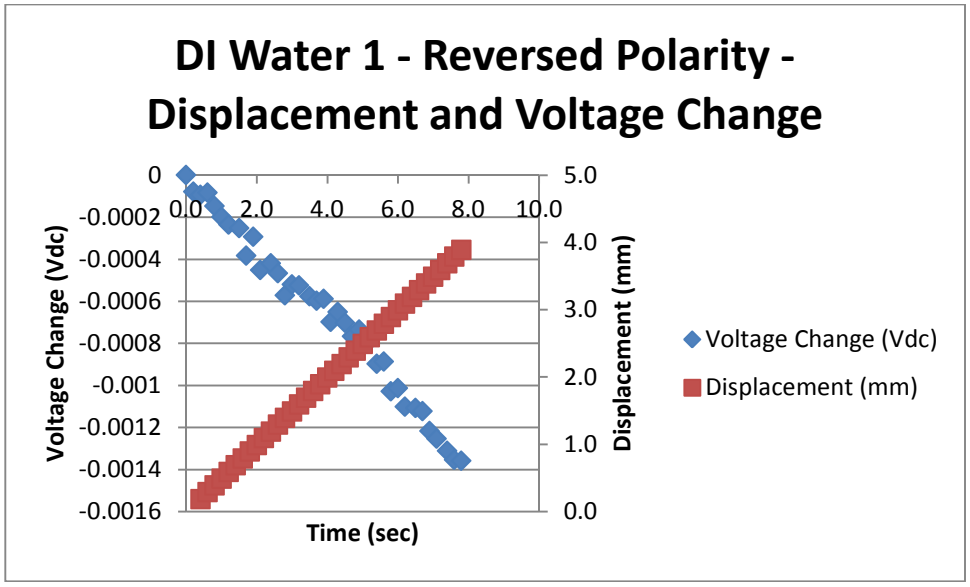

Figure 183
Trial 1 reversed polarity DI water electrolyte constant load scenario, displacement and voltage change

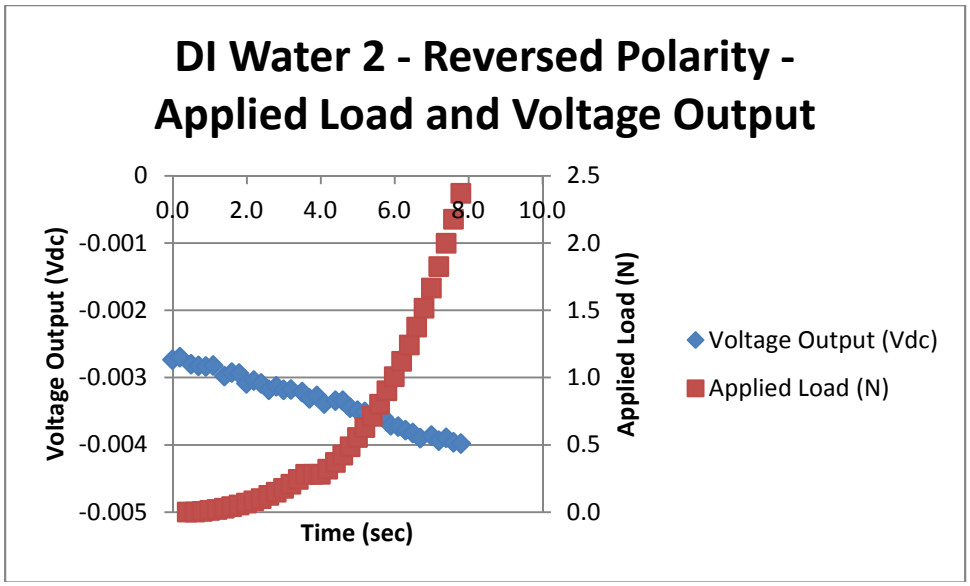

Figure 184

Trial 2 reversed polarity DI water electrolyte constant load scenario, load and raw voltage output

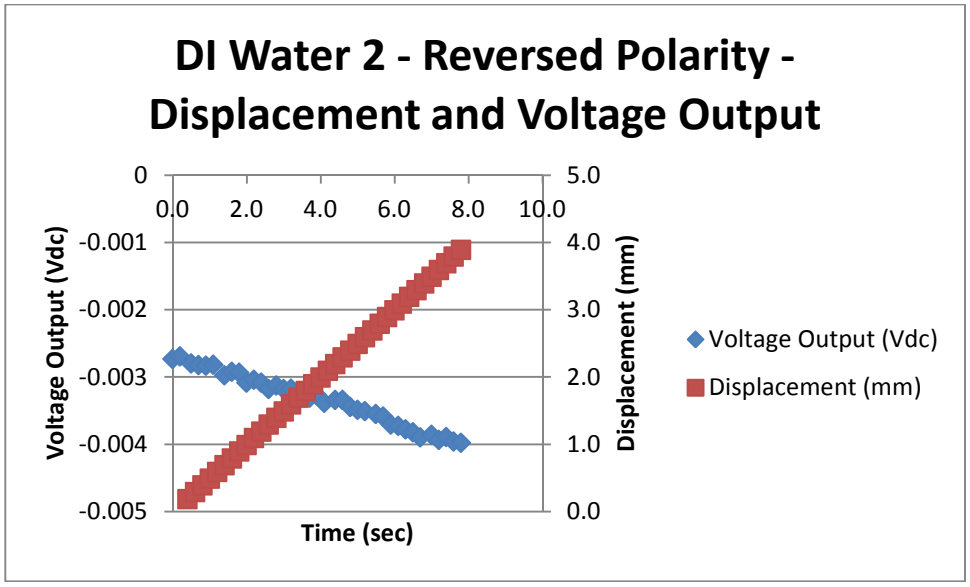

Figure 185

Trial 2 reversed polarity DI water electrolyte constant load scenario, displacement and raw voltage output

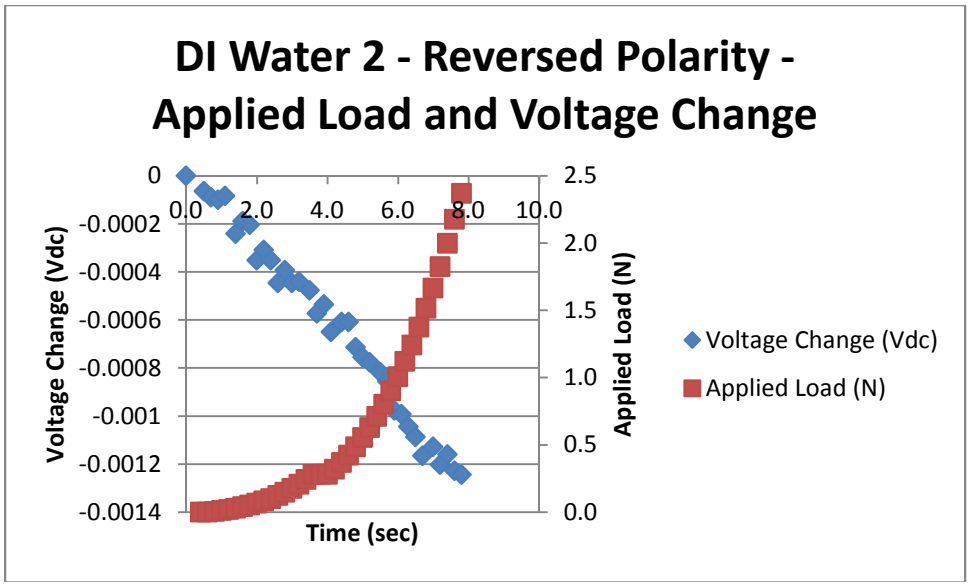

Figure 186
Trial 2 reversed polarity DI water electrolyte constant load scenario, load and voltage change

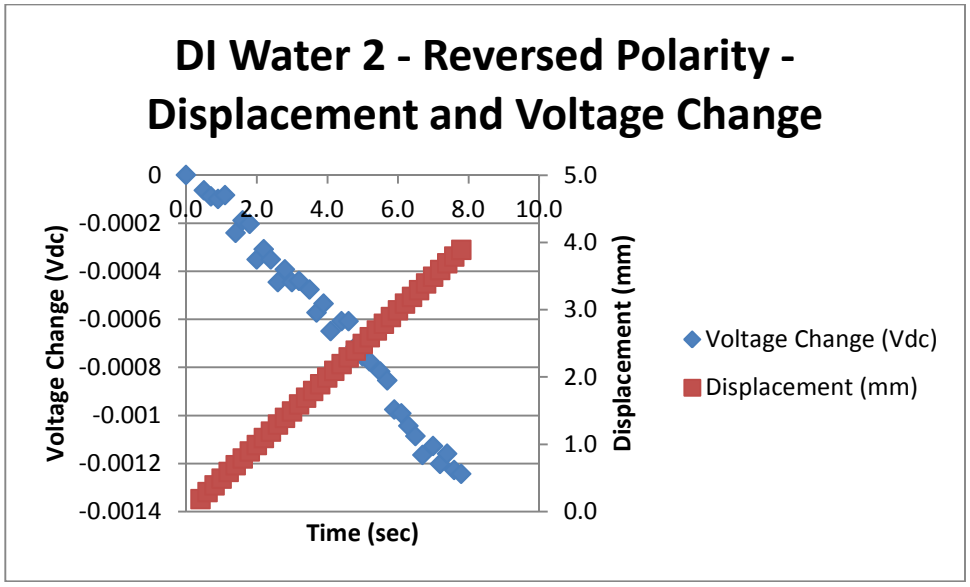

Figure 187
Trial 2 reversed polarity DI water electrolyte constant load scenario, displacement and voltage change

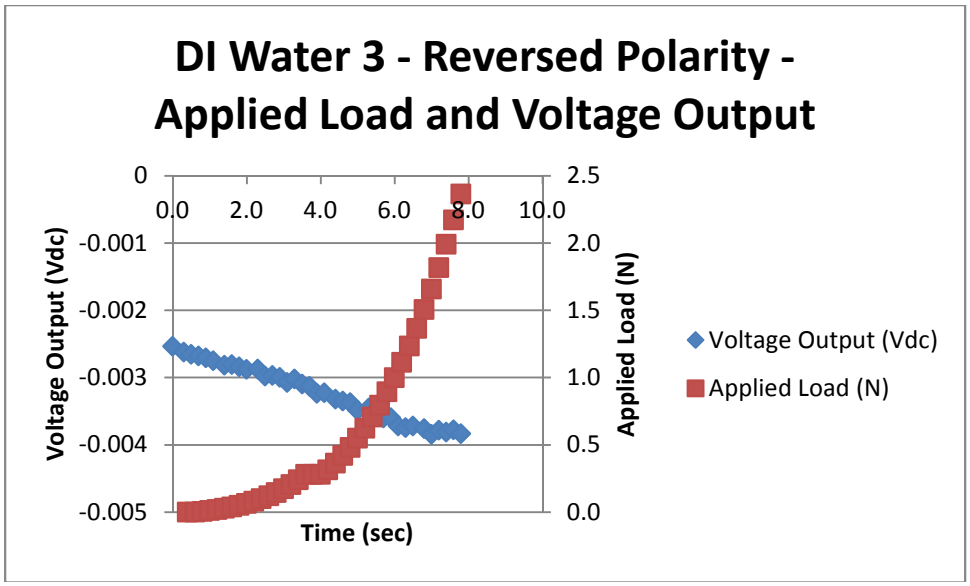

Figure 188

Trial 3 reversed polarity DI water electrolyte constant load scenario, load and raw voltage output

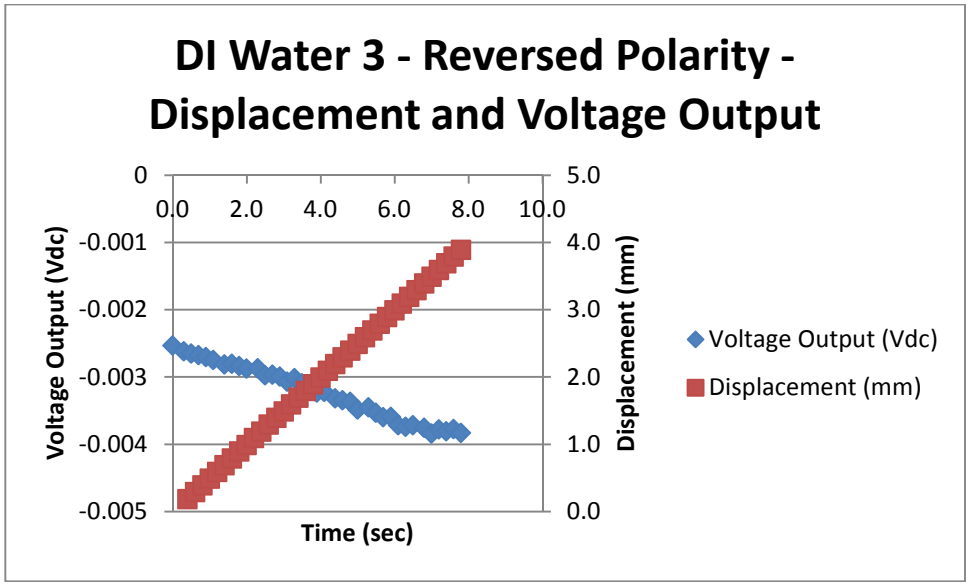

Figure 189

Trial 3 reversed polarity DI water electrolyte constant load scenario, displacement and raw voltage output

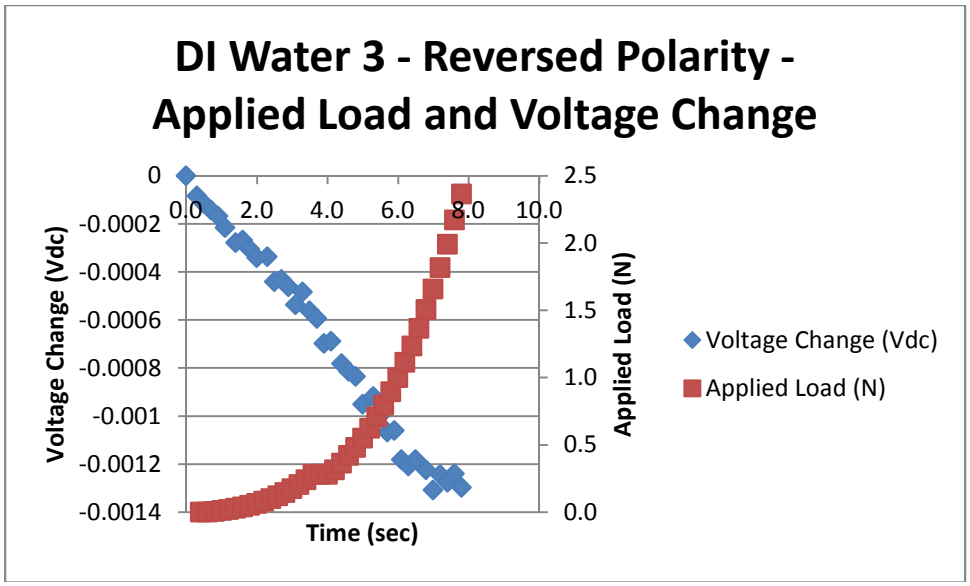

Figure 190
Trial 3 reversed polarity DI water electrolyte constant load scenario, load and voltage change

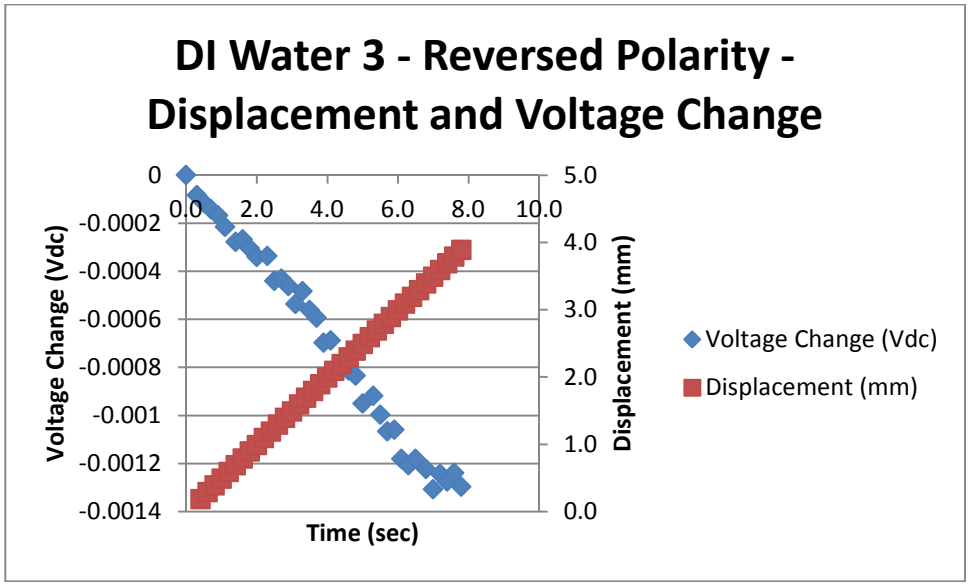

Figure 191
Trial 3 reversed polarity DI water electrolyte constant load scenario, displacement and voltage change

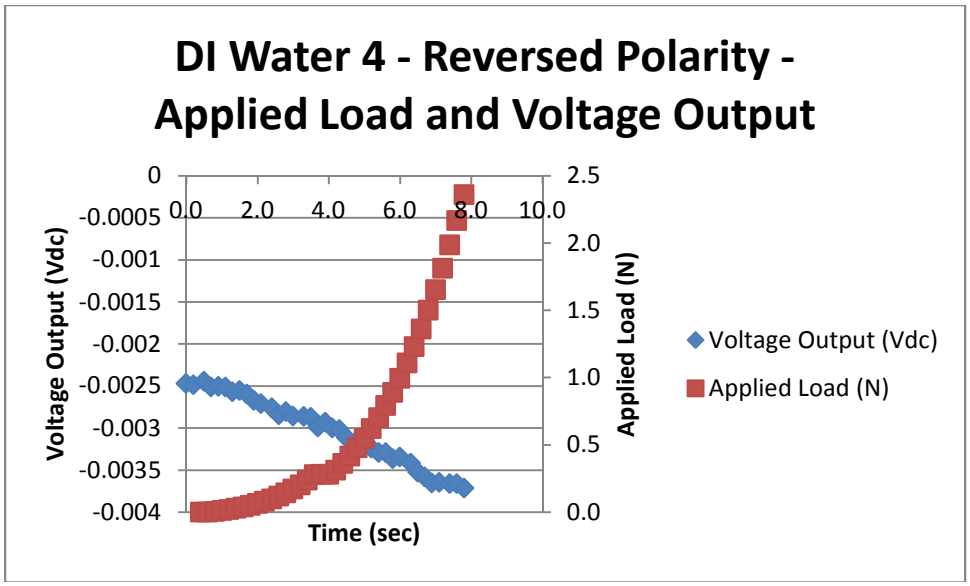

Figure 192

Trial 4 reversed polarity DI water electrolyte constant load scenario, load and raw voltage output

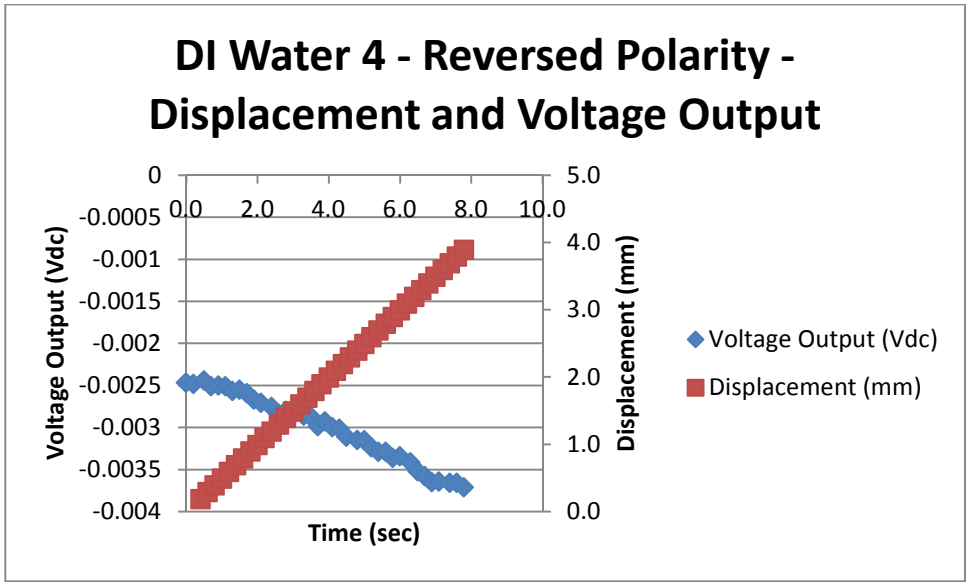

Figure 193

Trial 4 reversed polarity DI water electrolyte constant load scenario, displacement and raw voltage output

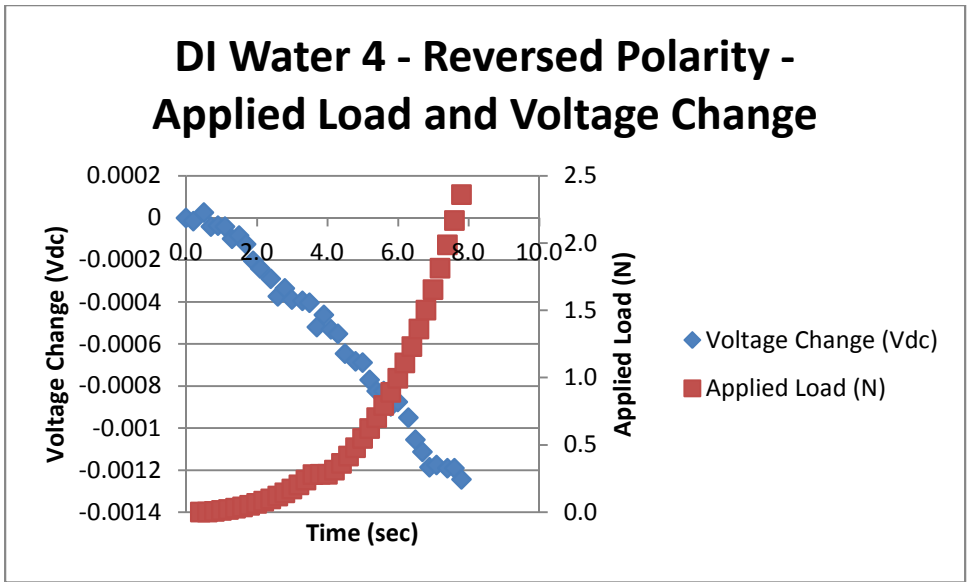

Figure 194
Trial 4 reversed polarity DI water electrolyte constant load scenario, load and voltage change

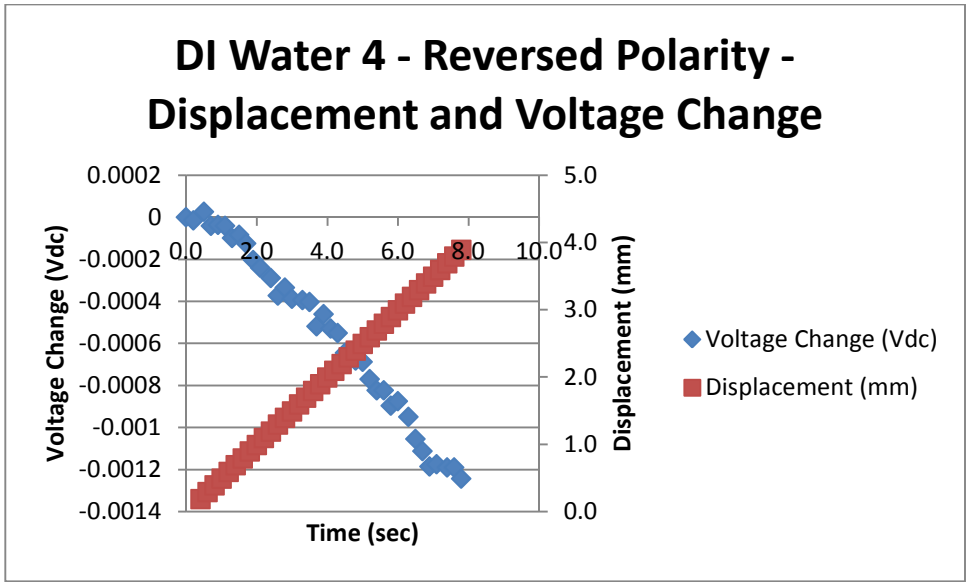

Figure 195
Trial 4 reversed polarity DI water electrolyte constant load scenario, displacement and voltage change

Appendix F

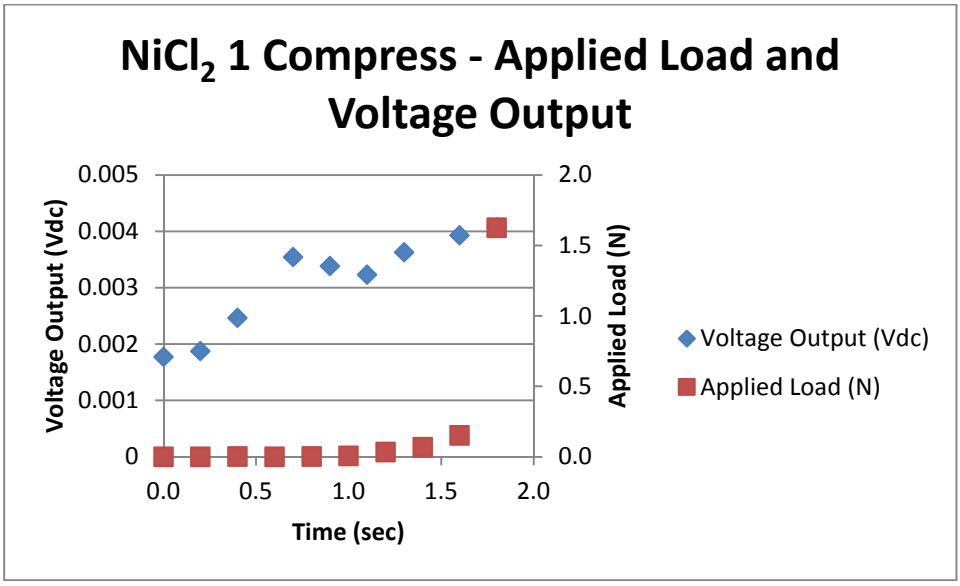

Figure 196

Trial 1 normal polarity $NiCl_2$ electrolyte constant compression load scenario, load and raw voltage output

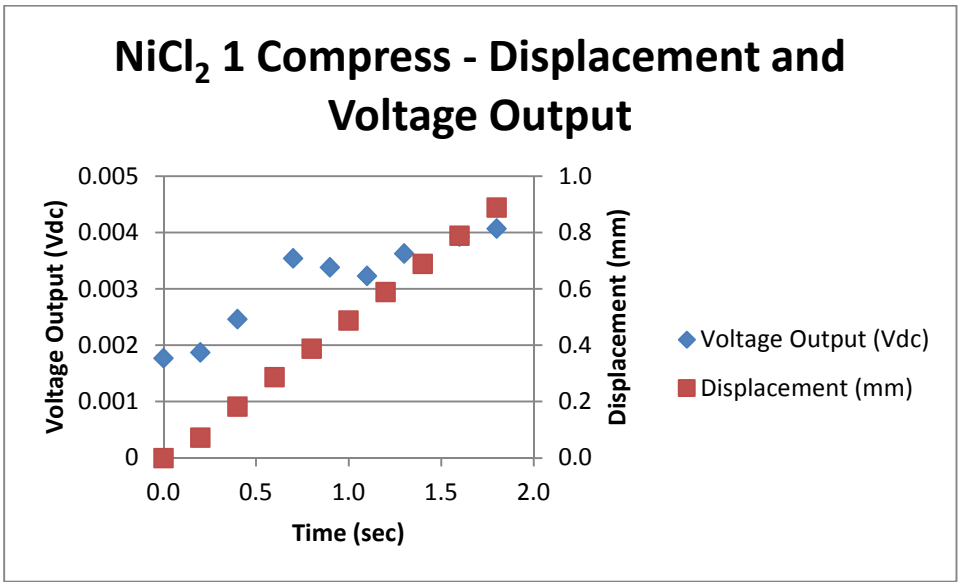

Figure 197

Trial 1 normal polarity $NiCl_2$ electrolyte constant compression load scenario, displacement and raw voltage output

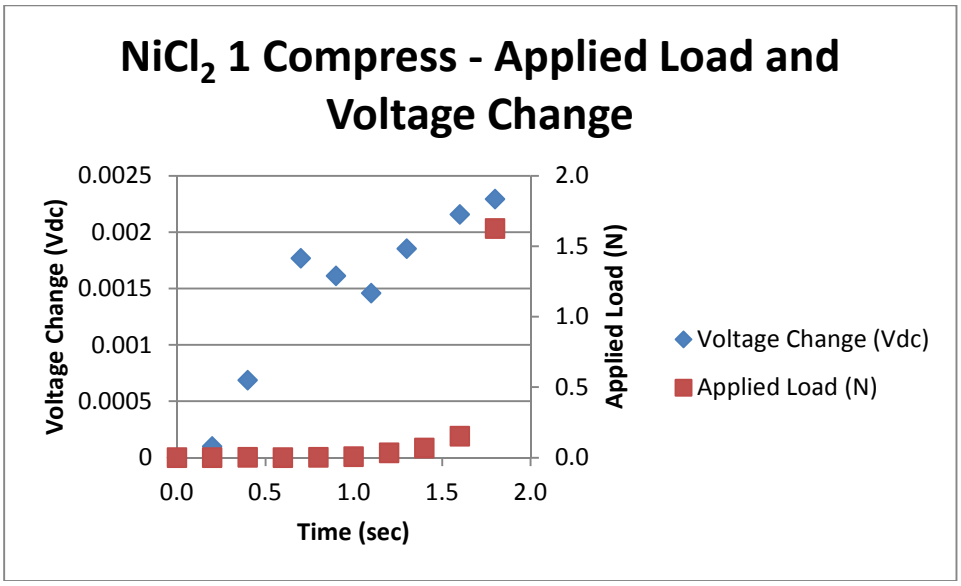

Figure 198

Trial 1 normal polarity $NiCl_2$ electrolyte constant compression load scenario, load and voltage change

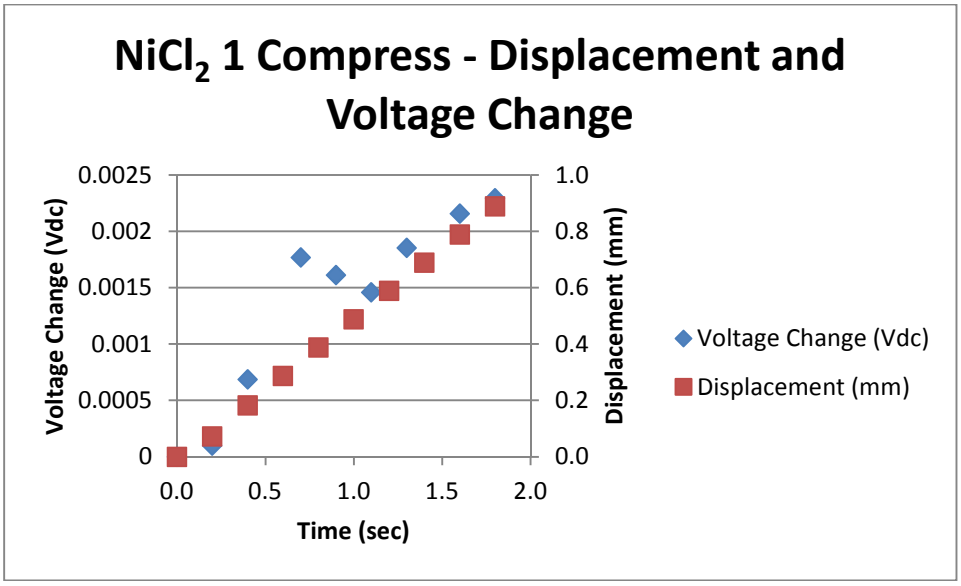

Figure 199

Trial 1 normal polarity $NiCl_2$ electrolyte constant compression load scenario, displacement and voltage change

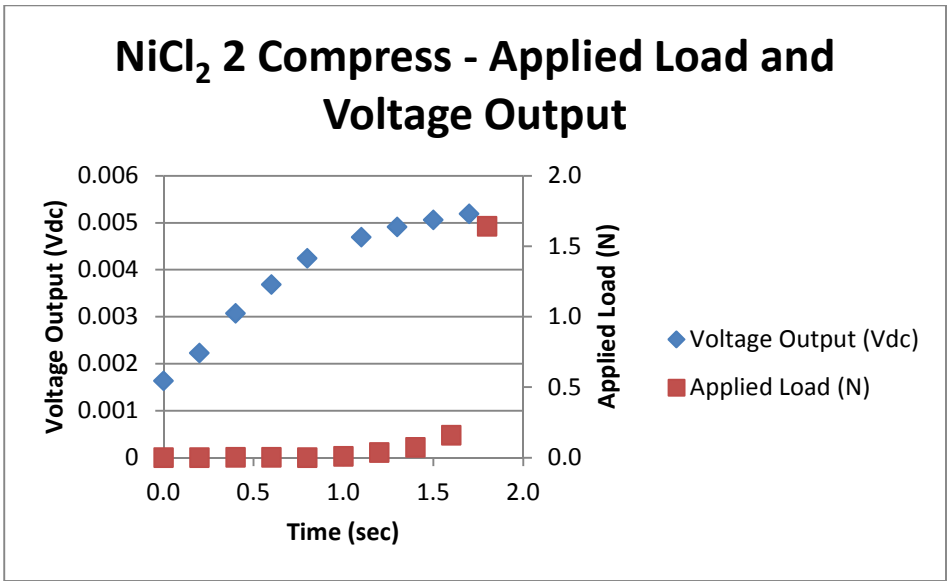

Figure 200

Trial 2 normal polarity $NiCl_2$ electrolyte constant compression load scenario, load and raw voltage output

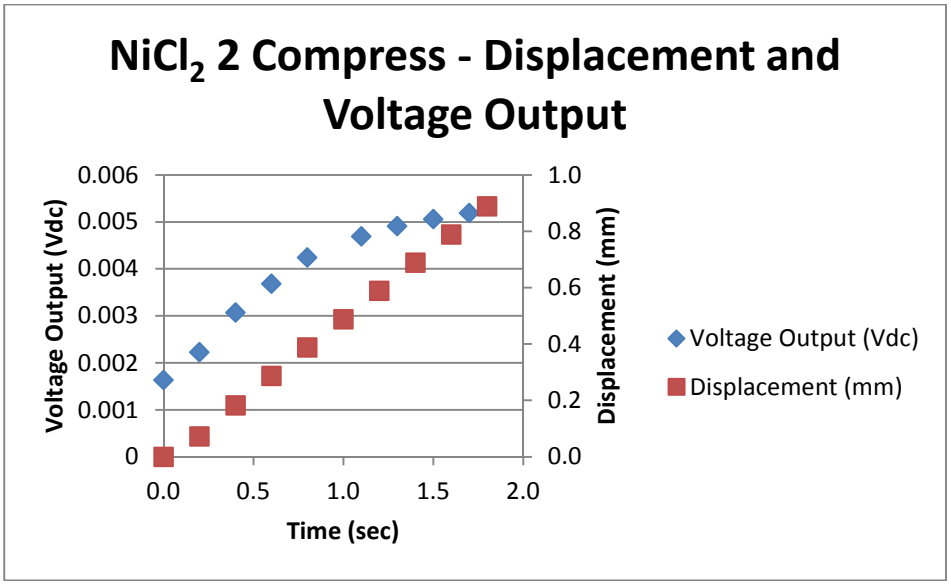

Figure 201

Trial 2 normal polarity $NiCl_2$ electrolyte constant compression load scenario, displacement and raw voltage output

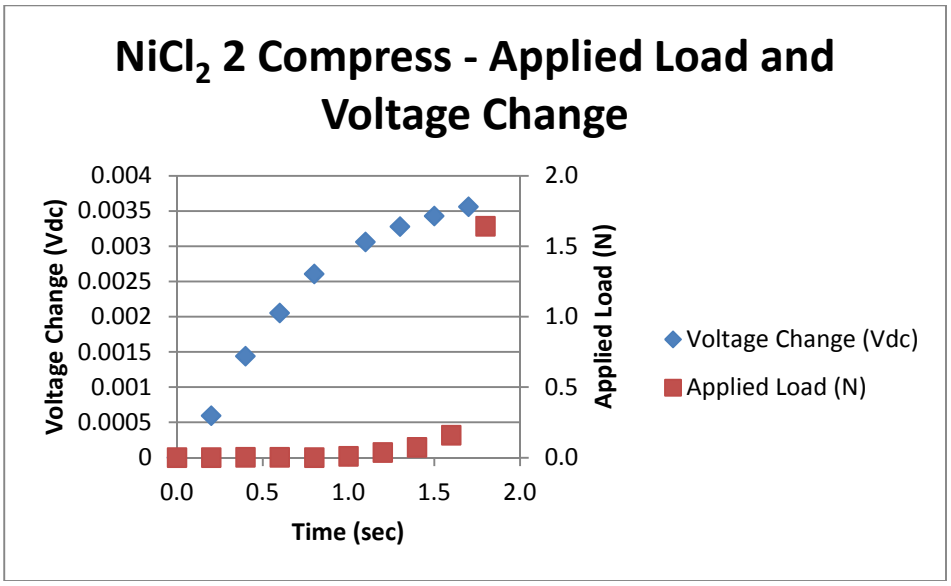

Figure 202

Trial 2 normal polarity $NiCl_2$ electrolyte constant compression load scenario, load and voltage change

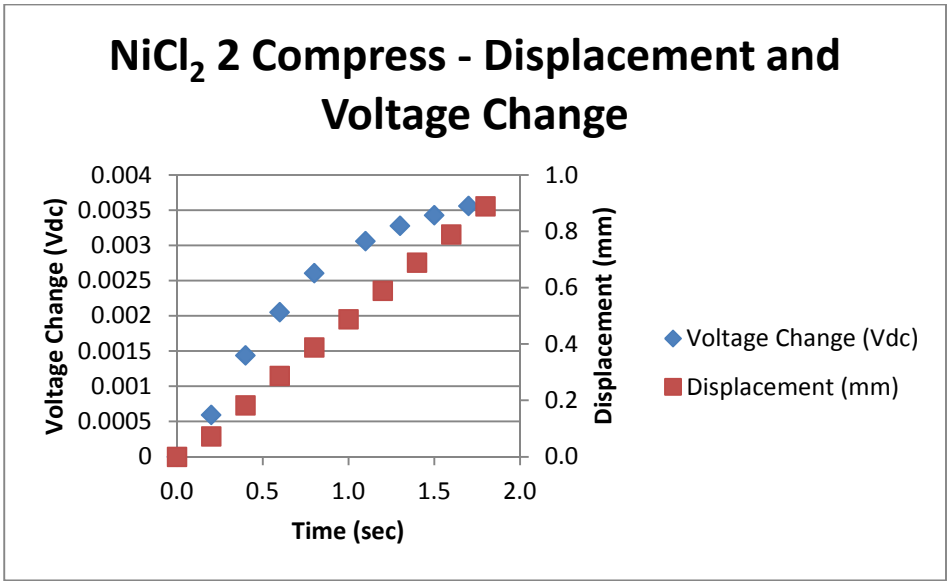

Figure 203

Trial 2 normal polarity $NiCl_2$ electrolyte constant compression load scenario, displacement and voltage change

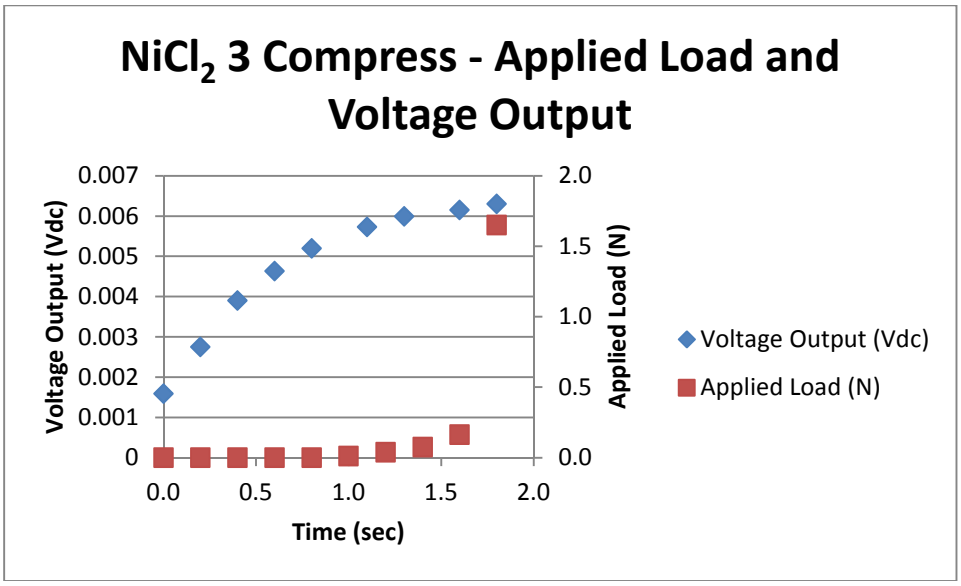

Figure 204

Trial 3 normal polarity $NiCl_2$ electrolyte constant compression load scenario, load and raw voltage output

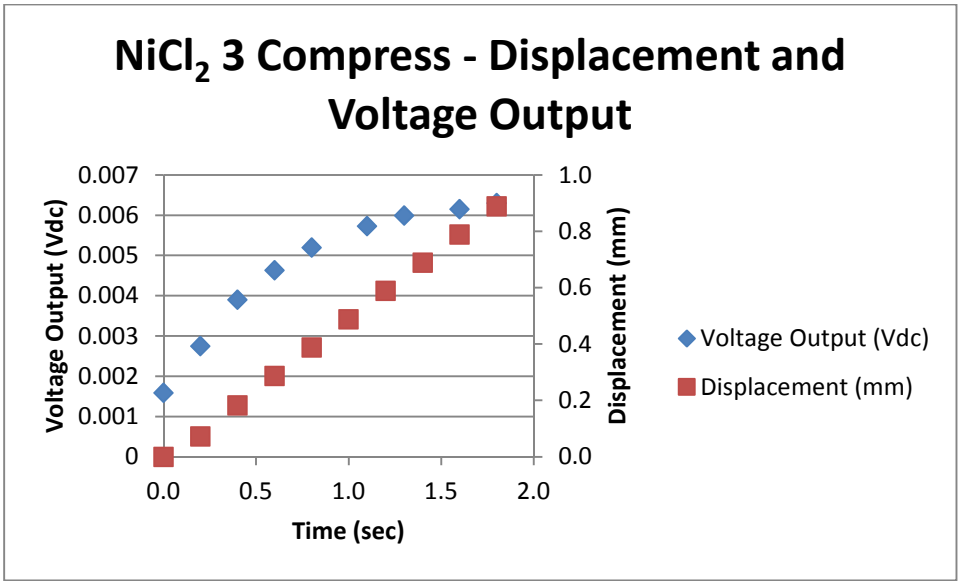

Figure 205

Trial 3 normal polarity $NiCl_2$ electrolyte constant compression load scenario, dispacement and raw voltage output

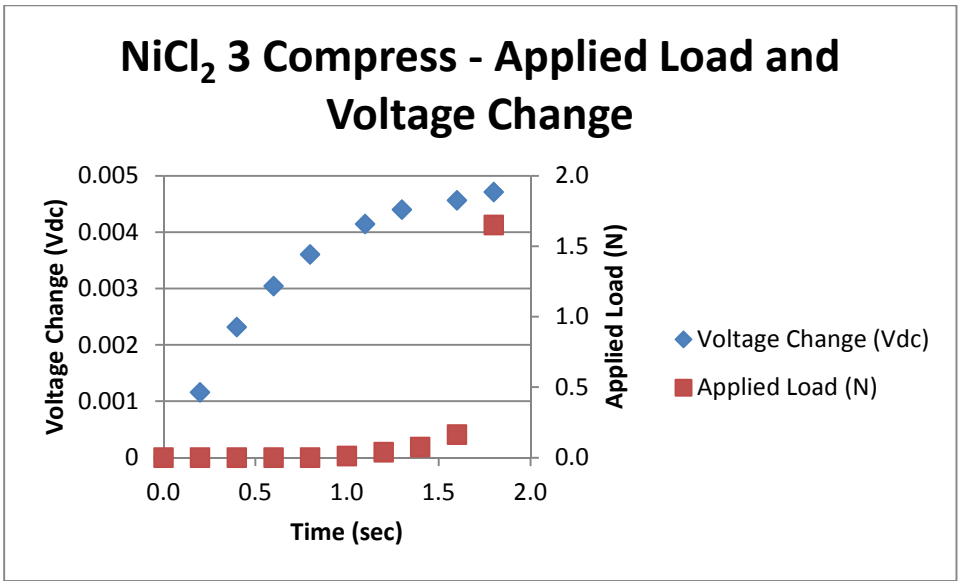

Figure 206

Trial 3 normal polarity $NiCl_2$ electrolyte constant compression load scenario, load and voltage change

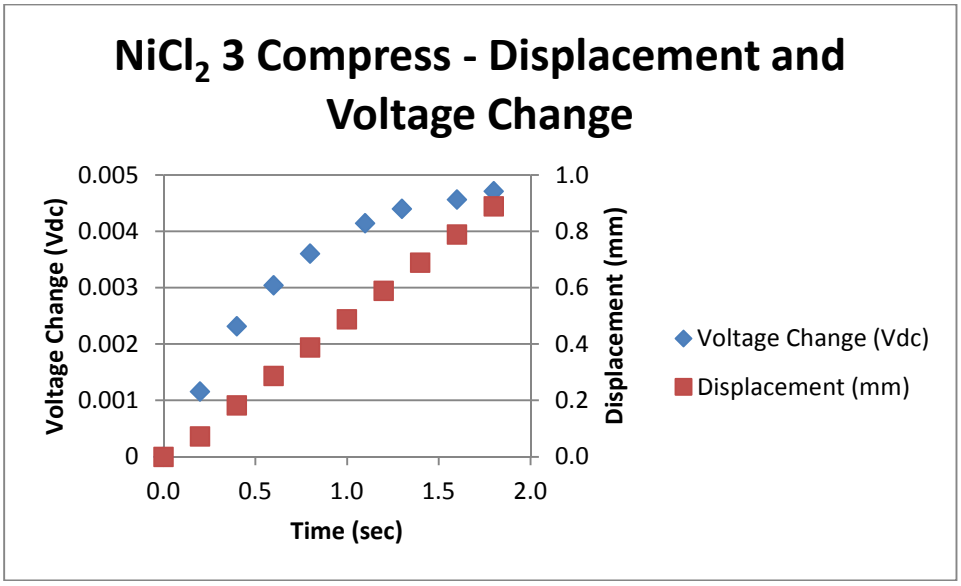

Figure 207

Trial 3 normal polarity $NiCl_2$ electrolyte constant compression load scenario, displacement and voltage change

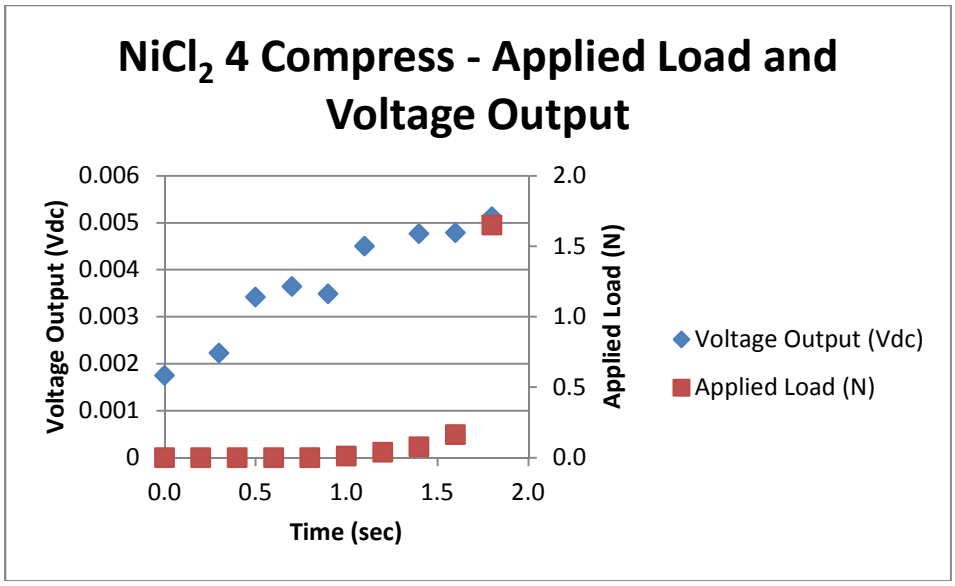

Figure 208

Trial 4 normal polarity $NiCl_2$ electrolyte constant compression load scenario, load and raw voltage output

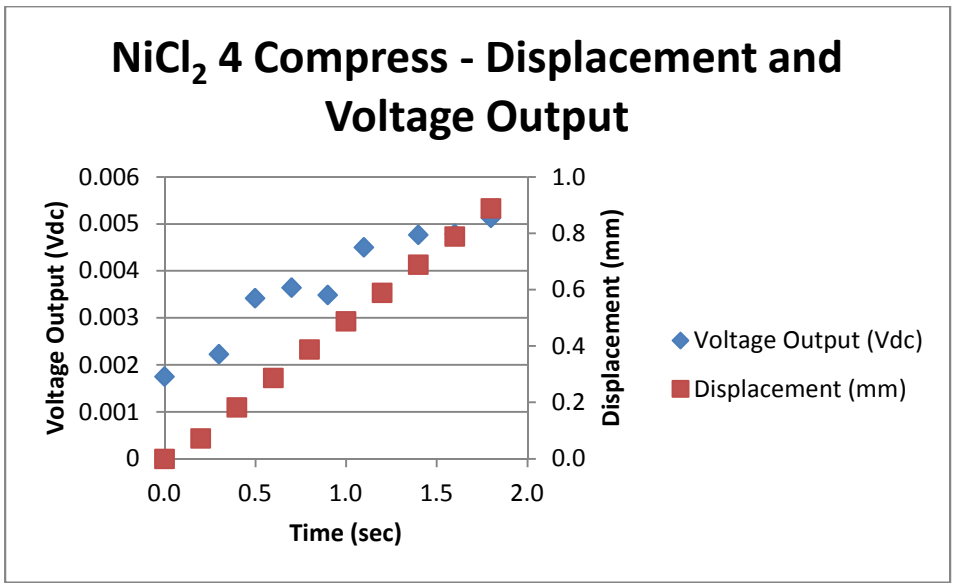

Figure 209

Trial 4 normal polarity $NiCl_2$ electrolyte constant compression load scenario, displacement and raw voltage output

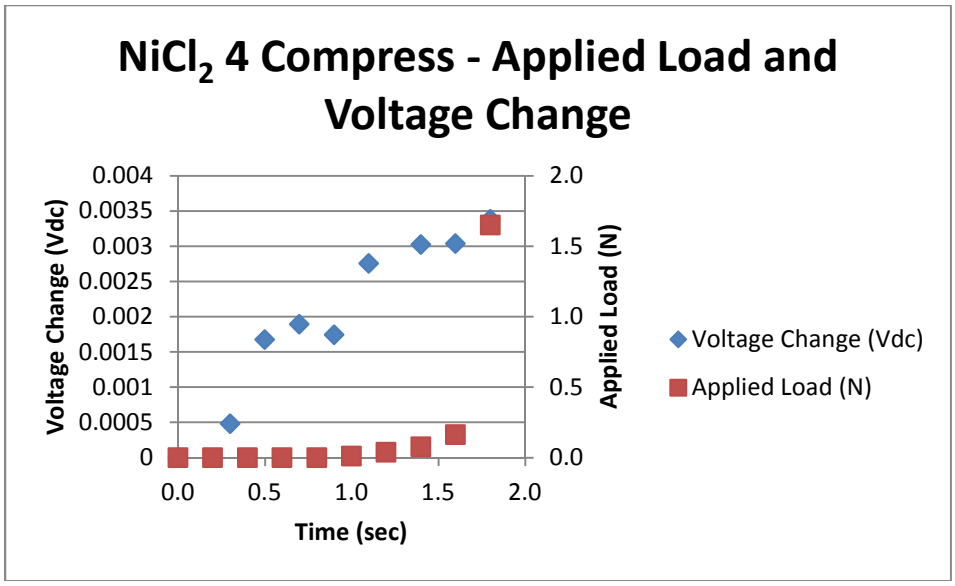

Figure 210

Trial 4 normal polarity $NiCl_2$ electrolyte constant compression load scenario, load and voltage change

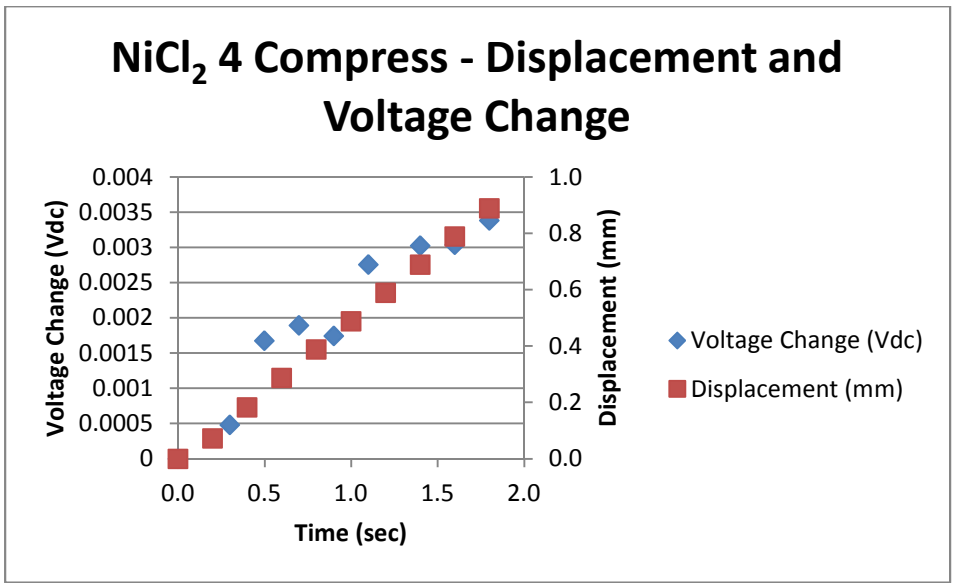

Figure 211

Trial 4 normal polarity $NiCl_2$ electrolyte constant compression load scenario, displacement and voltage change

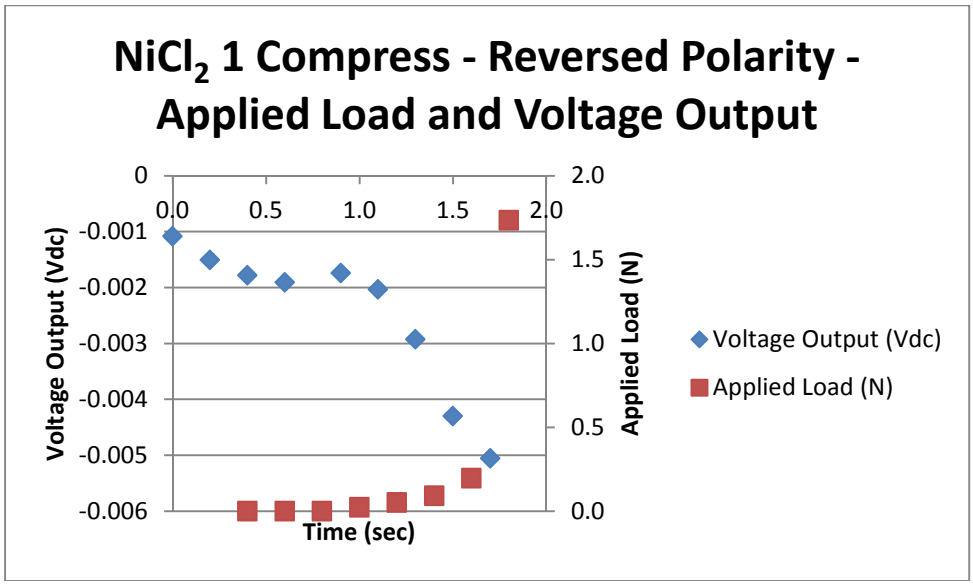

Figure 212

Trial 1 reversed polarity $NiCl_2$ electrolyte constant compression load scenario, load and raw voltage output

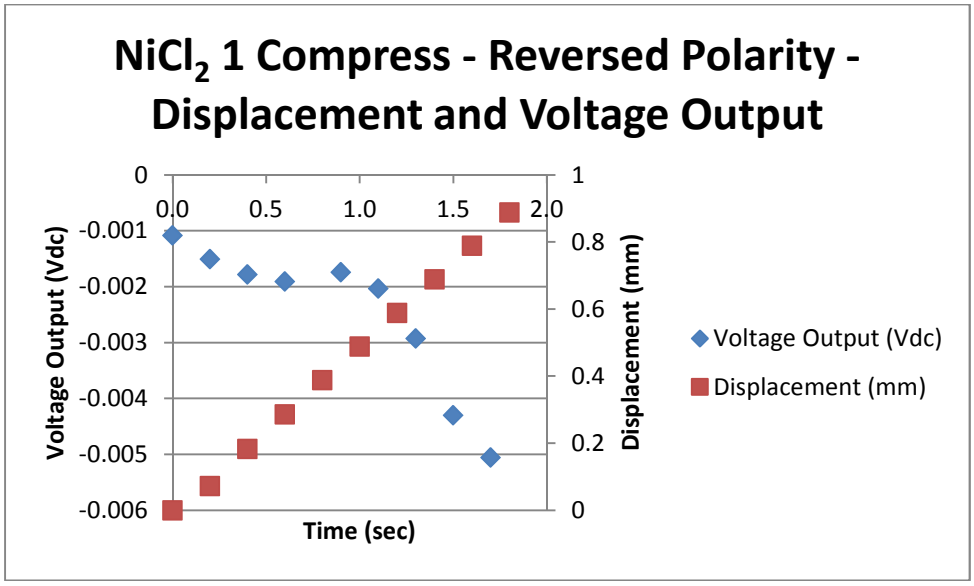

Figure 213

Trial 1 reversed polarity $NiCl_2$ electrolyte constant compression load scenario, displacement and raw voltage output

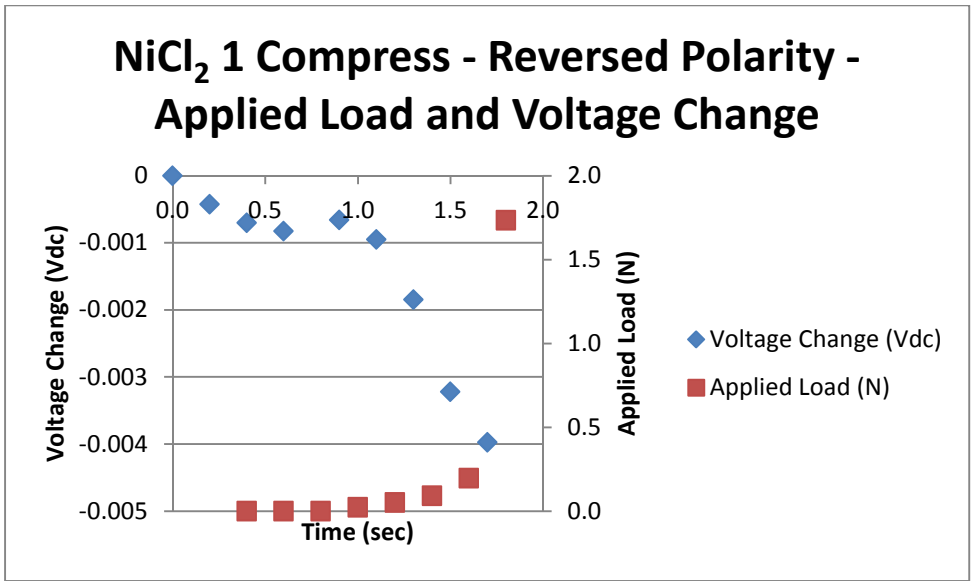

Figure 214

Trial 1 reversed polarity $NiCl_2$ electrolyte constant compression load scenario, load and voltage change

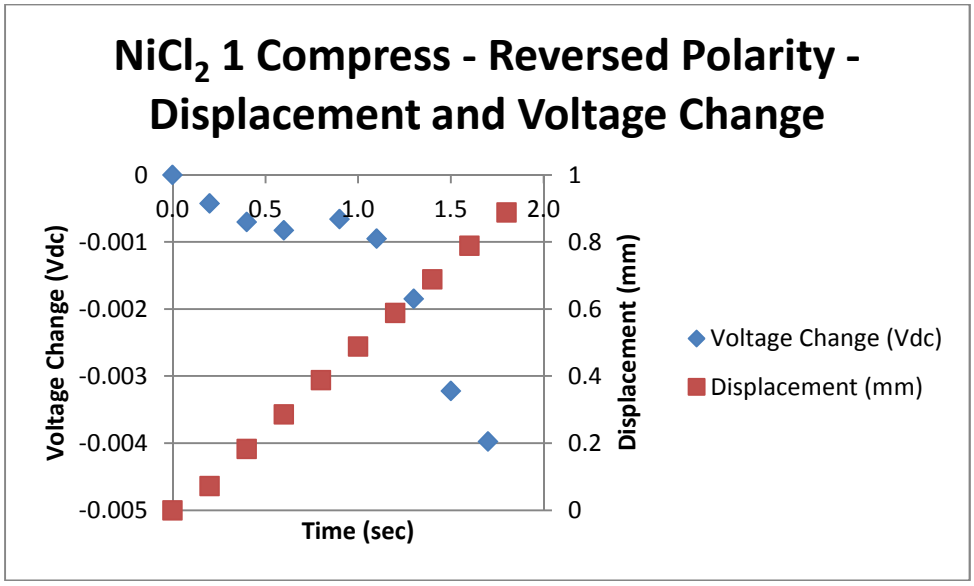

Figure 215

Trial 1 reversed polarity $NiCl_2$ electrolyte constant compression load scenario, displacement and voltage change

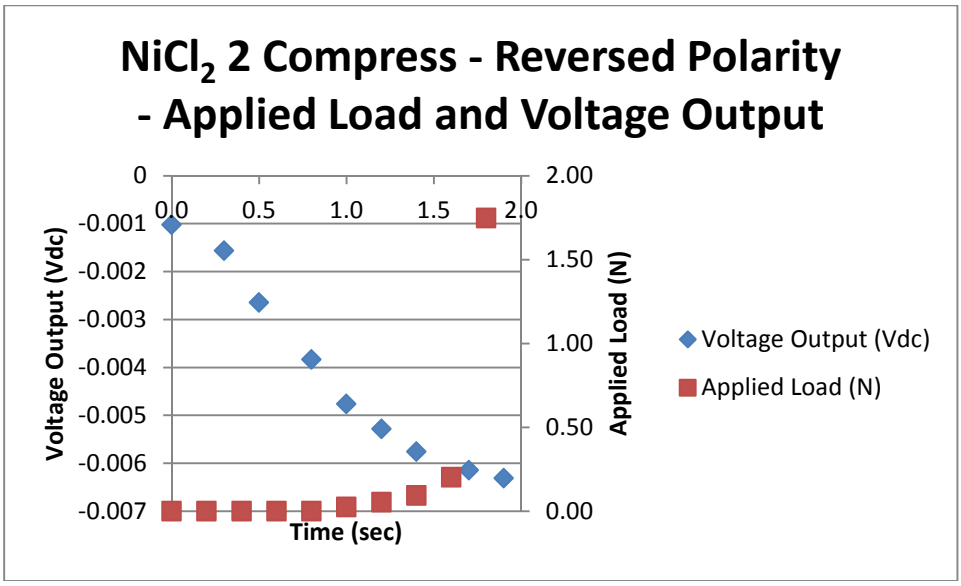

Figure 216

Trial 2 reversed polarity $NiCl_2$ electrolyte constant compression load scenario, load and raw voltage output

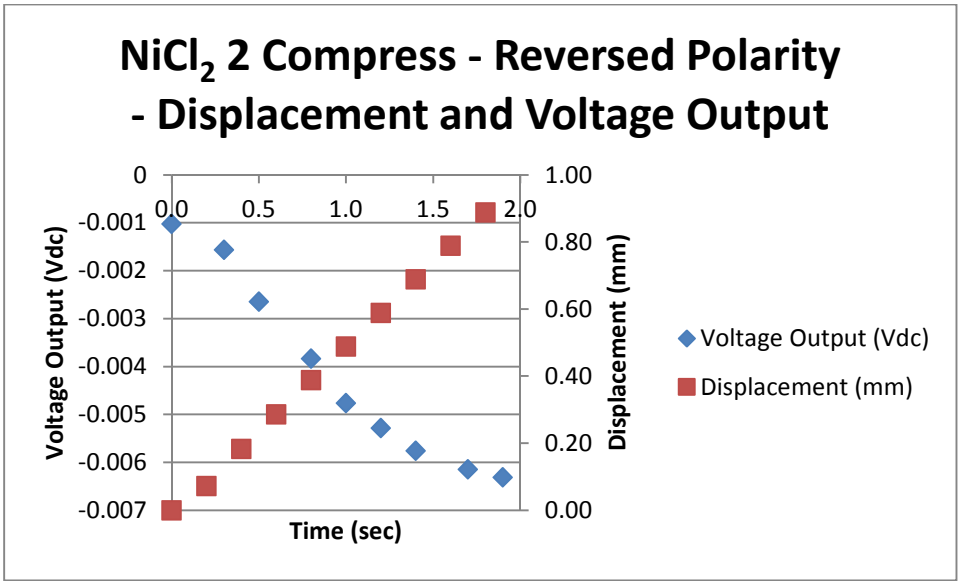

Figure 217

Trial 2 reversed polarity $NiCl_2$ electrolyte constant compression load scenario, displacement and raw voltage output

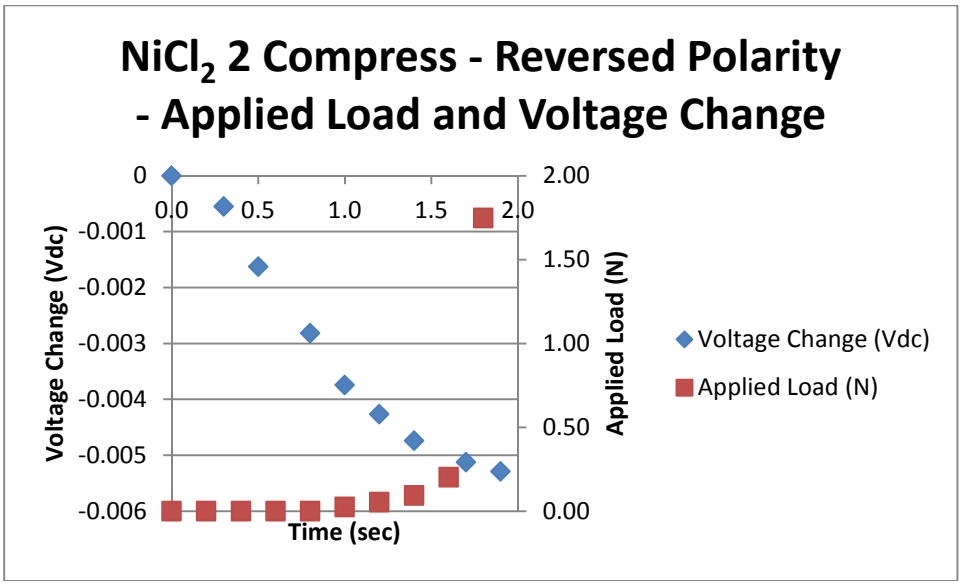

Figure 218

Trial 2 reversed polarity $NiCl_2$ electrolyte constant compression load scenario, load and voltage change

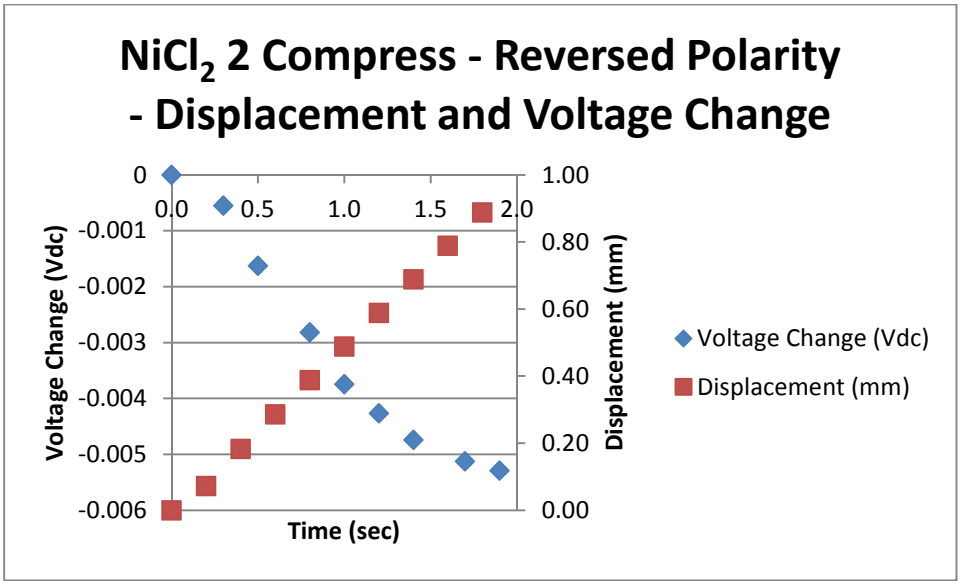

Figure 219

Trial 2 reversed polarity $NiCl_2$ electrolyte constant compression load scenario, displacement and voltage change

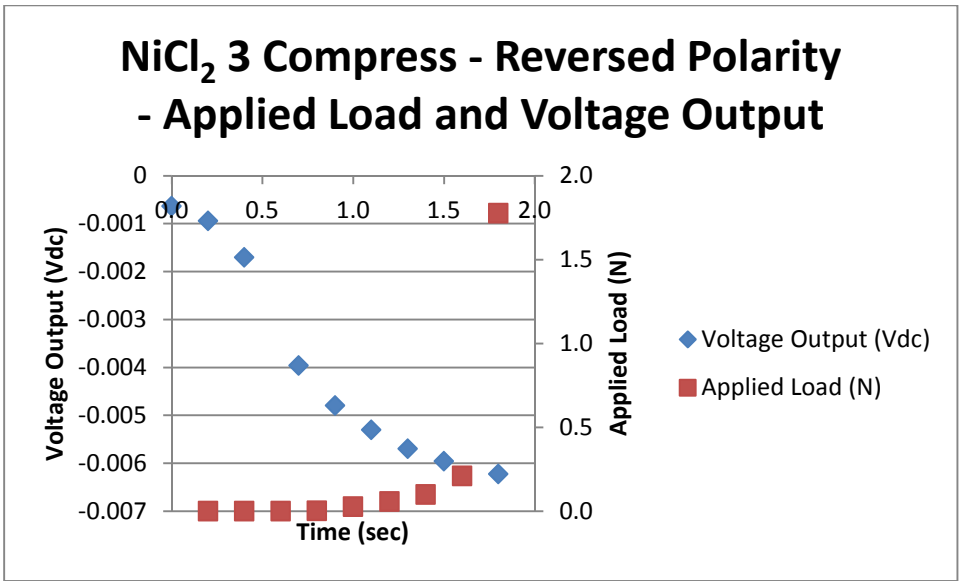

Figure 220

Trial 3 reversed polarity $NiCl_2$ electrolyte constant compression load scenario, load and raw voltage output

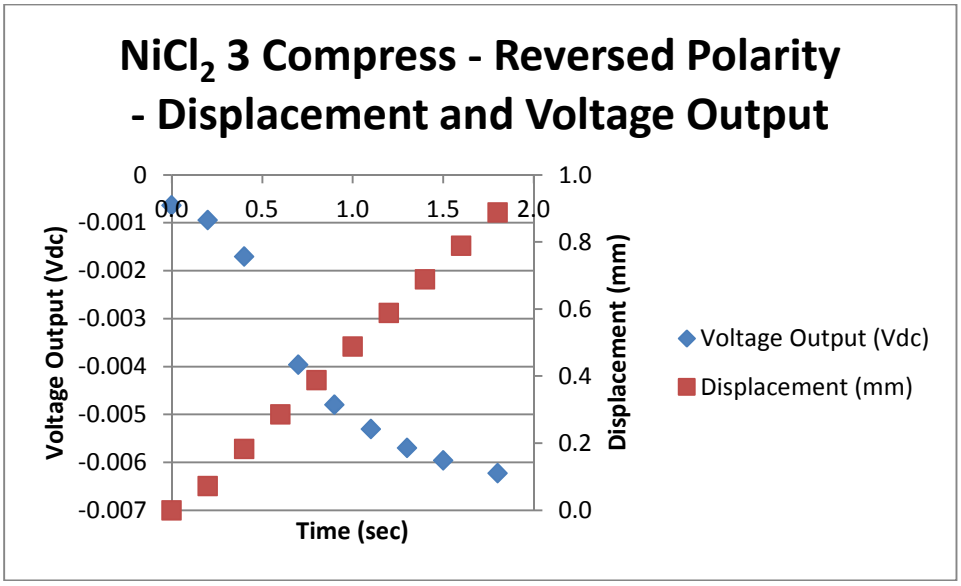

Figure 221

Trial 3 reversed polarity $NiCl_2$ electrolyte constant compression load scenario, displacement and raw voltage output

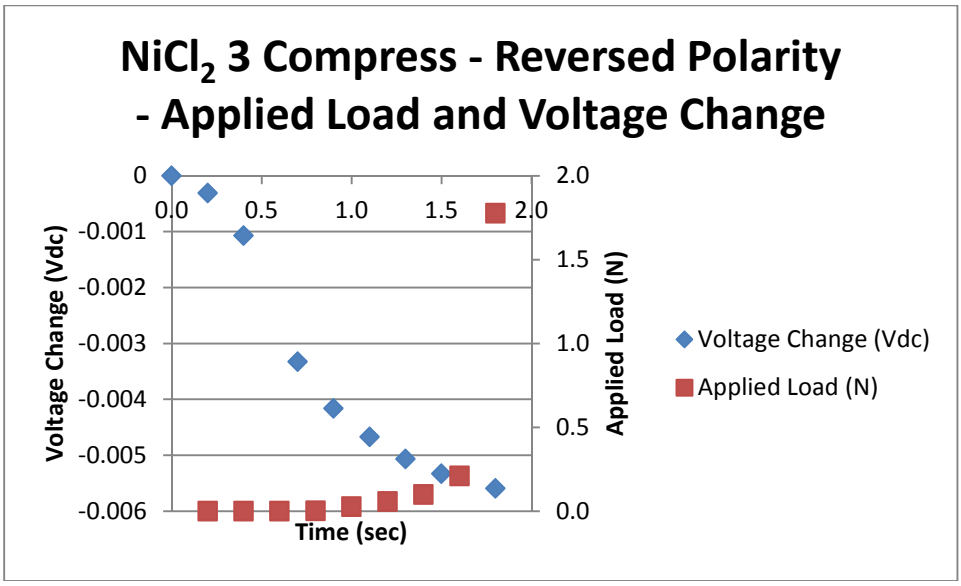

Figure 222

Trial 3 reversed polarity $NiCl_2$ electrolyte constant compression load scenario, load and voltage change

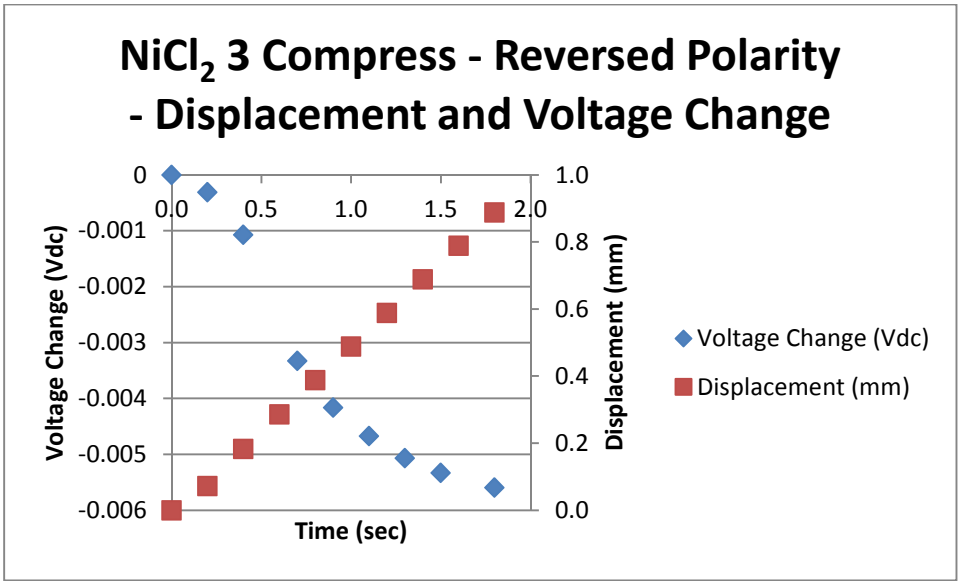

Figure 223

Trial 3 reversed polarity $NiCl_2$ electrolyte constant compression load scenario, displacement and voltage change

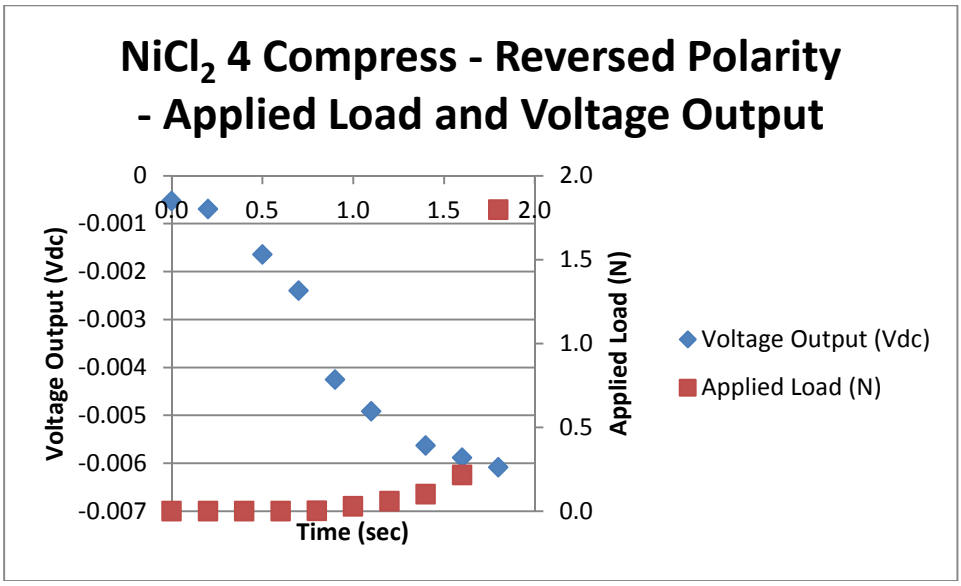

Figure 224

Trial 4 reversed polarity $NiCl_2$ electrolyte constant compression load scenario, load and raw voltage output

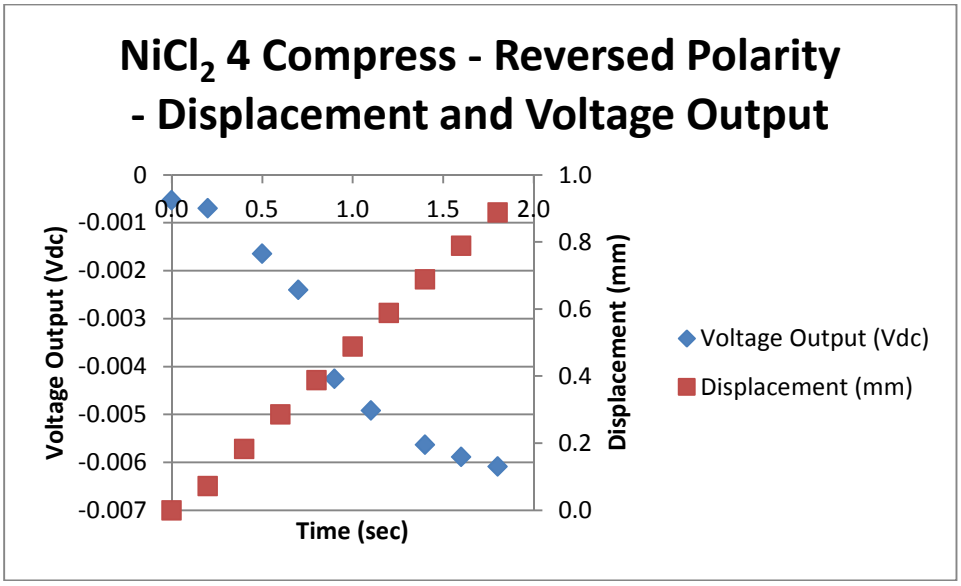

Figure 225

Trial 4 reversed polarity $NiCl_2$ electrolyte constant compression load scenario, displacement and raw voltage output

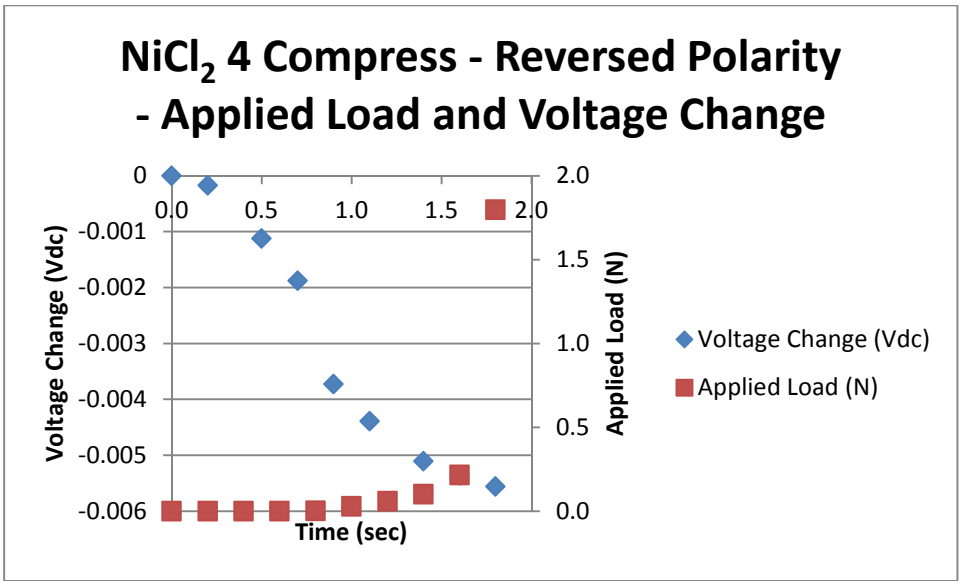

Figure 226

Trial 4 reversed polarity $NiCl_2$ electrolyte constant compression load scenario, load and voltage change

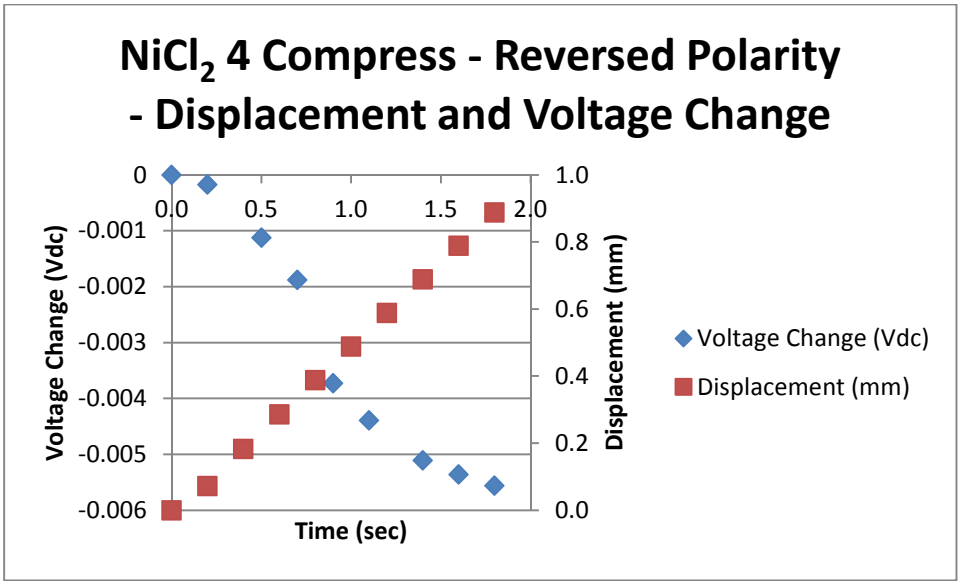

Figure 227

Trial 4 reversed polarity $NiCl_2$ electrolyte constant compression load scenario, displacement and voltage change

Appendix G

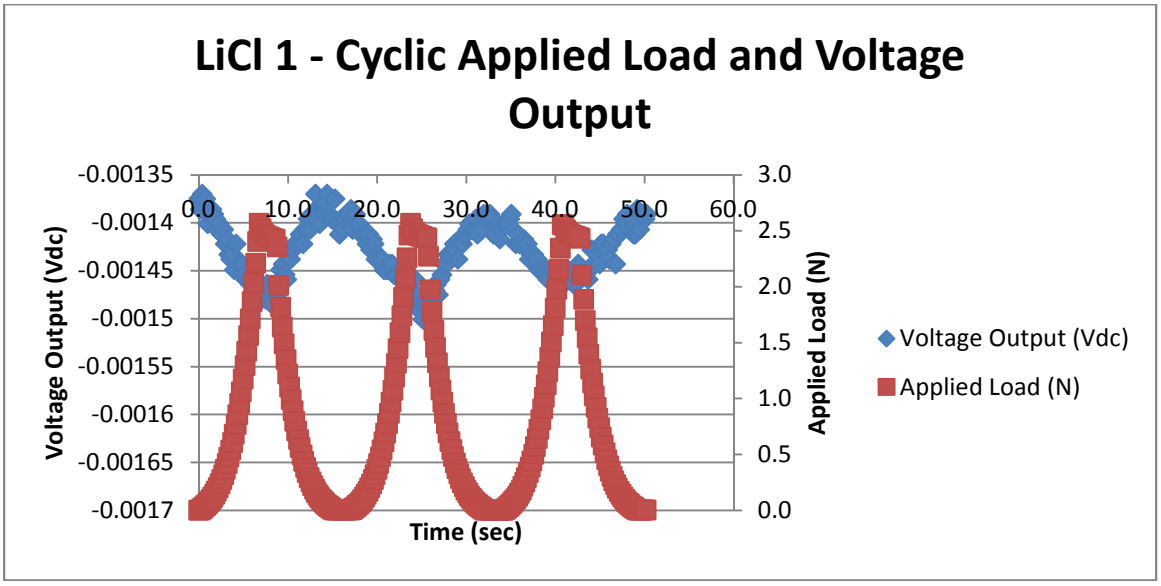

Figure 228
Trial 1 normal polarity LiCl electrolyte cyclic load scenario, load and raw voltage output

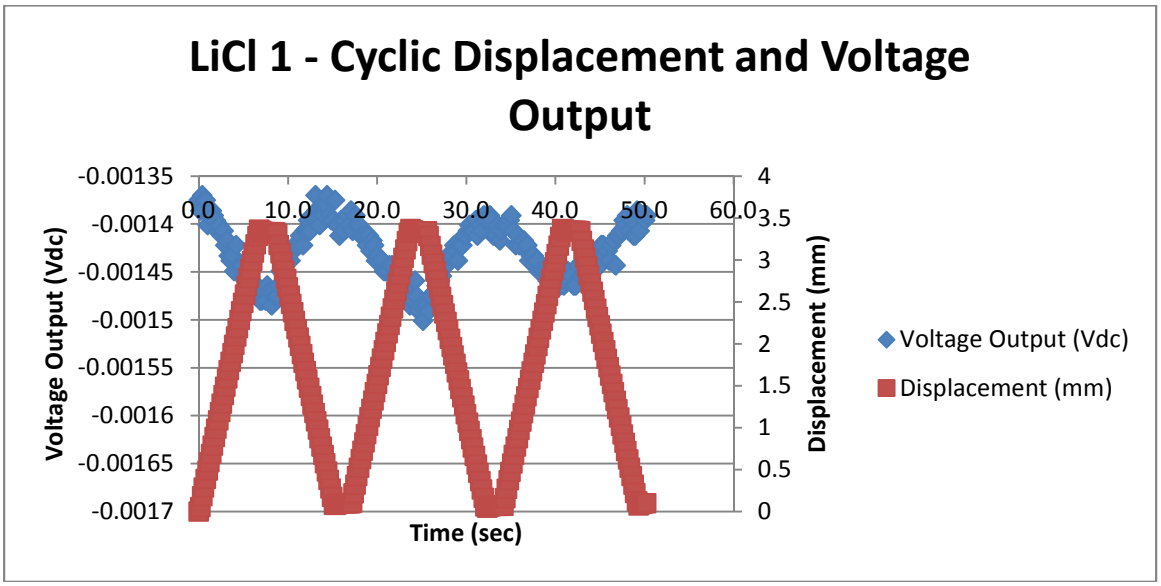

Figure 229
Trial 1 normal polarity LiCl electrolyte cyclic load scenario, displacement and raw voltage output

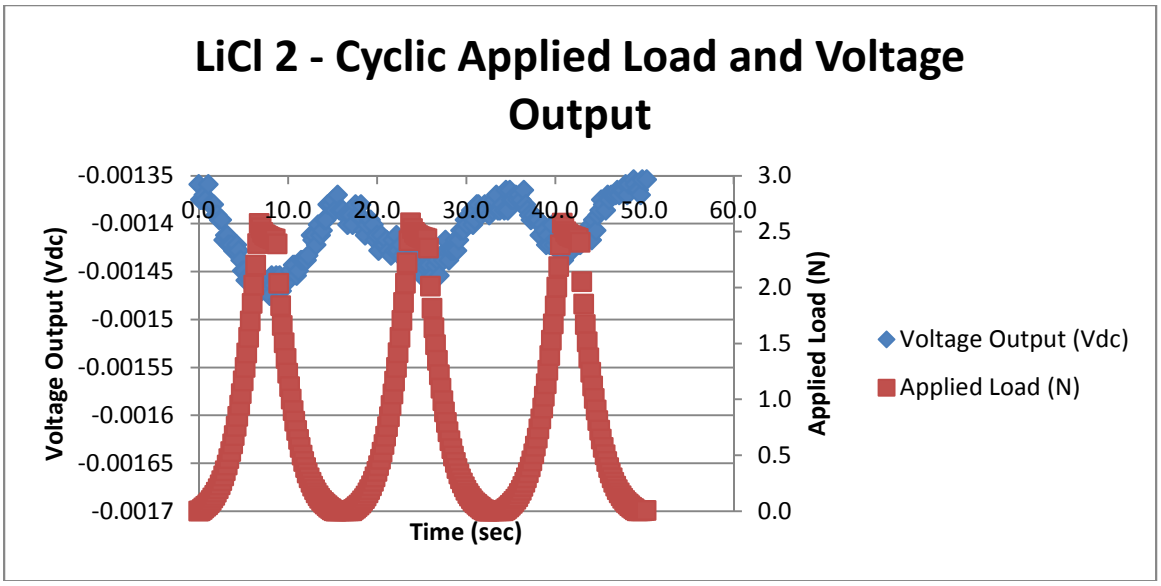

Figure 230
Trial 2 normal polarity LiCl electrolyte cyclic load scenario, load and raw voltage output

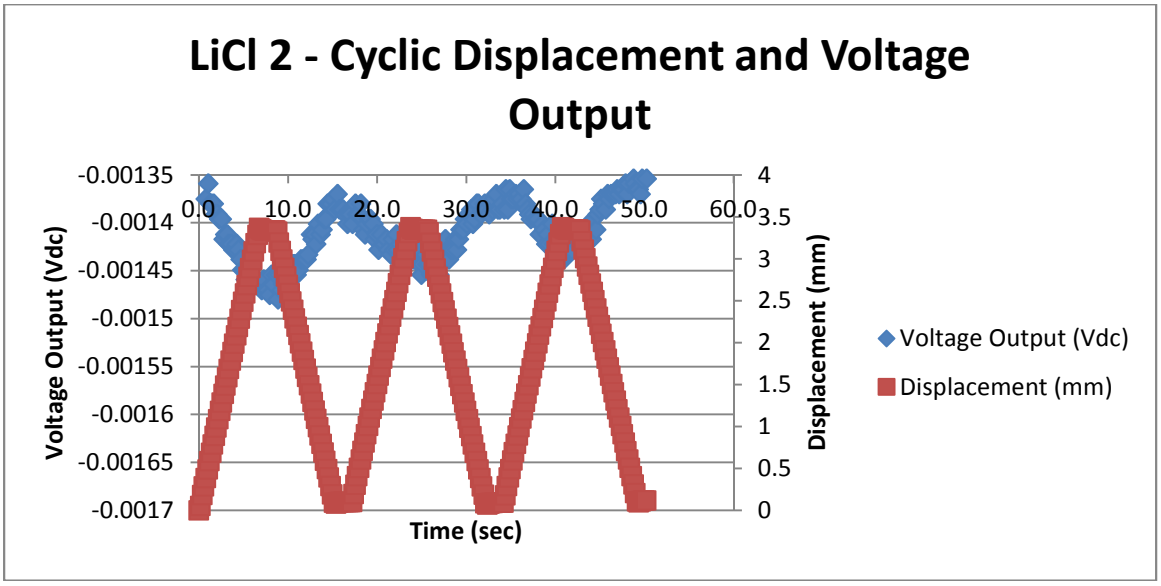

Figure 231
Trial 2 normal polarity LiCl electrolyte cyclic load scenario, displacement and raw voltage output

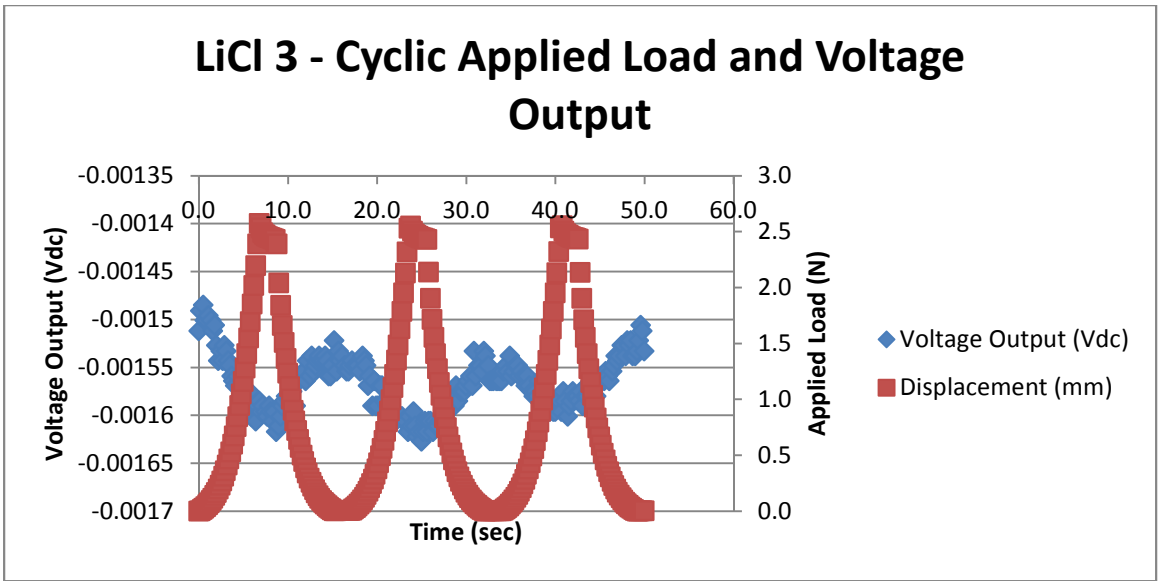

Figure 232
Trial 3 normal polarity LiCl electrolyte cyclic load scenario, load and raw voltage output

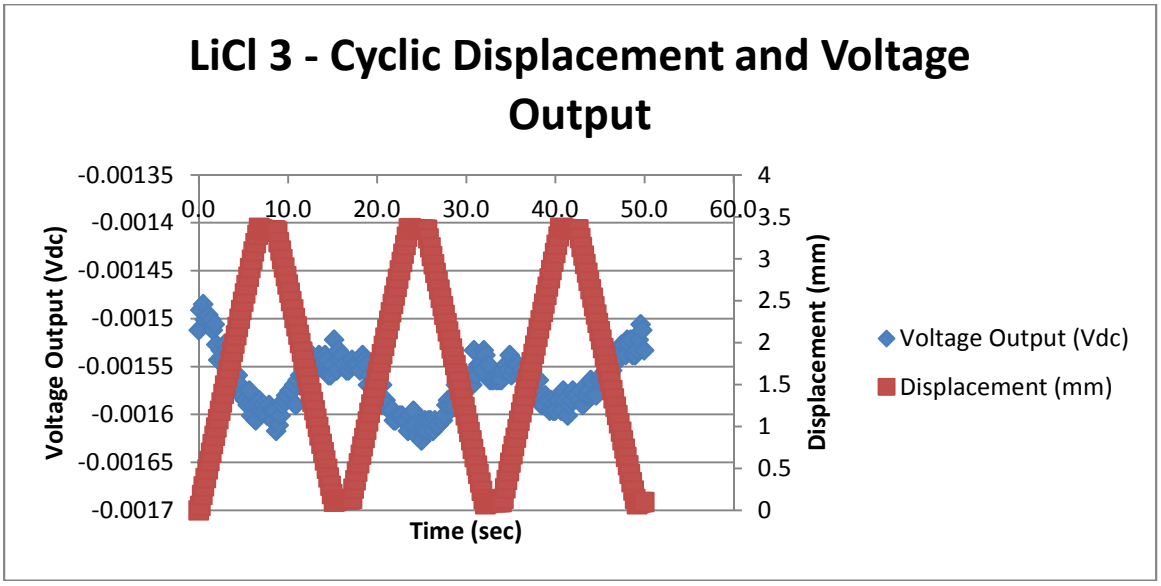

Figure 233
Trial 3 normal polarity LiCl electrolyte cyclic load scenario, displacement and raw voltage output

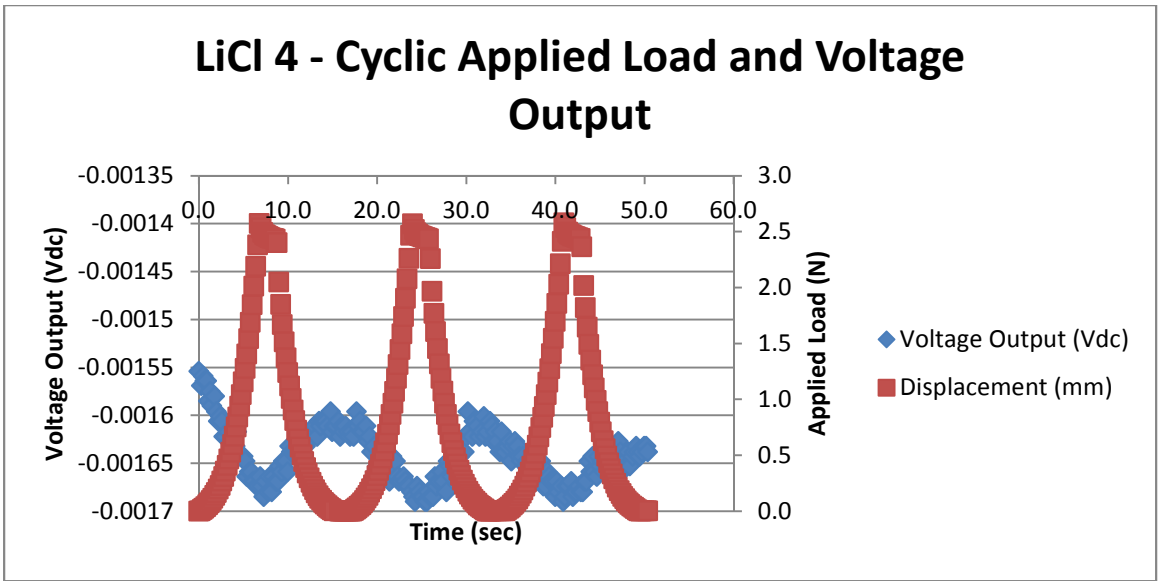

Figure 234
Trial 4 normal polarity LiCl electrolyte cyclic load scenario, load and raw voltage output

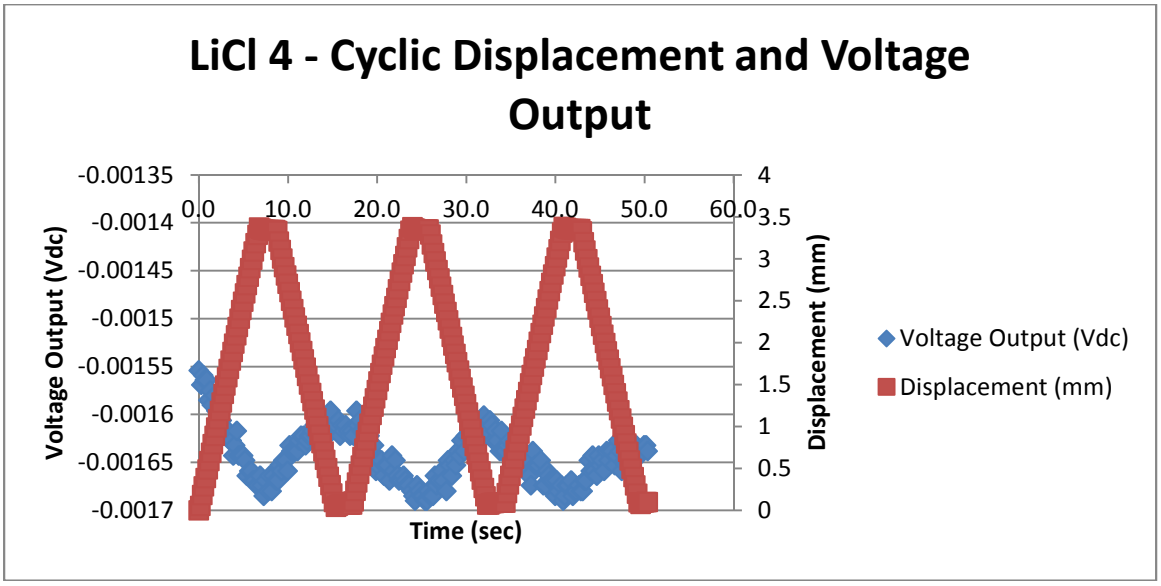

Figure 235
Trial 4 normal polarity LiCl electrolyte cyclic load scenario, displacement and raw voltage output

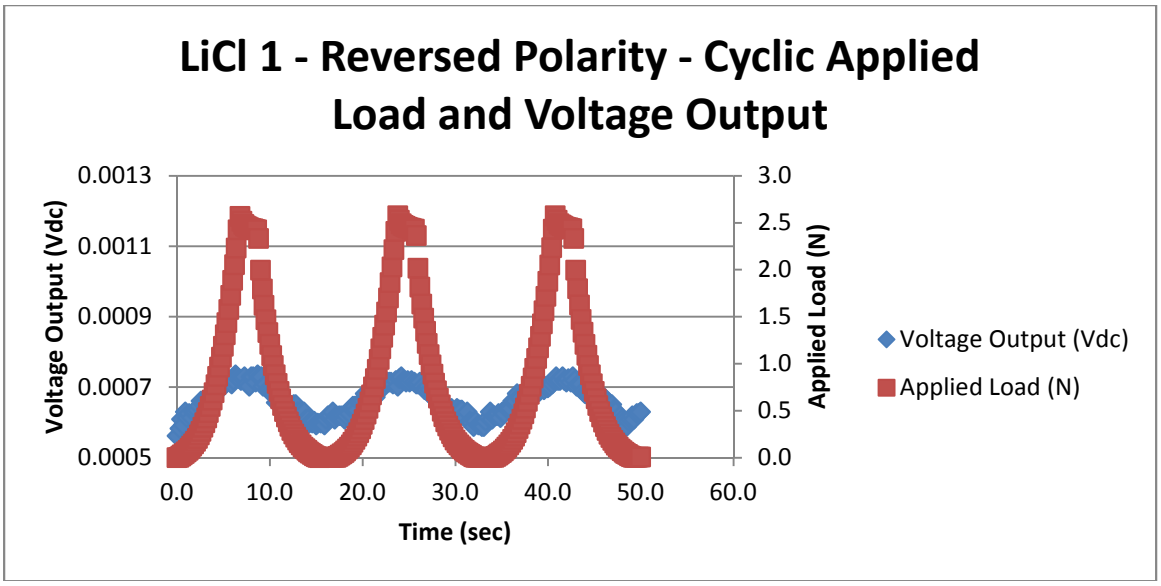

Figure 236
Trial 1 reversed polarity LiCl electrolyte cyclic load scenario, load and raw voltage output

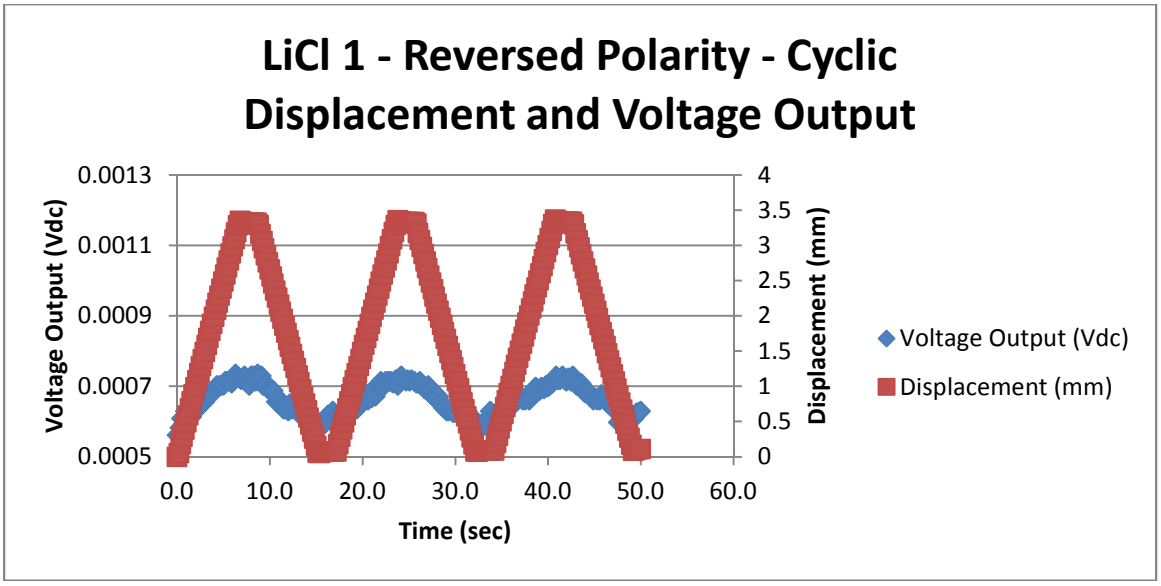

Figure 237
Trial 1 reversed polarity LiCl electrolyte cyclic load scenario, displacement and raw voltage output

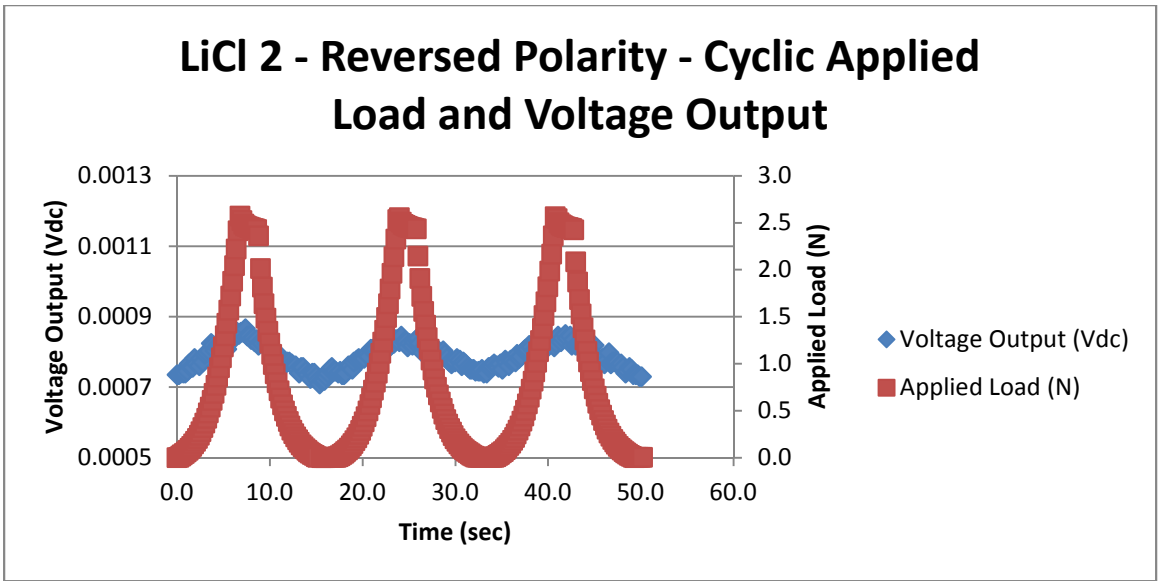

Figure 238
Trial 2 reversed polarity LiCl electrolyte cyclic load scenario, load and raw voltage output

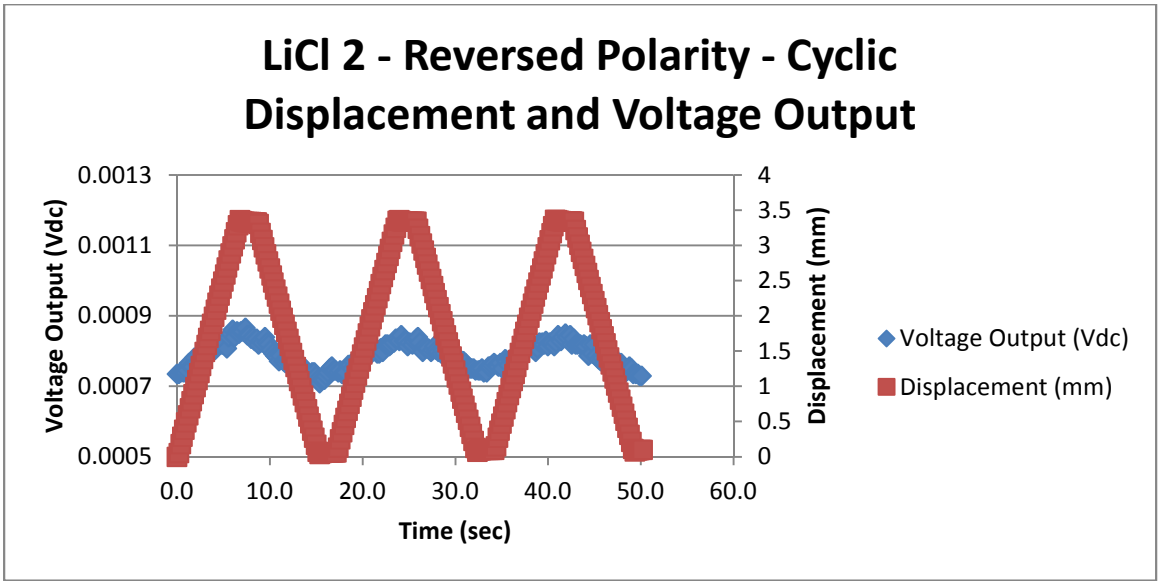

Figure 239
Trial 2 reversed polarity LiCl electrolyte cyclic load scenario, displacement and raw voltage output

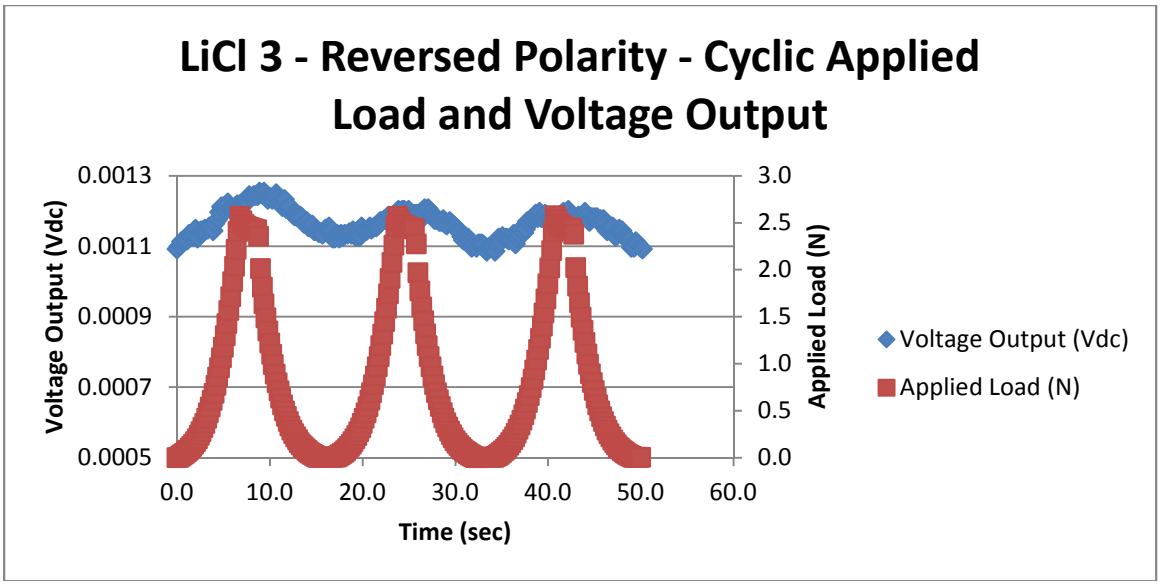

Figure 240
Trial 3 reversed polarity LiCl electrolyte cyclic load scenario, load and raw voltage output

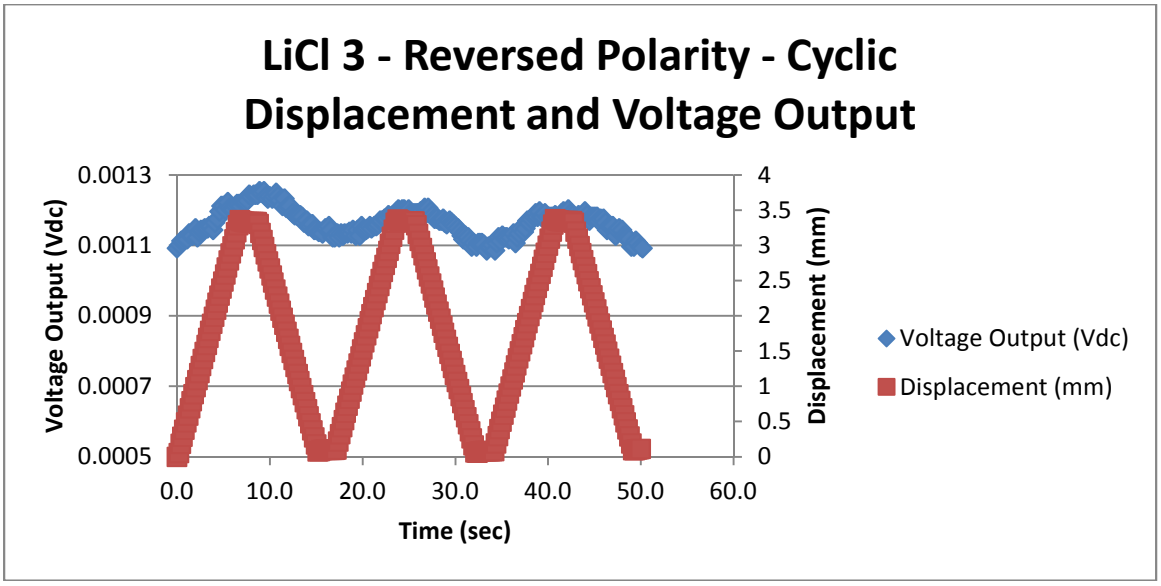

Figure 241
Trial 3 reversed polarity LiCl electrolyte cyclic load scenario, displacement and raw voltage output

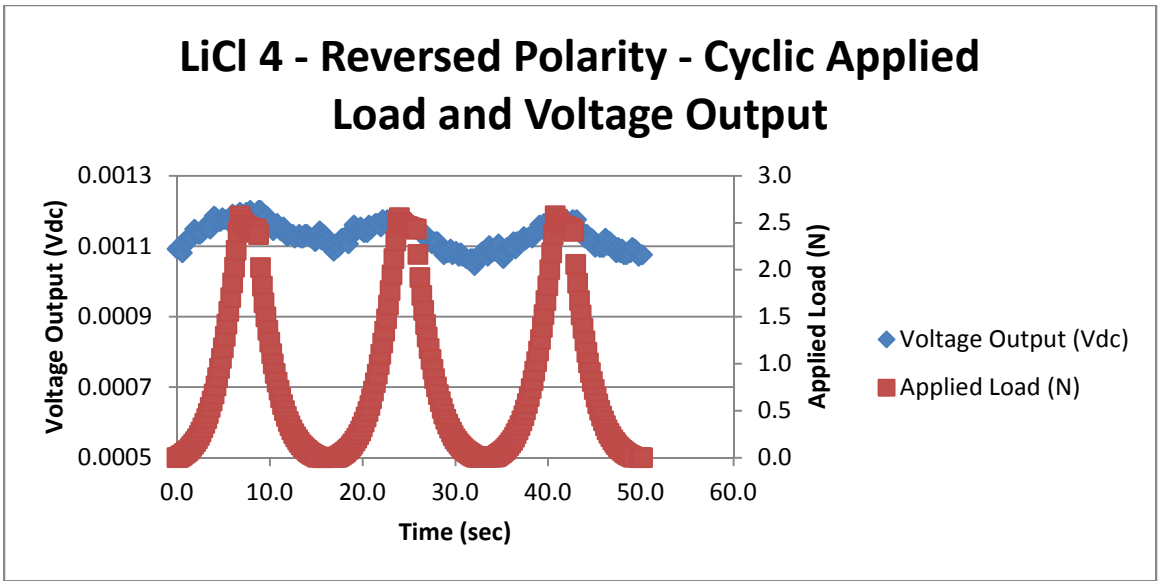

Figure 242
Trial 4 reversed polarity LiCl electrolyte cyclic load scenario, load and raw voltage output

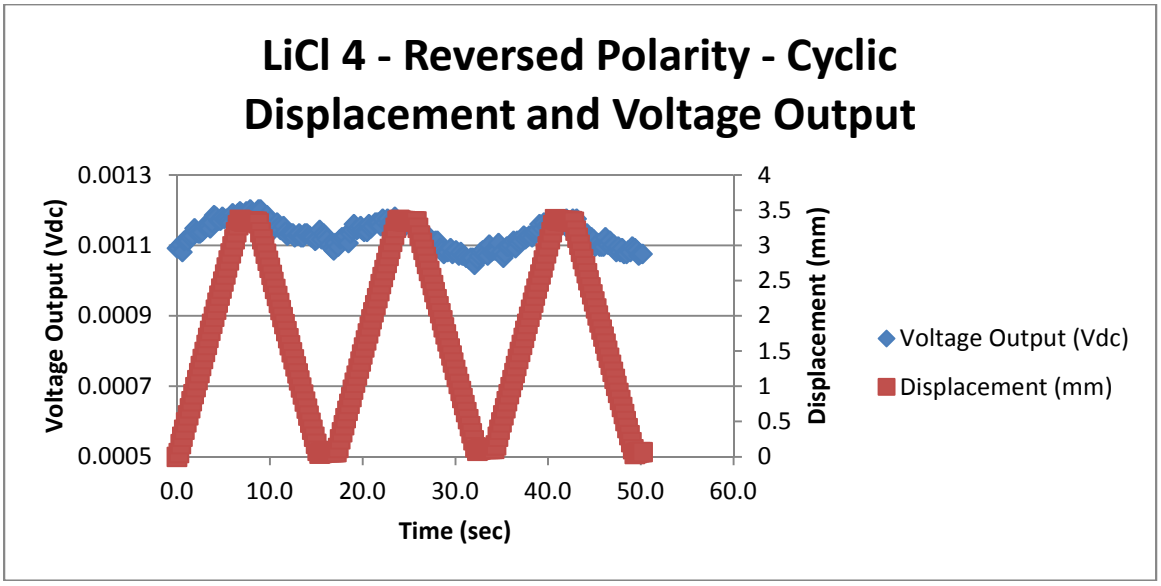

Figure 243
Trial 4 reversed polarity LiCl electrolyte cyclic load scenario, displacement and raw voltage output

Appendix H

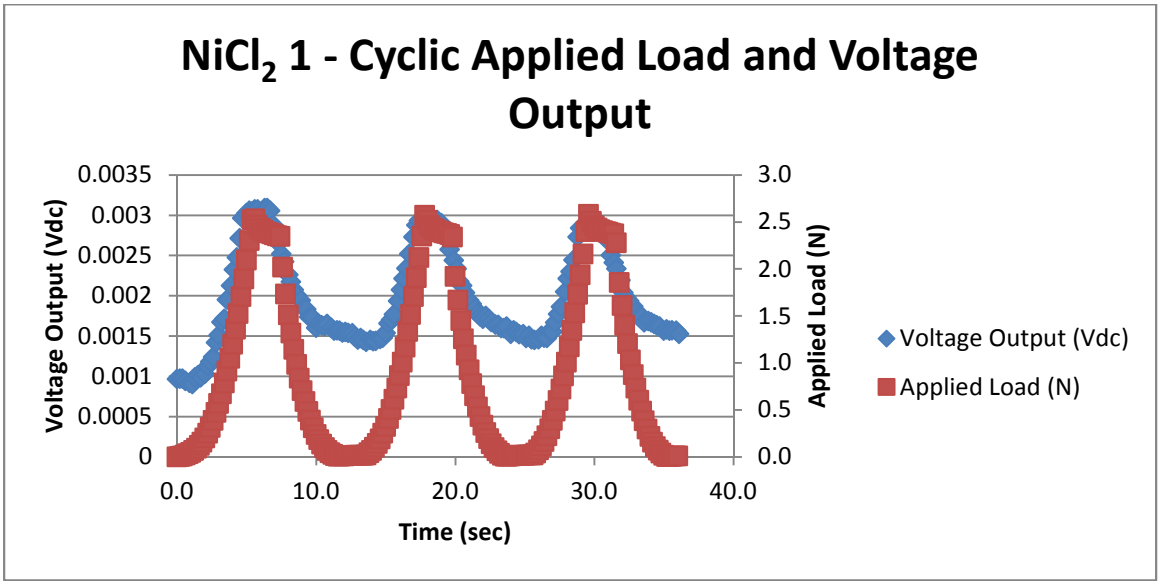

Figure 244

Trial 1 normal polarity $NiCl_2$ electrolyte cyclic load scenario, load and raw voltage output

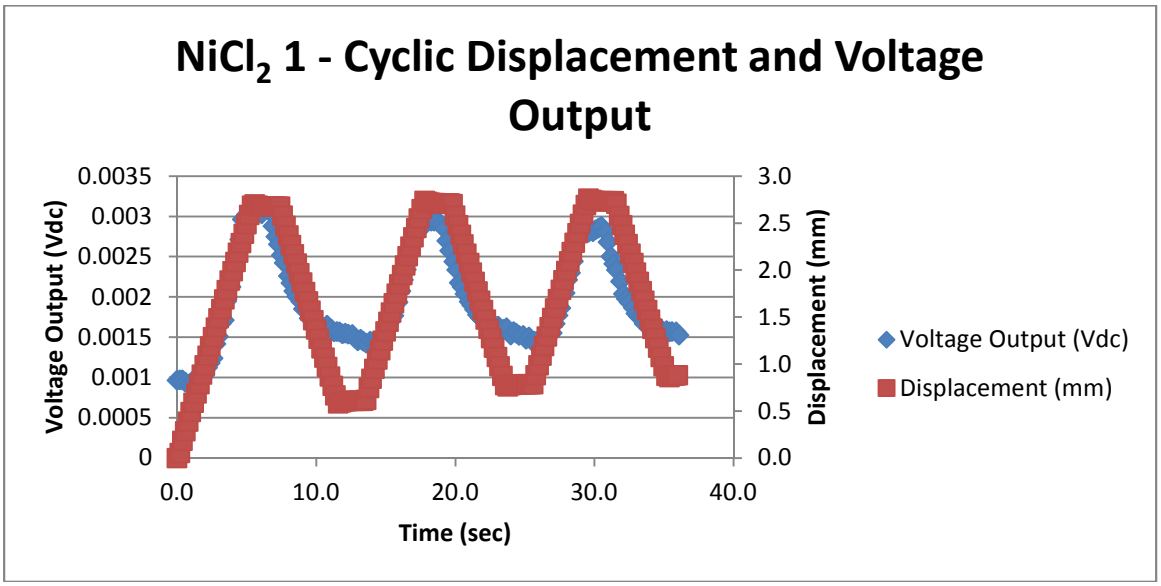

Figure 245

Trial 1 normal polarity $NiCl_2$ electrolyte cyclic load scenario, displacement and raw voltage output

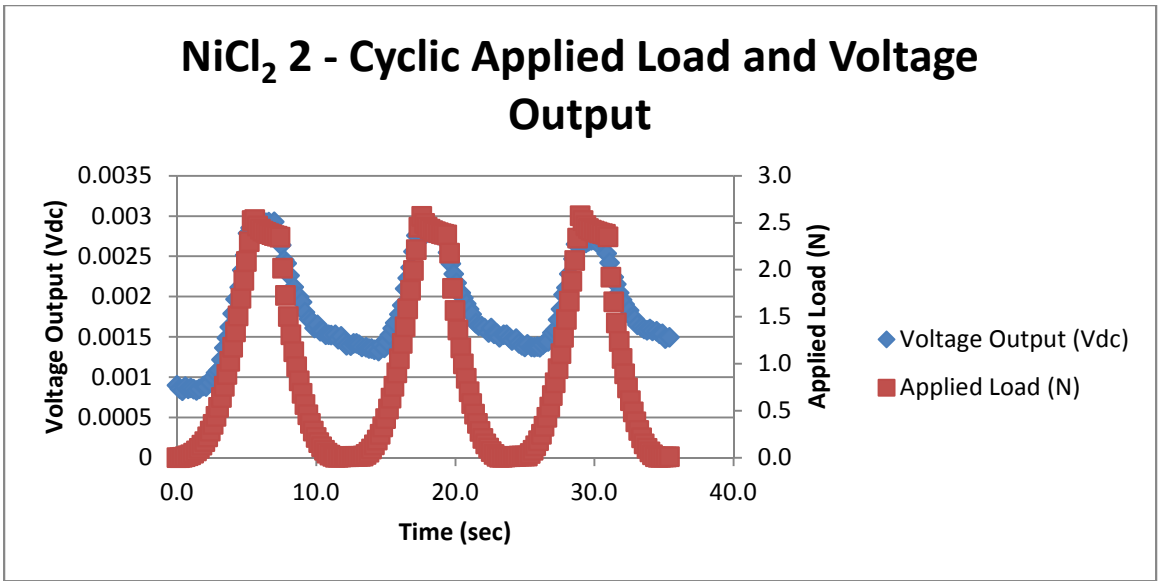

Figure 246
Trial 2 normal polarity $NiCl_2$ electrolyte cyclic load scenario, load and raw voltage output

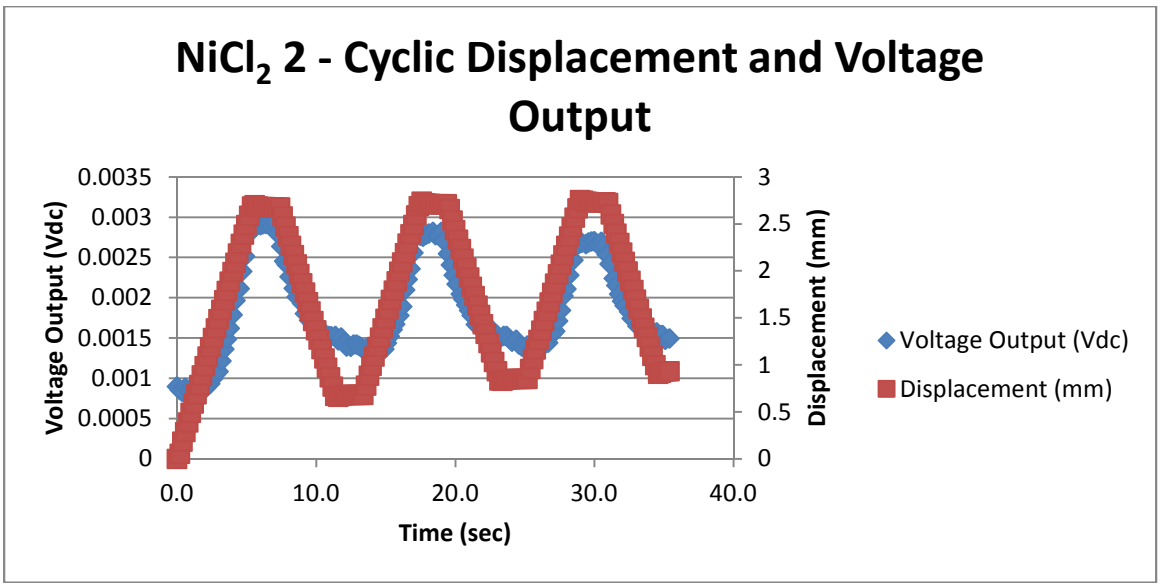

Figure 247
Trial 2 normal polarity $NiCl_2$ electrolyte cyclic load scenario, displacement and raw voltage output

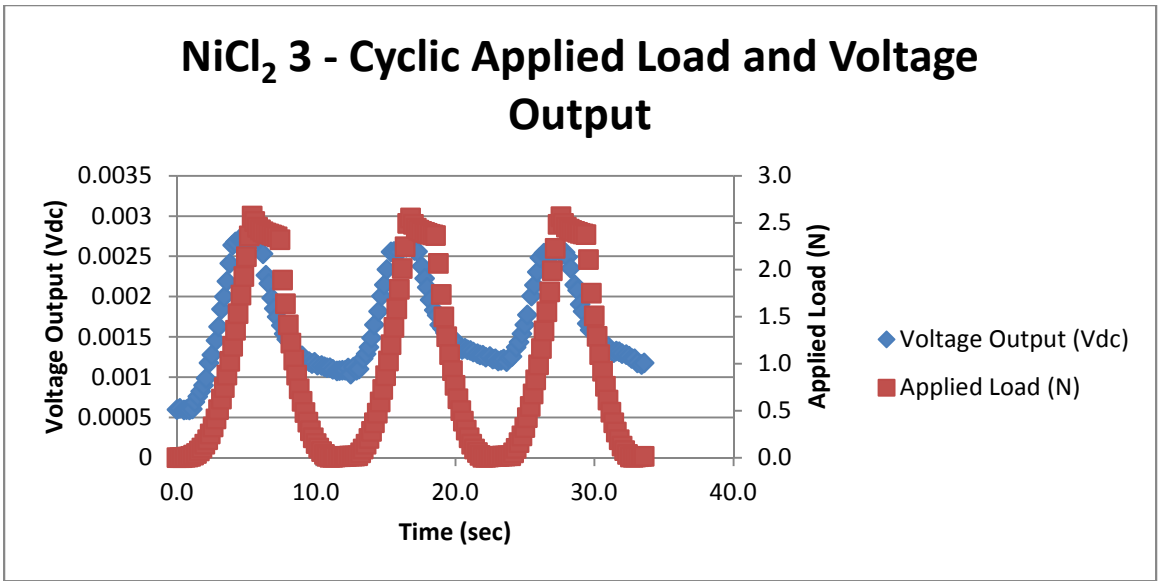

Figure 248

Trial 3 normal polarity $NiCl_2$ electrolyte cyclic load scenario, load and raw voltage output

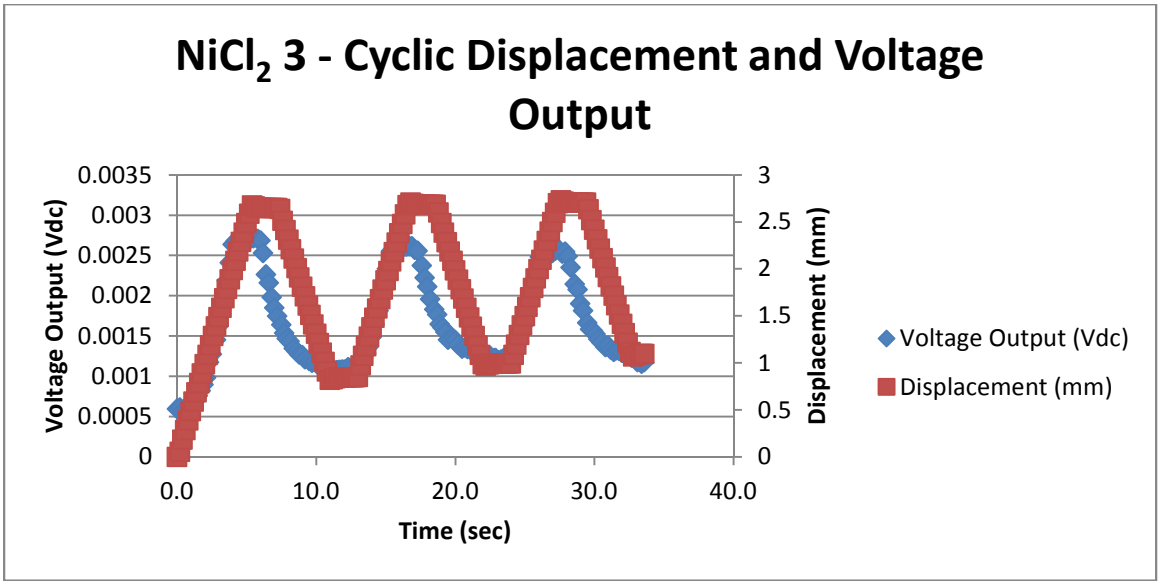

Figure 249

Trial 3 normal polarity $NiCl_2$ electrolyte cyclic load scenario, displacement and raw voltage output

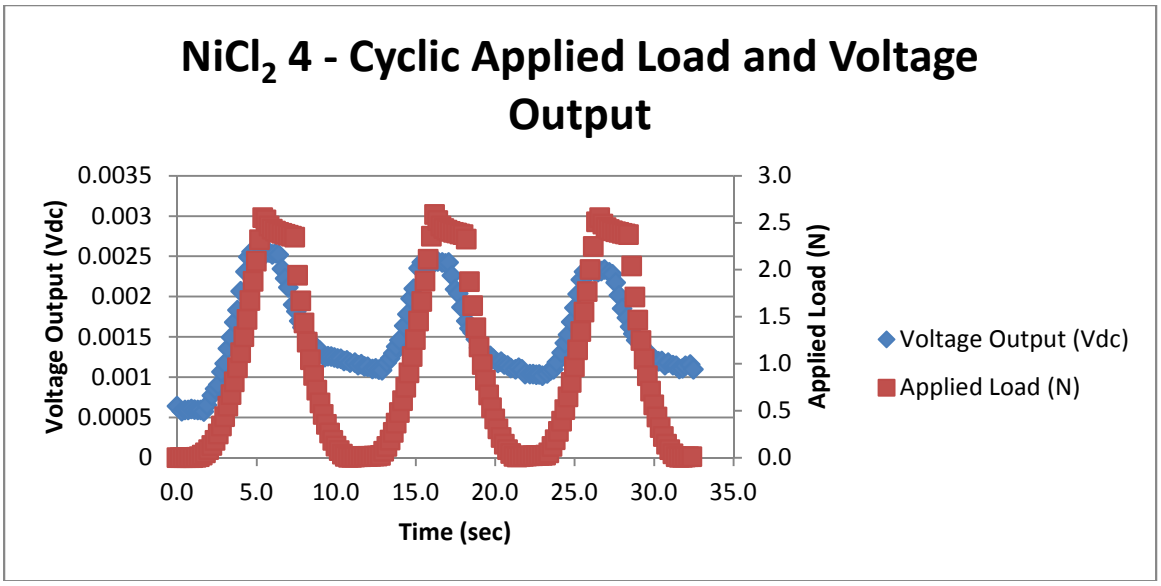

Figure 250
Trial 4 normal polarity $NiCl_2$ electrolyte cyclic load scenario, load and raw voltage output

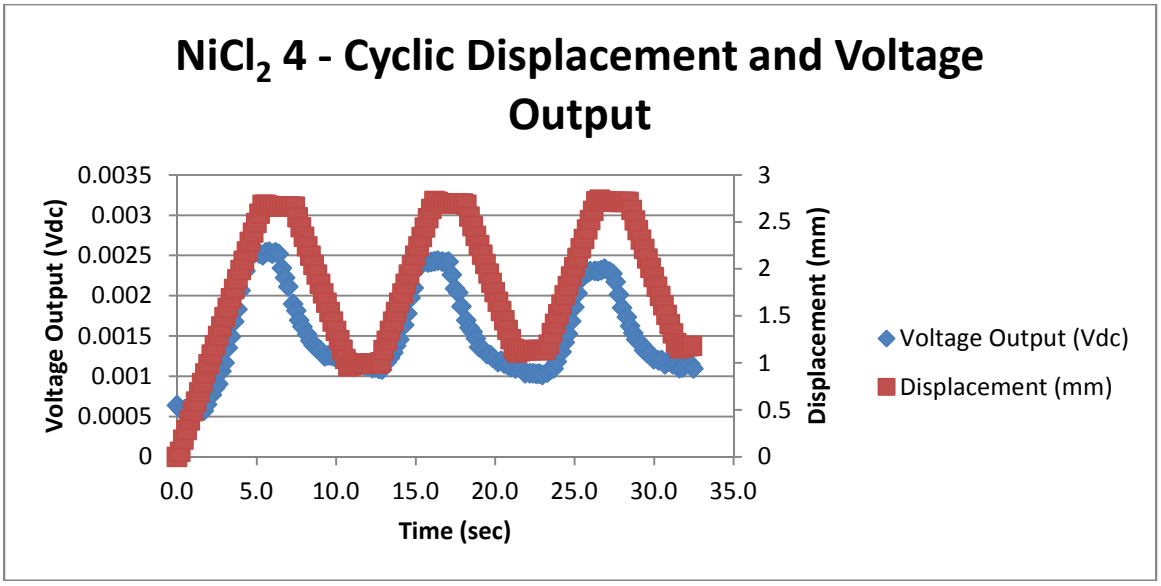

Figure 251
Trial 4 normal polarity $NiCl_2$ electrolyte cyclic load scenario, displacement and raw voltage output

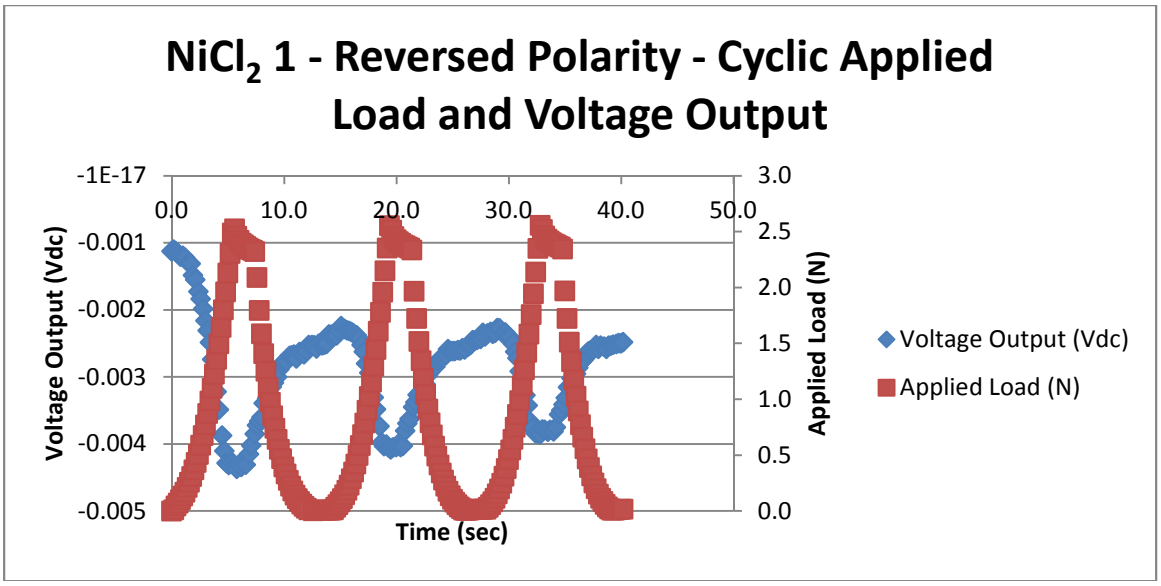

Figure 252
Trial 1 reversed polarity $NiCl_2$ electrolyte cyclic load scenario, load and raw voltage output

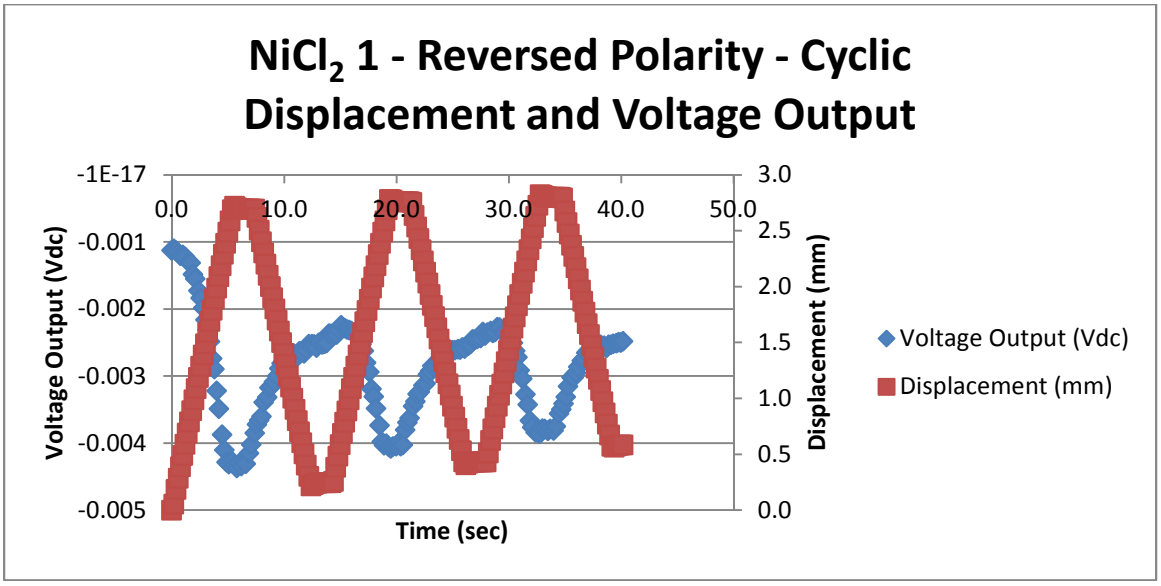

Figure 253
Trial 1 reversed polarity $NiCl_2$ electrolyte cyclic load scenario, displacement and raw voltage output

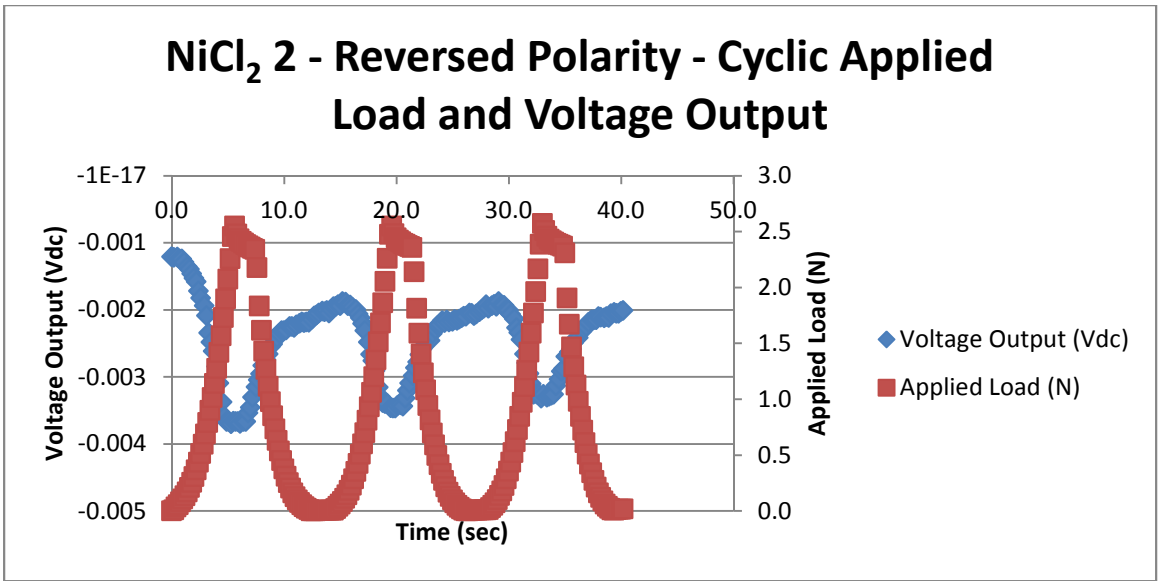

Figure 254
Trial 2 reversed polarity $NiCl_2$ electrolyte cyclic load scenario, load and raw voltage output

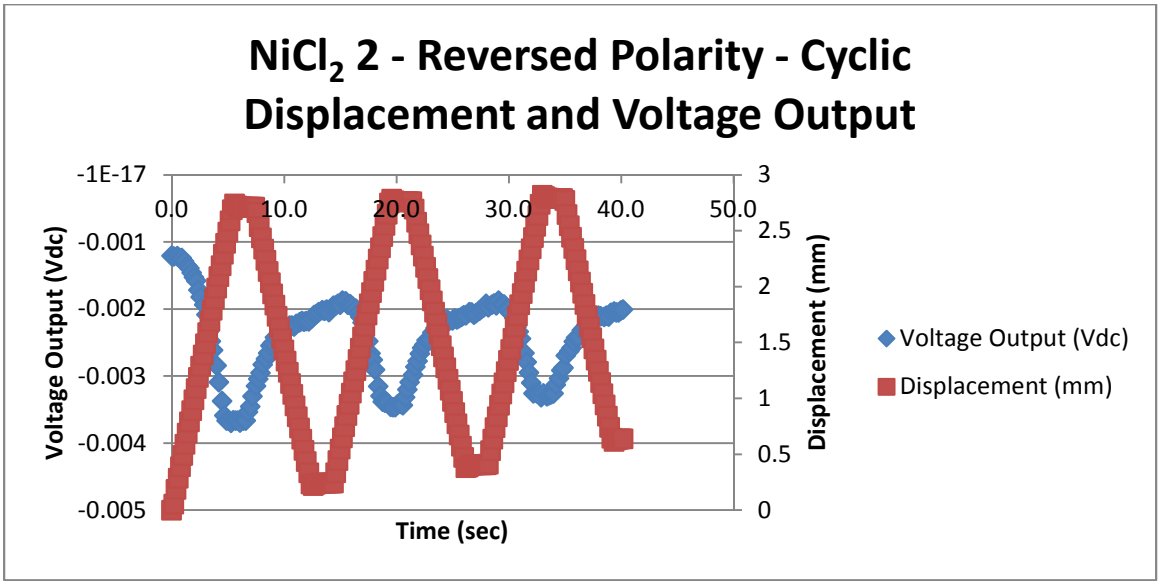

Figure 255
Trial 2 reversed polarity $NiCl_2$ electrolyte cyclic load scenario, displacement and raw voltage output

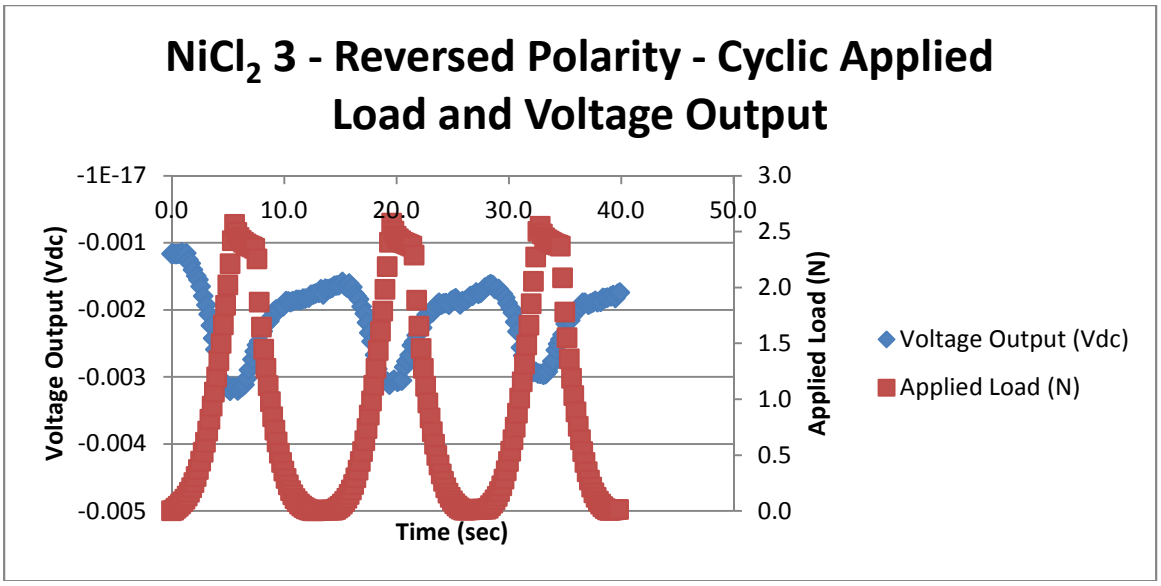

Figure 256
Trial 3 reversed polarity $NiCl_2$ electrolyte cyclic load scenario, load and raw voltage output

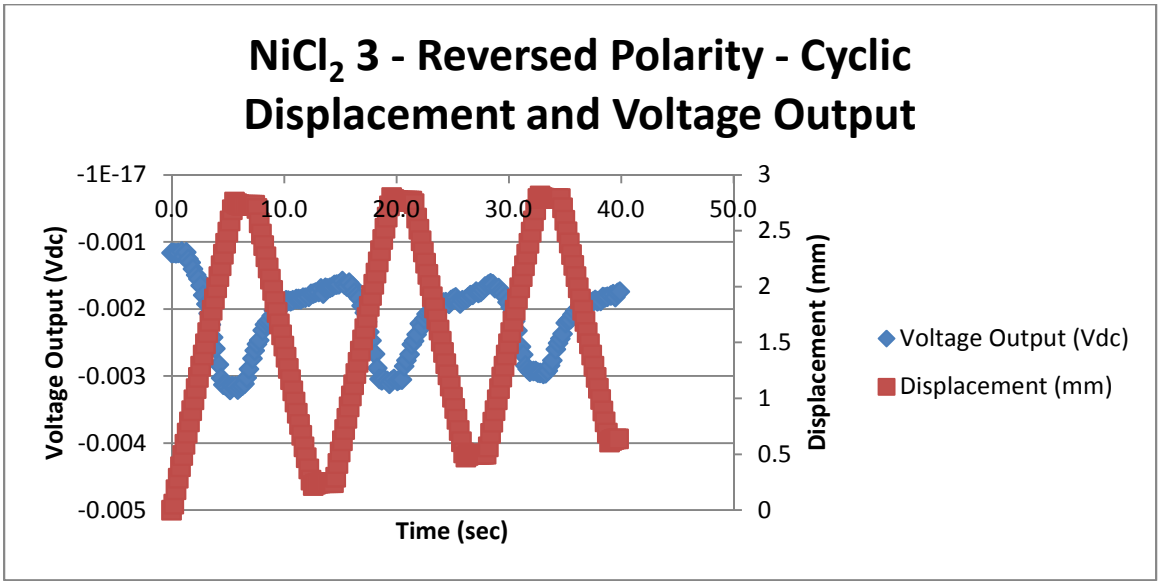

Figure 257
Trial 3 reversed polarity $NiCl_2$ electrolyte cyclic load scenario, displacement and raw voltage output

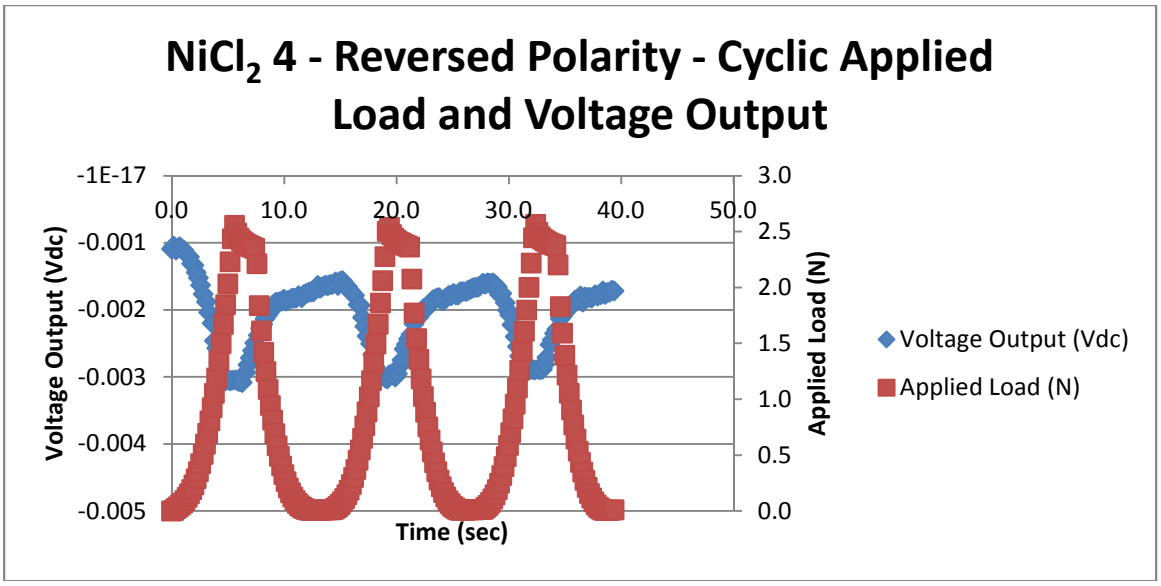

Figure 258
Trial 4 reversed polarity $NiCl_2$ electrolyte cyclic load scenario, load and raw voltage output

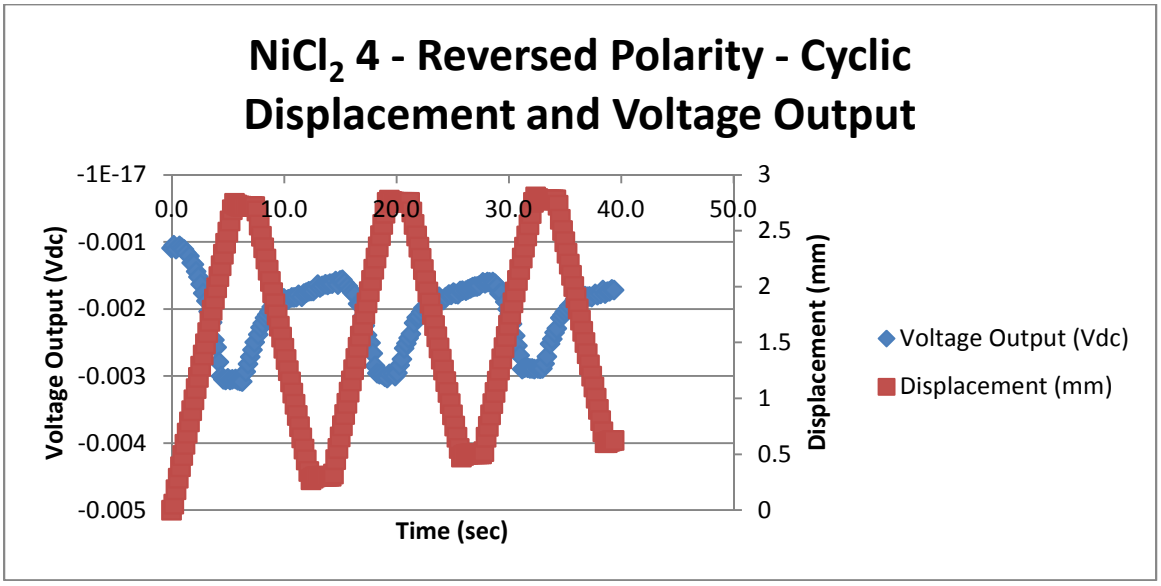

Figure 259
Trial 4 reversed polarity $NiCl_2$ electrolyte cyclic load scenario, displacement and raw voltage output

Appendix I

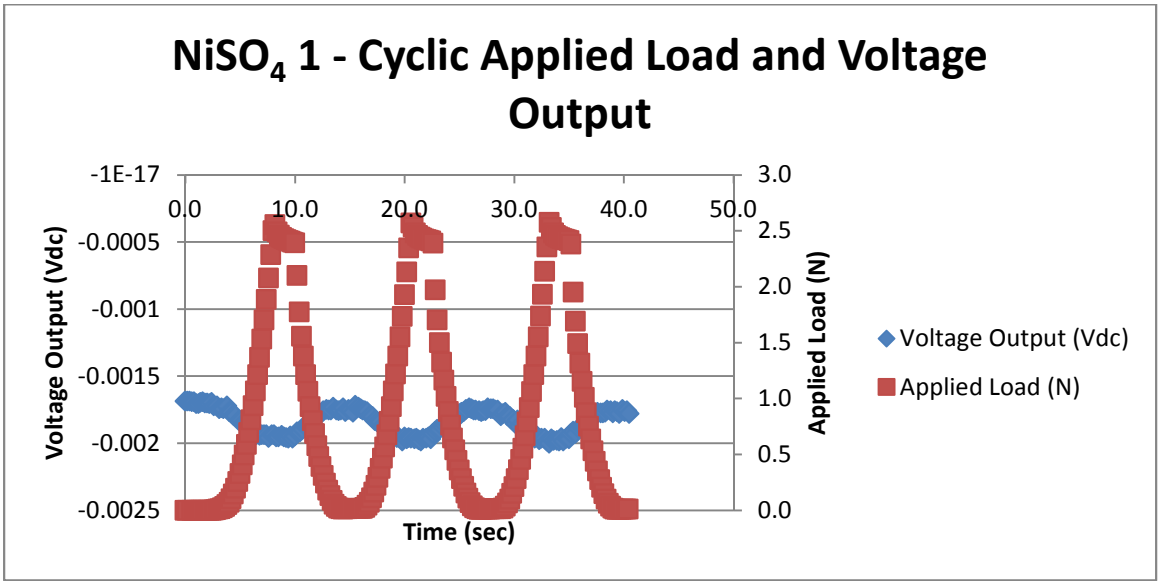

Figure 260
Trial 1 normal polarity $NiSO_4$ electrolyte cyclic load scenario, load and raw voltage output

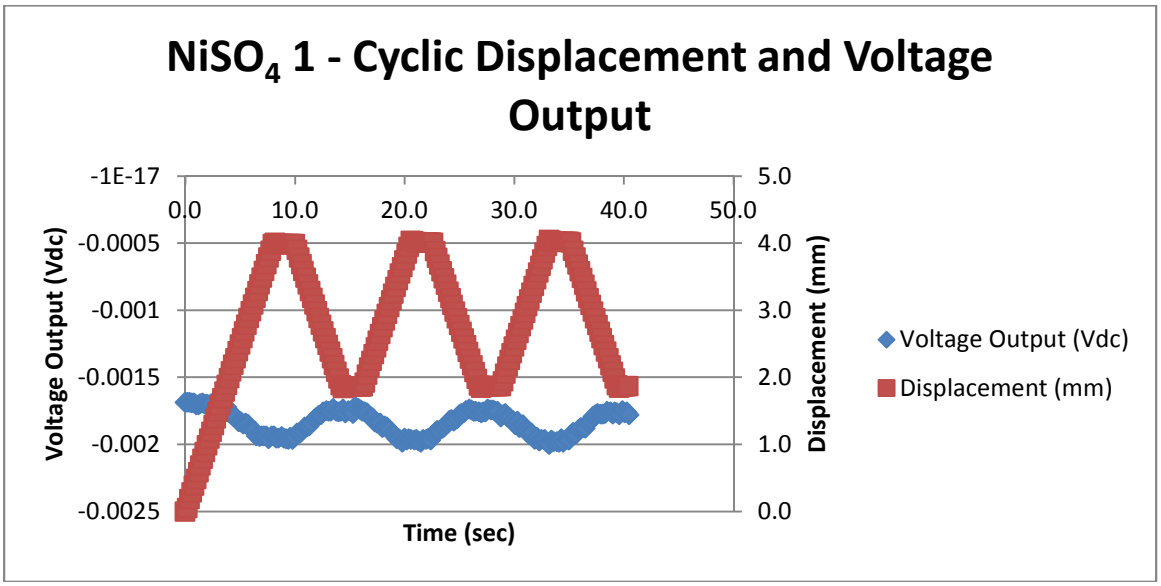

Figure 261
Trial 1 normal polarity $NiSO_4$ electrolyte cyclic load scenario, displacement and raw voltage output

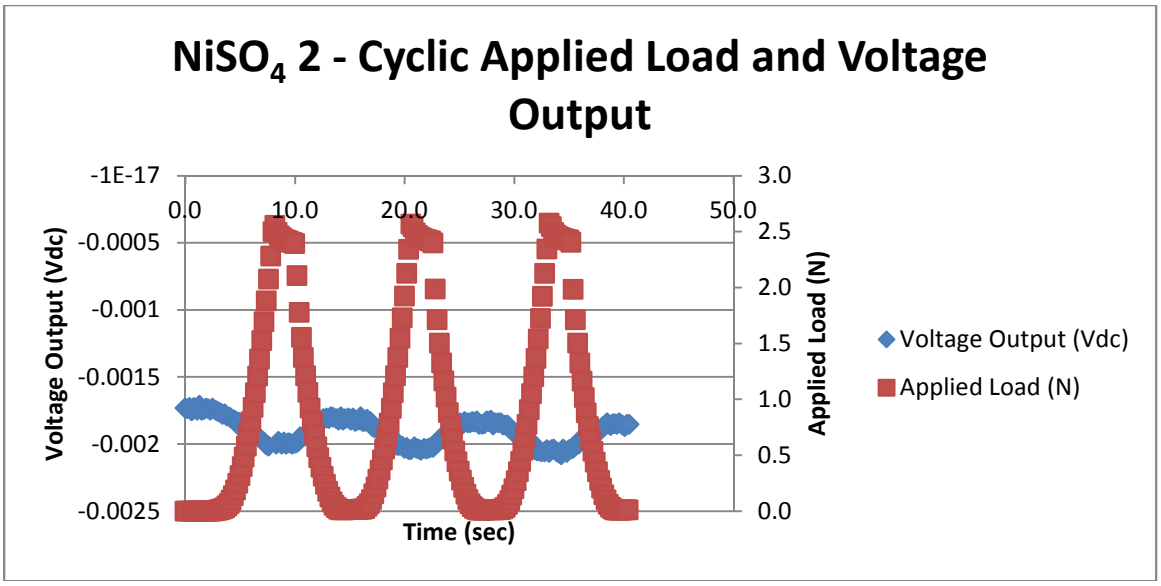

Figure 262
Trial 2 normal polarity $NiSO_4$ electrolyte cyclic load scenario, load and raw voltage output

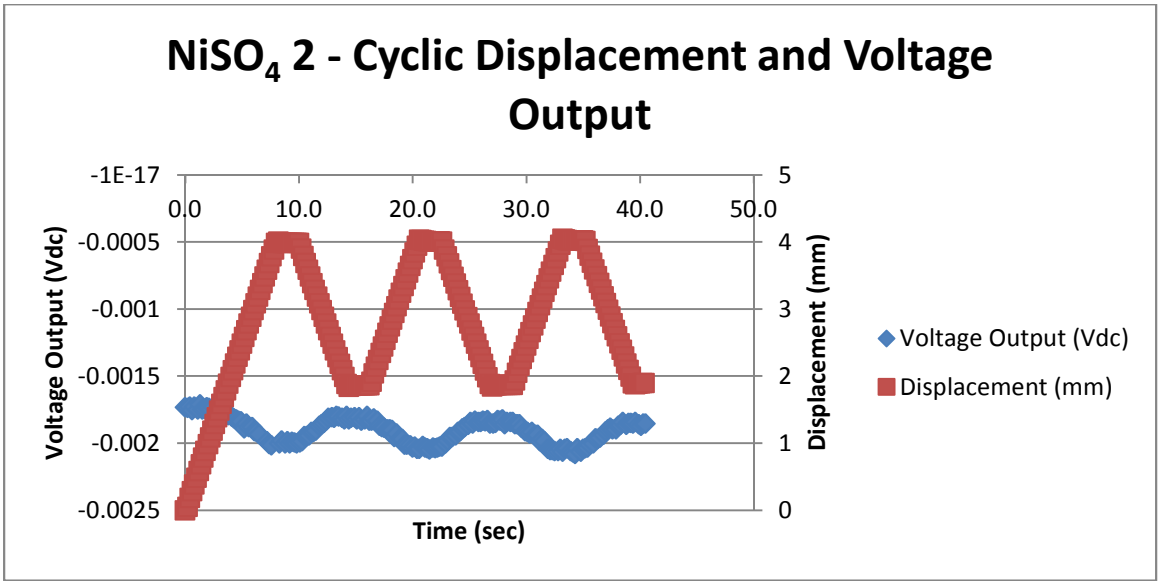

Figure 263
Trial 2 normal polarity $NiSO_4$ electrolyte cyclic load scenario, displacement and raw voltage output

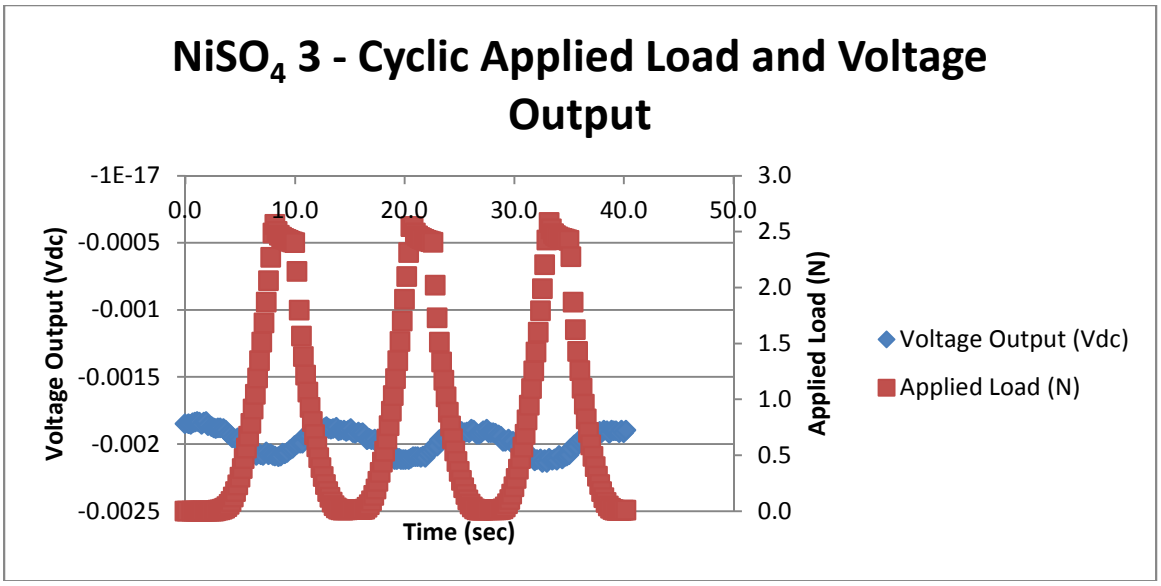

Figure 264
Trial 3 normal polarity $NiSO_4$ electrolyte cyclic load scenario, load and raw voltage output

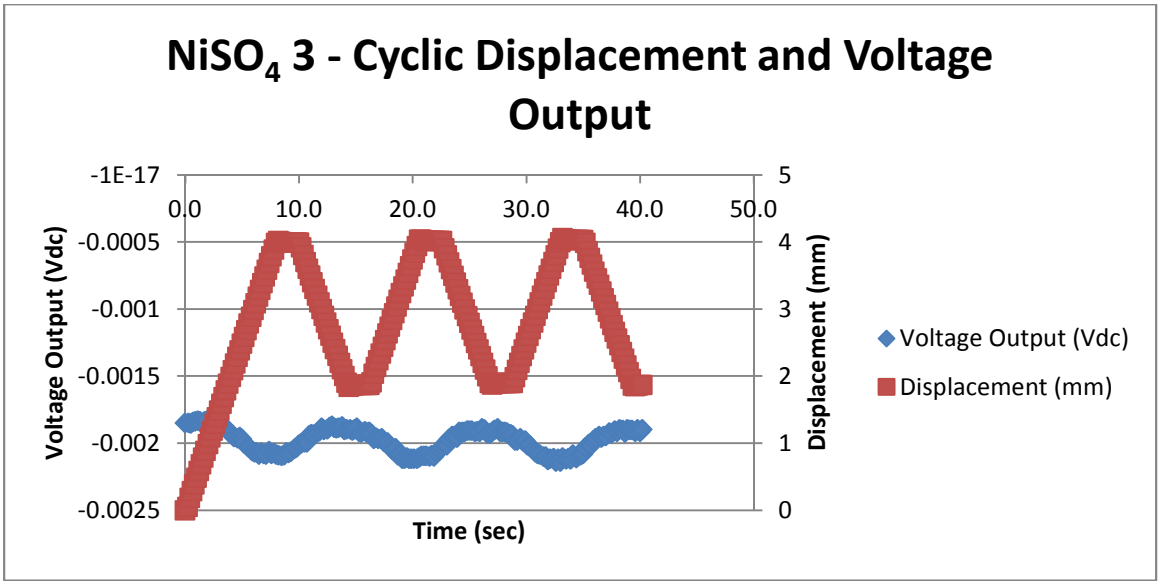

Figure 265
Trial 3 normal polarity $NiSO_4$ electrolyte cyclic load scenario, displacement and raw voltage output

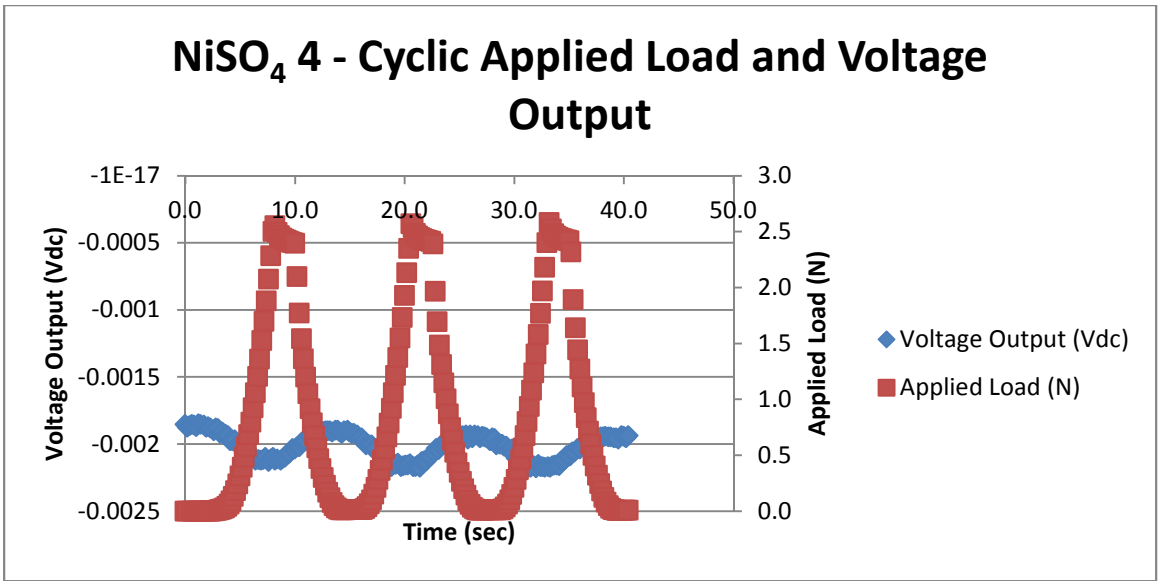

Figure 266
Trial 4 normal polarity $NiSO_4$ electrolyte cyclic load scenario, load and raw voltage output

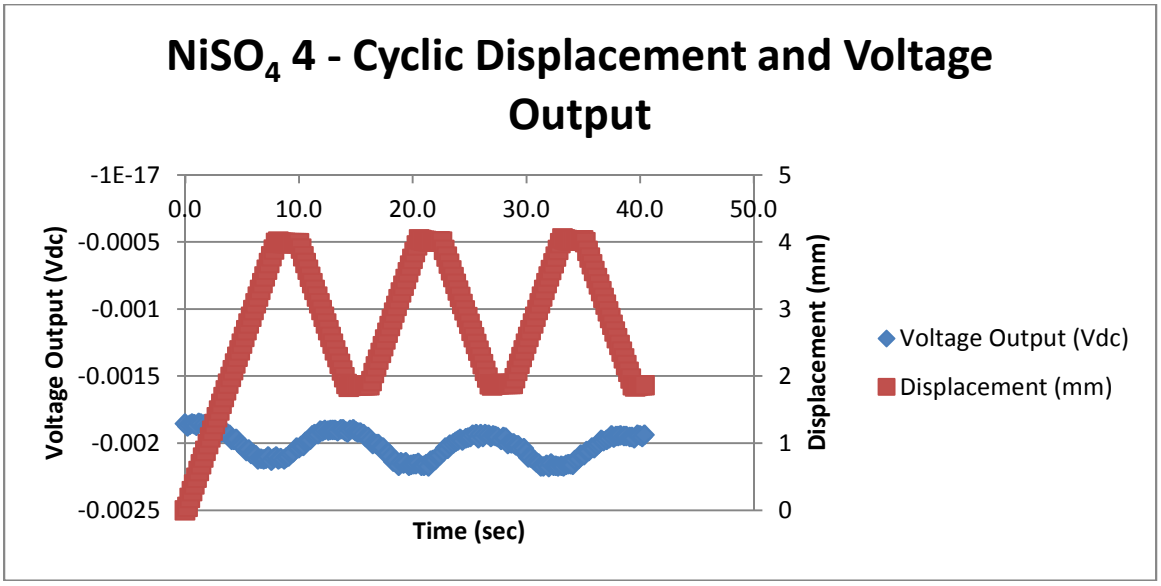

Figure 267
Trial 4 normal polarity $NiSO_4$ electrolyte cyclic load scenario, displacement and raw voltage output

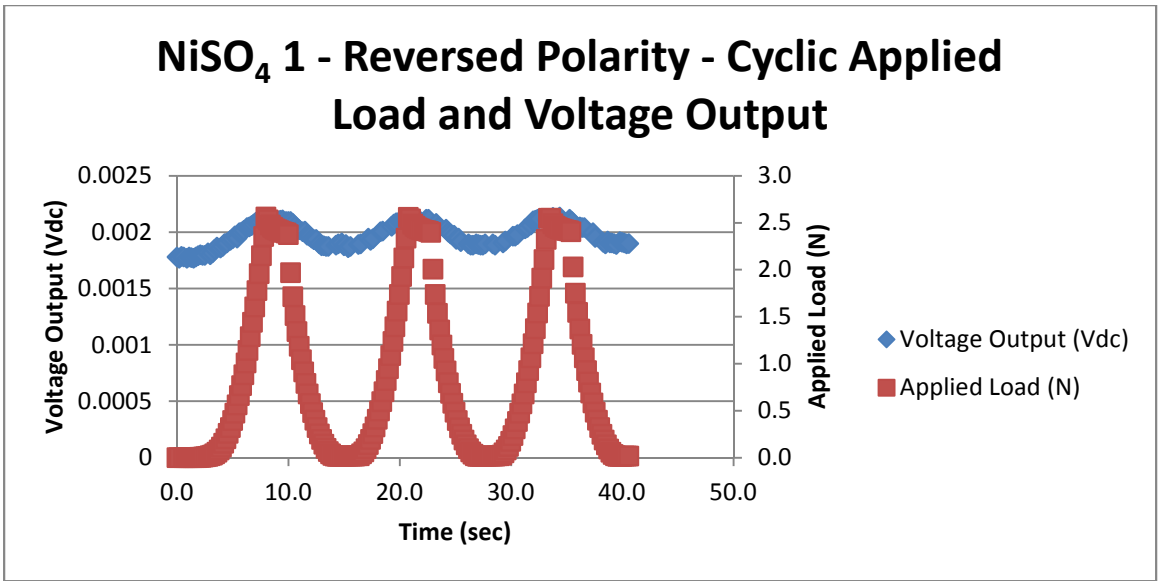

Figure 268
Trial 1 reversed polarity $NiSO_4$ electrolyte cyclic load scenario, load and raw voltage output

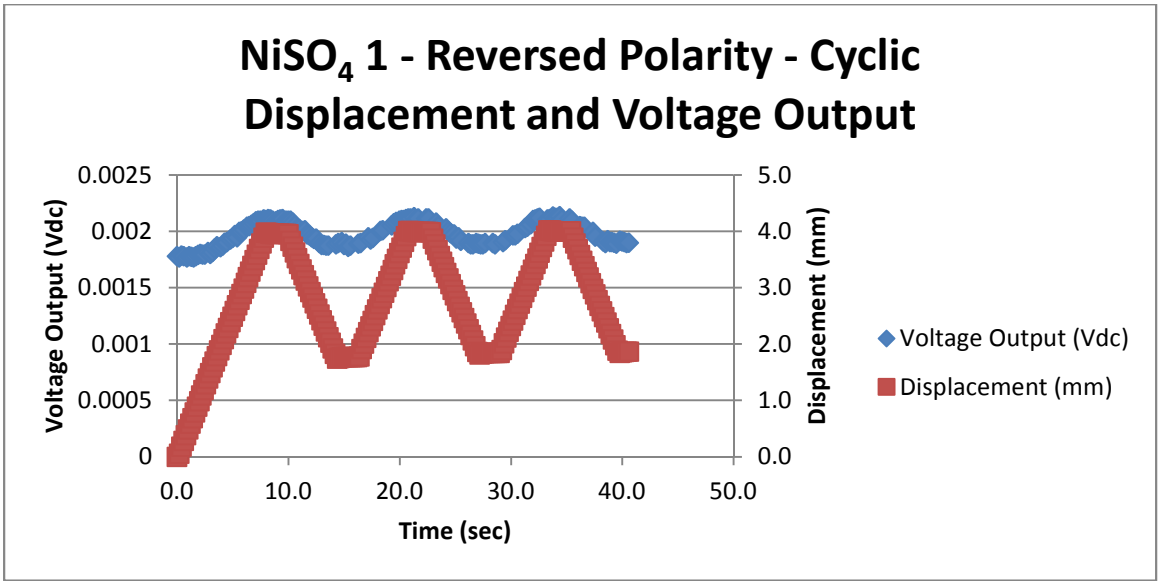

Figure 269
Trial 1 reversed polarity $NiSO_4$ electrolyte cyclic load scenario, displacement and raw voltage output

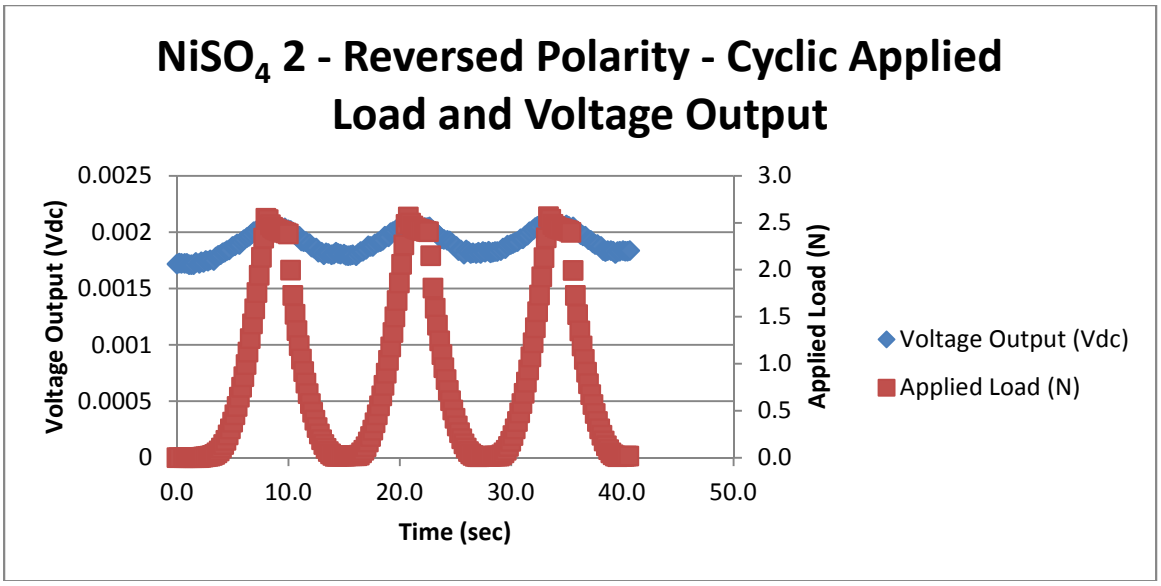

Figure 270
Trial 2 reversed polarity $NiSO_4$ electrolyte cyclic load scenario, load and raw voltage output

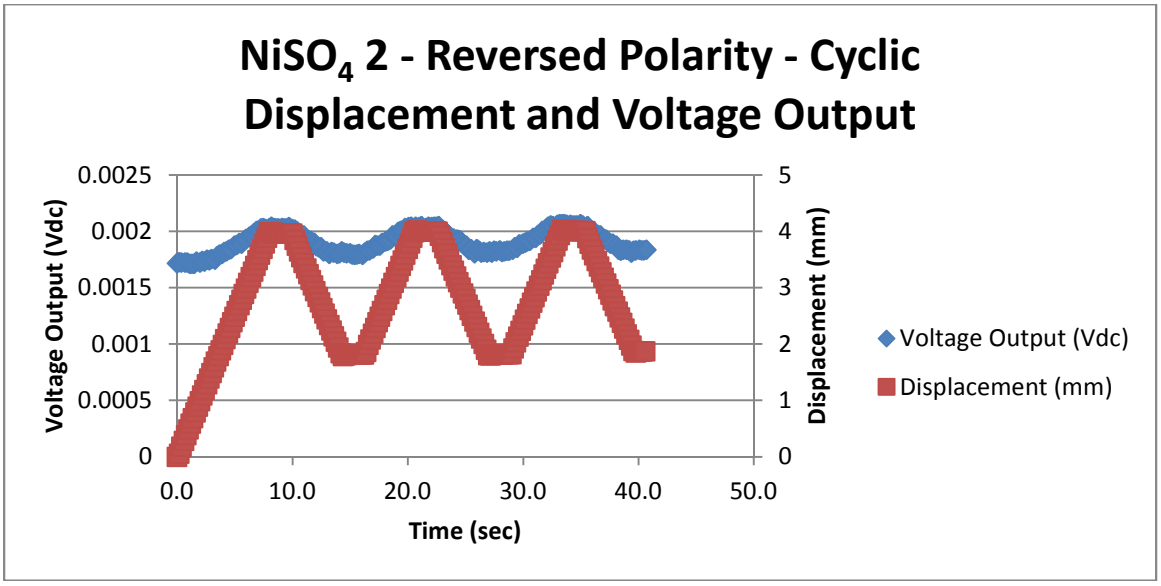

Figure 271
Trial 2 reversed polarity $NiSO_4$ electrolyte cyclic load scenario, displacement and raw voltage output

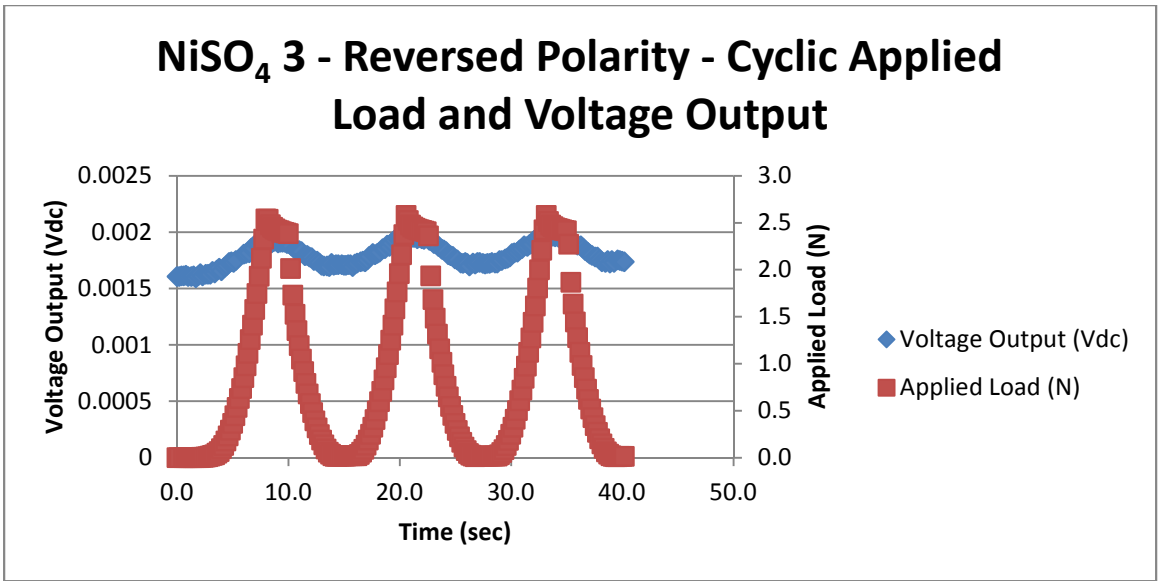

Figure 272
Trial 3 reversed polarity $NiSO_4$ electrolyte cyclic load scenario, load and raw voltage output

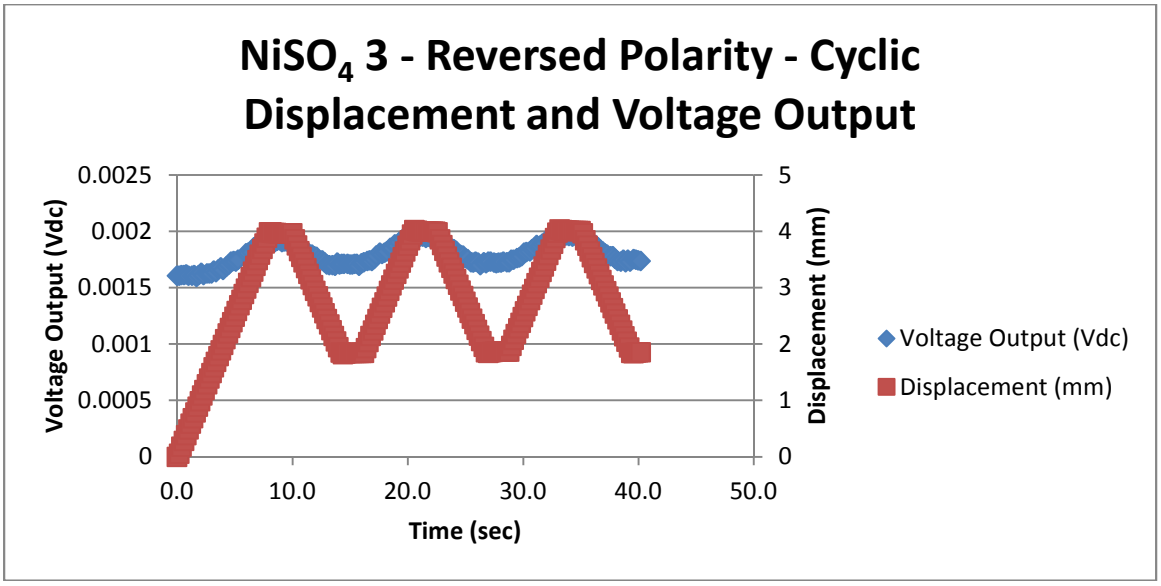

Figure 273
Trial 3 reversed polarity $NiSO_4$ electrolyte cyclic load scenario, displacement and raw voltage output

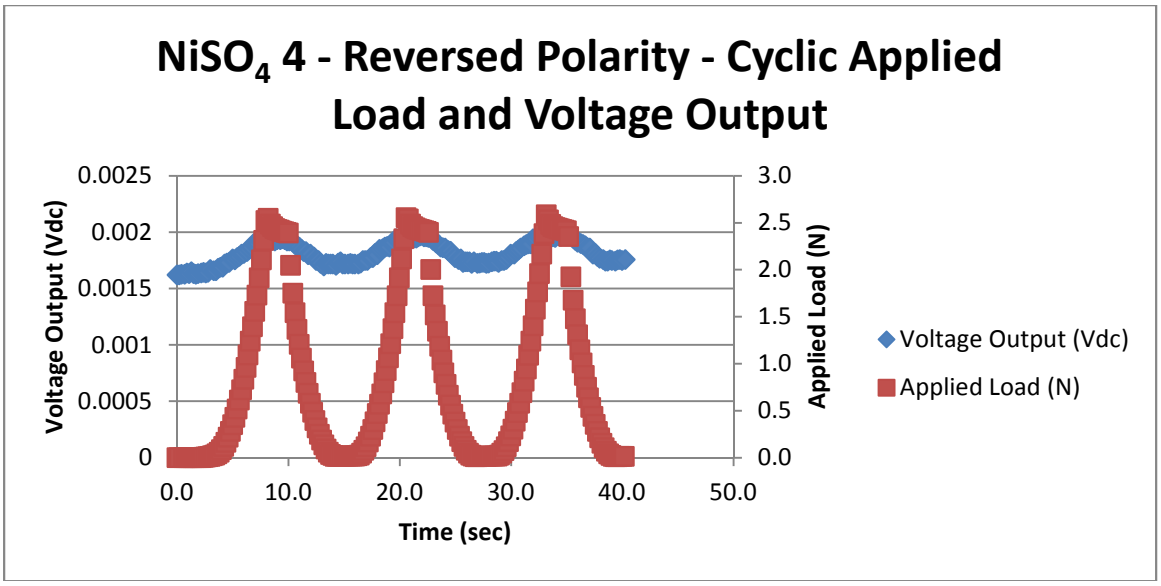

Figure 274
Trial 4 reversed polarity $NiSO_4$ electrolyte cyclic load scenario, load and raw voltage output

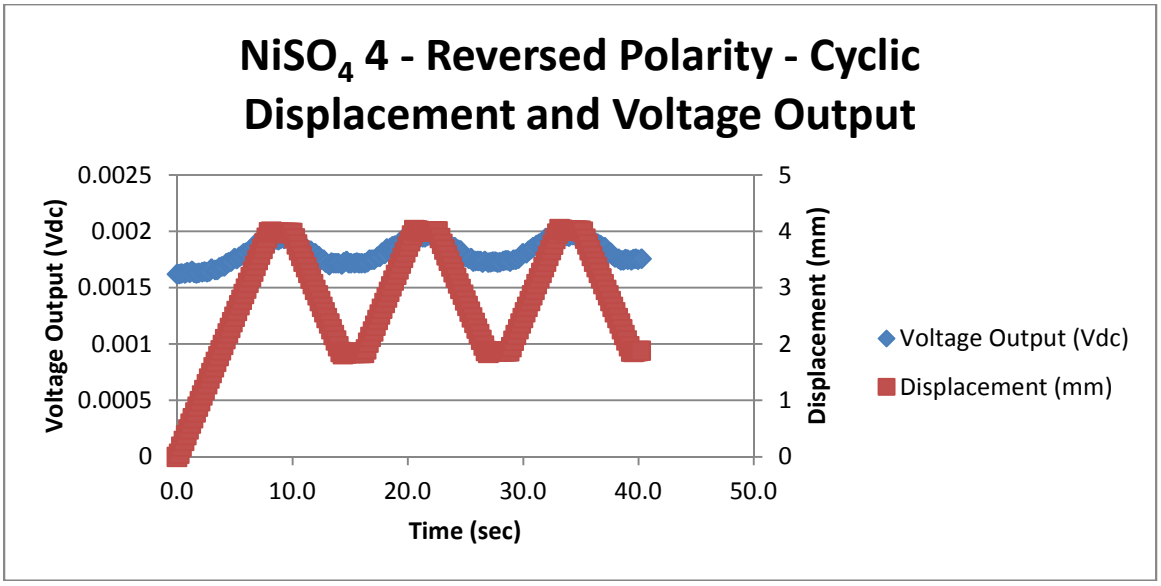

Figure 275
Trial 4 reversed polarity $NiSO_4$ electrolyte cyclic load scenario, displacement and raw voltage output

Appendix J

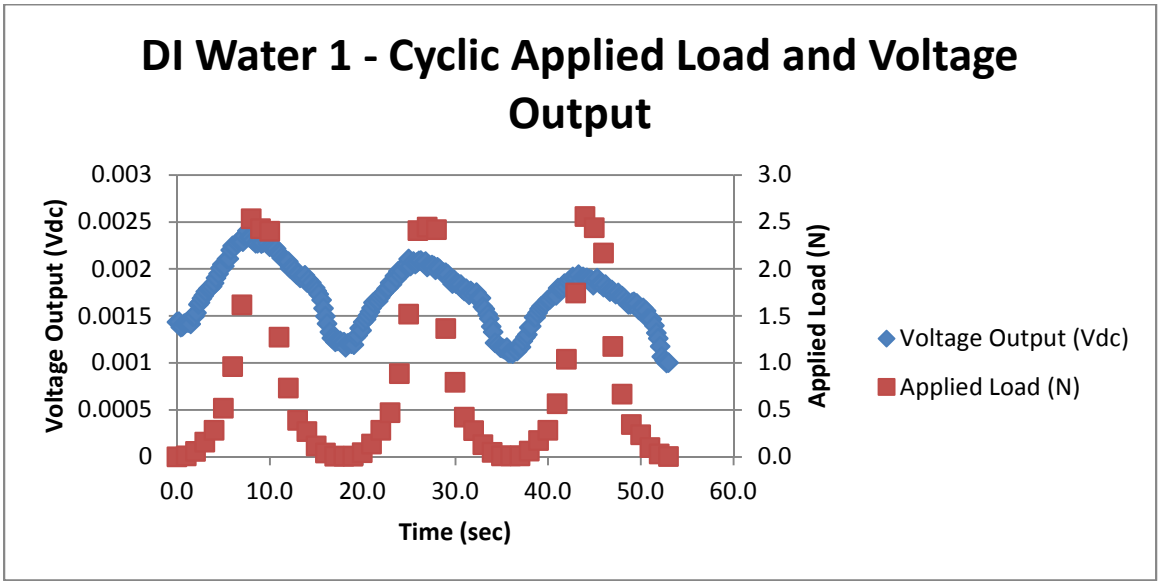

Figure 276
Trial 1 normal polarity DI water electrolyte cyclic load scenario, load and raw voltage output

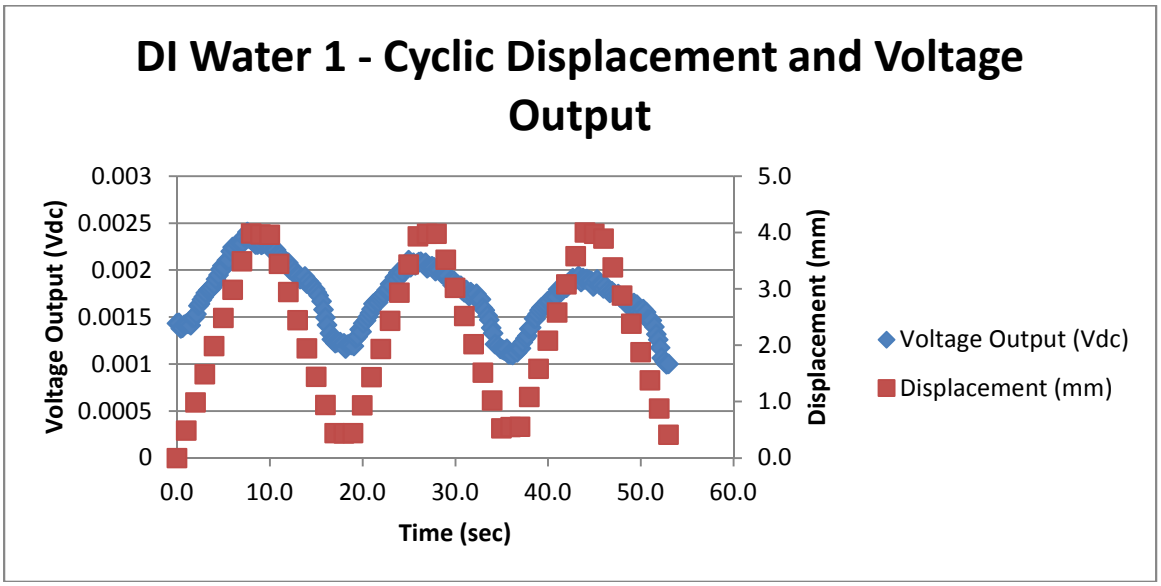

Figure 277
Trial 1 normal polarity DI water electrolyte cyclic load scenario, displacement and raw voltage output

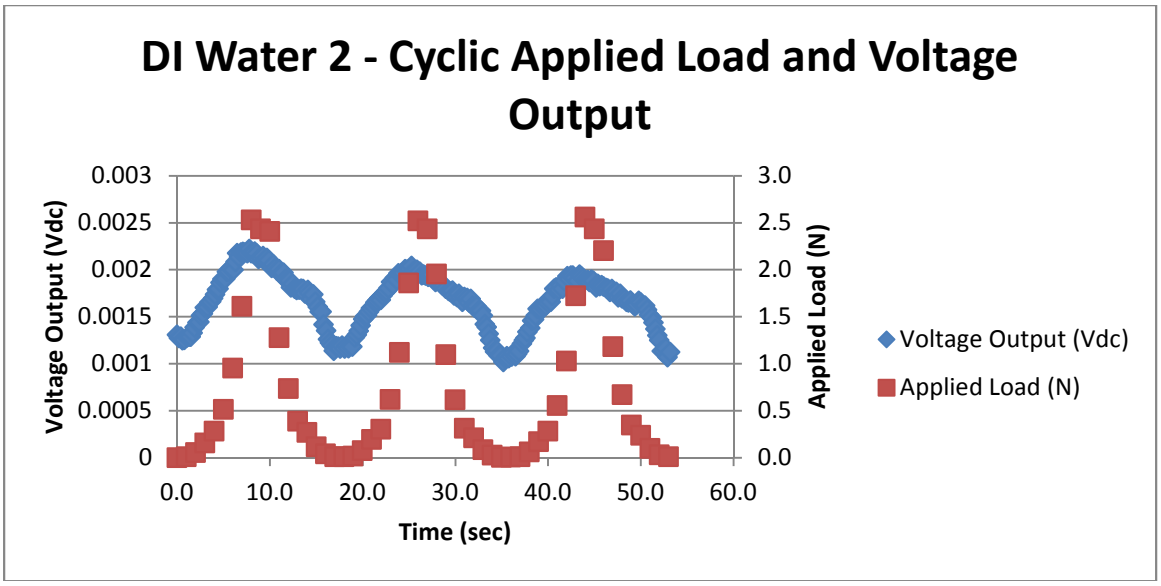

Figure 278
Trial 2 normal polarity DI water electrolyte cyclic load scenario, load and raw voltage output

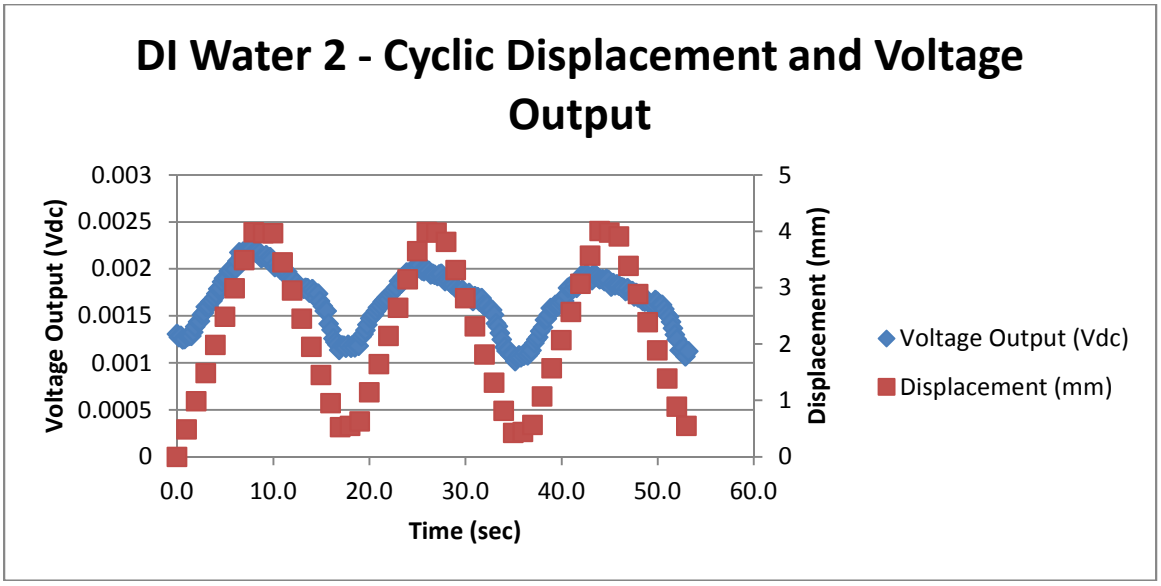

Figure 279
Trial 2 normal polarity DI water electrolyte cyclic load scenario, displacement and raw voltage output

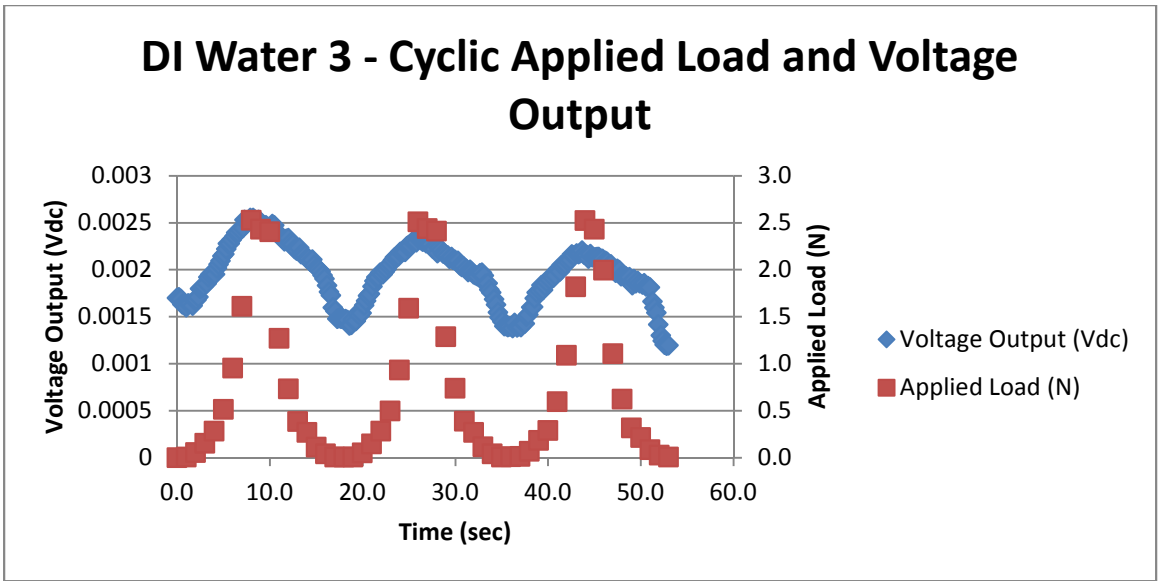

Figure 280
Trial 3 normal polarity DI water electrolyte cyclic load scenario, load and raw voltage output

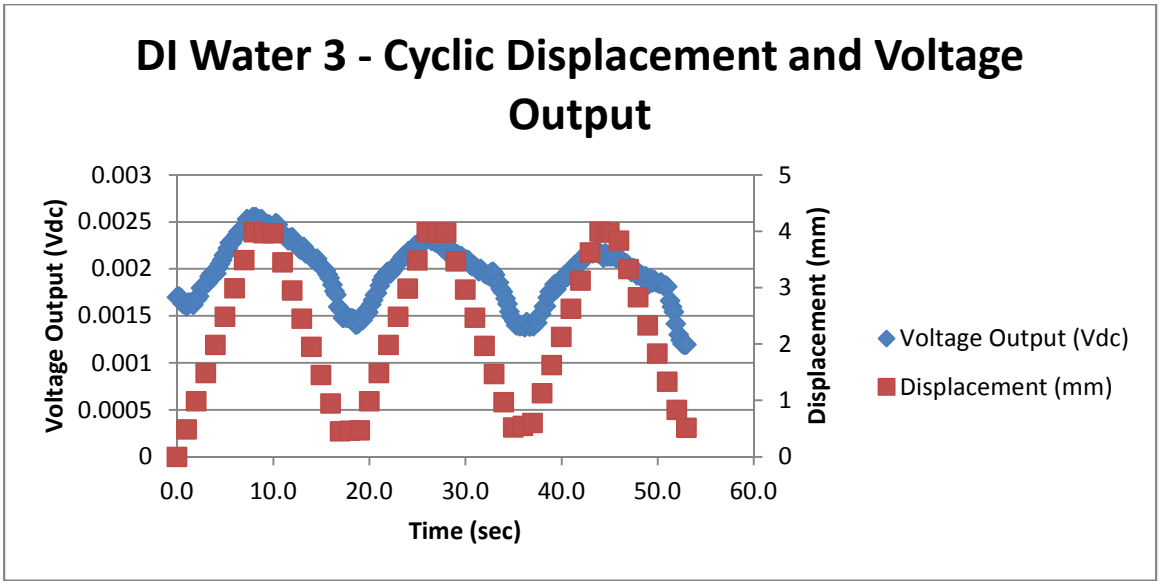

Figure 281
Trial 3 normal polarity DI water electrolyte cyclic load scenario, displacement and raw voltage output

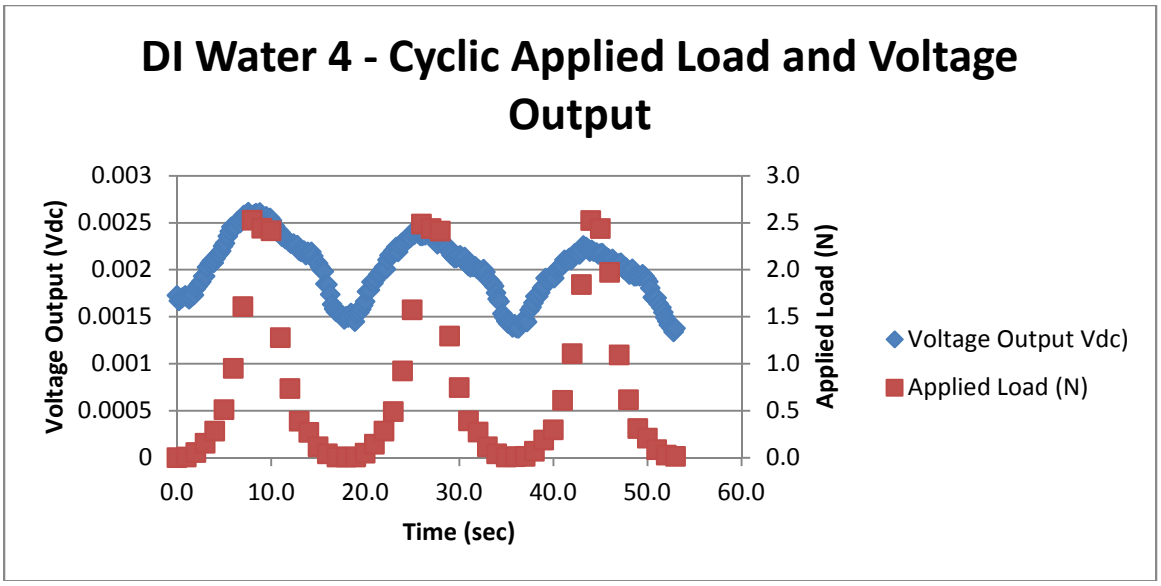

Figure 282
Trial 4 normal polarity DI water electrolyte cyclic load scenario, load and raw voltage output

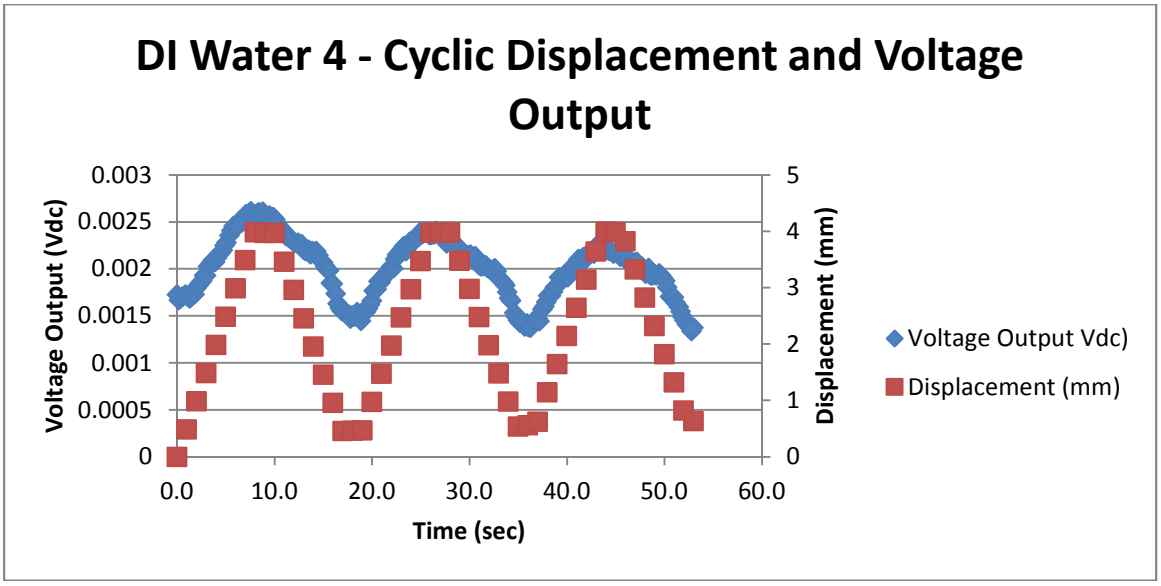

Figure 283
Trial 4 normal polarity DI water electrolyte cyclic load scenario, displacement and raw voltage output

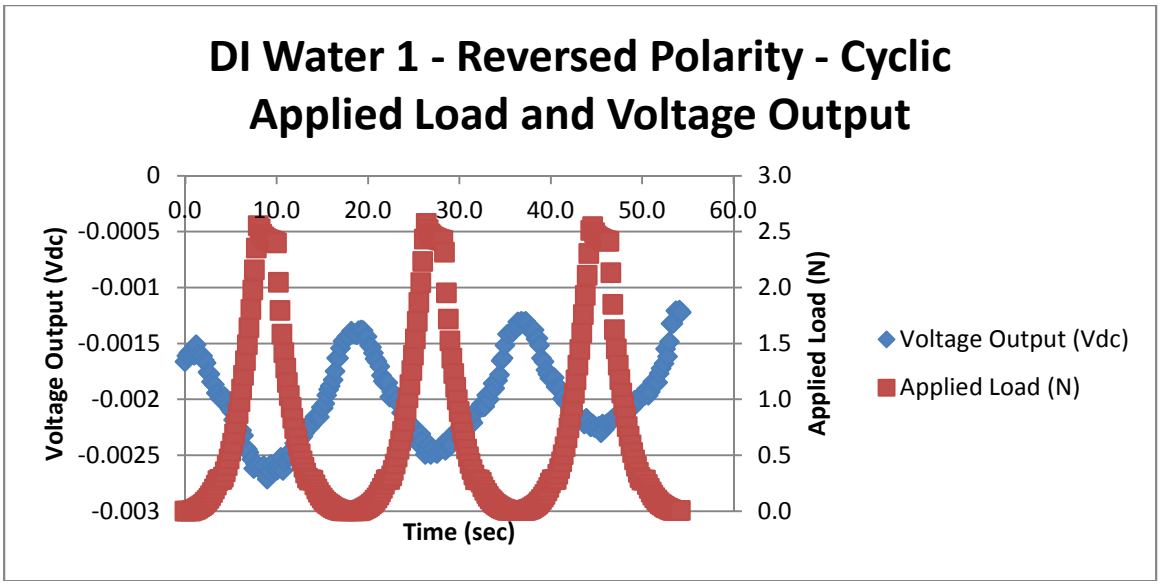

Figure 284
Trial 1 reversed polarity DI water electrolyte cyclic load scenario, load and raw voltage output

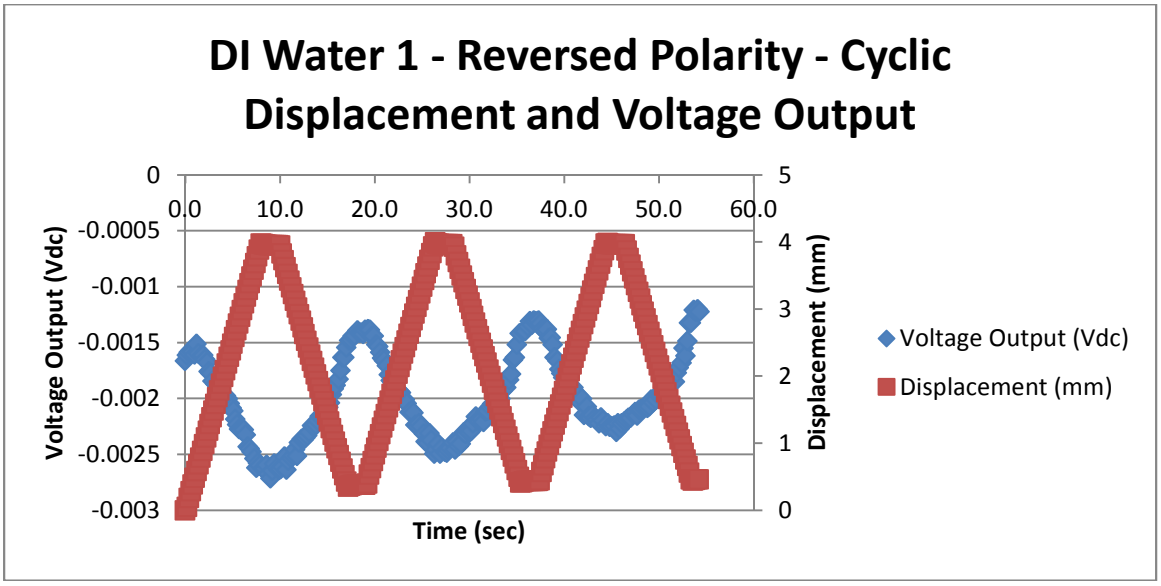

Figure 285
Trial 1 reversed polarity DI water electrolyte cyclic load scenario, displacement and raw voltage output

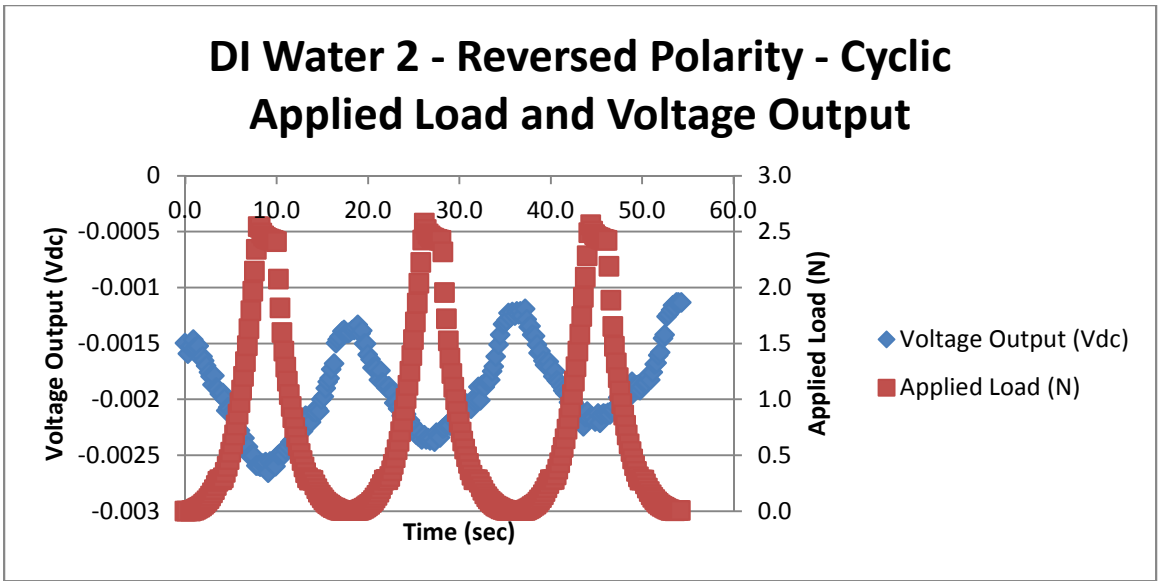

Figure 286
Trial 2 reversed polarity DI water electrolyte cyclic load scenario, load and raw voltage output

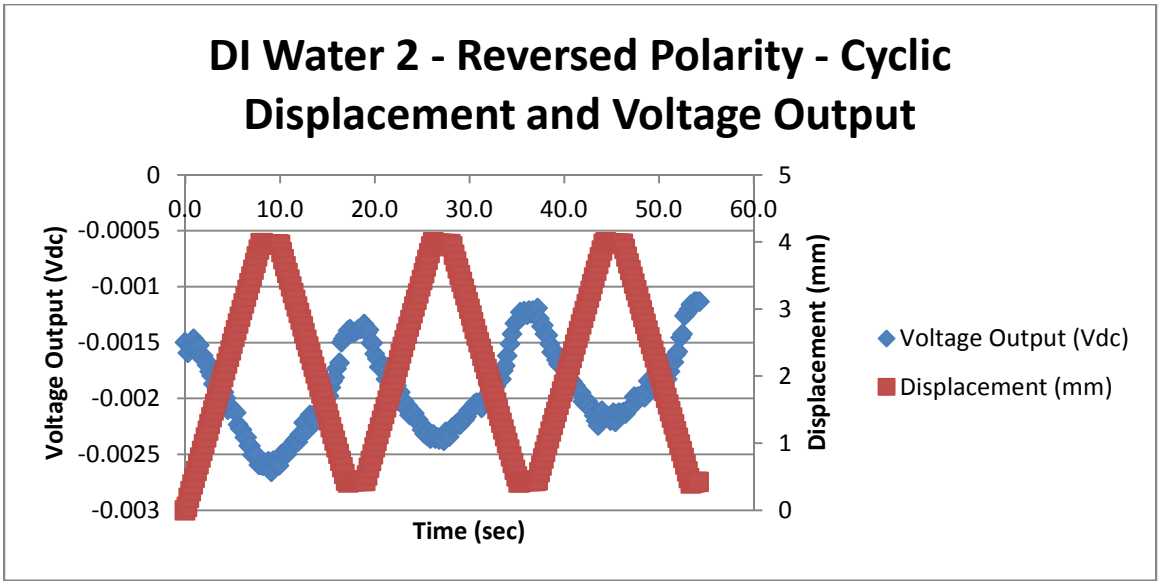

Figure 287
Trial 2 reversed polarity DI water electrolyte cyclic load scenario, displacement and raw voltage output

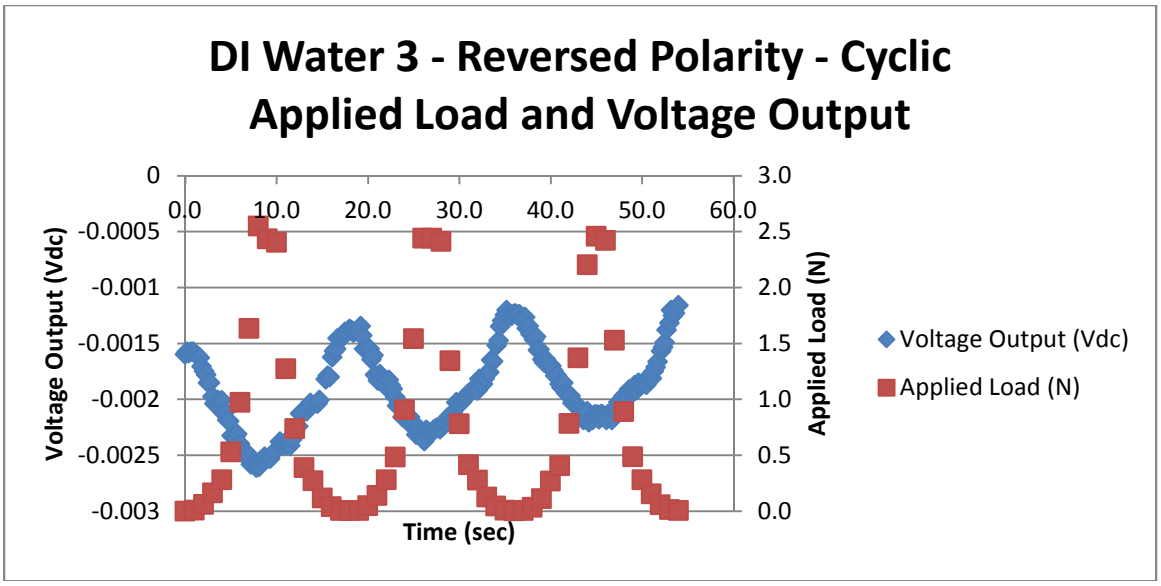

Figure 288
Trial 3 reversed polarity DI water electrolyte cyclic load scenario, load and raw voltage output

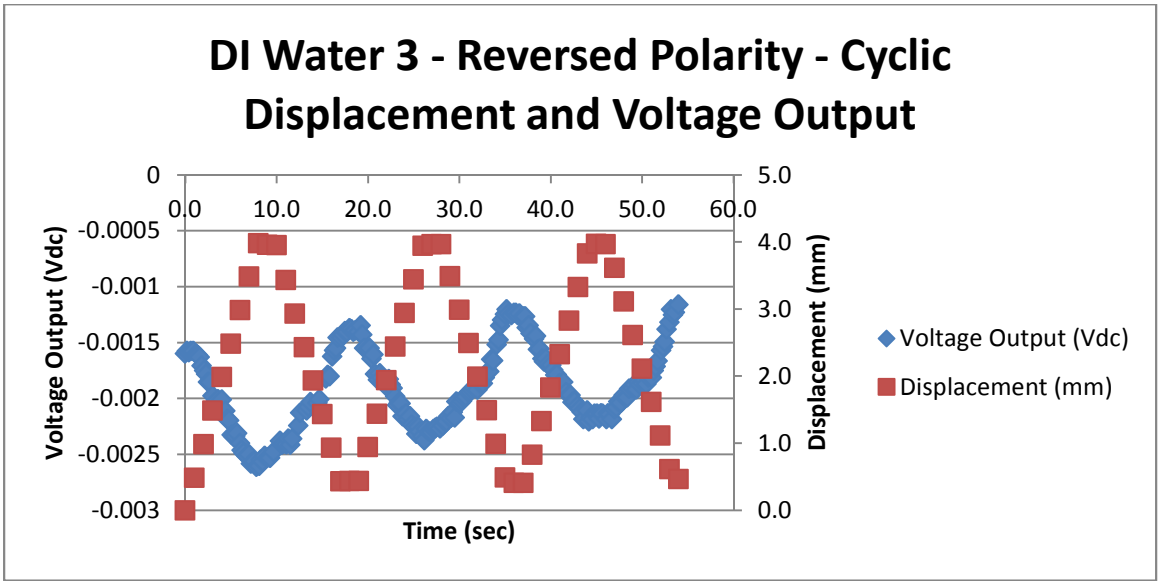

Figure 289
Trial 3 reversed polarity DI water electrolyte cyclic load scenario, displacement and raw voltage output

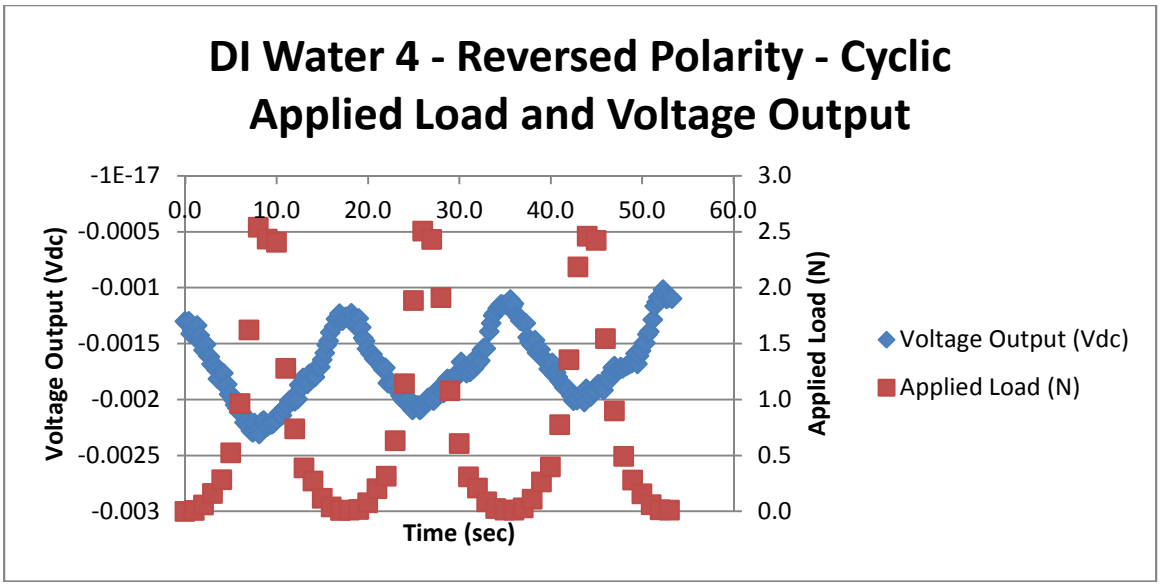

Figure 290

Trial 4 reversed polarity DI water electrolyte cyclic load scenario, load and raw voltage output

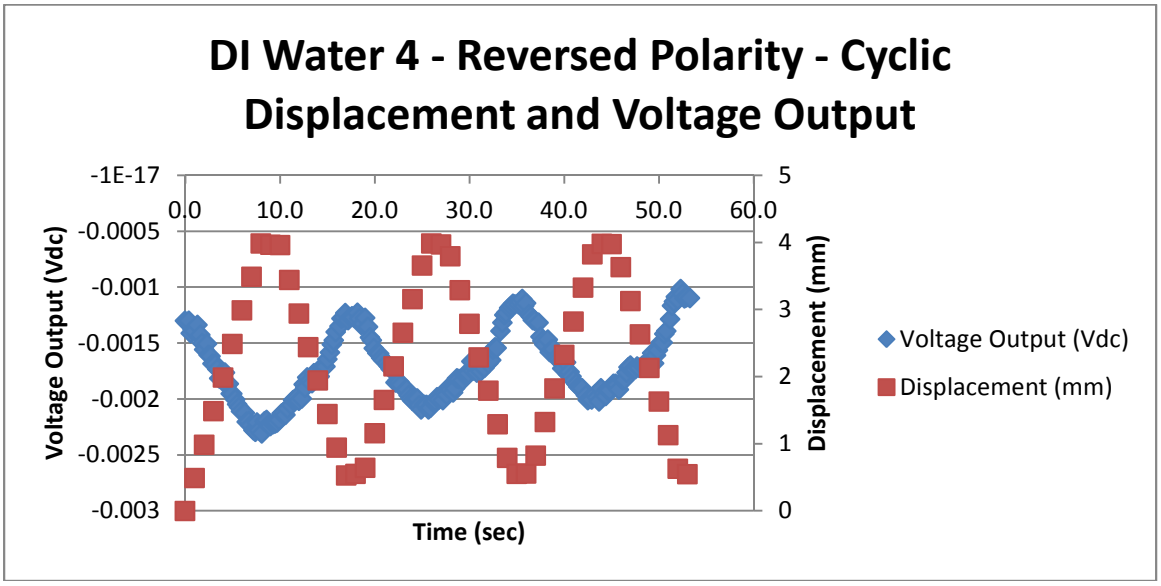

Figure 291

Trial 4 reversed polarity DI water electrolyte cyclic load scenario, displacement and raw voltage output

Appendix K

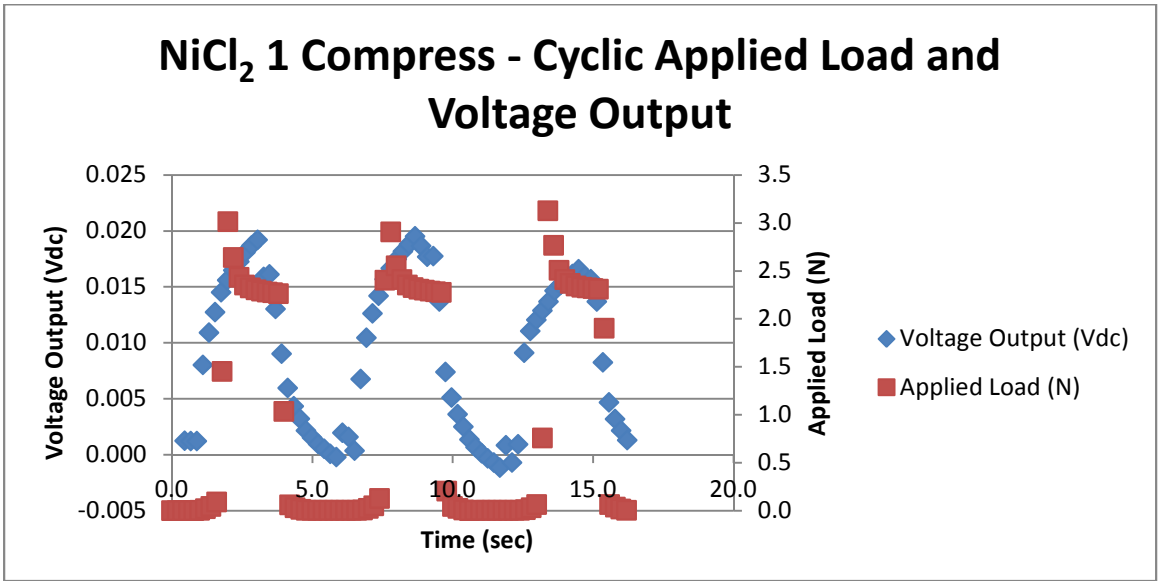

Figure 292

Trial 1 normal polarity $NiCl_2$ electrolyte cyclic compression load scenario, load and raw voltage output

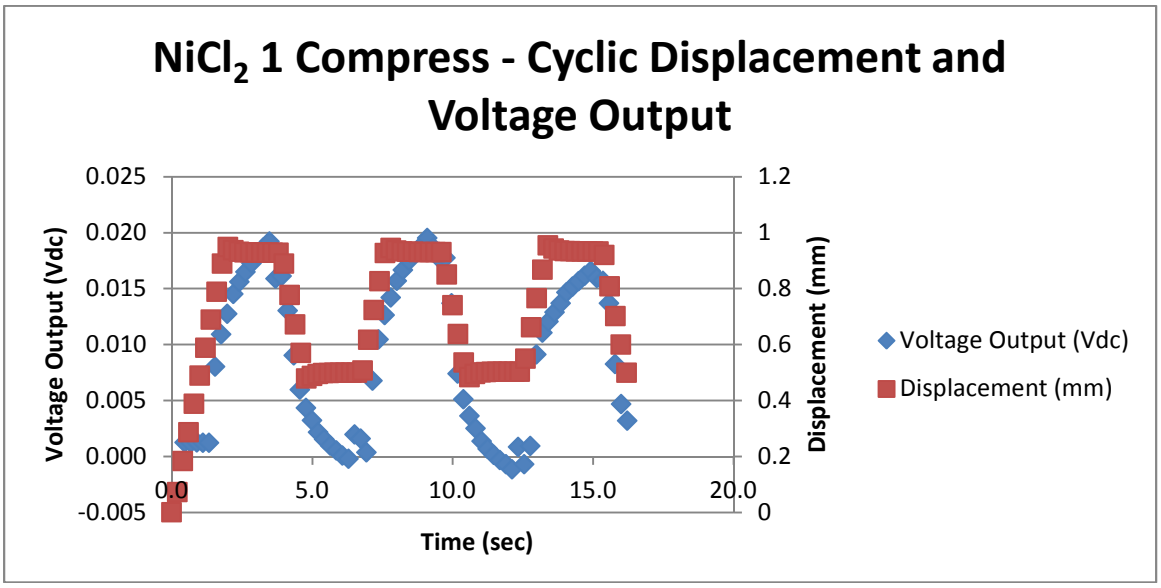

Figure 293

Trial 1 normal polarity $NiCl_2$ electrolyte cyclic compression load scenario, displacement and raw voltage output

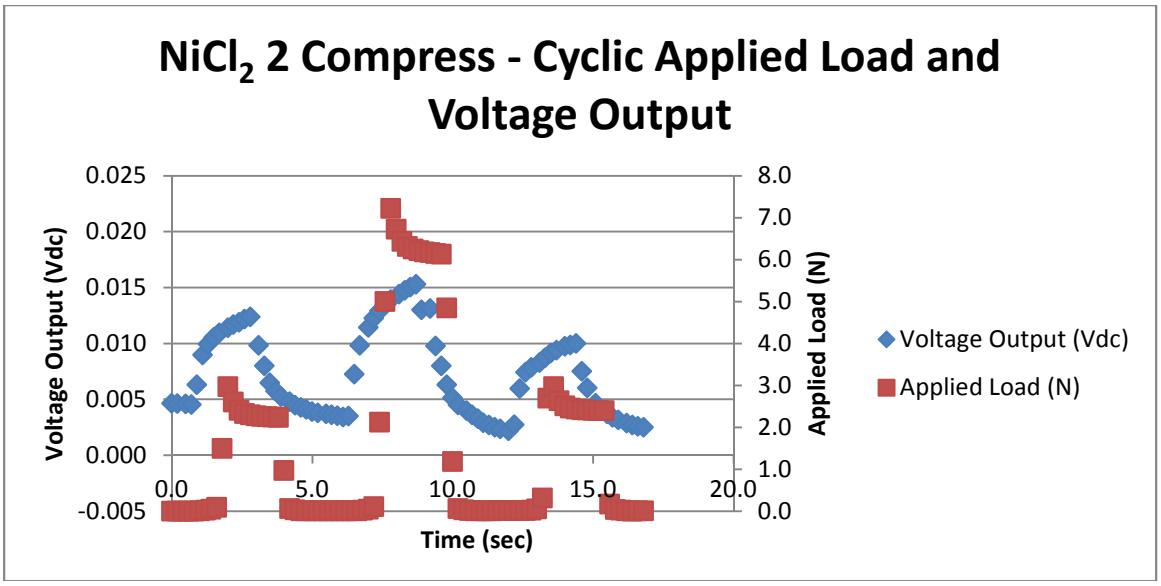

Figure 294

Trial 2 normal polarity $NiCl_2$ electrolyte cyclic compression load scenario, load and raw voltage output

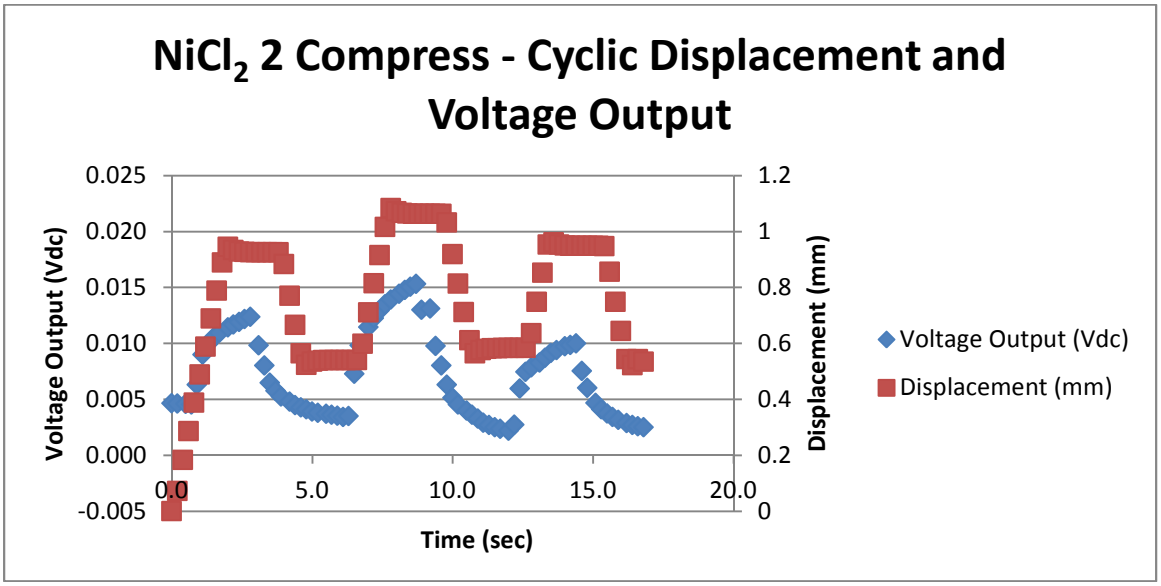

Figure 295

Trial 2 normal polarity $NiCl_2$ electrolyte cyclic compression load scenario, displacement and raw voltage output

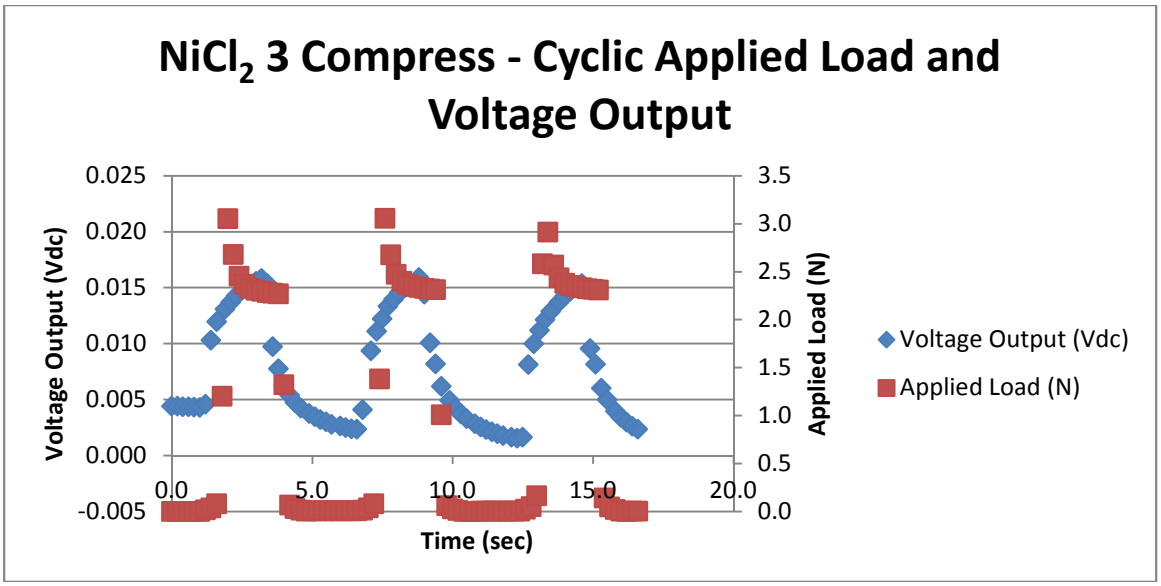

Figure 296

Trial 3 normal polarity $NiCl_2$ electrolyte cyclic compression load scenario, load and raw voltage output

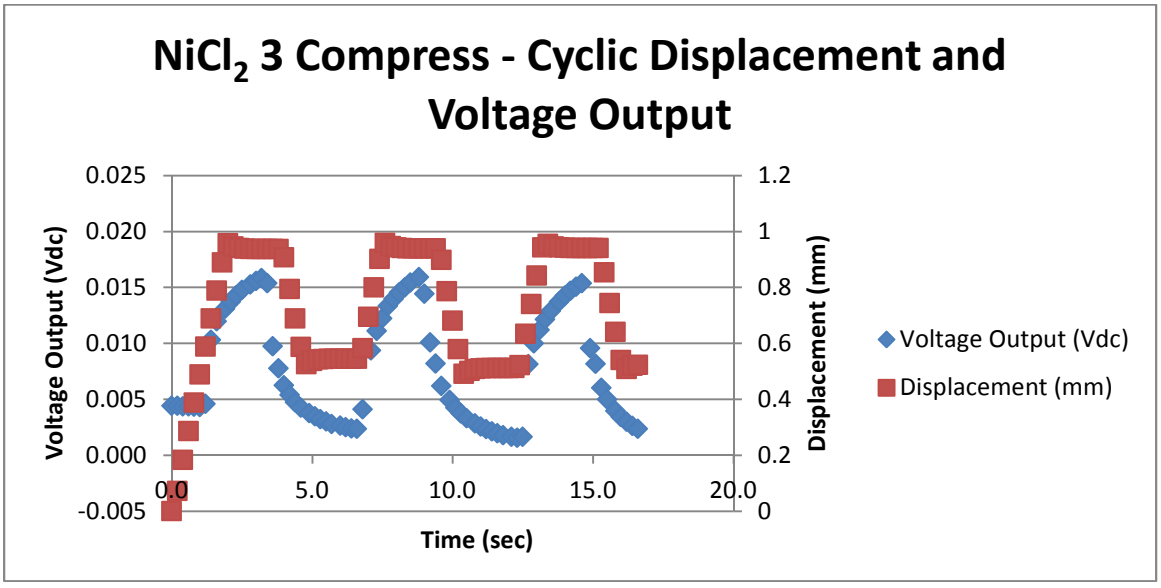

Figure 297

Trial 3 normal polarity $NiCl_2$ electrolyte cyclic compression load scenario, displacement and raw voltage output

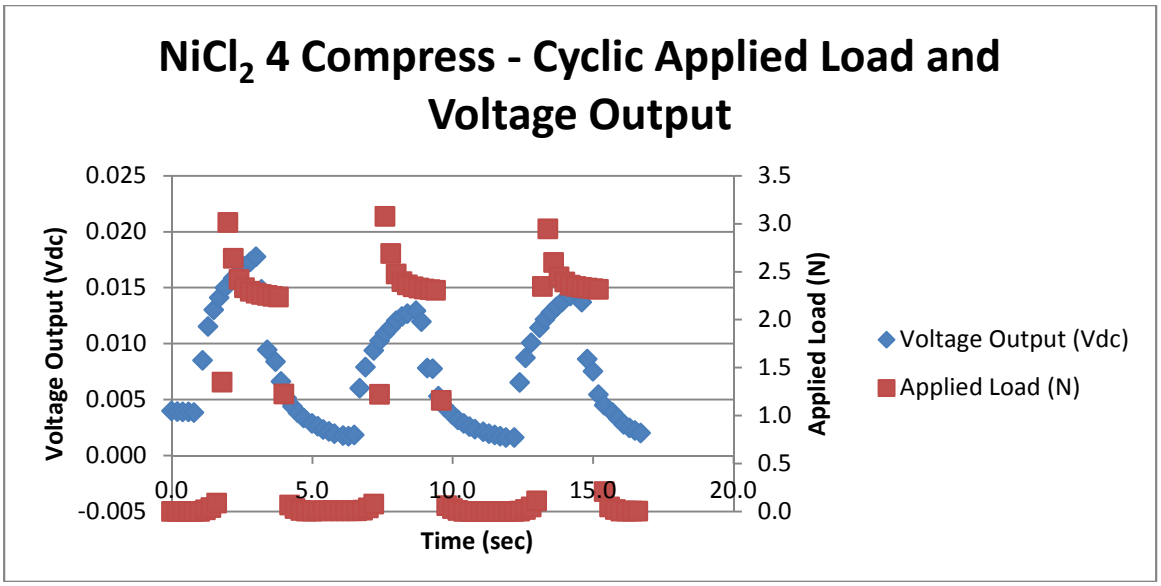

Figure 298

Trial 4 normal polarity $NiCl_2$ electrolyte cyclic compression load scenario, load and raw voltage output

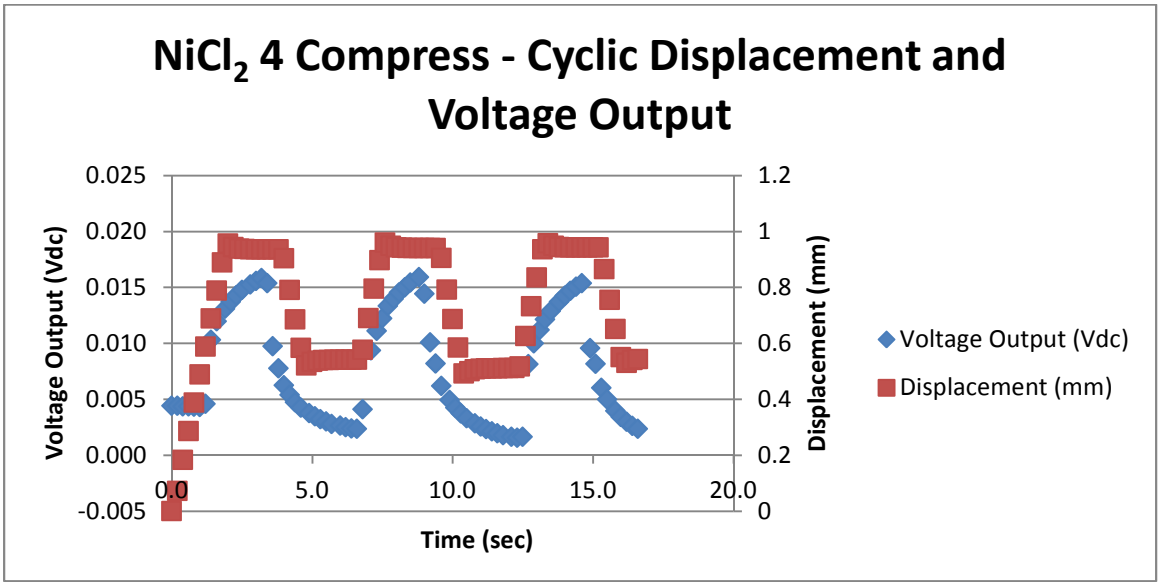

Figure 299

Trial 4 normal polarity $NiCl_2$ electrolyte cyclic compression load scenario, displacement and raw voltage output

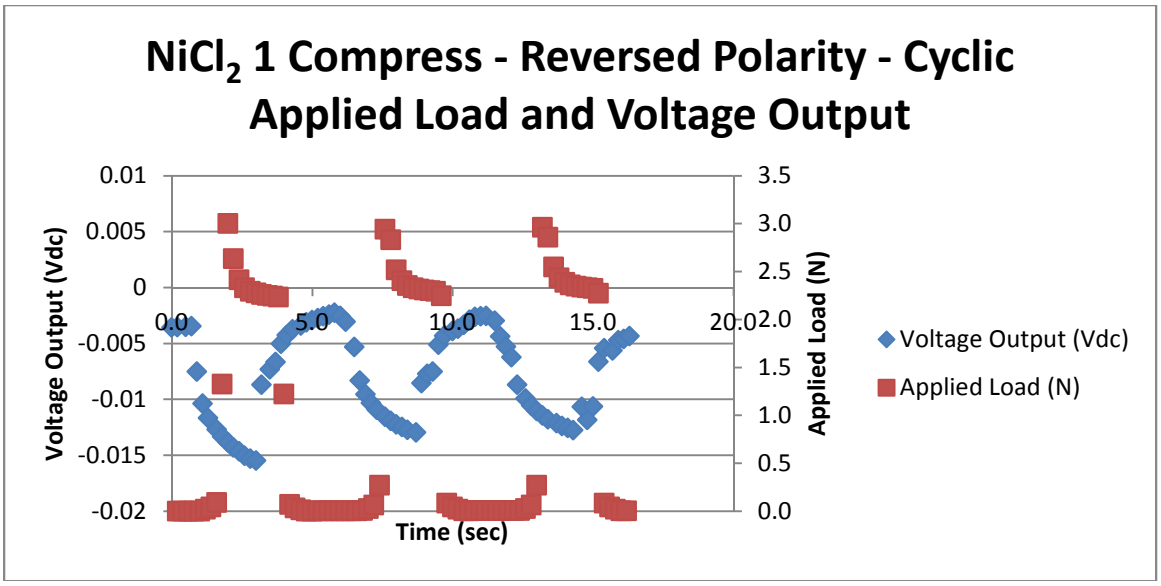

Figure 300

Trial 1 reversed polarity $NiCl_2$ electrolyte cyclic compression load scenario, load and raw voltage output

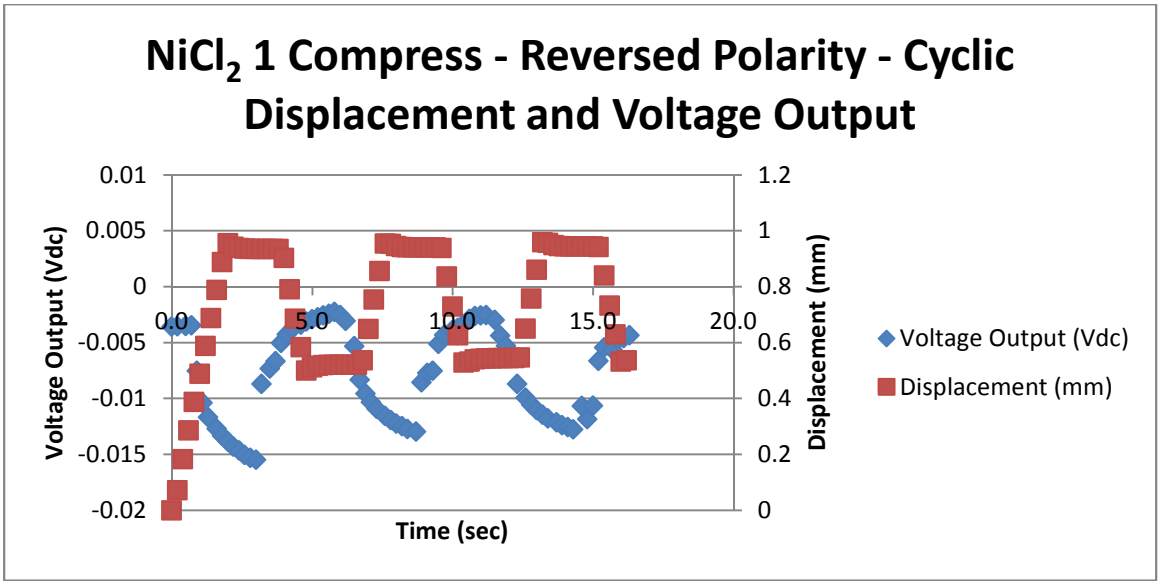

Figure 301

Trial 1 reversed polarity $NiCl_2$ electrolyte cyclic compression load scenario, displacement and raw voltage output

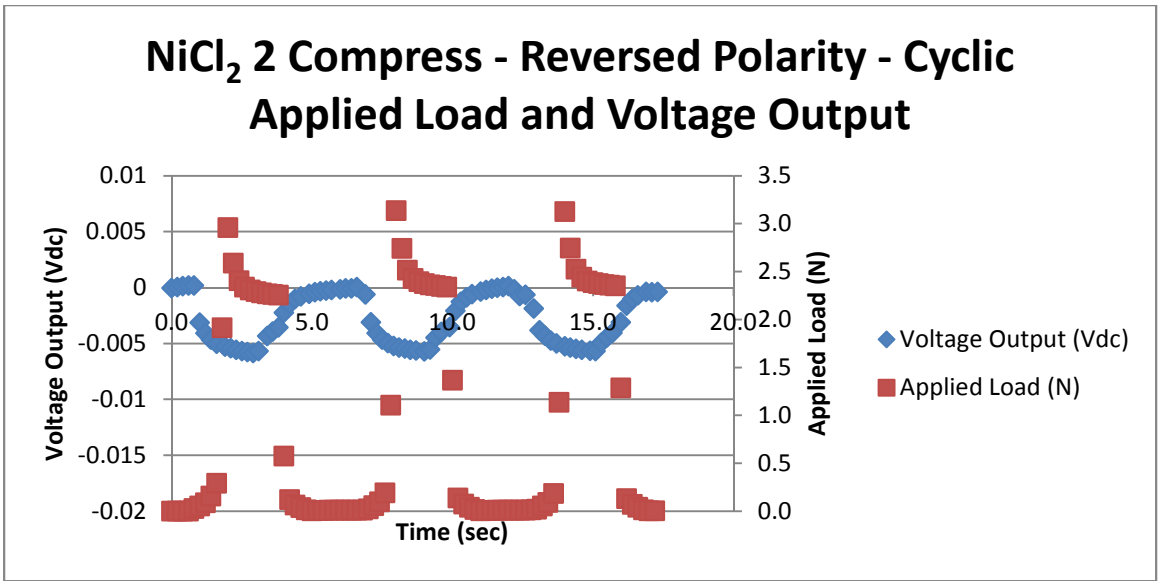

Figure 302

Trial 2 reversed polarity $NiCl_2$ electrolyte cyclic compression load scenario, load and raw voltage output

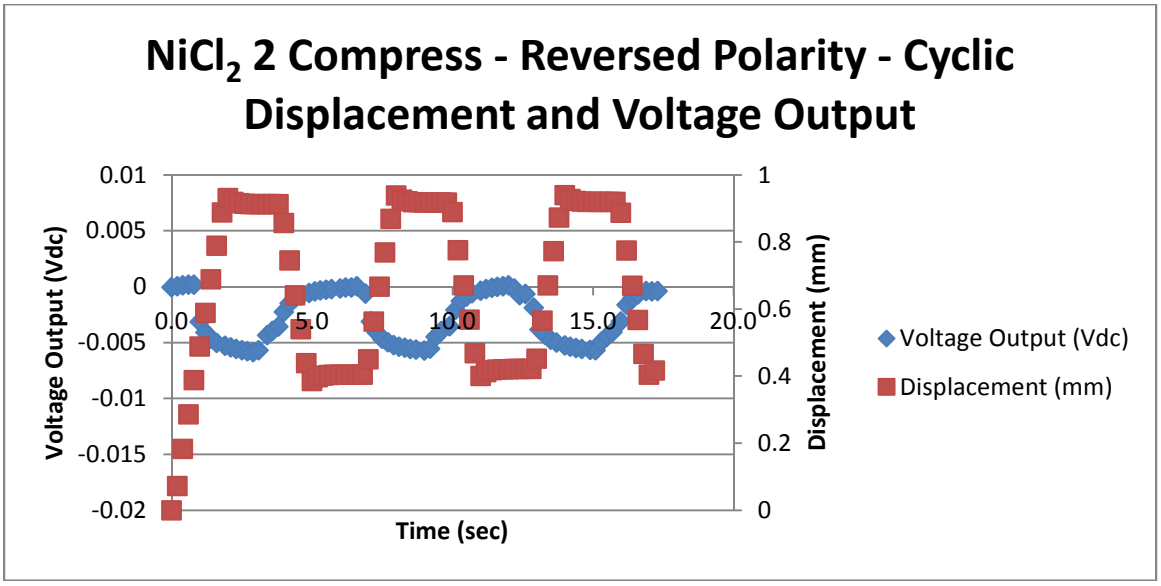

Figure 303

Trial 2 reversed polarity $NiCl_2$ electrolyte cyclic compression load scenario, displacement and raw voltage output

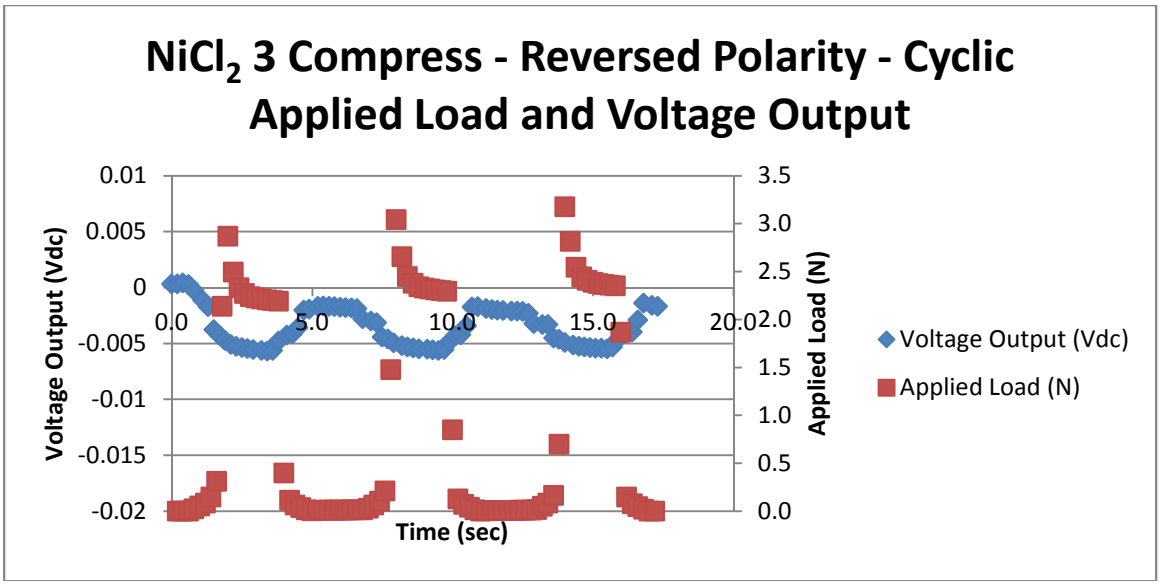

Figure 304

Trial 3 reversed polarity $NiCl_2$ electrolyte cyclic compression load scenario, load and raw voltage output

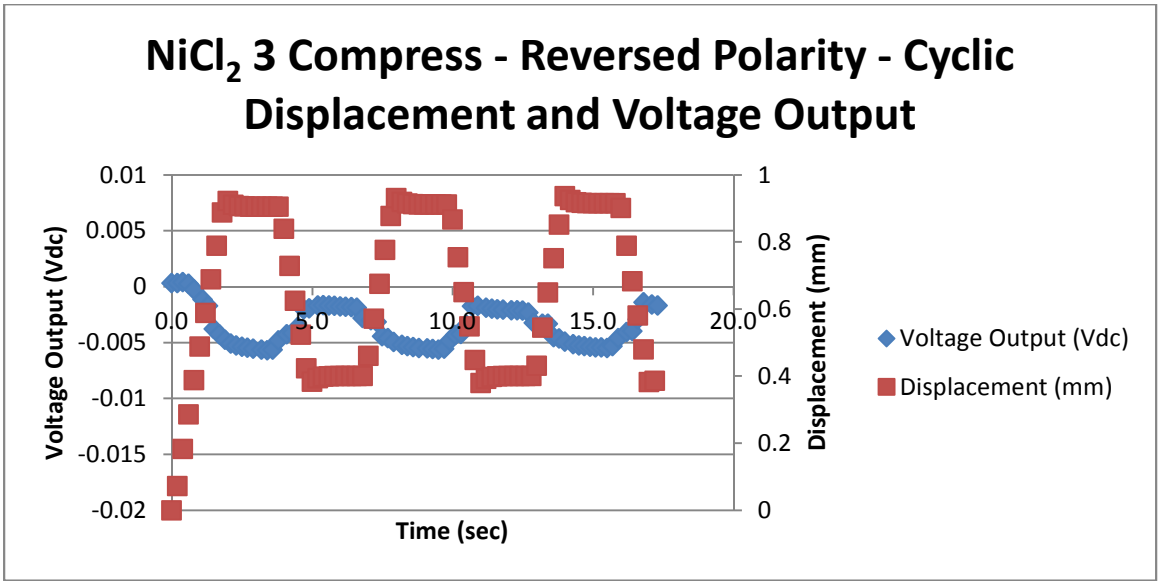

Figure 305

Trial 3 reversed polarity $NiCl_2$ electrolyte cyclic compression load scenario, displacement and raw voltage output

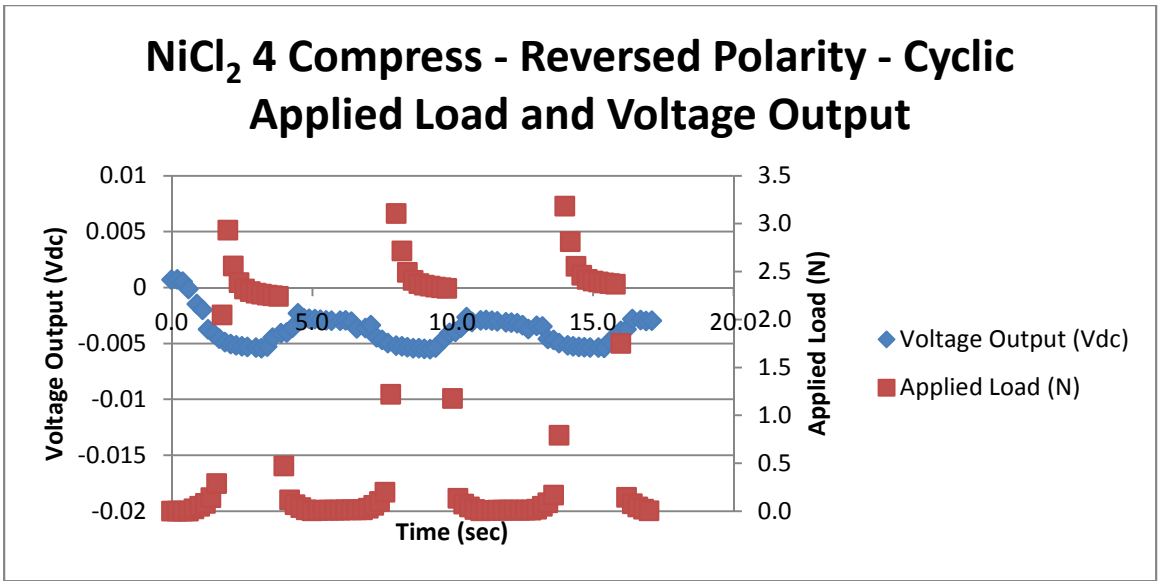

Figure 306

Trial 4 reversed polarity $NiCl_2$ electrolyte cyclic compression load scenario, load and raw voltage output

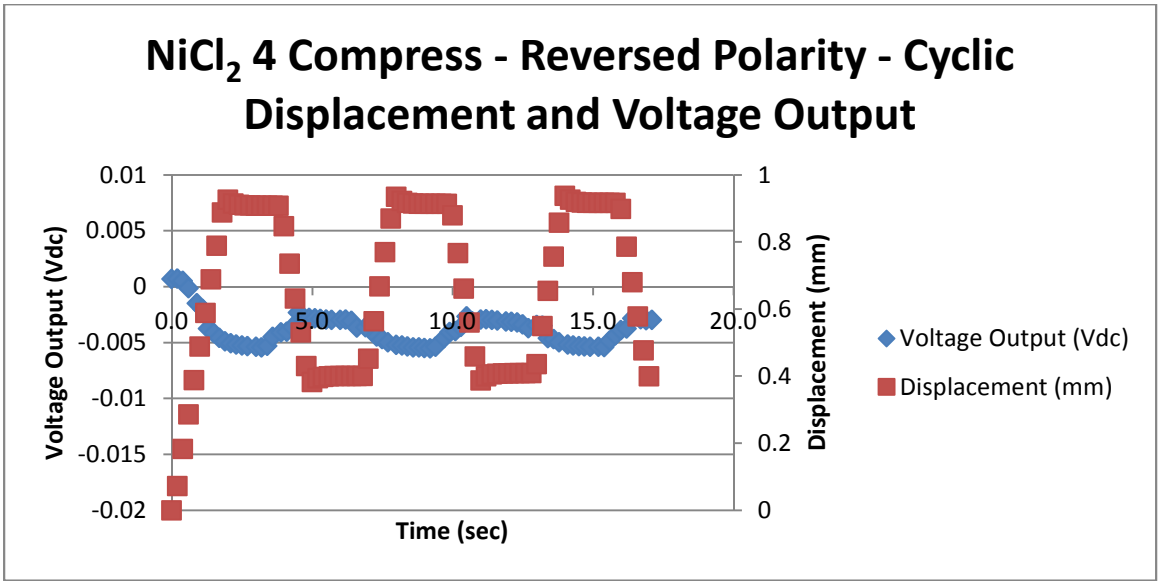

Figure 307

Trial 4 reversed polarity $NiCl_2$ electrolyte cyclic compression load scenario, displacement and raw voltage output

Appendix L

Preparation Procedure

Ion-Exchange Polymer Metal Composites (IPMC) Membranes

Adapted from [25]

Keisuke Oguro,

Osaka National Research Institute, AIST, Japan

This homepage is part of the Worldwide Electroactive Polymer (EAP) Webhub and it is maintained by the JPL's NDEAA Technologies Group

Supply

- Base polymer: Nafion 117 (duPont)
- Aqueous solution of platinum ammine complex ($[Pt(NH_3)_4]Cl_2$ or $[Pt(NH_3)_6]Cl_4$) [Can be purchased from: Aldrich Chemical Co., Milwackee, WI phone 800-558-9160, Catalog #275905]
- Sodium borohydride ($NaBH_4$, reducing agent for primary reduction)
- Hydrazine hydrate (NH_2NH_2- ~$1.5H_2O$, reducing agent for secondary reduction)
- Hydroxylamine hydrochloride (NH_2OH-HCl, reducing agent for secondary reduction)
- Dilute ammonium hydroxide solution (NH_4OH 5% solution)
- Dilute hydrochloric acid (HCl aq, 2 *N* solution and 0.1 *N* solution)
- Deionized water

1. Surface Roughening of the Membrane

a. Mild Sandblast: Sandblasting the surface of the membrane in order to increase the surface area. Use fine glass beads (GP 105A, Toshiba Co. Ltd.) that are blown onto the dry membrane by compressed air. The speed of sandblasting is ~1 sec/cm^2 membrane area. It is also possible to use emery paper to sand the material.

b. Ultrasonic Washing: Remove the glass beads and residues by washing the membrane with water preferably using ultrasonic cleaner.

c. Treatment with HCl: Boil the membrane in dilute hydrochloric acid (HCl aq, 2 *N* solution) for 30 minutes to remove impurities and ions in the membrane. Rinse it with deionized water.

d. Treatment with Water: Boil the membrane in deionized water for 30 minutes to remove acid and to swell the membrane. The roughened membrane can store in deionized water.

2. Ion-exchange (Adsorption)

Prepare a platinum complex ($[Pt(NH_3)_4]Cl_2$ or $[Pt(NH_3)_6]Cl_4$) solution of 2 mg Pt/ml. Although the adsorbing amount depends on charge of the complex, either complex gives good electrodes. Immerse the membrane in the solution containing more than 3 mg of Pt per cm^2 membrane area. For instance, more than 45 ml of the Pt solution is required for a membrane of 30 cm^2. Excess amount of the Pt solution is preferable. After immersing the membrane, add 1 ml of ammonium hydroxide solution (5 %) to neutralize. Keep the membrane in the solution at room temperature for more than 3 hours (one night usually).

3. Primary Plating (Reduction)

Prepare a 5 wt% aqueous solution of sodium borohydride. After rinsing the membrane with water, place the membrane of 30 cm^2 in stirring water of 180 ml in a water bath at 40°C. Then, add 2 ml of the sodium borohydride solution (5 wt% $NaBH_4$ aq) every 30 min for 7 times. The amount of the reagent should be proportional to the area of the membrane. In the sequence of addition, raise the temperature up to 60°C gradually. Then, add 20 ml of the reducing agent and stir for 1.5 hr at 60°C. Black layer of fine Pt particles deposits only on the surface of the membrane. Rinse the membrane with water and immerse it in dilute hydrochloric acid (0.1 *N*) for an hour.

4. Secondary Plating (Developing)

The amount of platinum deposited by the 1st plating (reduction process) is only less than 0.9 mg/cm^2, which depends on the ion exchange capacity, thickness of the membrane and the structure of the Pt complex. Additional amount of platinum is plated by developing process on the deposited Pt layer. When you add 2 mg/cm^2 of Pt on the area of 60 cm^2 (both sides of 30 cm^2 of membrane), you need Pt complex solution containing 120 mg of Pt. Prepare a 240 ml aqueous solution of the complex ($[Pt(NH_3)_4]Cl_2$ or $[Pt(NH_3)_6]Cl_4$) containing 120 mg of Pt and add 5 ml of the 5% ammonium hydroxide solution. Plating amount is determined by the content of Pt in the solution. Prepare a 5% aqueous solution of hydroxylamine hydrochloride (NH_2OH-HCl) and a 20% solution of hydrazine (NH_2NH_2). Place the membrane in the stirring Pt solution at 40°C. Add 6 ml of the hydroxylamine hydrochloride solution and 3 ml of the hydrazine solution every 30 minutes. In the sequence of addition, raise the temperature up to 60°C gradually for 4 hours, and gray metallic layers will form. At the end of this process, sample a small amount of the solution and boil it with the strong reducing agent ($NaBH_4$) to check the end point. It is

dangerous to add $NaBH_4$ powder in a hot solution, because of the gas explosion. So add $NaBH_4$ solution to a cold solution, then, warm the solution on a water bath. If any Pt ion remains in the plating solution, the color of the solution turns to black. In such cases, continue to develop Pt with addition of the NH_2OH-HCl and NH_2NH_2 solutions. If you check that there is none of Pt ion in the chemical plating solution, rinse the membrane with water, and boil in dilute hydrochloric acid (0.1 *N*) to remove the ammonium cation in the membrane. After washing with water, H^+ in the composite can be exchanged for any cation by immersing in a solution of the chloride salt of the cation.

ACKNOWLEDGMENT

The Editor of the WW-EAP Webhub would like to express his sincere appreciation to Dr. Keisuke Oguro for contributing his fabrication recipe. Dr. Oguro is one of the pioneers of the IPMC and leading EAP scientist. His contribution is a very important milestone for the field of EAP particularly since there is no recommended commercial source of such materials. The Editor would like to express his hope to seeing more scientists who are developing new EAP materials to share their recipe by allowing it to be published on the WW-EAP Webhub to promote progress in this emerging field of EAP.

Appendix M

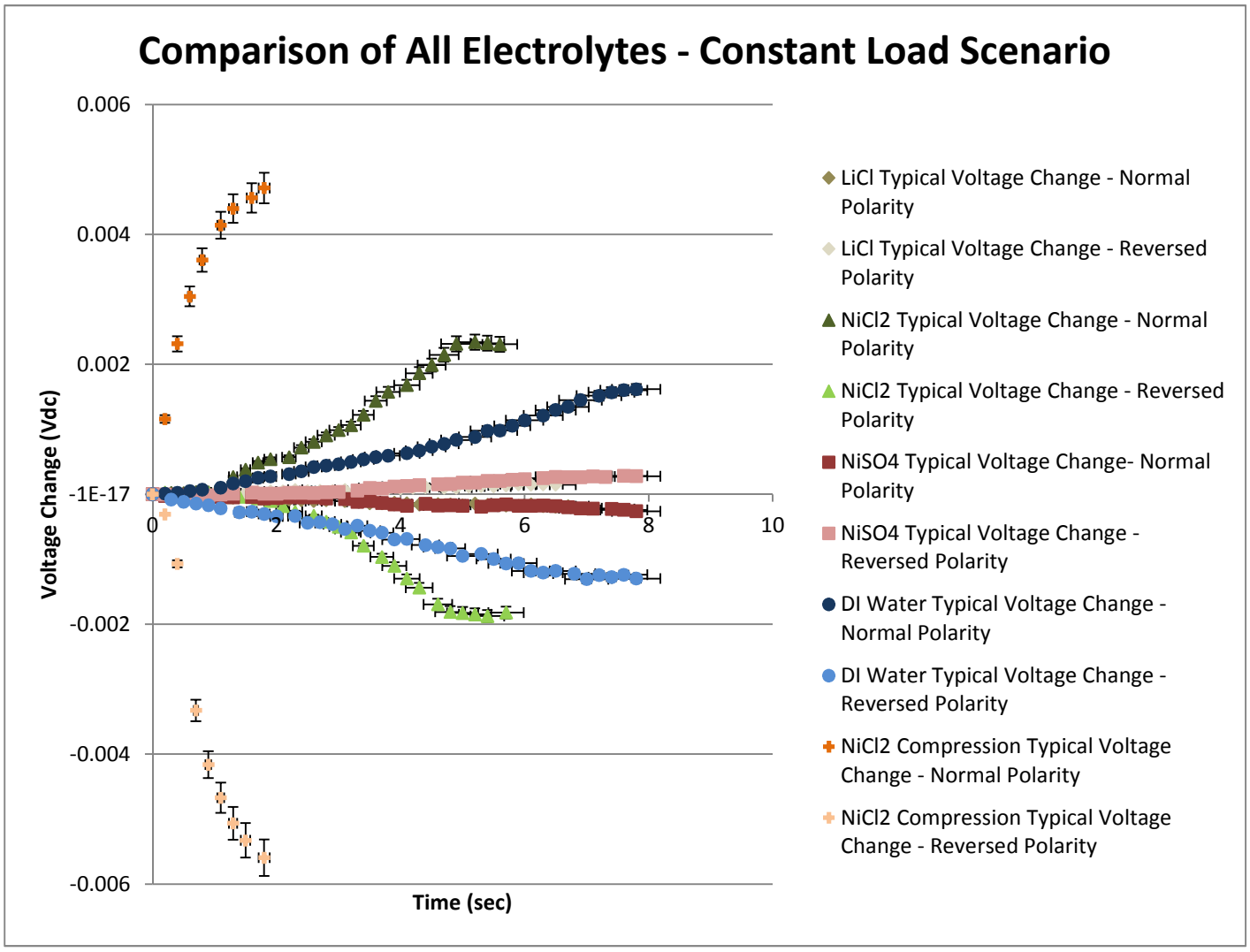

Figure 308. Comparison of All Electrolytes With Error Bars Constant Load Scenario

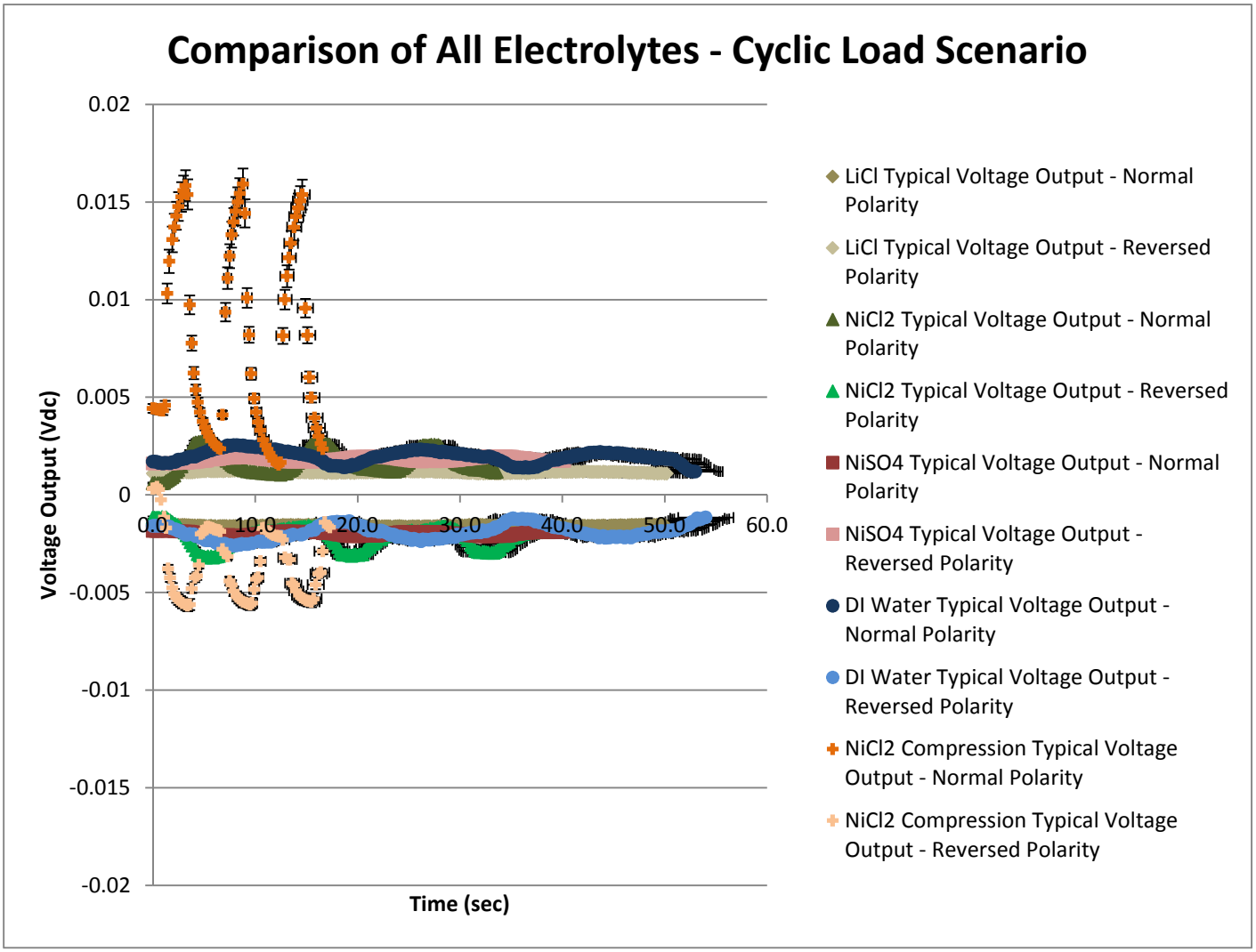

Figure 309. Comparison of All Electrolytes With Error Bars Cyclic Load Scenario